

Following London's Footsteps

-

Implications for Structure and Reactivity

Inauguraldissertation zur Erlangung des Doktorgrades der naturwissenschaftlichen Fachbereiche

im Fachgebiet Organische Chemie (Fachbereich 08)

der Justus-Liebig-Universität Gießen



vorgelegt von

Lars Rummel

angefertigt im Zeitraum von März 2019 bis Dezember 2022

am Institut für Organische Chemie

der Justus-Liebig-Universität Gießen

Betreuer: Prof. Dr. Peter R. Schreiner, PhD

Eidesstattliche Erklärung

Hiermit versichere ich, die vorgelegte Dissertation selbständig und ohne unerlaubte fremde Hilfe und nur mit den Hilfen angefertigt zu haben, die ich in der Dissertation angegeben habe. Alle Textstellen, die wörtlich oder sinngemäß aus veröffentlichten Schriften entnommen sind, und alle Angaben, die auf mündlichen Auskünften beruhen, sind als solche kenntlich gemacht.

Bei den von mir durchgeführten und in der Dissertation erwähnten Untersuchungen habe ich die Grundsätze guter wissenschaftlicher Praxis, wie sie in der „Satzung der JustusLiebig-Universität zur Sicherung guter wissenschaftlicher Praxis“ niedergelegt sind, eingehalten.

Frankfurt, 23.05.23

Ort, Datum

Unterschrift

Dekan: Prof. Dr. Thomas Wilke

Prodekan: Prof. Dr. Klaus Müller-Buschbaum

Studiendekan: Prof. Dr. Richard Göttlich

Erstgutachter: Prof. Dr. Peter R. Schreiner, PhD

Zweitgutachter: Prof. Dr. Richard Göttlich

Zusammenfassung

London'sche Dispersionswechselwirkungen sind in der Molekularchemie allgegenwärtig und bestimmen molekulare Aggregation, Erkennung sowie chemische Selektivität. Als attraktiver Teil der Van-der-Waals-Wechselwirkungen wird London'sche Dispersion dennoch als schwach und vernachlässigbar angesehen. Diese Arbeit zeigt durch Kombination experimenteller und quantenchemischer Untersuchungen den enormen Einfluss London'scher Dispersionswechselwirkungen auf molekulare Struktur sowie chemische Reaktivität auf. Während dieser Arbeit sind zahlreiche neuartige Moleküle hergestellt und analysiert worden, wobei der Schwerpunkt stets auf Qualifizierung und Quantifizierung nicht-kovalenter Wechselwirkungen gelegen hat. Die Ergebnisse dieser Arbeit sollen dazu beitragen einen zielgerichteten Einsatz von Dispersionsenergie-Donoren, beispielsweise in Synthese und Katalyse, zu ermöglichen. Durch ein besseres Verständnis nicht-kovalenter Wechselwirkungen können neue Moleküle dargestellt, Reaktionsmechanismen untersucht und Selektivitäten erhöht werden.

In der ersten Veröffentlichung sind quantenchemisch die unerwartete thermodynamische Stabilität von Hexaphenylethanderivaten höherer Tetrele untersucht worden. Durch Ausnutzung verschiedener computerchemischer Methoden zur Qualifizierung und Quantifizierung intra- und intermolekularer Wechselwirkungen ist die Hauptursache der hohen thermodynamischen Stabilität in einem idealen Verhältnis attraktiver London'scher Dispersionswechselwirkungen und abstoßender Pauli-Repulsion gefunden worden.

Die zweite und dritte Veröffentlichung konzentrieren sich auf die Rolle nicht-kovalenter Wechselwirkungen zwischen Silylgruppen und analysieren deren Potential als Dispersionsenergie-Donoren. Mittels experimenteller und quantenchemischer Analysen sind zwei molekulare Waagen basierend auf Cyclooctatetraen entworfen und untersucht worden. Während sich die zweite Veröffentlichung auf den sterischen Anspruch von Silylen konzentriert, betont die Dritte das feine Wechselspiel attraktiver London'scher Dispersionswechselwirkungen und Entropie.

Die vierte Publikation beschreibt die Rolle London'scher Dispersionswechselwirkungen auf die Konformation von Diphenylthioharnstoffen. Durch Verwendung von Dispersionsenergie-Donoren ist das bis dato selten betrachtete *syn-syn*-Konformer erzeugt worden. Unter Verwendung tieftemperatur-NMR-spektroskopischer Methoden konnte der Einfluss London'scher Dispersionswechselwirkungen qualifiziert und quantifiziert werden.

Während sich die ersten vier Publikationen auf molekulare Strukturen konzentrieren, befassen sich die nächsten Beiden mit dem Einfluss London'scher Dispersion auf chemische Reaktionen. Die fünfte Veröffentlichung beschreibt eine Hydrochlorierungsreaktion unter thermodynamischer Kontrolle. Es ist festgestellt worden, dass die Dispersionswechselwirkung der Schlüssel zur Rationalisierung des Produktverhältnisses ist. Das sechste Projekt beschreibt den Einfluss von Dispersionsenergie-Donoren auf eine kinetisch kontrollierte Reaktion. Hierbei konnte das Produktverhältnis der Johnson-Corey-Chaykovsky-Reaktion signifikant beeinflusst werden. Die Auswirkungen London'scher Dispersionswechselwirkungen auf Übergangszustände sind erneut experimentell qualifiziert und quantifiziert worden.

Abstract

London dispersion interactions are ubiquitously present in molecular chemistry and govern molecular aggregation, recognition as well as chemical selectivity. Nevertheless, as attractive part of the van der Waals interactions, London dispersion is generally regarded as weak and negligible. This work emphasizes the tremendous impact London dispersion interactions have on structural stability as well as chemical reactivity by focusing on a combination of experimental and computational investigations. During this work, numerous novel molecules were prepared and analyzed with the main focus on qualifying and quantifying noncovalent interactions. The results of this work might eventually enable a target-oriented use of dispersion energy donors, *e.g.* in synthesis and catalysis, to generate novel molecular structures, exploit reaction mechanisms or simply rationalize selectivities.

In the first publication, we computationally investigated the unexpected thermodynamic stability of hexaphenylethane derivatives with heavier tetrrels comprising the central bond. By exploiting various energy decomposition methods, the source of stabilization was found in an ideal ratio of attractive London dispersion interactions and repulsive Pauli exchange repulsion.

The second and third publication report an experimental and computational study on the effects of silyl groups on a molecular balance. While the second publication focuses on the steric size of such groups, the third one emphasizes the fine interplay between attractive London dispersion interactions and an entropic penalty due to increasing flexibility. In both publications, the cyclooctatetraene molecular balance was exploited.

The fourth publication describes the role of London dispersion on the conformational landscape of thiourea. By utilizing dispersion energy donors the *syn-syn* conformer was generated. The combination of low-temperature nuclear magnetic resonance experiments and computational analyses allowed quantification of London dispersion interactions.

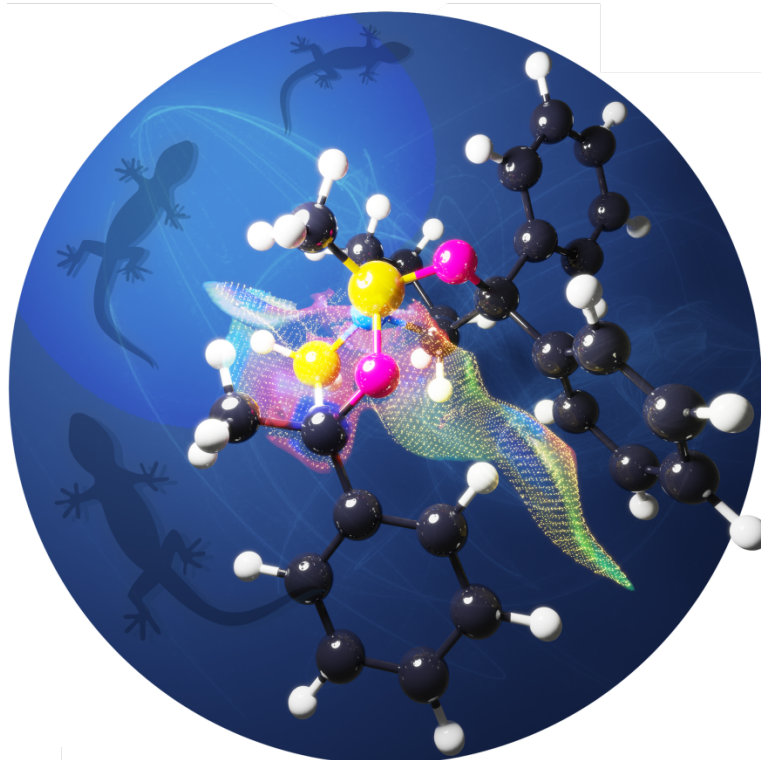
While the first four publications focus on structural ramifications of London dispersion, the next two cover the impact of London dispersion on reactivity. The fifth publication describes a hydrochlorination reaction under thermodynamic control. London dispersion was found to be key to rationalize product ratio.

The sixth project describes the impact of dispersion energy donors on a kinetically controlled reaction. We utilized the Johnson-Corey-Chaykovsky reaction to qualify and quantify the impact of London dispersion on transition states.

Table of Contents

Eidesstattliche Erklärung	3
Zusammenfassung	5
Abstract.....	7
1. Introduction	11
2. Publications	34
2.1 Hexaphenylditetrels – When Longer Bonds Provide Higher Stability.....	34
2.2 Gauging the Steric Effects of Silyl Groups with a Molecular Balance	39
2.3 Silyl Groups Are Strong Dispersion Energy Donors.....	50
2.4 London Dispersion Favors Sterically Hindered Diarylthiourea Conformers in Solution	61
2.5 London Dispersion Stabilizes Chloro-Substituted <i>cis</i> -Double Bonds	70
2.6 London Dispersion Favors <i>cis</i> -Selectivity in the Johnson-Corey-Chaykovsky Epoxidation.....	77
3. Acknowledgement - Danksagung.....	85

1. Introduction



Abstract:

London dispersion (LD) interactions are the main contribution of the attractive part of the van der Waals potential. Even though, LD effects are the driving force for molecular aggregation and recognition, the role of these omnipresent interactions in structure and reactivity had been largely underappreciated. However, in the recent years considerable efforts were made to thoroughly study LD interactions and their potential as a chemical design element for structures and catalysis. This was made possible through a fruitful combination of theory and experiment. This review highlights the recent results and advances in utilizing LD interactions as a structural motif to understand and utilize intra- and intermolecularly LD-stabilized systems. Additionally, we focus on the quantification of LD interactions and their fundamental role in chemical reactions.

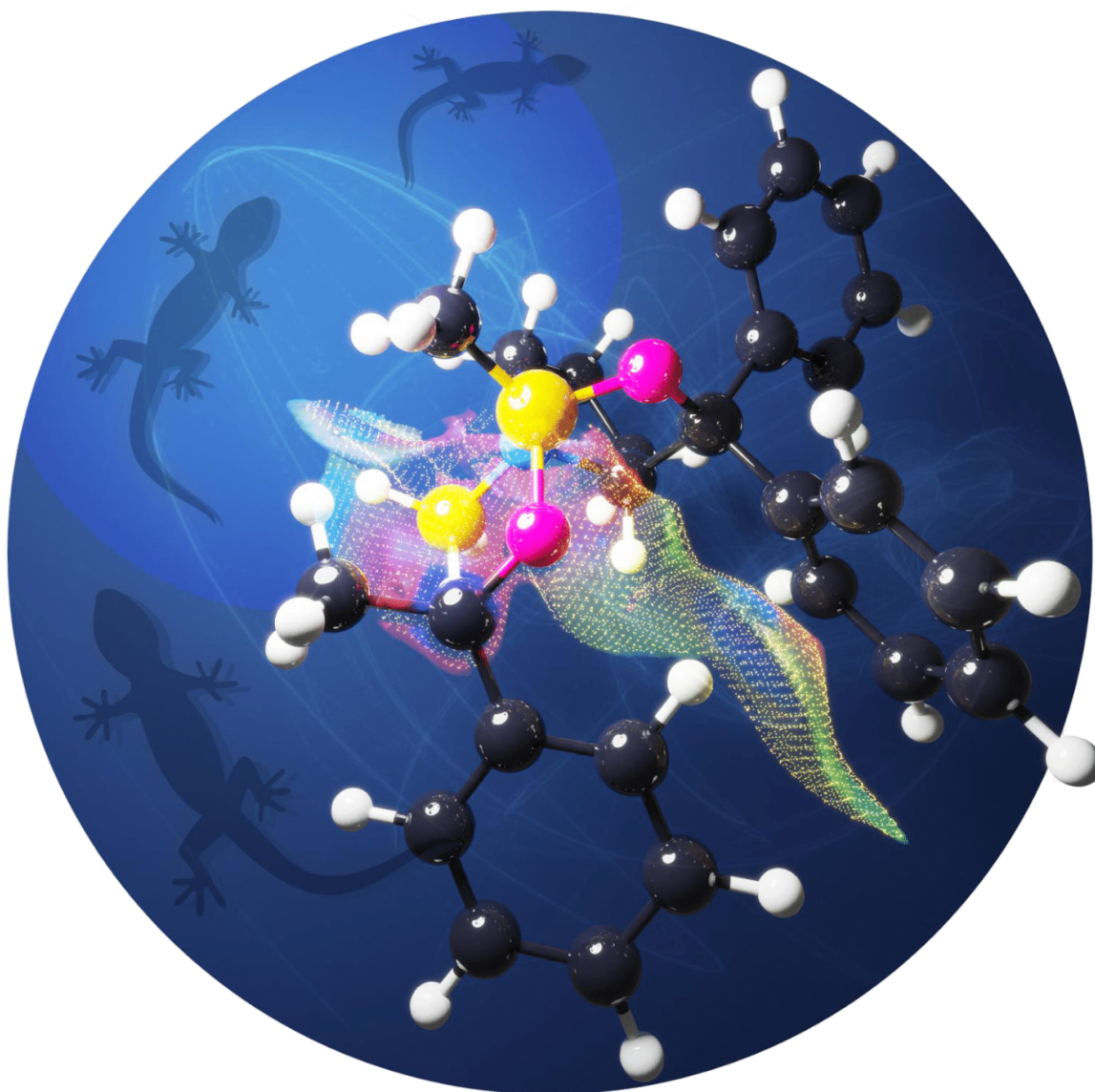
Reference:

Lars Rummel, and Peter R. Schreiner; *manuscript in preparation*.

Advances, Prospects, and Implications of London Dispersion Interactions in Molecular Chemistry

Lars Rummel and Peter R. Schreiner*

This paper is dedicated to the memory of Fritz London whose groundbreaking theoretical work now receives full recognition.



[*] L. Rummel, Prof. Dr. P. R. Schreiner
 Institute of Organic Chemistry
 Justus Liebig University
 Heinrich-Buff-Ring 17, 35392 Giessen (Germany)
 E-mail: prs@uni-giessen.de

Abstract: London dispersion (LD) interactions are the main contribution of the attractive part of the van der Waals potential. Even though, LD effects are the driving force for molecular aggregation and recognition, the role of these omnipresent interactions in structure and reactivity had been largely underappreciated. However, in the recent years considerable efforts were made to thoroughly study LD interactions and their potential as a chemical design element for structures and catalysis. This was made possible through a fruitful combination of theory and experiment. This review highlights the recent results and advances in utilizing LD interactions as a structural motif to understand and utilize intra- and intermolecularly LD-stabilized systems. Additionally, we focus on the quantification of LD interactions and their fundamental role in chemical reactions.

1. Introduction

J. D. van der Waals' famous maxim "*Matter will always display attraction*"^[1] essentially constitutes the basis of all chemical processes. The complexity of reaction mechanisms, catalytic cycles or structural motifs can all be reduced to the fact that matter always displays attraction. Hence, as a perpetual physical concept, van der Waals (vdW) interactions govern molecular structures and chemical reactions^[1a, 2] as they reach from the simplest case of two atoms attracting each other noncovalently (observable at a low enough temperature) complex systems, *e.g.*, the folding of peptides,^[3] catalyst-substrate recognition,^[4] or the orientation of molecules in a crystal lattice.^[5] One of the main contributors to the attractive part of vdW interactions stems from electron correlation effects referred to as London dispersion (LD) interactions.^[6] While molecular recognition and aggregation to a large extent is based on LD,^[7] the explicit consideration of LD interactions in molecular systems has only been conceptualized, quantified, and understood in the last few years.

LD interactions are described as quantum-mechanical fluctuations of the electron density leading to induced-dipole-induced-dipole interactions.^[8] Interestingly, London originally utilized spectroscopic properties to demonstrate the distance r^{-6} dependence of the attractive part of the vdW potential (1).^[9] As a result, he formulated the following mathematical equation, where C_6 represents an empirical polarization coefficient and r the distance between two atoms.

$$E_{\text{disp}} = -\frac{1}{2} \sum \frac{C_6}{r^6} \quad (1)$$

Although initially postulated by London in 1930 as the sum of pairwise interactions, σ - σ attraction has been mostly ignored for systems of larger size.^[6a, 9a] This is not surprising considering the strength of a single pairwise interaction in comparison to point-charges. Consequently, LD interactions are considered to be significantly weaker than Coulomb interactions and mostly outweighed by Pauli (exclusion) repulsion as well. However, the

dimerization of two atoms in the gas phase describes only the simplest case and can be extended by utilizing bulky moieties with multiple contacts, thereby accumulating the amount of LD interactions relative to other noncovalent interactions. The concept of utilizing bulky and highly polarizable groups in order to increase LD interactions has evoked the term "dispersion energy donor" (DED) for such groups, in analogy to electron-donor substituents.^[10] To quantify and qualify the effects of DED's on structure, molecular balances were designed. Accordingly, the equilibrium of 1,4- and 1,6-cyclooctatetraene (COT) is highly affected by the nature of the substituents attached.^[11] Since only the folded conformer benefits from attractive LD interactions, the equilibrium counterintuitively shifts towards more crowded and sterically more hindered 1,6-COT (Figure 1). This phenomenon can be observed throughout all organic solvents demonstrating the overwhelming importance of LD in molecular structure. In addition, modern computational methods, *e.g.* symmetry adapted perturbation theory^[12] (SAPT), can be utilized to predict DED strength. Accordingly, the rigid dimer scan of the isobutane (Figure 1) predicts the ideal ratio of LD and Pauli repulsion at a distance of around 2.5 Å.^[13]

In recent years the importance of LD interactions as a chemical design element has been assessed over a variety of research areas. Emphasis was placed on quantifying the interaction between various DED groups to utilize LD as a source of thermodynamic stability.

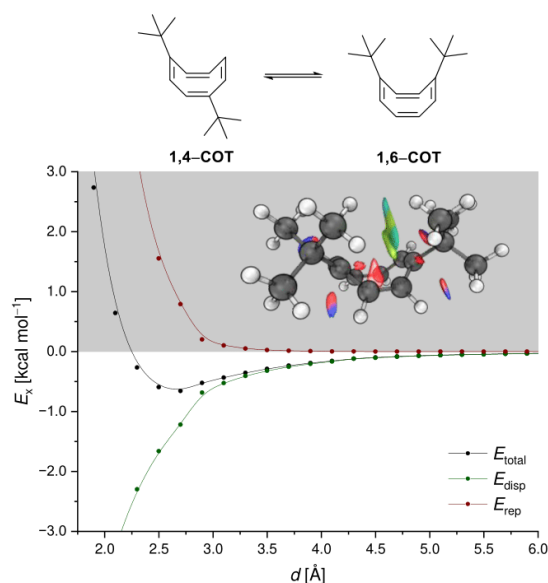


Figure 1. SAPT/6-311G(d,p) energy decomposition of a rigid dimer scan of isobutane dimer. The non-relaxed dimer scan is based on the geometries of the 1,6-COT. Every data point within the shaded area marks repulsive interactions.^[13]

REVIEW

As a consequence, new computational and experimental approaches had to be developed to measure and dissect LD from other noncovalent interactions. In this process many new structures were designed to determine the balance between attractive and repulsive interactions. Here, the focus was not only on the well-established π - π and σ - π interactions, but even more so on σ - σ attraction. To quantify such interactions many novel intra- and intermolecular dispersion-stabilized structures were prepared.

While the presence of LD interaction can be readily demonstrated both computationally and experimentally in the gas phase, the compensation of LD due to solvation was discussed extensively in recent years.^[13-14] Multiple systems were developed to investigate the interactions of bulky groups in various solvents or through direct comparison between gas phase and solvent measurements.

The most sizable effect of LD interactions is apparent through the control of reactivity due to incorporation of DEDs.^[7, 10] Especially in the area of catalysis, the role of LD interactions proved to be of key importance in molecular recognition, substrate activation, transition state lowering and as chemical driving force.

As a result, the use of LD interactions as a tool in synthesizing novel structures, increasing selectivities or facilitating alternative reaction pathways has gained greater significance. At the same time, LD interactions are introduced into educational chemistry to improve students' understanding of such structure-property relationships.^[15] This review intends to highlight the main advances in understanding, sizing, and controlling LD interactions. As the topic was reviewed here in 2015,^[7] we mostly focus on the developments of the last seven years. During this time a priority program on LD (SPP 1807) of the Deutsche Forschungsgemeinschaft (German Research Council) was formed to investigate the effects of LD on structure and reactivity.

1.1. Structure of the ReviewD

In order to fully outline the potential of LD interactions, various areas of research have to be examined and connected. In this review, we discuss these areas separately and then make the connections. For an introduction to LD interactions, we refer the reader to our review article of 2015.^[7]

A thorough examination of LD interactions can only be achieved through a tight interplay between theory, spectroscopy, and synthesis. Therefore, we begin with methods to elucidate LD and noncovalent interactions in general. Theoretical considerations and experimental approaches to quantify LD interactions have been extended and refined in recent years. In the first section, we provide an overview of newly developed approaches to single out LD interactions.

The second section focuses on implications of LD on molecular structures. By demonstrating exceptional structural motifs only accessible through LD, we shift our focus to the spectroscopic prospects and advancements made by studying small energy differences.

Finally, we consider reactivity and highlight its correlation with LD interactions. Here, we bring all topics discussed before in focus again by demonstrating the influence of LD on catalysis.

Lars Rummel studied chemistry and biology at the Justus Liebig University Giessen, Germany, to become a teacher. In parallel, he received his B.Sc. degree in chemistry in 2018. He joined the group of Peter R. Schreiner as research associate in 2019. Currently, he is carrying out his doctoral studies. His research focuses on the effects of London dispersion interactions on molecular structure and reactivity. In the years 2021 and 2022, he served as the scientific secretary of the priority program on dispersion (SPP 1807) of the Deutsche Forschungsgemeinschaft (German Research Council).



Peter R. Schreiner is professor of organic chemistry and Liebig-Chair at the Justus Liebig University Giessen, Germany. He studied chemistry in his native city at the University of Erlangen-Nürnberg, Germany, where he received his Dr. rer. nat. (1994) in Organic Chemistry. Simultaneously, he obtained a Ph.D. (1995) in Computational Chemistry from the University of Georgia, USA. He completed his habilitation at the University of Göttingen (1999), before becoming associate professor at the University of Georgia (Athens, USA), and head of the institute in Giessen in 2002. P. R. Schreiner is an elected member of the Leopoldina – German National Academy of Sciences, the North Rhine-Westphalian Academy of Sciences, Humanities, and the Arts, the Academy of Science and Literature (Mainz), and the Berlin-Brandenburg Academy of Sciences. He received the Dirac Medal (2003) and the Adolf-von-Baeyer Memorial Award of the German Chemical Society in 2017. He has been a visiting professor at the CNRS in Bordeaux, the Technion in Haifa, the Australian National University in Canberra, and the University of Florida in Gainesville. His research interests include organic reaction dynamics and reactive intermediates, quantum mechanical tunneling as well as London dispersion interactions as probed in the realm of nanodiamonds and organocatalysis.



2. Elucidation of London Dispersion Interactions

The knowledge of the attractive ability, which molecules ubiquitously have, has been around for over 150 years.^[1a, 6] Nevertheless, the methods to quantify LD interactions and distinguish between them and other effects have been developed only in recent years. In the first part of this section we discuss the current computational advances to analyze and describe LD interactions, while the second part concentrates on their experimental evidence. By highlighting the advantages and disadvantages of molecular balances, we outline ways to assess LD interactions in solution, thereby emphasizing the influence of solvents on LD interactions in solution.

2.1. Theory and Computations

In recent years, computational chemistry has made important progress in identifying and quantifying LD interactions. We consider advances made in density functional theory (DFT) and wave function theory (WFT). One of the most common and

REVIEW

popular approaches to account for LD interactions is to utilize an empirical dispersion correction (often denoted as DFT-D n , with $n = 1-4$).^[16] Grimme and coworkers have developed these approaches over the last decade. A force-field-type term is added *a posteriori* to a DFT energy.^[17] The amount of LD in a system can be estimated using simple isodesmic equations and by comparison of the energies computed with or without inclusion of a DFT-D n correction.^[18] This *ad hoc* correction is one of the most popular approaches of dealing with LD interactions since its computational cost is quite reasonable.^[17] Whereas other methods utilize the electron density to take local dispersion coefficients into account, Grimme's DFT-D n corrections only use the atomic positions to generate the dispersion coefficients with respect to the neighboring atoms from reference values.^[19] Additionally, damping functions are employed at close interatomic distances to deal with high variations of dispersion forces.^[20] The most recently published D4 correction is an improvement over the DFT-D3 correction, which did not handle charged systems properly.^[21] D4 is still solely based on geometries and atomic positions but includes a scaling of the dispersion coefficients based on atomic charges and electronegativity (Figure 2). Although D4 generally outperforms D3, the differences are most apparent for transition metal complexes.^[22]

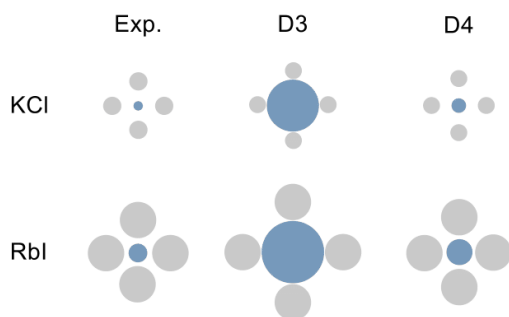


Figure 2. Schematic representation of anionic (grey) and cationic (blue) polarizability values of KCl (top) and RbI (bottom) in a comparison between experimental results (left), computed D3 (center) and D4 (right) atomic polarizabilities.^[22a]

The analysis and quantification of LD interactions is not only important for DFT computations but also in WFT. With this in mind, Neese *et al.*^[23] reported in 2016 a novel way to decompose interaction energies of the domain-based local pair natural orbital coupled-cluster (DLPNO-CCSD(T)) method into physically interpretable components. The method, called Local Energy Decomposition (LED), differentiates between electrostatic, electronic promotion, exchange, dynamic charge polarization, and LD interactions ranging from weakly to strongly bound dimers. It can be applied to an optional number of fragments giving accurate results at the coupled cluster level. Using the counterpoise correction of Boys and Bernardi,^[24] the method intrinsically accounts for the basis set superposition error. Within this supramolecular approach the bond dissociation energy (ΔE_{BDE}) is initially decomposed into an electronic interaction term (ΔE_{int}) and a geometric preparation energy ($\Delta E_{\text{geo-prep}}$), which accounts for the energy necessary to deform the monomers into the dimer structure (2).

$$\Delta E_{\text{BDE}} = \Delta E_{\text{int}} + \Delta E_{\text{geo-prep}} \quad (2)$$

The interaction energy is further split into a Hartree-Fock and a correlation contribution. By decomposing both Hartree-Fock and correlation energy, Neese *et al.* developed a nonperturbative approach to compute intermolecular interactions. The method allows dissecting a variety of noncovalent interactions ranging from dispersively bound dimers to ionic interactions into chemically useful energies. As shown below, the energy decomposition analysis (EDA) results in a detailed characterization of the dissociation energy whereas electronic preparation (intrafragment contribution $\Delta E_{\text{el-prep}}^{\text{HF}}$), electrostatic (E_{elst}), and exchange (E_{exch}) interactions result from decomposition of the HF term. The correlation energy can be separated into charge-transfer (E_{ct}), dispersion (E_{disp}), and electronic preparation ($\Delta E_{\text{el-prep}}^{\text{C}}$) contributions as well (3).^[23]

$$\begin{aligned} \Delta E_{\text{BDE}} = & \Delta E_{\text{el-prep}}^{\text{HF}} + E_{\text{elst}} + E_{\text{exch}} + \Delta E_{\text{el-prep}}^{\text{C}} \\ & + E_{\text{ct}} + E_{\text{disp}} + \Delta E_{\text{geo-prep}} \end{aligned} \quad (3)$$

The main advantage over symmetry adapted perturbation theory^[25] (SAPT) is that LED allows to dissect strong and weak interactions at the same level of theory whereas SAPT only examines weak interactions *via* its perturbative approach. Interestingly, the intermolecular exchange term differs from the exchange contribution in SAPT.^[23] Whereas the exchange term represents a repulsive interaction in SAPT, it is a stabilizing term within LED. Nevertheless, a comparison of SAPT and LED has shown that both energy decompositions to be in good agreement with the distance-dependence of noncovalent interactions. The LED method was utilized by Neese *et al.*^[26] for investigations of LD effects in frustrated Lewis pairs (FLPs). Accordingly, increasing DED size increases thermodynamic FLP stability. Additionally, Bistoni and coworkers showed that LD significantly contributes to the stability of metal complexes through coordination to C-H σ -bonds. They studied agostic complexes^[27] where around 50% of attraction is due to LD, and a variety of direct σ -complexes,^[28] in which dispersion energy amounts to at least 67% of the overall binding energy. Other noncovalent interactions, *e.g.*, H-bonding, can be studied with the LED method as well.^[23, 29] Furthermore, it can also be applied to open-shell systems by computing energies at the UHF-DLPNO-CCSD(T) level of theory.^[30]

A subsequent non-empirical method applicable to very large systems is the newly developed Hartree-Fock plus London dispersion (HFLD) scheme.^[31] In HFLD, the interaction energies are computed at the HF level of theory and corrected with a LD term computed at CCSD. Since all other intramolecular correlation energies compensate each other and can therefore be neglected, the method efficiently quantifies intermolecular interactions.

Since SAPT^[32] is still the most popular energy decomposition analysis to date, we will briefly present its main features. As mentioned before, SAPT allows computing the interaction energy of two molecular fragments using a perturbation of the Hamiltonian of both fragments.^[25] Thus, the energy is partitioned into electrostatics (E_{elst}), exchange (E_{exch}), induction (E_{in}), and dispersion (E_{disp}) according to the following equation (4):

$$\Delta E_{\text{int}} = E_{\text{elst}} + E_{\text{exch}} + E_{\text{in}} + E_{\text{disp}} \quad (4)$$

REVIEW

Here, the electrostatics describe the interaction of charge densities of multipoles and hence is attractive. Different from LED, the exchange term describes repulsive interactions caused by an overlap of wave functions (Pauli repulsion). Due to different definitions, this term cannot be compared to the LED exchange term. In a second-order expansion, SAPT generates energies for LD and induction, *i.e.*, the redistribution of an electric charge due to the electric field of the opposing monomer.^[25] Since SAPT and LED are based on different theories, only electrostatics and dispersion energies can be readily compared. Additionally, due to the perturbative approach only weak interactions can be described properly with SAPT.^[23] Improvements of the SAPT scheme focus on adjusting the second-order induction and dispersion energies. By employing the GW approximation and response functions from Bethe-Salpeter equation (BSE),^[33] Klopper and coworkers achieved more accurate results as compared to DFT-SAPT.^[34] In order to address the slow basis set convergence in conventional perturbational dispersion approaches, Patkowski *et al.*^[35] utilized a method from explicitly correlated (F12) electronic structure theory. The method was utilized to investigate complexes involving heavy elements such as gold, mercury and bismuth.^[36] Utilizing SAPT, Herbert *et al.*^[37] revisited the dimerization of benzene and larger polycyclic hydrocarbons. While benzene dimers are commonly described as a result of quadrupolar electrostatic interactions, the C₆H₆-C₆F₆ dimer already contradicts the model based on quadrupolar effects as it also favors the periplanar offset dimer. Alternatively, a competition between LD and Pauli repulsion dictates π - π interactions resulting in the offset stacked benzene dimer. In stark contrast to textbook knowledge, electrostatic interactions are not decisive for this geometric preference (Figure 3).^[38]

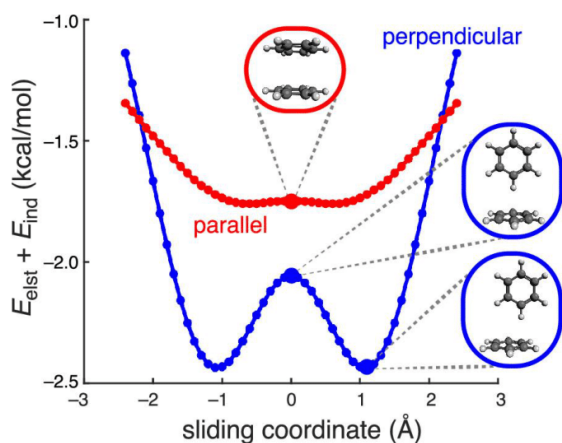


Figure 3. Polarized electrostatic and inductive interactions along a sliding coordinate with benzene either parallel (red) or perpendicular (blue) oriented. Note that $E_{\text{elst}} + E_{\text{ind}}$ fail to predict the geometric preference of a benzene dimer. Data was extracted from Herbert.^[38]

Visualizing LD greatly helps understand effect of DEDs between interacting molecules or moieties. Popular are noncovalent interaction (NCI),^[39] Dispersion Interaction Density (DID) plots,^[40] and London Dispersion Potential (LDP) maps.^[41] The NCI approach is based on a 2D plot of the reduced density gradient and the electron density. By depicting isosurfaces of the

reduced density gradient together with electron densities, the strength of noncovalent bonding can be represented. High densities represent strong interactions, whereas lower densities hint to weaker interactions. By accounting for the sign of the electron density values, attractive and repulsive interactions can be separated and visualized according to a color-code. Strongly repulsive interactions *via* Pauli repulsion are depicted in red, while strongly attractive forces are coded blue. Green isosurfaces represent weak interactions like dispersion or dipole interactions.^[39] In order to properly distinguish between the types of weak interaction, dispersion interaction density (DID)^[40] plots can be utilized, visualizing LD interactions to locate the origin of stabilization. These plots are usually depicted as a voxel or wireframe plot through coloring of the local intermolecular interaction density. Here, the color scheme ranges from red (strong LD interaction) over green to blue (no dispersion interaction). Additionally, Pollice and Chen introduced London dispersion potential (LDP) maps as quantitative LD descriptors.^[41] By using a parameter P based on homoatomic dispersion coefficients, the authors defined P_{int} , which not only accounts for the spatial polarization distribution but also for the ionization potentials in molecules with respect to their vdW surface.^[41-42] This parameter was then applied to the periodic table and DEDs to highlight the coherence of dispersion coefficients and atomic radii. By projecting the P values onto the electron density isosurface, a three-dimensional depiction quantifies and visualizes LD interactions within molecules. The color scheme was chosen to coincide with DID plots. In comparison to the other depictions, LDP portrays the dimer LD contact areas, while DID plots highlight the origin of these interactions. Figure 4 displays a comparison of all visualization tools according to Pollice and Chen.^[41]

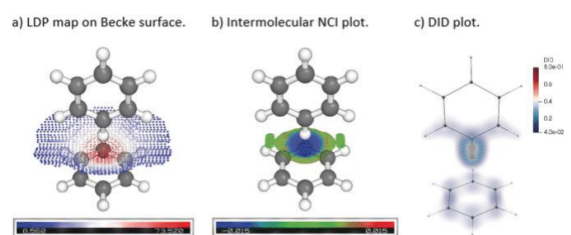


Figure 4. Visualization methods of NCIs in the T-shaped benzene dimer. a) LDP mapped onto the intermolecular Becke surface (values in kcal mol^{-0.5}). b) Intermolecular NCI plot (values in au). c) DID plot (values in kJ mol⁻¹ Bohr⁻³). Data was extracted from Pollice and Chen.^[41]

2.2. Experimental Manifestations of London Dispersion Interactions

Molecular balances have been the workhorse to analyze LD interactions experimentally.^[14a, 43] Hereby, interactions between various hydrocarbon groups are in focus, and the acquired knowledge can readily be transferred to every area in chemistry.

Molecular balances measure the thermodynamic energy differences of conformers of configurational isomers and the equilibrium constants are indicative of noncovalent interactions that affect the isomers to different degrees (Figure 5). An obvious criterion still worth mentioning is that the geometric change must be readily quantifiable by means of spectroscopic

REVIEW

techniques. Additionally, intramolecular interactions have to be definable and separable. Just as well, ionic interactions^[44] or hydrogen bonding^[45] which might exceed LD interactions in magnitude for intermolecular contacts must be considered. Thus, systems including heteroatoms have to be treated with caution. Solvent effects have to be taken into account as well.^[13, 46] Especially in solvents with high polarity, solvophobic effects were reported, which minimize balance-solvent interactions while maximizing stronger solvent-solvent interactions.^[47]

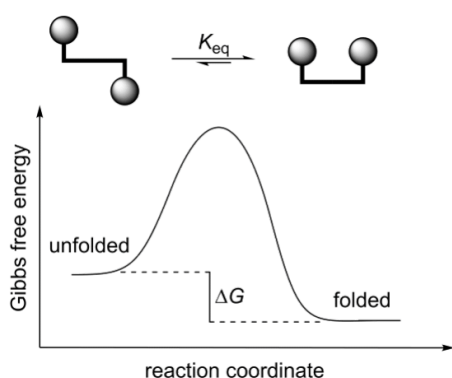


Figure 5. Schematic illustration of a molecular balance consisting of a folded and unfolded conformers.

The most well-known molecular balance was reported by Wilcox and coworkers in 1994.^[48] The rigid scaffold, based on Tröger's base, limits the number of thermodynamically accessible conformers to two torsional isomers that interconvert at room temperature. Based on NMR analysis, Wilcox and coworkers determined the ratio of folded to unfolded isomers, whereby noncovalent edge-to-face aromatic interactions in the folded conformer were assigned to having a stabilizing effect. On the other hand, entropy drives the equilibrium towards the unfolded isomer. The expected CH- π interactions between the aromatic groups could be observed by NMR and X-ray crystallography and stabilize the folded conformer by around $\Delta G_{\text{fold}} = -0.24 \text{ kcal mol}^{-1}$. Additional substitution in *para* position of the aromatic ester favors the T-shaped noncovalent contact even further. By substituting the aromatic ester with a cyclohexyl or *tert*-butyl ester, Wilcox and coworkers noticed that the resulting σ - π interactions were as dominant as the edge-to-face interactions. This suggests large LD interactions between aromatics and alkyl groups rather than electrostatic attraction.^[49] Additionally, Wilcox also noticed a slight variation in the hinge angle of the backbone of the torsion balance, thereby maximizing the attractive interactions.^[48]

By focusing on alkyl-alkyl interactions, Cockroft and coworkers substituted Wilcox' balance with long alkyl chains ($R = n$ -heptyl; $R' = n$ -hexyl) in the aromatic *para*-positions of the Wilcox balance (Figure 6).^[46] Measuring the equilibria in various polar, apolar, and fluoruous solvents, they came to the conclusion that solvophobic effects largely cancel LD interactions. This was demonstrated by dissecting the interaction energy of the alkyl substituents using a double mutant cycle. This, however, contradicts Wilcox original findings that no significant solvent effects can be observed.^[46, 48] Subsequent studies by the Cockroft group using perfluoroalkyl chains ($R = R' = \text{perfluoro-}n$ -

hexyl) as substituents demonstrated the competition of intramolecular and intermolecular LD, respectively.^[50] By correlating Gibbs free energies of alkyl or perfluoroalkyl substituents with the cohesive energy densities of the solvents, a linear regression analysis demonstrated that LD interactions as well as solvophobic effects are responsible for the folding of the Wilcox balance. While the former is dominant in apolar organic and fluoruous solvents, the latter is most important in aqueous and highly polar solvents.^[50a, 51]

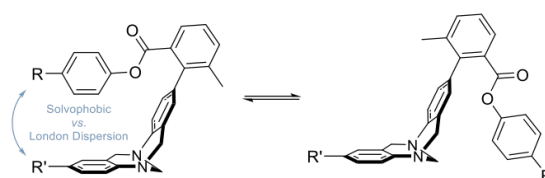


Figure 6. Molecular balance utilized by Cockroft and coworkers to partition solvophobic and LD interactions in various solvents.^[50a]

In order to study aromatic stacking interactions, Shimizu and coworkers designed a molecular balance based on a bicyclic *N*-arylimide scaffold. In comparison to Wilcox' balance, which was used to quantify edge-to-face aromatic interactions, Shimizu and coworkers set up a framework with a distance of 3.75 Å between arene groups to measure face-to-face interactions.^[52] After studying substituent effects^[53], Shimizu focused on quantifying LD interactions influencing the stacking behavior of arene groups.^[14c] By accounting for conflicting effects (*e.g.*, solvophobic or linker effects) using the corresponding control balances and double mutant cycles, Shimizu and coworkers quantified the LD interactions required for molecular folding. Conflicting with computational studies,^[54] they came to the result that LD interactions only play a minor role in the stacking behavior of aromatics. Furthermore, they suggested LD compensation due to solvent effects.

Later, Shimizu *et al.* demonstrated the importance of LD while studying σ - π interactions (Figure 7).^[55] Depending on the attached group and the substitution pattern, either attractive or repulsive interactions dominate. By exchanging one side of their balance with *meta* or *para* substituted benzenes, the distance dependence of LD and Pauli repulsion was deduced. As a result, they concluded an optimal distance for σ - π interactions of 2.5 to 3.0 Å.

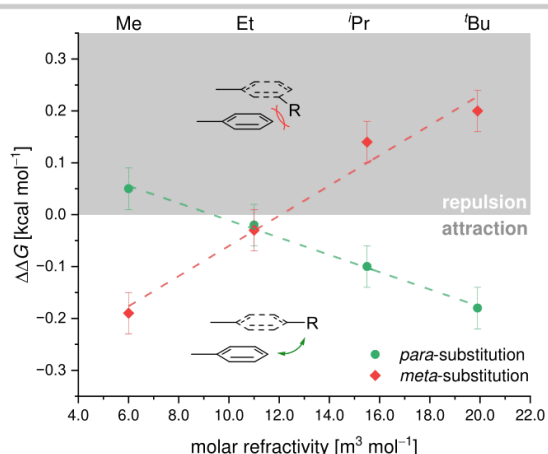


Figure 7. Differential interaction free energies $\Delta\Delta G$ derived from a double-mutant cycle for alkyl- π interactions. While *meta* substitution (red markings) shows repulsive interactions, the *para* substitution pattern (green markings) highlights attractive LD.^[55]

Other than conformational balances based on slow rotation around single bonds, Chen *et al.* developed a method to quantify LD interactions using dissociation energies of weakly bound dimers.^[14d] They used protonated *N*-heterocyclic compounds that can dimerize *via* hydrogen bonding (Figure 8). In addition to this central connection, every monomer possesses remote substituents interacting intermolecularly *via* LD. As a result, LD interactions can only be at work in the proton-bound dimer. The dissociation energies were thoroughly studied using a large set of different protonated *N*-heterocyclic compounds ranging from amines to pyridines and quinolones. The dimerization process was investigated computationally and experimentally, both in the gas phase and in solution. As a result, Chen *et al.*^[14d, 56] found considerable influence of LD interactions in the gas phase. By performing threshold collision-induced-dissociation measurements (T-CID), they could directly compare computational and experimental data. In order to account for solvent effects, free bond dissociation energies were measured in dichloromethane *via* variable temperature NMR experiments. As a result, a compensation of around 70% of intermolecular LD was reported due to additional solvent-solute interactions. Interestingly, these effects could not be reproduced exactly by computational means using state-of-the-art solvent models. Implicit solvent models, *e.g.*, SMD^[57] and COSMO-RS,^[58] should therefore be treated with caution when accounting for LD interactions.

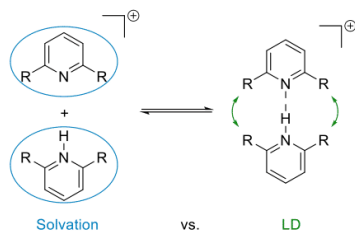


Figure 8. LD supported formation of proton-bound dimers and compensating solvation effects.^[14d]

In 2017, Albrecht and coworkers investigated the effect of LD on the dimerization processes of metal complexes (Figure 9).^[47] Using helicate-type titanium(IV) triscatecholates complexes, they measured the equilibrium constant of the dimerization in the presence of lithium ions. The catechols were systematically substituted by altering the ester moiety. The effect of linear, branched, *n*-fluorinated, and cyclic substituents were taken into account. *Via* a van't Hoff analysis enthalpy and entropy values were determined in addition to the equilibrium constants. By elongating the alkyl chains, the dimerization process becomes enthalpically more favorable. On the other hand, entropy disfavors the dimeric structure due to restrictions of torsional motions. The equilibrium was shifted to monomeric titanium complexes with branched alkyl attachments. This suggests an increase in repulsion in the dimer. The entropic penalty of close alkyl-alkyl contacts was slightly decreased in cyclic compounds, making the dimer the energetically preferred structure. The trend of fluorinated *n*-alkyl chains was comparable to hydrogenated chains but significantly smaller. By comparing the equilibrium constants of the *iso*-propyl and cyclobutyl system, Albrecht *et al.*^[47] noticed a substantial difference although both groups are comparable in size. Since this difference is caused by larger enthalpic stabilities due to attractive LD rather than the bulkiness of the molecules under consideration, they deduced that solvophobicity of the alkyl groups plays a minor role in their system. In a second study, the cyclohexyl substituted system was investigated with respect to the conformational axial/equatorial preference in the dimeric structure.^[59] Counterintuitively, the axial orientation is favored due to a combination of LD and solvophobic effects, while the equatorial position does not offer stabilizing noncovalent interactions between neighboring groups.

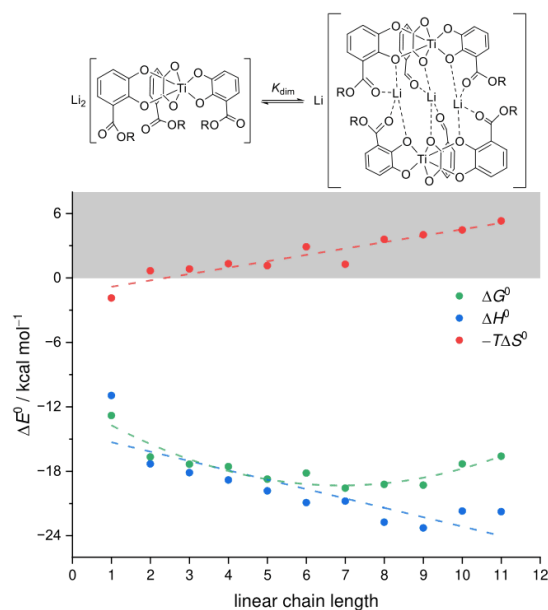


Figure 9. Energy contributions of titanium complexes with increasingly long linear alkyl substituents. Enthalpy (blue markings) and entropy (red markings) are experimentally determined *via* van't Hoff analysis. Gibbs free energies (green markings) indicate stabilizing effects with increasing chain length.^[47]

REVIEW

A purely hydrocarbon based molecular balance can be designed using cyclooctatetraene (COT), initially presented by Streitwieser *et al.*^[11b] in 1981. Since it avoids heteroatoms, it minimizes alternative noncovalent binding interactions, *e.g.*, hydrogen bonding or electrostatic interactions. Streitwieser *et al.*^[11b] noticed an unusual behavior of the 1,4-di-*tert*-butyl-COT, which was later experimentally confirmed by Hanzawa *et al.*,^[60] this molecular balance was also computationally investigated.^[61] Even though COT is non-planar, it undergoes a valence-bond isomerization that exchanges the 1,4- with the 1,6-substituent positions. While the 1,4-isomer places the *tert*-butyl groups far away from each other, the 1,6-isomer brings them in close proximity. As recognized already by Streitwieser *et al.*^[11] this close contact is stabilizing, even in solution as evident from the determination of the equilibrium constant *via* NMR in CDCl₃. In 1992, Anderson and Kirsch reported on additional substitution patterns, demonstrating the LD distance-dependence.^[62] By varying the sizes of the attached groups and investigating the equilibrium *via* NMR analysis, they observed a preference for the 1,6 isomer. With increasing DED size from methyl to *tert*-butyl, the ensuing enthalpic stabilization increasingly favors one valence bond isomer. In 2021, Schreiner *et al.*^[13] reinvestigated the 1,4-/1,6-COT balance to determine the solvent effects on the equilibrium. By measuring equilibrium constants in 16 different organic solvents *via* variable-temperature NMR experiments, LD could be correlated with solvent polarizability. Interestingly, in each case the more crowded 1,6-isomer dominates at r.t., whereas only at high temperatures the equilibrium slightly favors the entropically favored 1,4-isomer. There is clear-cut correlation of polarity or polarizability with the ability to compensate LD in solvents was not observed. Accordingly, a more complex interplay of solvent parameters has to be taken into account.

The COT backbone was further exploited to study the effects of silyl groups with respect to their steric size^[63] and role to act as DEDs (Figure 10).^[10] By directly attaching silyl groups at the COT molecular backbone, the relative bulkiness of such groups was investigated and successfully correlated to literature known steric parameters, such as A-values,^[64] solvolysis rates,^[65] and Tolman's steric parameter θ .^[66] The main driving force favoring the unfolded isomer was found to be an internal strain within the COT backbone. On the other hand, by including a -CH₂O- spacer group between COT and silyl groups, LD interactions were identified to alter the equilibrium due to σ - σ or CH- π contacts. Counterintuitively, NMR measurements revealed that the bulky TIPS group shifts the equilibrium between 1,4- and 1,6-disubstituted COT furthest towards the folded and more crowded valence isomer. With a computationally derived internal strain for TIPS-COT of 1.2 kcal mol⁻¹, attractive LD is responsible for the remaining 0.7 kcal mol⁻¹. However, flexibility due to the -CH₂O- spacer comes at the cost of unfavorable folding entropy.

Finally, the COT molecular backbone was further exploited to experimentally study hydrogen bonding *via* a model system resembling a cyclic water dimer.^[67] Interestingly, an energy decomposition analysis demonstrated that hydrogen bonding is largely dominated by electrostatic and LD interactions. While the first constitutes around 65% of the total hydrogen bonding interaction energy, the latter is responsible for around 25% stabilization.

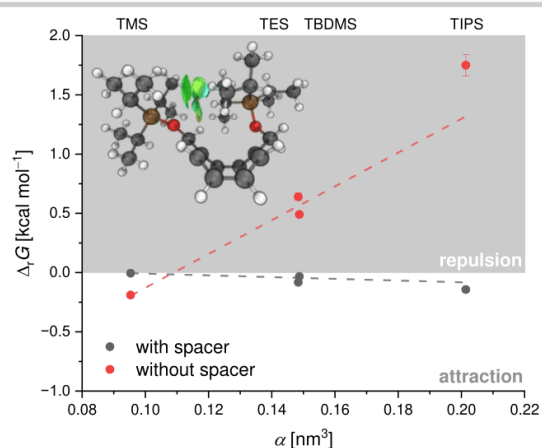


Figure 10. Gibbs free energies for the equilibrium of silyl substituted COT without (red markings) and with (grey markings) spacer group.^[63, 68]

Another purely hydrocarbon-based molecular balance was described by Schreiner *et al.*^[69] in 2022. By substituting a 9,9'-bifluorenylidene backbone in 2,2'-position with various alkyl groups, the system can be equilibrated thermally or photochemically between *Z*- and *E*-configurations. Originally, Minabe *et al.*^[70] synthesized 2,2'-diacyl balances as fullerene precursors and noticed an unexpected *Z/E* ratio after connecting two fluorene moieties in 9,9'-position. While the 2,2'-diacetyl derivative gave a *Z/E* ratio of 30/70, the 2,2'-distearoyl balance afforded a 90/10 ratio in favor of the sterically more demanding *Z* conformer; this demonstrated the "sticky" properties of fatty acids. Minabe and coworkers already suggested LD as the key factor for selectivity.^[70] In 2022, Schreiner *et al.*^[69] reinvestigated the system removing the acyl functional groups to isolate and quantify the LD interactions. By systematically exchanging alkyl groups in 2,2'-position with increasing polarizability the interplay of repulsive and attractive interactions as well as solvent effects were studied *via* NMR spectroscopy. While linear alkyl chains favor the folded *Z*-isomer despite an entropic penalty, the experimental ratios of bulky substituents, *e.g.* *tert*-butyl and cyclohexyl substituents, do not systematically increase with substituent size (Figure 11). A computational analysis revealed a more complex interplay of LD, steric hindrance, and solvent accessibility, and ultimately resulted in identifying cyclohexyl ($\Delta G = -0.60$ kcal mol⁻¹ in cyclohexane) as the strongest DED. Whereas methyl substitution results in a 1:1 mixture of *Z*- and *E*-isomers, ethyl as well as *iso*-propyl groups shift the equilibrium towards the more crowded *Z*-isomer (Figure 11). The fine line between attraction and repulsion is best observed by comparing cyclohexyl to *tert*-butyl substitution. While cyclohexyl favors the *Z*-form by maximizing LD due to perfect alignment of both cyclohexyl substituents, the more rigid *tert*-butyl substituent on the other hand reverses the effect due to increasing repulsive interactions. Additionally, Schreiner *et al.*^[69] focused on the role of intermolecular solute-solvent interactions. Whereas many studies^[14d, 46] suggest a decrease of LD in solution, the 9,9'-bifluorenylidene molecular balance gave similar experimental results for all solvents employed (cyclohexane, toluene, benzene, bromobenzene, pyridine, nitrobenzene, and acetic acid).

REVIEW

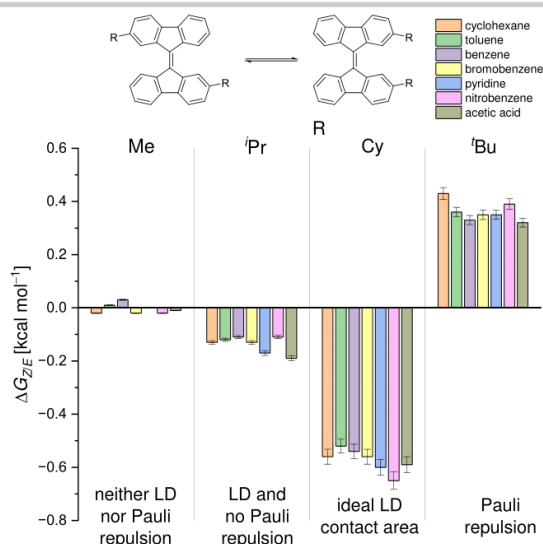


Figure 11. Gibbs free energies for the equilibrium between *Z*- and *E*-isomers of the 9,9'-bifluorenylidene molecular balance at 333 K in various solvents.^[69]

2.3. London Dispersion in Solution

As already addressed before, in all balances a compensation of LD can be observed when comparing computations or gas phase interaction energies with those in solution. While the importance of solvation is undisputable, the effects of LD in solution are still being elaborated. Numerous examples can be found in which a change of solvent has a tremendous impact on the structure or reactivity of the solute. Therefore, it is not surprising that molecular balances are also influenced in solution.

In general, two reasons can be identified as counteracting forces opposing the dimerization process. The first factor compensating attractive interactions is entropy, which is usually negative for a dimerization.^[47, 71] Additionally, by increasing the size of monomers the enthalpic gain due to LD is always compensated by an increasing entropic penalty due to restrictions in rotational and vibrational freedom. The number of atoms present in a dimerization process does not only rapidly increase the number of pairwise interactions but also the degrees of freedom in the monomers. For flexible molecules the tight interplay of solvation and entropy must be taken into account when evaluating Gibbs free energies.^[68, 72] In every balance discussed above this entropic penalty counteracts LD.^[47, 71] By weighing LD against cation- π interactions utilizing large flexible pyridinium cations Chen and coworkers highlighted the challenges to *in silico* predict the complex interplay of LD and entropic compensation. While computations predicted LD to be dominant, gas-phase cryogenic ion vibrational predissociation (CIVP) spectroscopy found the effects of *tert*-butyl groups to be modest at best.^[73]

While computational investigations suggest LD to play a dominant role for molecular aggregation in the gas phase, its effects in solution are still discussed extensively.^[13-14, 74] Although stabilizing LD effects were demonstrated with various molecular balances and even catalytic processes, studies suggest a partial compensation of LD by solute-solvent

interactions (Figure 12). Interestingly, both phenomena (solute-solute as well as solute-solvent interactions) can be evoked by LD interactions.^[14c, 71] Instead of intramolecular stabilization, the energy gain *via* intermolecular solute-solvent contacts hamper molecular dimerization.

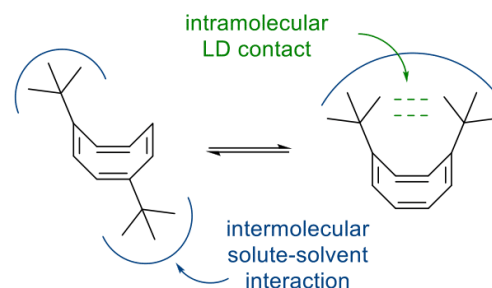


Figure 12. Schematic illustration of intra- and intermolecular interactions of the cyclooctatetraene molecular balance.

Initially, Houk described an equilibrium between intramolecular van der Waals contacts and intermolecular solute-solvent interactions by computationally studying Wilcox' torsional balance.^[75] An overestimation of 1-3 kcal mol⁻¹ of the preferred folded conformer in the gas phase could only be explained by taking solvation effects into account. Thereby, a compensation of the relative instability of the unfolded balance was achieved by including interactions between solvent molecules and the molecular balance itself. The same balance was subject to experimental approaches to dissect the role LD plays in solution.^[46] By utilizing a double-mutant cycle, Cockroft *et al.*^[46] extracted the interaction energy of alkyl chains (heptyl-hexyl) in multiple solvents. The study suggests a large compensation of LD in solution for linear alkyl chains and, instead, claims cohesive solvent interactions, *i.e.*, solvophobic effects^[76] as the main driving force for aggregation. In a second study, Cockroft and coworkers focused on separating LD interactions from solvophobic effects using a perfluoroalkyl substituted balance.^[50a] While a correlation with the cohesive energy density (ced) gave rise to the solvophobic effect, LD interactions were dissected using the bulk solvent polarizability. As a result, both effects were found to contribute to the dimerization of apolar alkyl groups with LD being more prominently in apolar organic and fluoruous solvents. Pollice and Chen^[42] investigated the intermolecular interactions of alkanes and perfluoroalkanes computationally (Figure 13). Whereas fluorinated substituents or molecules are generally argued to interact only weakly *via* LD interactions, the study elucidated the opposite. The computations showed that perfluorinated molecules such as tetrafluoromethane provide higher LD energy due to fluorine-fluorine contacts. On the other hand, their conformational rigidity does not allow an ideal alignment thereby reducing the interaction energies.

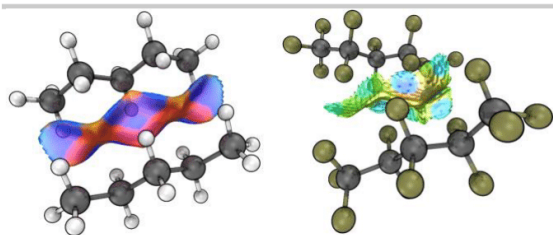


Figure 13. Strong LD and repulsive interactions between an *n*-pentane dimer (left) and the corresponding perfluorinated dimer (right). Due to a lack of flexibility, the perfluorinated dimer cannot exploit the full LD strength.^[42]

In an experimental and computational study on the bond dissociation reactions of proton-bound dimers, Chen *et al.*^[14d] noticed a large compensation of inter- and intramolecular interactions in dichloromethane (about 70%). Nevertheless, the effects of LD on the dissociation energies were not completely overridden by solute-solvent interactions. Further studies^[56] of the same group focused on polar and nonpolar aprotic solvents. A comparison between experimental and computational data showed that implicit solvent models utilized to verify the observed trends underestimate solvent effects significantly. Apart from thermodynamic compensation, kinetic investigations on the unfolding process of azobenzenes substituted with increasingly longer alkyl chains contradict the sentiment that LD does not play a major role in solution. Wegner *et al.*^[71, 77] identified alkyl-alkyl contacts in transition structures to be the dominant source of stabilization in the thermal equilibration of azobenzene switches (molecular balances). By utilizing an unsymmetrically substituted azobenzene derivative, Wegner *et al.*^[78] demonstrated the decisive role of LD in stabilizing the (*Z*)-isomer *via* aryl-alkyl interactions. In contrast, the electronic structure of the aryl moieties was found to be negligible for isomerization. Additionally, the Wegner group introduced surface tension as a parameter that influences *Z*- to *E*-isomerizations.^[77]

In 2021, Schreiner and coworkers^[13] revisited the cyclooctatetraene molecular balance to investigate solvation effects on the equilibrium of the folded and unfolded diastereomer by performing van't Hoff analyses on di-*tert*-butyl substituted cyclooctatetraene in various different solvents (Figure 14). Even though LD is partially compensated by solvation and entropy, the sterically more demanding folded diastereomer was preferred independent of the solvent. Whereas the interaction energy between both *tert*-butyl groups is diminished in hexane and cyclohexane, DMSO and DMF shift the equilibrium towards the folded conformer *via* a combination of LD and solvophobic effects. Although a compensation can be significant in comparison to computational data, finely balanced systems can benefit significantly from the attractive potential of LD.

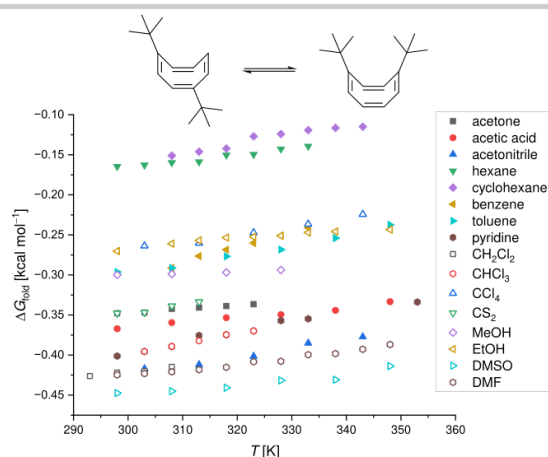


Figure 14. Temperature-dependent Gibbs free energies for the equilibrium of 1,4- and 1,6-cyclooctatetraene in different solvents. While the absolute energy values vary, LD never vanishes completely. Consequently, 1,6-cyclooctatetraene is always preferred in solution.^[13]

3. London Dispersion as a Design Element for Molecular Structures

One of the most prominent examples demonstrating the role LD plays in stabilizing structures is the counterintuitive case of hexaphenylethane (HPE).^[79] The unsubstituted HPE initially suggested by Gomberg^[80] dissociates into monomeric triphenyl methyl radicals and recombines to the well-known quinoid structure.^[81] Understandably, steric hindrance between the phenyl moieties were taken as the origin for the very facile dissociation of HPE, which was considered unattainable.^[82] Counterintuitively, sterically much more crowded all-*meta tert*-butyl HPE can be isolated (Figure 15).^[83] LD was found to be the origin of stability outweighing Pauli exchange repulsion by forming an LD stabilized "corset" of *tert*-butyl groups surrounding the fragile central C-C bond (Figure 16).^[84] Accordingly, alkyl substitution was utilized to study the balance between attraction and repulsion not only in HPE but also in the head-to-head dimer of the triphenylmethyl radical.^[85] Alternatively, an extension of the central bond by including higher tetrel derivatives also results in stable HPE-like compounds.^[86] While the central C-C bond (~1.70 Å) of unsubstituted HPE is too short and Pauli exchange repulsion dominates, a more favorable ratio of repulsion and LD was found in higher tetrel congeners, where even unsubstituted phenyl moieties act as DEDs. This also contradicts the (physically unfounded) concept that longer bonds are weaker and dissociate more readily, because higher tetrel HPE derivatives form remarkably stable compounds due to strong LD interactions.^[86]

REVIEW

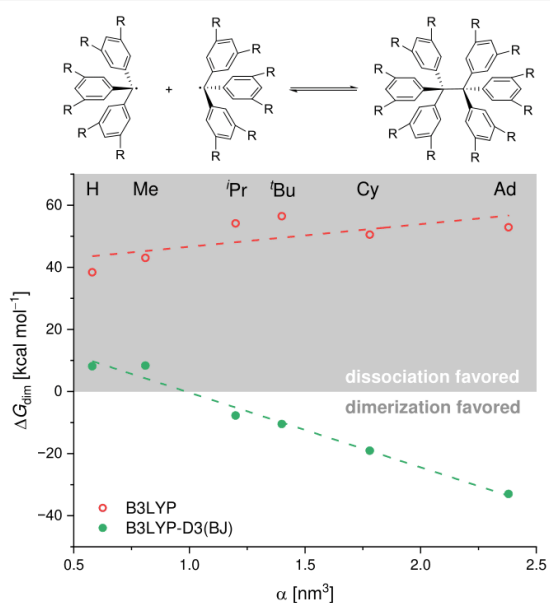


Figure 15. Dimerization energies ΔG_{dim} of all-*meta* substituted triphenyl methyl radicals including (green markings) and excluding (red markings) LD interactions. Note that only by including LD the HPE-like radical dimerization can be rationalized.^[83d]

A similar bond stabilization can be utilized to connect bulky adamantyl moieties and circumvent dissociation *via* numerous attractive LD contacts. For instance, the resulting alkyl-alkyl contacts between diamondoids are sufficiently strong to yield exceptionally long central C-C bonds (~1.71 Å) in directly connected diamondoid dimers.^[18, 87] A combination of single-crystal X-ray diffraction, gas-phase electron diffraction, combined GED/microwave (MW) spectroscopy, as well as quantum chemical computations confirmed the remarkable C-C bond length in the covalently bound diamantyl and oxadiamantyl dimers in the solid and gas phase.^[88] Recently, Suzuki *et al.*^[89] synthesized a pure hydrocarbon consisting of a central intramolecular C-C bond distance of 1.77 Å. By utilizing bulk *tert*-butyl groups they observed a bond contraction due to close LD contacts. In marked contrast to the expected structural consequences of steric repulsion, the bulky substituents pull both molecular fragments together and prohibit bond dissociation. As for intramolecular stabilization, intermolecular dimerization of triphenylmethane derivatives benefits from the same interactions. While the unsubstituted triphenylmethane dimerizes in a head-to-tail fashion, the all-*meta tert*-butyl derivative enforces a head-to-head structure yielding an incredibly short H-H contact (~1.57 Å). Although such a short intermolecular contact (still the shortest on record to date in the Cambridge Crystallographic Data Centre) entails significant Pauli repulsion, an energy decomposition analysis reveals a total interaction energy of $E_{\text{tot}} = -37$ kcal mol⁻¹ between both monomers with LD as the main origin of stabilization (up to $E_{\text{disp}} = -52$ kcal mol⁻¹).^[90]

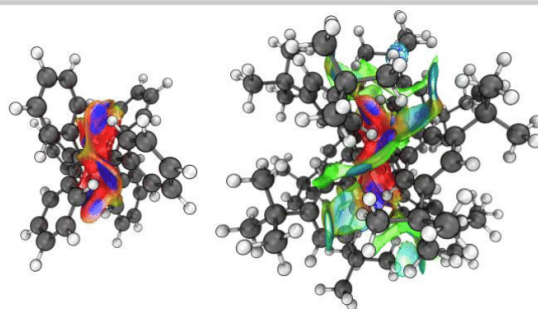


Figure 16. NCI plots of the unsubstituted hexaphenylethane (left) and *tert*-butyl substituted derivative (right). While the unsubstituted system is strongly affected by repulsion (red isosurfaces), the substituted molecule benefits from stabilizing LD contacts (green isosurfaces).^[83d]

Even though LD is the dominant stabilizing factor in molecular (hydrocarbon) crystals, the observed triphenylmethane derivative dimer structures prevail in the gas phase as shown by ionization loss stimulated Raman spectroscopy in molecular beam experiments.^[91] Recently, the knowledge gained from head-to-head dimerization was utilized to enhance the interaction energy between amine-borane frustrated Lewis pairs (FLPs) to generate a crystalline Lewis complex. Accordingly, N(3,5-^tBu₂C₆H₃)₃ and B(3,5-^tBu₂C₆H₃)₃ were mixed and crystallized with the aim to stabilize the heterodimer of fleeting encounter complex. While LD supports dimerization not only for heterodimer (N(3,5-^tBu₂C₆H₃)₃/B(3,5-^tBu₂C₆H₃)₃) formation but also for the homodimer (N(3,5-^tBu₂C₆H₃)₃/N(3,5-^tBu₂C₆H₃)₃) as well as B(3,5-^tBu₂C₆H₃)₃/B(3,5-^tBu₂C₆H₃)₃, no distinct characterization of an encounter complex has been reported.^[92] Apart from very bulky substituents the LD fingerprint can already be detected by studying the aggregation of small molecules. In a multi-pronged spectroscopic approach, Gerhards *et al.* investigated the structural preferences of diphenyl ether-alcohol aggregates to bind *via* OH-O or OH- π interactions (Figure 17).^[93] In a series of publications, a counterintuitive trend that larger alcohols favor OH-O arrangement was rationalized by accounting for LD and a deformation of the ether upon aggregation. Interestingly, by altering the flexibility of the ether by utilizing dibenzofuran as a rigid docking site, the trends reverse and OH- π interactions are favored for bulkier alcohols.^[94]

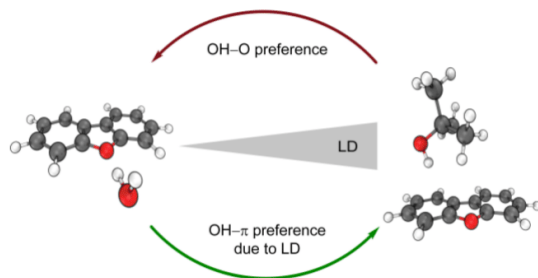


Figure 17. Preferred binding motif from oxygen-bound to π -bound structures with increasing solvent size.^[94]

REVIEW

Utilizing rotational spectroscopy Schnell *et al.*^[95] investigated the dimerization of dibenzofuran, diphenylether and fluorene. With 60-70% of the total interaction energy, LD was identified as the main driving force for molecular aggregation of all dimers. The aggregation of alcohols of increasing size with diadamantyl ether showed a competition of electrostatically and LD driven dimerization. Whereas water prefers hydrogen bonding resulting in close OH-O bond distances governed by electrostatic interactions, bulkier alcohols such as *tert*-butanol sacrifice electrostatic stabilization by maximizing LD contacts.^[96] As a result, the OH-O hydrogen bond distance increases with the number of close *tert*-butyl-adamantyl contacts.^[97] The same method was applied to study the impact of fluorination in aromatic-diadamantyl ether aggregates *via* rotational spectroscopy.^[98] In the same way, fluorinated benzene is expected to significantly alter its binding mechanism towards diadamantyl ether. As a matter of fact, the exchange of one hydrogen with fluorine is sufficient to change the preferred docking site of the benzene derivative to diadamantyl ether. SAPT investigations demonstrate that in contrast to the common notion that fluorine is a poor DED, LD is always the main driving force for aggregation (around 70% of the total interaction energy).

In a series of publications, Suhm and coworkers^[99] utilized a variety of spectroscopic tools to investigate the role of LD in dimerization and aggregation processes. In general, LD was found to be essential to determine the correct dimer geometries of molecules such as cyclohexanediol,^[100] benzyl alcohols,^[101] and *trans*-N-methylacetamide.^[102] In addition, the docking preferences of alcohols and ketones were studied in supersonic jet expansion experiments and by measuring their spectroscopic signatures.^[103]

In line with the HPE case, LD has been more appreciated as an additional source of stabilization for labile complexes and otherwise unstable molecules.^[5, 18] Initially, the “corset effect” was introduced to account for stabilizing interactions between steric bulk based on a “protective shell” around a reactive center. In this way, the synthesis of tetra-*tert*-butyltetrahedane was accomplished.^[84a] Bulky *tert*-butyl groups successfully stabilized the fleeting tetrahedrane molecule as well as silyl groups due to a “protective LD shell”.^[104] Recently, Cummins *et al.*^[105] attributed the remarkable stability of the bulky phosphatetrahedranes (tBuC_3P) to a network of close H \cdots H contacts.^[106] The computational study revealed a total of nine H \cdots H contacts with a stabilizing effect of $-0.7 \text{ kcal mol}^{-1}$ per contact due to LD.^[105]

While such H \cdots H contacts counteract the ring strain of tetrahedrane, *tert*-butyl substituents are usually utilized to introduce steric hindrance. In an attempt to quantify steric effects experimental parameters such as the Winstein-Holness A-value^[107] were constructed to define steric hindrance. Based on the ratio of axial vs. equatorial monosubstituted cyclohexane, the A-value is sensitive to destabilizing contacts in the axial position. Recently, the experimental data were revisited computationally with the goal to conceptualize a DED scale.^[64c] Whereas steric bulk is the factor defining the thermodynamic stability of monosubstituted cyclohexane, LD was found to play a non-negligible part to rationalize the experimental data (Figure 18). This is particularly apparent for the counterintuitive A-values of pinacol boronic acid (Bpin) and glycol boronic acid (Bgly).^[108] While Bpin (A-value of $0.42 \text{ kcal mol}^{-1}$) is clearly the smaller substituent in comparison to Bgly (A-value of $0.73 \text{ kcal mol}^{-1}$), it does not favor the axial position as much as

Bgly. In contrast to Bgly, Bpin benefits from addition H-H contacts stabilizing the axial conformer due to LD. Apart from alkyl contacts, halogen-alkyl and halogen-halogen interactions were identified to be valuable DEDs influencing the landscape of the potential energy surface significantly.^[109]

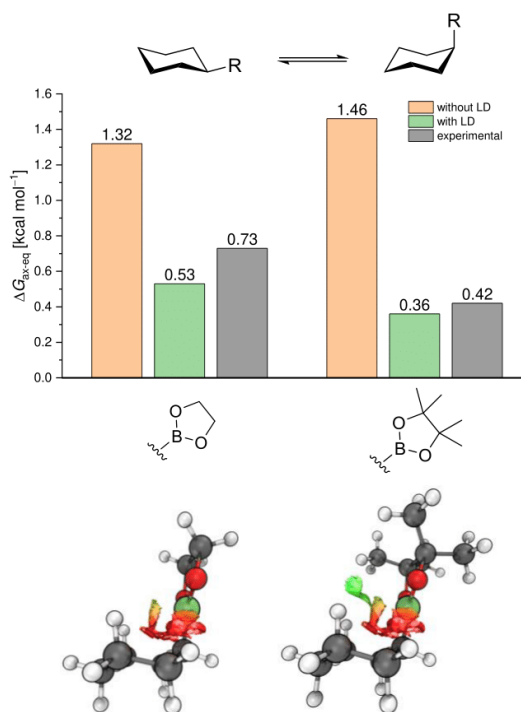


Figure 18. Computed and experimental $\Delta G_{\text{ax-eq}}$ (A-values) for pinacol boronic acid (right) and glycol boronic acid (left) substituted cyclohexane (top). The corresponding NCI plots (bottom) visualize noncovalent interactions. Note that the experimental data can only be reproduced computationally by including LD.^[64c]

4. London Dispersion as a Driving Force for Reactivity and Catalysis

Since LD interactions significantly influence the conformational landscape of molecules and can be used as the thermodynamic driving force for chemical reactions, it becomes apparent that these manifestations can be transferred to catalytic processes as well. In the field of catalysis the rather incomplete concept of steric hindrance (aka Pauli exchange repulsion) is commonly utilized.^[110] The hard-sphere classical mechanics model is the basis for this misconception. While this might be true for some cases, most early studies on catalytic processes lacked a detailed analysis of the role of noncovalent interactions. Although observations that steric crowding enhances reaction rates and increases selectivities are often attributed to repulsive interactions, LD interactions must be investigated to account for the physical reality. Since Pauli repulsion is always destabilizing in its nature, it cannot be the origin of higher reaction rates. Therefore, a balance between attractive and repulsive interactions must be found to design

REVIEW

new and highly selective catalysts. Stabilizing LD interactions on energy minima on the hypersurface can be directly transferred to loosely bound transition structures as well.^[7, 111]

Since LD interactions are ubiquitous and omnidirectional, not only productive reaction steps are promoted. This becomes apparent when catalytically inactive conformers of a catalyst are favored due to LD, thereby inhibiting catalysis. For instance, thiourea catalysis is based on substrate activation due to double hydrogen bonding of the unfolded (*anti-anti*) conformer of diphenylthiourea derivatives.^[112] While this has been confirmed experimentally and computationally for *N,N'*-bis[3,5-bis(trifluoromethyl)phenyl]thiourea, the implementation of bulky substituents in all-*meta* position inhibits catalysis.^[112d] In a recent study, LD interactions were identified to shift the conformational preference of diphenylthiourea derivatives towards the sterically more crowded *syn-syn* conformer (Figure 19).^[113] Systematic low-temperature NMR studies helped quantify the effects of LD on the equilibrium of *syn-syn* and *syn-anti* diphenylthiourea derivatives. Accordingly, the incorporation of bulky all-*meta-tert*-butyl substituents shifts the equilibrium towards the *syn-syn* conformer by around 1.7 kcal mol⁻¹. A double-mutant-cycle dissected the interaction energy between DEDs into stabilizing alkyl-alkyl contacts (around 30% of the total interaction energy) and σ - π interactions between DED and the opposing phenyl moiety (70%). The preference for the *syn-anti* and *syn-syn* conformers restricts effective catalytic processes.^[113]

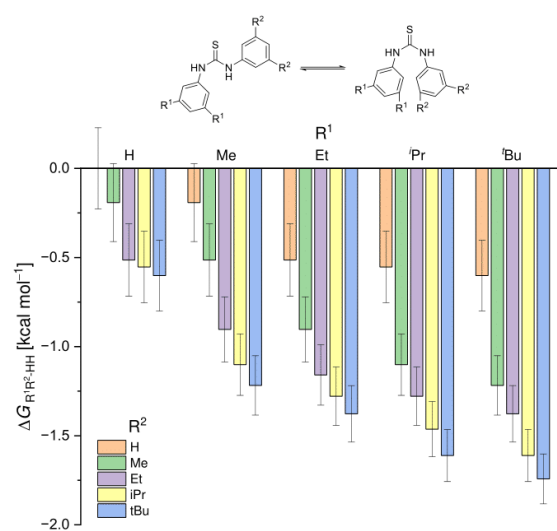


Figure 19. Gibbs free energy values for the equilibrium of *syn-syn* and *syn-anti* diphenylthiourea at 193 K substituted with DEDs in all-*meta* position. $\Delta G < 0$ corresponds to a shift towards the *syn-syn* conformer.^[113]

Whereas LD can reduce the catalytic activity of thiourea derivatives, the opposite effect is observed for a chiral bismuth-rhodium paddlewheel catalyst (Figure 20). By utilizing LD, Fürstner *et al.*^[114] locked the chiral calyx of a bismuth-rhodium catalyst in place. A combination of TIPS and *tert*-butyl substituents stabilize the active catalyst conformer.^[115] Computations reveal up to -11.6 kcal mol⁻¹ stabilization due to LD, whereas the TIPS and *tert*-butyl butyl groups account for

$\sim 32\%$ and $\sim 12\%$ respectively. A new generation of Rh-Bi catalysts outperformed the old set in selectivity as well as in reactivity. Whereas a cyclopropanation reaction using *N*-phthalimido substituents on the *tert*-leucine ligands gave full conversion in >3 h, the new set of ligands completed the reaction within 10 min with outstanding selectivity. Since the more sterically hindered catalyst proceeds with higher reaction rates, *stabilizing* LD interactions must be responsible for the increase in reactivity.^[114a]

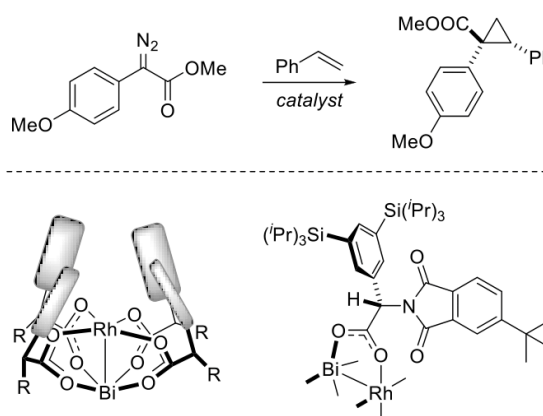


Figure 20. Cyclopropanation of styrene utilizing a heterobimetallic bismuth-rhodium paddlewheel complex.^[114a]

Bistoni *et al.*^[116] examined an asymmetric intramolecular hydroalkoxylation of terminal olefins catalyzed by bulky Brønsted acids.^[117] By studying the conformational flexibility in the transition state of the reaction, the interplay of catalyst and substrate was of capital importance. The authors observed a distortion of the catalyst to maximize intermolecular interaction with the substrate. The energy penalty arising from conformational distortion was overwritten by a number of LD interactions.^[116]

Accordingly, attractive interactions dominate enzyme-substrate interactions whereas steric hindrance prevents close contact. Thus, rate acceleration can only be rationalized due to the presence of attractive noncovalent interactions. Selectivity, on the other hand, can be evoked by both, repulsive steric interactions decelerating the reaction to one product and steric attraction favoring the reaction to the other. Size-dependent rate acceleration was observed in competition experiments between secondary alcohols and silyl reagents of varying size (Figure 21). While silyl groups are commonly utilized to introduce steric bulk^[63-64, 65] and prohibit chemical reactions, Zipse *et al.*^[118] observed a systematic rate increase of a silylation reaction using large DED substituents. In a combined experimental and computational study, Zipse and coworkers isolated LD interactions as dominant factor for a rate increase. Whereas small silyl reagents (*e.g.* TMSCl) lack a sufficient number of LD contacts, large aromatic substituents increase the reaction rates.

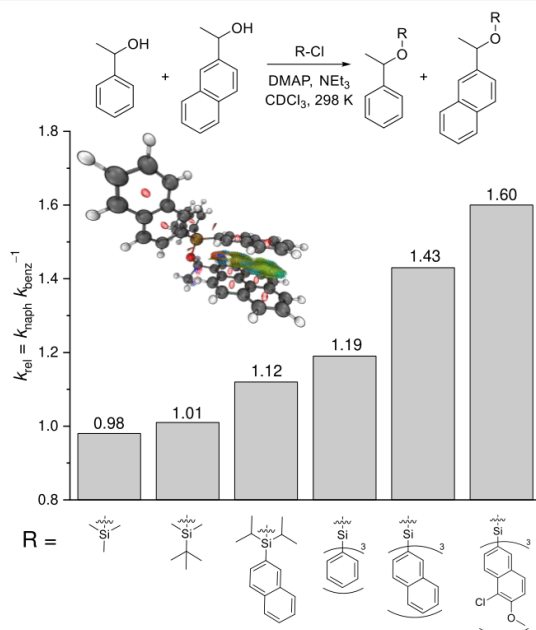


Figure 21. Relative rate constants k_{rel} for competition experiments between 1-phenylethanol and 1-naphthylethanol with increasingly larger silyl chlorides. The NCI plot highlights π - π (LD) interactions (green isosurface).^[118]

The same effect was taken advantage of in the kinetic resolution of secondary alcohols.^[119] By utilizing chiral pyridine derivatives with increasingly larger aromatic side chains, the rate accelerate by a factor up of 40. Computational investigations revealed that the most crowded transition structure was favored by around 1.6 kcal mol⁻¹ resulting in high kinetic selectivity factors ($s \geq 50$). The origin for the stabilization lies in attractive CH- π and π - π interactions. Accordingly, the concept of steric attraction (*via* LD) was successfully utilized to increase reaction rates and improve enantioselectivities.^[119]

The Corey-Bakshi-Shibata (CBS) reduction^[120] of prochiral ketones is a striking example where stereoselectivity is explained solely on the basis of a classic steric repulsion model. The proposed (and widely accepted) mechanism for the enantioselective reduction of ketones by oxazaborolidines (OXB) is based on repulsive interactions^[121] between the boron substituent R on the catalyst and the largest substituents R_L of the ketone. Repulsive interactions between R and R_L are designated as to disfavor the six membered boat-like transition state to the (*S*)-product, delivering the (*R*)-enantiomer with high selectivity. While this concept can qualitatively predict the enantioselectivities for many substrates, it fails for ketones such as 1-cyclopropyl-2-methylpropan-1-one.^[121b]

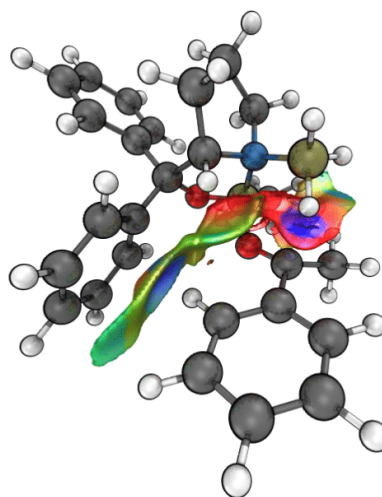


Figure 22. NCI plot of the lowest-lying transition structure for the reduction of acetophenone with OXB. Stabilizing CH- π interactions highlight the role of the phenyl moieties at the carbonyl position of OXB in the transition structure. Rather than steric hindrance they provide an anchor to fix the substrate *via* LD interactions.^[14c]

Since both substituents are similar in steric size, poor selectivity would be predicted. Nevertheless, the (*R*)-enantiomer formed in 91% *ee*. Schreiner *et al.*^[4b] investigated the origin of this selectivity by focusing on both the steric repulsion argument but also by including LD in the mechanistic and structural rationale. In contrast to Corey's model, the reactions are actually more selective upon removal of the large phenyl substituent on boron. Instead, LD interactions between the OXB carbonyl phenyl groups interact favorably with the substrate (Figure 22). With this improved mechanistic and more physically sound understanding of the CBS reduction it was possible to modify the catalyst to show improved enantioselectivities even for the most challenging substrate like butanone (Figure 23). This most difficult methyl-ethyl discrimination challenge was improved from 60% *ee* to 72% *ee* with a DED-enhanced OXB catalyst.

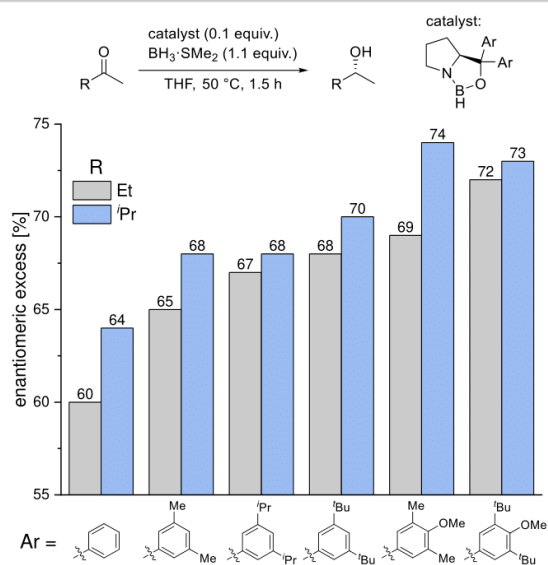


Figure 23. CBS reductions of butanone (grey) and 3-methyl-2-butanone (blue) employing modified catalysts of growing size.^[4b]

Since LD is accumulative and highly dependent of the number of short-range contacts, large molecules, such as peptides or the double helix of DNA, greatly benefit from LD. Bistoni *et al.*^[122] as well as Hobza and coworkers^[123] demonstrated the importance of LD on the intrinsic stability of the duplex structure of DNA using advanced quantum mechanical methods. Even in the presence of multiple noncovalent contacts, LD is essential for the stability of large molecular structures. Accordingly, large peptide catalysts are prone to utilize LD interactions to stabilize transition structures.

In the enantioselective kinetic resolution of *trans*-cyclohexane-1,2-diols through monoacylation a non-natural oligopeptide catalysts was utilized.^[124] While the nucleophilic *N*- π -methylhistidine moiety is catalytically active and performs the enantioselective acyl transfer, cyclohexylalanine was incorporated to act as a DED. Both, computational and experimental evidence suggest the formation of an enzyme-like pocket in which the substrate is bound *via* hydrogen bonding and LD interactions.^[125] The molecular aggregation due to LD was probed using advanced NMR methods.^[125b] The investigations included a conformational analysis of the organocatalyst as well as the aggregation of substrate and catalyst *via* nuclear-Overhauser effect (NOE)-based NMR spectroscopy. As a result, the NOE-contact between the substrate (*trans*-1,2-cyclohexyldiol) and the cyclohexyl moiety of the oligopeptide catalyst could be observed.

A similar catalyst-substrate binding was exploited to develop the first enantioselective Dakin-West reaction (Figure 24).^[126] Due to racemization of two intermediates, stereoselective catalysis was difficult to achieve. While the oligopeptide catalyzed the Steglich rearrangement as well as the final decarboxylation and re-protonation, stereoselectivity was only realized during the latter. A combination of LD and enolate binding hold the substrate in place for stereoselective re-protonation of the terminal enol. Again, cyclohexyl groups proved most effective as DEDs due to their flexibility and yet

high electron density (Figure 24). The same catalyst was also utilized in site-selective acylation of pyranosides.^[127] LD is likely to bind the carbohydrate in the catalyst's pocket thereby facilitate site-selectivity.

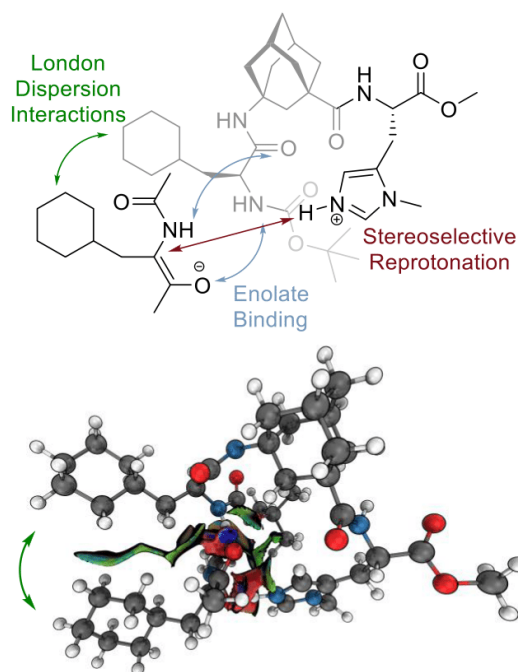


Figure 24. Association of protonated catalyst and substrate in the first enantioselective Dakin-West reaction. The NCI plot highlights the importance of attractive alkyl-alkyl contacts fixing the substrate in the catalyst's pocket.^[126]

In the Brønsted acid catalyzed transfer hydrogenation of imines, the incorporation of bulky DEDs significantly enhances enantioselectivities due to stabilization of the *Z*-imine transition state. In a systematic study, Gramüller and Gschwind^[128] developed a dispersion-controlled catalytic cycle by investigating the impact of *tert*-butyl groups on the conformational preference of the starting material and the termolecular transition structure (Figure 25). Although the *E*-imine is in general the preferred conformer, sophisticated NMR techniques revealed a shift of the equilibrium between the *E*- and *Z*-imine to the more crowded *Z*-imine by around 1 kcal mol⁻¹. While the dimerization of starting material and catalyst significantly favors the *Z*-imine, the stabilizing effects of *tert*-butyl substituents prevail throughout the entire reaction process. This leads to a significant increase of enantioselectivity.

REVIEW

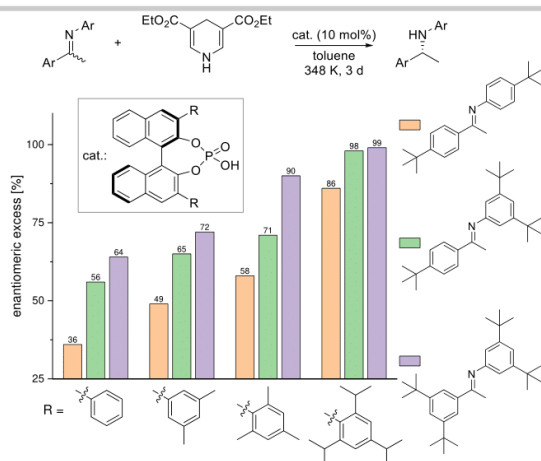


Figure 25. Enantioselectivities for the transfer hydrogenation of imines utilizing *tert*-butyl groups for efficient catalyst-substrate binding.^[128]

Chiral phosphoric acids were also used to achieve high enantioselectivities in the Minisci reaction of alcohols. Phipps *et al.*^[129] reported the first enantioselective Minisci reaction that uses α -hydroxy radicals instead of commonly employed α -amino radicals. Both, experimental and computational investigations point to a deprotonation as the selectivity- and rate-determining step with noncovalent interactions being responsible for enantiodiscrimination. While the formation of the major product is stabilized by LD between the substrate and 3,3'-substituents of the phosphate catalyst, the transition structure of the minor product lacks such stabilization. The consideration of LD in the computational analysis led to excellent agreement of experimental and computational data. Toste *et al.*^[130] studied an enantioselective allenolate-claisen rearrangement *via* chiral phosphoric acid catalysts. In coordination to sodium cation a catalytic pocket formed which maximizes noncovalent interactions. Since phosphoric acid catalysts are readily substituted, they might prove valuable DEDs in the future.

Studying bioorthogonal reactions Franzini and coworkers^[131] noticed an unexpected rate increase in the cycloaddition of 3,6-dialkyl-tetrazines and (2-isocyanoethyl)benzene by introducing steric bulk (Figure 26). Accordingly, the introduction of *tert*-butyl groups at tetrazine increased the reaction rate by a factor of eight. Since repulsive interactions cannot be responsible for rate increases, LD interactions were studied in detail. A computational analysis revealed increasing LD interactions (~ -6.0 kcal mol⁻¹) in the rate-determining transition structure with increasing steric bulk for the reaction with *iso*-nitriles. Due to the linear structure of the *iso*-nitrile group repulsive steric hindrance was estimated to be minimal (~ 1.0 kcal mol⁻¹).

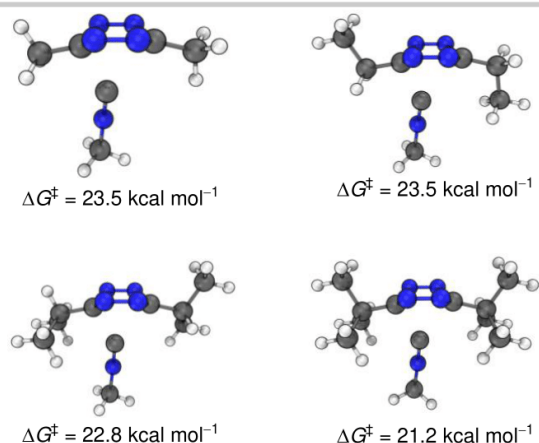


Figure 26. Computed structures and Gibbs free energies for the transition structure of the model reaction of substituted tetrazines with methylisonitrile.^[131a]

To efficiently use attractive noncovalent interactions in catalysis, substrate and catalyst need to be geometrically compatible with each other.^[132] While this compatibility is usually achieved by utilizing functional groups, Karton *et al.*^[133] recently demonstrated that simple pristine graphene catalyzes the racemization chiral 1,1'-binaphthyl-2,2'-diol (BINOL) *via* a large area of noncovalent contacts. By utilizing a single-layer graphene (*R*)-BINOL (>99:1 *e.r.*) was fully converted to a racemic mixture. Computations showed a combination of LD and electrostatic interactions (with the former being most prominent) are the basis for catalytic activity. Similar effects were observed for bowl-to-bowl inversion of corannulene and sumanene using graphene and h-BN as catalysts.^[134]

The stereo- and regiochemical outcomes of photochemical dearomative cycloadditions were found to be significantly influenced by LD. Brown and coworkers reported a cycloaddition of quinoline derivatives with alkenes proceeding *via* a stepwise radical reaction (Figure 27).^[135] After initial reversible radical addition the *endo* product formed preferably in a selectivity determining radical recombination. Accordingly, the more sterically demanding product forms; this is also true for the extremely bulky adamantyl substituent. Computational investigations found LD to be decisive for selectivity. A comparison between dispersion corrected functionals and those excluding LD demonstrated that only by including LD the selectivity was reproduced. Thus, methyl substitution favors the *endo* transition structure by -0.7 kcal mol⁻¹. Additionally, σ - π interactions increase with steric bulk favoring the *endo* reaction path by -1.8 kcal mol⁻¹ with *tert*-butyl substitution.^[135]

REVIEW

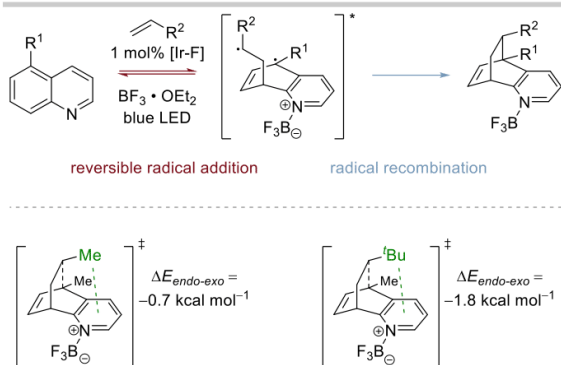


Figure 27. Photochemical reaction of a quinolone derivative with an alkene (top). Selectivity determining transition structure (bottom) with methyl and *tert*-butyl substituents.^[135]

In the field of transition-metal catalysis, electronic and steric arguments (as if they were separable!) are commonly utilized to rationalize ligand effects.^[136] While the first is described as a through-bond^[137] effect, bulky substituents in the periphery of the metal center mostly affect the catalyst-substrate through-space interactions.^[111, 138] Both effects greatly influence the catalytic performance by altering rate determining transition structures. Typically, the through-space interaction is described as steric repulsion.^[139] This argument effectively rationalizes an increase in selectivity due to repulsive interactions by shielding certain parts of the metal catalyst. However, the notion that higher steric bulk, *i.e.*, a *destabilization*, increases reaction rates must be called into question.

Naturally, LD interactions can override steric repulsion due to a large number of attractive ligand-substrate contacts.^[140] Nevertheless, attractive noncovalent interactions are rarely discussed in transition-metal catalysis even though a ligand that is able to attractively interact with a substrate is crucial for reactivity and selectivity.^[141] While systematic studies of LD effects on organic reactions or structures are feasible, polarized metal centers prove difficult when it comes to dissecting between various noncovalent interactions. For instance, a thorough analysis of through-space interactions was performed for a copper-catalyzed hydroamination reaction of unactivated olefins by Liu *et al.*^[14a] The reaction proceeds *via* a hydrocupration on to the olefin as the rate determining step. Whereas commonly utilized ligands, such as SEGPHOS, hardly catalyze the reaction for unactivated substrates, the introduction of bulky *tert*-butyl substituents counterintuitively increases reaction rates and yields. Liu *et al.*^[14a] utilized a ligand-substrate interaction model to dissect the through-bond and -space interactions into the main contributors to the activation barrier (Figure 28). *Via* a combination of experimental and computational investigations, they identified LD interactions to be the dominant factor in the transition structure of the reaction. By incorporating bulky di-*tert*-butyl-methoxy (DTBM) substituents, the substrate scope and reactivity increased significantly. In a later study, the catalysts' performance towards in a hydroboration reaction was further increased by exchanging bulky *tert*-butyl substituents with higher tetrel congeners.^[142] By utilizing trimethylsilyl (TMS) and trimethylgermanium (TMG) as DEDs the interactions between the catalyst and substrates was

further optimized resulting in higher yields and faster reactions. Thereby, the incorporation of higher tetrels enhances LD interactions between catalyst and substrate due to their increased size and polarizabilities. A similar effect is responsible for the observed stability of higher tetrel hexaphenylethane congeners, whereas the original carbon-based hexaphenylethane has not been prepared to date.^[86] Other studies also indicate that silyl groups can be utilized as DEDs despite their large steric demand.^[63, 68, 114a, 118-119, 143] Similar to the SEGPHOS ligand, prolinol-phosphine ligands bearing DTBM groups were successfully utilized in silver catalyzed asymmetric aldol reactions as decisive structural feature for stereoselectivity. Computational investigations point to a combination of non-classical C–H...O hydrogen bonding and LD interactions stabilizing the rate-determining transition structure.^[144]

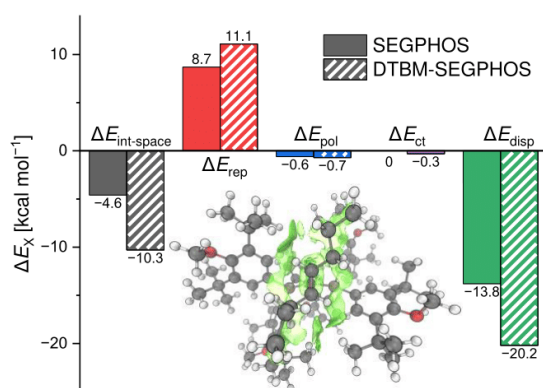


Figure 28. Energy decomposition analysis of the ligand-substrate interaction energies in the transition structure of the hydrocupration reaction of *trans*-4-octene reacting with SEGPHOS (bold markings) and DTBM-SEGPHOS (striped markings).^[14a]

In 2018, Sawamura *et al.*^[145] introduced the copper-catalyzed asymmetric alkynylation of α -ketoesters. A combination of hydrogen bonding and LD interactions between the chiral phosphine ligand and substrate was identified as the origin for the observed enantioselectivities. Apart from transition state stabilization, LD interactions significantly alter the reactions' energy profile. Computations of the Cobalt-catalyzed C–H cyanation reaction show that, both, energy barriers and minima are stabilized by LD.^[146] Here, the Cp* ligand was utilized to interact as DED and stabilize labile complexes with the Co catalyst. An LD analysis revealed strong LD interactions of up to 12 kcal mol⁻¹ between the CP* ligand and the substrate. Consequently, the CP* ligand does not interact *via* steric shielding but rather stabilizes the complex due to CH- π contacts.^[146b] Similar effects were reported for a Mn-catalyzed C–H-bond functionalization.^[147] LD was computed to play a dominant role in stabilizing the key transition structures. As a consequence, the role of bulky ligands^[148] in transition metal catalysis should be carefully considered and re-evaluated. The noninnocence of steric bulk can usually be traced back to a fine interplay of Pauli repulsion and LD in enantioinduction.^[149]

Accordingly, in the developing field of dual transition metal catalysis noncovalent interactions have begun to move into the spotlight. Here, LD is utilized as a tool to enable face-selectivity

REVIEW

via π - π interactions.^[150] Pursuant to this, Rios *et al.*^[151] observed in the field of synergistic catalysis where LD is the key attractive interaction stabilizing the rate determining step in the synthesis of dihydroacridines. In the zirconocene catalyzed ethylene polymerization, Ess and coworkers computationally investigated the role of LD during α -olefin co-monomer incorporation. Both fields are largely based on the concept steric hindrance rather than attractive noncovalent interaction. Counterintuitively, they identified LD as decisive factor for selectivity and incorporated LD as a ligand design feature.^[152]

Whereas chemical reactions can benefit from LD interactions due to lower energy barriers of the rate determining step, LD can also help in elucidating mechanisms of catalytic processes. Berkessel and coworkers^[153] utilized bulky 2,6-bis(2-propyl)phenyl (Dipp) and 2,4,6-trimethylphenyl (Mes) substituents attached to *N*-heterocyclic carbenes to stabilize and characterize the elusive Breslow intermediate. Computations suggest LD to be the major component of the thermodynamic stability of the intermediate.

While LD can be regarded as the key interaction to stabilize metal-NHC^[141b, 154] complexes, the selectivity of such catalysts was studied experimentally and computationally with respect to the role of noncovalent interactions in the rate determining transition state.^[155] A ruthenium catalyst bearing NHC ligands can be utilized for enantioselective hydrogenation of heteroarenes to generate saturated heterocycles.^[156] The corresponding mechanism consists of a hydride and a subsequent proton shift with the first being rate determining. Enantioselectivity is determined by substrate coordination via the *re* or *si*-face of the substrate. Glorius *et al.*^[156] located a decisive structural feature for binding of the substrate which affects the energy of all subsequent reaction steps. While *re*-face coordination is dominated by a flat interaction surface of the catalyst and while there is no steric hindrance, a more crowded catalyst-substrate complex forms via *si*-face coordination (Figure 29). Still, *si*-face coordination yields the major enantiomer. In line with the induced fit model,^[157] the catalyst bends around the substrate and forms a pocket by maximizing LD interactions. While this pocket cannot form upon *re*-face coordination, LD stabilizes the more hindered pathway. With a difference in Gibbs free energy of the transition structure of 1.9 kcal mol⁻¹ (experimentally determined) the reaction yields the (*R*)-configured product with 96:4 *e.r.*^[156] Similar effects were observed by Bistoni *et al.*^[158] who computationally assessed the mechanism and stereoselectivities of asymmetric catalytic Diels-Alder reactions. LD was found to be an indispensable feature of catalyst-substrate aggregation.

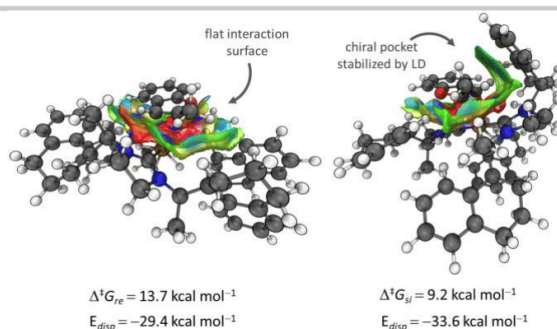


Figure 29. NCI plot and computed energies of the rate determining transition structure of the ruthenium NHC-catalyzed asymmetric heteroarene hydrogenation. The *si* transition structure (right) results in major enantiomer.^[156]

The role of NHC ligands as the origin for additional stabilization via LD has also been taken advantage of in hydroarylation reactions of unactivated alkenes. Very bulky and highly substituted NHCs and a nickel catalyst were demonstrated to increase reactivities and selectivities due to a combination of LD and electrostatic interactions.^[159]

A comparable impact of LD was reported for the Pd catalyzed stereoselective synthesis of tetrasubstituted chromanones. The chiral pyridine-dihydroisoquinoline ligand (PyDHIQ) utilized to induce excellent stereoselectivities consists of a floppy benzyl group substituted with steric bulk to make use of steric hindrance as a directing effect.^[160] Andreola and Wheeler^[161] computationally found stabilizing hydrogen bonding and LD interactions as the main origin for observed selectivities. Accordingly, the floppy benzyl substituent at PyDHIQ favors a closed conformation in the transition structure, thereby interacting with the substrate.

5. Conclusions

LD interactions are ubiquitously present in all areas of molecular chemistry. Nevertheless, the general assumption remains largely intact that LD are negligible in comparison to other noncovalent interaction and is largely cancelled by Pauli repulsion. With this review, we have tried to demonstrate that LD can be significant and must be considered when discussing structure, reactivity, catalysis, or spectroscopy.

In the recent years, great progress has been made in quantifying LD interactions. DEDs are now regularly used to influence structural stability or enforce selectivity. Especially, labile and highly reactive molecules benefit from LD and can now be studied in more detail (e.g. HPE).

In catalysis, the fine interplay of LD and Pauli repulsion between catalyst and substrate is often responsible for reactivity and selectivity. Accordingly, fine-tuning the ratio of LD and repulsive interactions greatly affects the catalysts activity and expands the possibility of diastereo- as well as enantioselection.

In the future, LD can be readily utilized as a design element to systematically adjust thermodynamic stability as well as reactivity.

Acknowledgements

This work was supported by the priority program "Control of London Dispersion in Molecular Chemistry" (SPP1807) of the Deutsche Forschungsgemeinschaft. With the end of the program, we thank all principle investigator contributing for a successful collaboration. We thank Jan M. Schümann for fruitful discussions.

Keywords: noncovalent interactions • van der Waals forces • molecular balance • spectroscopy • structure and reactivity

- [1] a) J. D. Van der Waals, *Over de Continuïteit van den Gas- en Vloeistoftoestand, Vol. 1*, Sijthoff, **1873**; b) J. D. Waals, *Die Continuïteit des gasförmigen und flüssigen Zustandes*, JA Barth, **1881**; c) J. D. Van Der Waals, J. S. Rowlinson, *On the continuity of the gaseous and liquid states*, Courier Corporation, **2004**; d) K.-T. Tang, J. P. Toennies, *Angew. Chem. Int. Ed.* **2010**, *49*, 9574-9579.
- [2] A. Stone, in *Molecular Liquids*, Springer, **1984**, pp. 1-34.
- [3] H.-J. Schneider, *Angew. Chem. Int. Ed.* **2009**, *48*, 3924-3977.
- [4] a) G. Lu, R. Y. Liu, Y. Yang, C. Fang, D. S. Lambrecht, S. L. Buchwald, P. Liu, *J. Am. Chem. Soc.* **2017**, *139*, 16548-16555; b) C. Eschmann, L. Song, P. R. Schreiner, *Angew. Chem. Int. Ed.* **2021**, *60*, 4823-4832.
- [5] D. J. Liptrot, P. P. Power, *Nat. Chem. Rev.* **2017**, *1*, 0004.
- [6] a) F. London, *Z. Phys.* **1930**, *63*, 245-279; b) F. London, *Trans. Faraday Soc.* **1937**, *33*, 8b-26.
- [7] J. P. Wagner, P. R. Schreiner, *Angew. Chem. Int. Ed.* **2015**, *54*, 12274-12296.
- [8] J. N. Israelachvili, in *Intermolecular and Surface Forces (Third Edition)* (Ed.: J. N. Israelachvili), Academic Press, San Diego, **2011**, pp. 107-132.
- [9] a) R. Eisenschitz, F. London, *Z. Phys.* **1930**, *60*, 491-527; b) D. G. Truhlar, *J. Chem. Educ.* **2019**, *96*, 1671-1675.
- [10] S. Grimme, R. Huenerbein, S. Ehrlich, *ChemPhysChem* **2011**, *12*, 1258-1261.
- [11] a) M. J. Miller, M. H. Lyttle, A. Streitwieser Jr, *J. Org. Chem.* **1981**, *46*, 1977-1984; b) M. H. Lyttle, A. Streitwieser Jr, R. Q. Kluttz, *J. Am. Chem. Soc.* **1981**, *103*, 3232-3233.
- [12] K. Szalewicz, *WIREs Comput. Mol. Sci.* **2012**, *2*, 254-272.
- [13] J. M. Schümann, J. P. Wagner, A. K. Eckhardt, H. Quanz, P. R. Schreiner, *J. Am. Chem. Soc.* **2021**, *143*, 41-45.
- [14] a) C. A. Hunter, *Angew. Chem. Int. Ed.* **2004**, *43*, 5310-5324; b) K. D. Shimizu, *Nat. Chem.* **2013**, *5*, 989-990; c) J. Hwang, B. E. Dial, P. Li, M. E. Kozik, M. D. Smith, K. D. Shimizu, *Chem. Sci.* **2015**, *6*, 4358-4364; d) R. Pollice, M. Bot, I. J. Kobylanski, I. Shenderovich, P. Chen, *J. Am. Chem. Soc.* **2017**, *139*, 13126-13140.
- [15] a) N. Becker, K. Noyes, M. Cooper, *J. Chem. Educ.* **2016**, *93*, 1713-1724; b) K. Noyes, M. M. Cooper, *J. Chem. Educ.* **2019**, *96*, 1821-1832; c) K. Noyes, R. L. McKay, M. Neumann, K. C. Haudek, M. M. Cooper, *J. Chem. Educ.* **2020**, *97*, 3923-3936.
- [16] a) S. Grimme, *WIREs Comput. Mol. Sci.* **2011**, *1*, 211-228; b) S. Grimme, A. Hansen, J. G. Brandenburg, C. Bannwarth, *Chem. Rev.* **2016**, *116*, 5105-5154.
- [17] S. Ehrlich, J. Moellmann, S. Grimme, *Acc. Chem. Res.* **2013**, *46*, 916-926.
- [18] P. R. Schreiner, L. V. Chernish, P. A. Gunchenko, E. Y. Tikhonchuk, H. Hausmann, M. Serafin, S. Schlecht, J. E. P. Dahl, R. M. K. Carlson, A. A. Fokin, *Nature* **2011**, *477*, 308-311.
- [19] a) S. Grimme, J. Antony, S. Ehrlich, H. Krieg, *J. Chem. Phys.* **2010**, *132*, 154104; b) J. Klimeš, A. Michaelides, *J. Chem. Phys.* **2012**, *137*, 120901.
- [20] E. R. Johnson, A. D. Becke, *J. Chem. Phys.* **2005**, *123*, 024101.
- [21] a) E. Caldeweyher, C. Bannwarth, S. Grimme, *J. Chem. Phys.* **2017**, *147*, 034112; b) E. Caldeweyher, S. Ehlert, A. Hansen, H. Neugebauer, S. Spicher, C. Bannwarth, S. Grimme, *J. Chem. Phys.* **2019**, *150*, 154122.
- [22] a) M. Bursch, E. Caldeweyher, A. Hansen, H. Neugebauer, S. Ehlert, S. Grimme, *Acc. Chem. Res.* **2019**, *52*, 258-266; b) E. Caldeweyher, J.-M. Mewes, S. Ehlert, S. Grimme, *Phys. Chem. Chem. Phys.* **2020**, *22*, 8499-8512.
- [23] W. B. Schneider, G. Bistoni, M. Sparta, M. Saitow, C. Riplinger, A. A. Auer, F. Neese, *J. Chem. Theory Comput.* **2016**, *12*, 4778-4792.
- [24] S. F. Boys, F. Bernardi, *Mol. Phys.* **1970**, *19*, 553-566.
- [25] T. M. Parker, L. A. Burns, R. M. Parrish, A. G. Ryno, C. D. Sherrill, *J. Chem. Phys.* **2014**, *140*, 094106.
- [26] G. Bistoni, A. A. Auer, F. Neese, *Chem. Eur. J.* **2017**, *23*, 865-873.
- [27] Q. Lu, F. Neese, G. Bistoni, *Angew. Chem. Int. Ed.* **2018**, *57*, 4760-4764.
- [28] Q. Lu, F. Neese, G. Bistoni, *Phys. Chem. Chem. Phys.* **2019**, *21*, 11569-11577.
- [29] A. Altun, F. Neese, G. Bistoni, *Beilstein J. Org. Chem.* **2018**, *14*, 919-929.
- [30] A. Altun, M. Saitow, F. Neese, G. Bistoni, *J. Chem. Theory Comput.* **2019**, *15*, 1616-1632.
- [31] A. Altun, F. Neese, G. Bistoni, *J. Chem. Theory Comput.* **2019**, *15*, 5894-5907.
- [32] K. Patkowski, *WIREs Comput. Mol. Sci.* **2020**, *10*, e1452.
- [33] a) E. E. Salpeter, H. A. Bethe, *Phys. Rev.* **1951**, *84*, 1232-1242; b) S.-H. Ke, *Phys. Rev. B* **2011**, *84*, 205415.
- [34] C. Holzer, W. Klopper, *J. Chem. Phys.* **2017**, *147*, 181101.
- [35] M. Kodrycka, C. Holzer, W. Klopper, K. Patkowski, *J. Chem. Theory Comput.* **2019**, *15*, 5965-5986.
- [36] C. Holzer, W. Klopper, *Mol. Phys.* **2017**, *115*, 2775-2781.
- [37] a) K. Carter-Fenk, J. M. Herbert, *Chem. Sci.* **2020**, *11*, 6758-6765; b) K. Carter-Fenk, J. M. Herbert, *Phys. Chem. Chem. Phys.* **2020**, *22*, 24870-24886; c) K. Carter-Fenk, K. U. Lao, J. M. Herbert, *Acc. Chem. Res.* **2021**, *54*, 3679-3690.
- [38] J. M. Herbert, *J. Phys. Chem. A* **2021**, *125*, 7125-7137.
- [39] a) E. R. Johnson, S. Keinan, P. Mori-Sánchez, J. Contreras-García, A. J. Cohen, W. Yang, *J. Am. Chem. Soc.* **2010**, *132*, 6498-6506; b) J. Contreras-García, E. R. Johnson, S. Keinan, R. Chaudret, J.-P. Piquemal, D. N. Beratan, W. Yang, *J. Chem. Theory Comput.* **2011**, *7*, 625-632.
- [40] A. Wuttke, R. A. Mata, *J. Comput. Chem.* **2017**, *38*, 15-23.
- [41] R. Pollice, P. Chen, *Angew. Chem. Int. Ed.* **2019**, *58*, 9758-9769.
- [42] R. Pollice, P. Chen, *J. Am. Chem. Soc.* **2019**, *141*, 3489-3506.
- [43] a) I. K. Mati, S. L. Cockroft, *Chem. Soc. Rev.* **2010**, *39*, 4195-4205; b) M. A. Strauss, H. A. Wegner, *Eur. J. Org. Chem.* **2019**, *2019*, 295-302.
- [44] T. Grawe, T. Schrader, R. Zadnard, A. Kraft, *J. Org. Chem.* **2002**, *67*, 3755-3763.
- [45] A. H. Heindl, R. C. Wende, H. A. Wegner, *Beilstein J. Org. Chem.* **2018**, *14*, 1238-1243.
- [46] L. Yang, C. Adam, G. S. Nichol, S. L. Cockroft, *Nat. Chem.* **2013**, *5*, 1006-1010.
- [47] D. Van Craen, W. H. Rath, M. Huth, L. Kemp, C. Rüber, J. M. Wollschläger, C. A. Schalley, A. Valkonen, K. Rissanen, M. Albrecht, *J. Am. Chem. Soc.* **2017**, *139*, 16959-16966.
- [48] S. Paliwal, S. Geib, C. S. Wilcox, *J. Am. Chem. Soc.* **1994**, *116*, 4497-4498.
- [49] E.-i. Kim, S. Paliwal, C. S. Wilcox, *J. Am. Chem. Soc.* **1998**, *120*, 11192-11193.
- [50] a) C. Adam, L. Yang, S. L. Cockroft, *Angew. Chem. Int. Ed.* **2015**, *54*, 1164-1167; b) L. Yang, C. Adam, S. L. Cockroft, *J. Am. Chem. Soc.* **2015**, *137*, 10084-10087.
- [51] S. Otto, *Chem. Sci.* **2013**, *4*, 2953-2959.
- [52] W. R. Carroll, P. Pellechia, K. D. Shimizu, *Org. Lett.* **2008**, *10*, 3547-3550.
- [53] J. Hwang, P. Li, W. R. Carroll, M. D. Smith, P. J. Pellechia, K. D. Shimizu, *J. Am. Chem. Soc.* **2014**, *136*, 14060-14067.
- [54] C. D. Zeinalipour-Yazdi, D. P. Pullman, *J. Phys. Chem. B* **2006**, *110*, 24260-24265.
- [55] J. Hwang, P. Li, M. D. Smith, K. D. Shimizu, *Angew. Chem. Int. Ed.* **2016**, *55*, 8086-8089.

REVIEW

- [56] R. Pollice, F. Fleckenstein, I. Shenderovich, P. Chen, *Angew. Chem. Int. Ed.* **2019**, *58*, 14281-14288.
- [57] A. V. Marenich, C. J. Cramer, D. G. Truhlar, *J. Phys. Chem. B* **2009**, *113*, 6378-6396.
- [58] F. Eckert, A. Klamt, *AIChE J.* **2002**, *48*, 369-385.
- [59] M. Schlottmann, D. Van Craen, J. Baums, I. Funes-Ardoiz, C. Wiederhold, I. M. Oppel, M. Albrecht, *Inorg. Chem.* **2020**, *59*, 1758-1762.
- [60] L. A. Paquette, G. J. Hefferon, R. Samodral, Y. Hanzawa, *J. Org. Chem.* **1983**, *48*, 1262-1266.
- [61] a) N. Allinger, M. Frierson, F. Van-Catledge, *J. Am. Chem. Soc.* **1982**, *104*, 4592-4593; b) C. Tosi, *J. Comput. Chem.* **1984**, *5*, 248-251.
- [62] J. E. Anderson, P. A. Kirsch, *J. Chem. Soc., Perkin Trans. 2* **1992**, 1951-1957.
- [63] H. F. König, L. Rummel, H. Hausmann, J. Becker, J. M. Schümann, P. R. Schreiner, *J. Org. Chem.* **2022**, *87*, 5492-5493.
- [64] a) E. L. Eliel, H. Satici, *J. Org. Chem.* **1994**, *59*, 688-689; b) C. H. Marzabadi, J. E. Anderson, J. Gonzalez-Outeiriro, P. R. J. Gaffney, C. G. H. White, D. A. Tocher, L. J. Todaro, *J. Am. Chem. Soc.* **2003**, *125*, 15163-15173; c) E. Solel, M. Ruth, P. R. Schreiner, *J. Am. Chem. Soc.* **2021**, *143*, 20837-20848.
- [65] S. Nobujiro, T. Naohide, Y. Sigefumi, I. Takahiko, *Chem. Lett.* **1993**, *22*, 1807-1810.
- [66] C. A. Tolman, *Chem. Rev.* **1977**, *77*, 313-348.
- [67] H. F. König, H. Hausmann, P. R. Schreiner, *J. Am. Chem. Soc.* **2022**.
- [68] L. Rummel, H. F. König, H. Hausmann, P. R. Schreiner, *J. Org. Chem.* **2022**.
- [69] F. M. Wilming, B. Marazzi, P. P. Debes, J. Becker, P. R. Schreiner, *J. Org. Chem.* **2022**.
- [70] a) M. Minabe, T. Oba, M. Tanaka, K. Kanno, M. Tsubota, *Chem. Lett.* **2000**, *29*, 498-499; b) M. Minabe, A. Yamazaki, T. Imai, T. Takanezawa, M. Karikomi, *B. Chem. Soc. Jpn.* **2006**, *79*, 1758-1765.
- [71] M. A. Strauss, H. A. Wegner, *Angew. Chem. Int. Ed.* **2019**, *58*, 18552-18556.
- [72] J. Gorges, S. Grimme, A. Hansen, P. Pracht, *Phys. Chem. Chem. Phys.* **2022**.
- [73] a) A. Tsybizova, L. Fritsche, V. Gorbachev, L. Miloglyadova, P. Chen, *J. Chem. Phys.* **2019**, *151*, 234304; b) V. Gorbachev, A. Tsybizova, L. Miloglyadova, P. Chen, *J. Am. Chem. Soc.* **2022**, *144*, 9007-9022.
- [74] a) C. A. Hunter, *Chem. Sci.* **2013**, *4*, 834-848; b) C. Bravin, J. A. Piekos, G. Licini, C. A. Hunter, C. Zonta, *Angew. Chem. Int. Ed.* **2021**, *60*, 23871-23877.
- [75] K. Nakamura, K. N. Houk, *Org. Lett.* **1999**, *1*, 2049-2051.
- [76] a) D. Chandler, *Nature* **2005**, *437*, 640-647; b) A. Elmi, S. L. Cockroft, *Acc. Chem. Res.* **2021**, *54*, 92-103; c) F. M. Wilming, J. Becker, P. R. Schreiner, *J. Org. Chem.* **2022**, *87*, 1874-1878.
- [77] M. A. Strauss, H. A. Wegner, *Angew. Chem. Int. Ed.* **2021**, *60*, 779-786.
- [78] D. Schatz, A. Kunz, A. R. Raab, H. A. Wegner, *Synlett* **2022**, *0*.
- [79] S. Rösel, P. R. Schreiner, *Isr. J. Chem.* **2022**, *62*, e202200002.
- [80] a) M. Gomberg, *Ber. Dtsch. Chem. Ges.* **1900**, *33*, 3150-3163; b) M. Gomberg, A. I. O. T. Carbon, *J. Am. Chem. Soc.* **1900**, *22*, 757-771.
- [81] H. Lankamp, W. T. Nauta, C. MacLean, *Tetrahedron Lett.* **1968**, *9*, 249-254.
- [82] a) W. D. Hounshell, D. A. Dougherty, J. P. Hummel, K. Mislow, *J. Am. Chem. Soc.* **1977**, *99*, 1916-1924; b) E. Osawa, Y. Onuki, K. Mislow, *J. Am. Chem. Soc.* **1981**, *103*, 7475-7479.
- [83] a) M. Stein, W. Winter, A. Rieker, *Angew. Chem. Int. Ed.* **1978**, *17*, 692-694; b) B. Kahr, D. Van Engen, K. Mislow, *J. Am. Chem. Soc.* **1986**, *108*, 8305-8307; c) N. Yannoni, B. Kahr, K. Mislow, *J. Am. Chem. Soc.* **1988**, *110*, 6670-6672; d) S. Rösel, C. Balestrieri, P. R. Schreiner, *Chem. Sci.* **2017**, *8*, 405-410.
- [84] a) G. Maier, S. Priem, U. Schäfer, R. Matusch, *Angew. Chem. Int. Ed.* **1978**, *17*, 520-521; b) S. Grimme, P. R. Schreiner, *Angew. Chem. Int. Ed.* **2011**, *50*, 12639-12642.
- [85] S. Rösel, J. Becker, W. D. Allen, P. R. Schreiner, *J. Am. Chem. Soc.* **2018**, *140*, 14421-14432.
- [86] L. Rummel, J. M. Schümann, P. R. Schreiner, *Chem. Eur. J.* **2021**, *27*, 13699-13702.
- [87] A. A. Fokin, L. V. Chernish, P. A. Gunchenko, E. Y. Tikhonchuk, H. Hausmann, M. Serafin, J. E. P. Dahl, R. M. K. Carlson, P. R. Schreiner, *J. Am. Chem. Soc.* **2012**, *134*, 13641-13650.
- [88] A. A. Fokin, T. S. Zhuk, S. Blomeyer, C. Pérez, L. V. Chernish, A. E. Pashenko, J. Antony, Y. V. Vishnevskiy, R. J. F. Berger, S. Grimme, C. Logemann, M. Schnell, N. W. Mitzel, P. R. Schreiner, *J. Am. Chem. Soc.* **2017**, *139*, 16696-16707.
- [89] Y. Ishigaki, T. Shimajiri, Y. Kawakami, S. Kawaguchi, Y. Hayashi, K. Hada, T. Suzuki, *Synlett* **2022**, *0*.
- [90] S. Rösel, H. Quanz, C. Logemann, J. Becker, E. Mossou, L. Cañadillas-Delgado, E. Caldeweyher, S. Grimme, P. R. Schreiner, *J. Am. Chem. Soc.* **2017**, *139*, 7428-7431.
- [91] D. Maué, P. H. Strebart, D. Bernhard, S. Rösel, P. R. Schreiner, M. Gerhards, *Angew. Chem. Int. Ed.* **2021**, *60*, 11305-11309.
- [92] F. Holtrop, C. Helling, M. Lutz, K. Van Leest, B. de Bruin, C. Sloatweg, *Synlett*, *0*.
- [93] a) C. Medcraft, S. Zinn, M. Schnell, A. Poblitzki, J. Altnöder, M. Heger, M. A. Suhm, D. Bernhard, A. Stamm, F. Dietrich, M. Gerhards, *Phys. Chem. Chem. Phys.* **2016**, *18*, 25975-25983; b) D. Bernhard, C. Holzer, F. Dietrich, A. Stamm, W. Klopfer, M. Gerhards, *ChemPhysChem* **2017**, *18*, 3634-3641; c) D. Bernhard, F. Dietrich, M. Fatima, C. Perez, A. Poblitzki, G. Jansen, M. A. Suhm, M. Schnell, M. Gerhards, *Phys. Chem. Chem. Phys.* **2017**, *19*, 18076-18088; d) F. Dietrich, D. Bernhard, M. Fatima, C. Pérez, M. Schnell, M. Gerhards, *Angew. Chem. Int. Ed.* **2018**, *57*, 9534-9537; e) D. Bernhard, F. Dietrich, M. Fatima, C. Perez, H. C. Gottschalk, A. Wuttke, R. A. Mata, M. A. Suhm, M. Schnell, M. Gerhards, *Beilstein J. Org. Chem.* **2018**, *14*, 1642-1654.
- [94] D. Bernhard, M. Fatima, A. Poblitzki, A. L. Steber, C. Pérez, M. A. Suhm, M. Schnell, M. Gerhards, *Phys. Chem. Chem. Phys.* **2019**, *21*, 16032-16046.
- [95] M. Fatima, A. L. Steber, A. Poblitzki, C. Pérez, S. Zinn, M. Schnell, *Angew. Chem. Int. Ed.* **2019**, *58*, 3108-3113.
- [96] a) C. Pérez, A. Krin, A. L. Steber, J. C. López, Z. Kiesel, M. Schnell, *J. Phys. Chem. Lett.* **2016**, *7*, 154-160; b) S. Zinn, C. Medcraft, T. Betz, M. Schnell, *Angew. Chem. Int. Ed.* **2016**, *55*, 5975-5980; c) S. R. Domingos, C. Pérez, M. Schnell, *J. Chem. Phys.* **2016**, *145*, 161103; d) C. Pérez, J. C. López, S. Blanco, M. Schnell, *J. Phys. Chem. Lett.* **2016**, *7*, 4053-4058.
- [97] M. M. Quesada Moreno, P. Pinacho, C. Pérez, M. Šekutor, P. R. Schreiner, M. Schnell, *Chem. Eur. J.* **2020**, *26*, 10817-10825.
- [98] M. M. Quesada-Moreno, P. Pinacho, C. Pérez, M. Šekutor, P. R. Schreiner, M. Schnell, *Chem. Eur. J.* **2021**, *27*, 6198-6203.
- [99] A. Poblitzki, H. C. Gottschalk, M. A. Suhm, *J. Phys. Chem. Lett.* **2017**, *8*, 5656-5665.
- [100] B. Hartwig, M. Lange, A. Poblitzki, R. Medel, A. Zehnacker, M. A. Suhm, *Phys. Chem. Chem. Phys.* **2020**, *22*, 1122-1136.
- [101] a) R. Medel, M. A. Suhm, *Phys. Chem. Chem. Phys.* **2020**, *22*, 25538-25551; b) R. Medel, A. Camiruaga, R. T. Saragi, P. Pinacho, C. Pérez, M. Schnell, A. Lesarri, M. A. Suhm, J. A. Fernández, *Phys. Chem. Chem. Phys.* **2021**, *23*, 23610-23624.
- [102] T. Forsting, H. C. Gottschalk, B. Hartwig, M. Mons, M. A. Suhm, *Phys. Chem. Chem. Phys.* **2017**, *19*, 10727-10737.
- [103] a) M. Heger, J. Altnöder, A. Poblitzki, M. A. Suhm, *Phys. Chem. Chem. Phys.* **2015**, *17*, 13045-13052; b) A. Poblitzki, J. Altnöder, M. A. Suhm, *Phys. Chem. Chem. Phys.* **2016**, *18*, 27265-27271; c) H. C. Gottschalk, J. Altnöder, M. Heger, M. A. Suhm, *Angew. Chem. Int. Ed.* **2016**, *55*, 1921-1924; d) C. Zimmermann, T. L. Fischer, M. A. Suhm, *Molecules* **2020**, *25*, 5095; e) C. Zimmermann, H. C. Gottschalk, M. A. Suhm, *Phys. Chem. Chem. Phys.* **2020**, *22*, 2870-2877; f) C. Zimmermann, M. Lange, M. A. Suhm, *Molecules* **2021**, *26*, 4883.

REVIEW

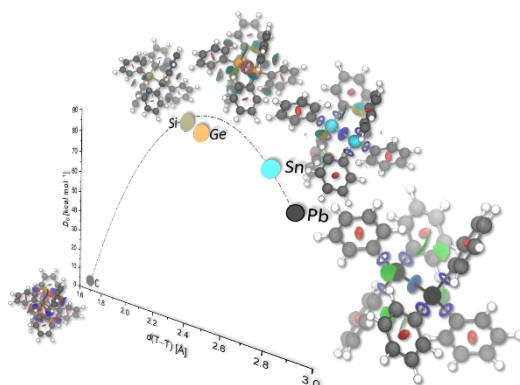
- [104] a) G. Maier, J. Neudert, O. Wolf, D. Pappusch, A. Sekiguchi, M. Tanaka, T. Matsuo, *J. Am. Chem. Soc.* **2002**, *124*, 13819-13826; b) C. F. Matta, J. Hernández-Trujillo, T.-H. Tang, R. F. W. Bader, *Chem. Eur. J.* **2003**, *9*, 1940-1951.
- [105] M.-L. Y. Riu, G. Bistoni, C. C. Cummins, *J. Phys. Chem. A* **2021**, *125*, 6151-6157.
- [106] M.-L. Y. Riu, R. L. Jones, W. J. Transue, P. Müller, C. C. Cummins, *Science Advances* **2020**, *6*, eaaz3168.
- [107] a) S. Winstein, N. J. Holness, *J. Am. Chem. Soc.* **1955**, *77*, 5562-5578; b) F. R. Jensen, C. H. Bushweller, B. H. Beck, *J. Am. Chem. Soc.* **1969**, *91*, 344-351.
- [108] V. Fasano, A. W. McFord, C. P. Butts, B. S. L. Collins, N. Fey, R. W. Alder, V. K. Aggarwal, *Angew. Chem. Int. Ed.* **2020**, *59*, 22403-22407.
- [109] a) H.-J. Schneider, *Acc. Chem. Res.* **2015**, *48*, 1815-1822; b) E. Solel, M. Ruth, P. R. Schreiner, *J. Org. Chem.* **2021**, *86*, 7701-7713.
- [110] a) R. R. Knowles, E. N. Jacobsen, *P. Natl. Acad. Sci. USA* **2010**, *107*, 20678-20685; b) K. T. Mahmudov, A. V. Gurbanov, F. I. Guseinov, M. F. C. Guedes da Silva, *Coordin. Chem. Rev.* **2019**, *387*, 32-46; c) F. Holtrop, K. W. Visscher, A. R. Jupp, J. C. Slootweg, in *Advances in Physical Organic Chemistry*, Vol. 54 (Eds.: I. H. Williams, N. H. Williams), Academic Press, **2020**, pp. 119-141; d) A. Fanourakis, P. J. Docherty, P. Chuentragool, R. J. Phipps, *ACS Catal.* **2020**, *10*, 10672-10714; e) K. L. Mears, P. P. Power, *Acc. Chem. Res.* **2022**, *55*, 1337-1348.
- [111] A. J. Neel, M. J. Hilton, M. S. Sigman, F. D. Toste, *Nature* **2017**, *543*, 637-646.
- [112] a) P. R. Schreiner, A. Wittkopp, *Org. Lett.* **2002**, *4*, 217-220; b) A. Wittkopp, P. R. Schreiner, *Chem. Eur. J.* **2003**, *9*, 407-414; c) P. R. Schreiner, *Chem. Soc. Rev.* **2003**, *32*, 289-296; d) K. M. Lippert, K. Hof, D. Gerbig, D. Ley, H. Hausmann, S. Guenther, P. R. Schreiner, *Eur. J. Org. Chem.* **2012**, *30*, 5919-5927.
- [113] L. Rummel, M. H. J. Domanski, H. Hausmann, J. Becker, P. R. Schreiner, *Angew. Chem. Int. Ed.* **2022**, *n/a*.
- [114] a) S. Singha, M. Buchsteiner, G. Bistoni, R. Goddard, A. Fürstner, *J. Am. Chem. Soc.* **2021**, *143*, 5666-5673; b) M. Buchsteiner, S. Singha, J. Decaens, A. Fürstner, *Angew. Chem. Int. Ed.* **2022**, *61*, e202212546.
- [115] L. P. Wolters, R. Koekkoek, F. M. Bickelhaupt, *ACS Catal.* **2015**, *5*, 5766-5775.
- [116] I. Harden, F. Neese, G. Bistoni, *Chem. Sci.* **2022**, *13*, 8848-8859.
- [117] N. Tsuji, J. L. Kennemur, T. Buyck, S. Lee, S. Prévost, P. S. J. Kaib, D. Bykov, C. Farès, B. List, *Science* **2018**, *359*, 1501-1505.
- [118] M. Marin-Luna, B. Pöllöth, F. Zott, H. Zipse, *Chem. Sci.* **2018**, *9*, 6509-6515.
- [119] B. Pöllöth, M. P. Sibi, H. Zipse, *Angew. Chem. Int. Ed.* **2021**, *60*, 774-778.
- [120] E. J. Corey, R. K. Bakshi, S. Shibata, C. P. Chen, V. K. Singh, *J. Am. Chem. Soc.* **1987**, *109*, 7925-7926.
- [121] a) E. J. Corey, J. O. Link, R. K. Bakshi, *Tetrahedron Lett.* **1992**, *33*, 7107-7110; b) E. J. Corey, C. J. Helal, *Tetrahedron Lett.* **1995**, *36*, 9153-9156; c) E. J. Corey, C. J. Helal, *Angew. Chem. Int. Ed.* **1998**, *37*, 1986-2012.
- [122] A. Altun, M. Garcia-Ratés, F. Neese, G. Bistoni, *Chem. Sci.* **2021**, *12*, 12785-12793.
- [123] a) J. Vondrášek, T. Kubař, F. E. Jenney Jr., M. W. W. Adams, M. Kožišek, J. Černý, V. Sklenář, P. Hobza, *Chem. Eur. J.* **2007**, *13*, 9022-9027; b) R. Sedlák, P. Jurečka, P. Hobza, *J. Chem. Phys.* **2007**, *127*, 075104; c) J. Šponer, K. E. Riley, P. Hobza, *Phys. Chem. Chem. Phys.* **2008**, *10*, 2595-2610; d) O. A. Stasyuk, D. Jakubec, J. Vondrášek, P. Hobza, *J. Chem. Theory Comput.* **2017**, *13*, 877-885.
- [124] a) C. E. Müller, L. Wanka, K. Jewell, P. R. Schreiner, *Angew. Chem. Int. Ed.* **2008**, *47*, 6180-6183; b) C. E. Müller, P. R. Schreiner, *Angew. Chem. Int. Ed.* **2011**, *50*, 6012-6042.
- [125] a) C. E. Müller, D. Zell, R. Hrdina, R. C. Wende, L. Wanka, S. M. M. Schuler, P. R. Schreiner, *J. Org. Chem.* **2013**, *78*, 8465-8484; b) E. Procházková, A. Kolmer, J. Ilgen, M. Schwab, L. Kaltschnee, M. Fredersdorf, V. Schmidts, R. C. Wende, P. R. Schreiner, C. M. Thiele, *Angew. Chem. Int. Ed.* **2016**, *55*, 15754-15759.
- [126] R. C. Wende, A. Seitz, D. Niedek, S. M. M. Schuler, C. Hofmann, J. Becker, P. R. Schreiner, *Angew. Chem. Int. Ed.* **2016**, *55*, 2719-2723.
- [127] a) A. Seitz, R. C. Wende, E. Roesner, D. Niedek, C. Topp, A. C. Colgan, E. M. McGarrigle, P. R. Schreiner, *J. Org. Chem.* **2021**, *86*, 3907-3922; b) A. Seitz, R. Wende, P. R. Schreiner, *Chem. Eur. J.* **2022**, *n/a*.
- [128] J. Gramüller, M. Franta, R. M. Gschwind, *J. Am. Chem. Soc.* **2022**.
- [129] A. C. Colgan, R. S. J. Proctor, D. C. Gibson, P. Chuentragool, A. S. K. Lahdenperä, K. Ermanis, R. J. Phipps, *Angew. Chem. Int. Ed.* **2022**, *61*, e202200266.
- [130] J. Miró, T. Gensch, M. Ellwart, S.-J. Han, H.-H. Lin, M. S. Sigman, F. D. Toste, *J. Am. Chem. Soc.* **2020**, *142*, 6390-6399.
- [131] a) J. Tu, D. Svatoněk, S. Parvez, A. C. Liu, B. J. Levandowski, H. J. Eckvahl, R. T. Peterson, K. N. Houk, R. M. Franzini, *Angew. Chem. Int. Ed.* **2019**, *58*, 9043-9048; b) T. Deb, R. M. Franzini, *Synlett* **2020**, *31*, 938-944.
- [132] L. Pauling, *Nature* **1948**, *161*, 707-709.
- [133] A. A. Kroeger, J. F. Hooper, A. Karton, *ChemPhysChem* **2020**, *21*, 1675-1681.
- [134] A. Karton, *J. Phys. Chem. A* **2020**, *124*, 6977-6985.
- [135] R. Guo, S. Adak, P. Bellotti, X. Gao, W. W. Smith, S. N. Le, J. Ma, K. N. Houk, F. Glorius, S. Chen, M. K. Brown, *J. Am. Chem. Soc.* **2022**, *144*, 17680-17691.
- [136] F. H. John, *Organotransition metal chemistry: from bonding to catalysis*, University Science Books, **2010**.
- [137] a) N. Fey, *Dalton T.* **2010**, *39*, 296-310; b) D. J. Nelson, S. P. Nolan, *Chem. Soc. Rev.* **2013**, *42*, 6723-6753.
- [138] M. Raynal, P. Ballester, A. Vidal-Ferran, P. W. N. M. van Leeuwen, *Chem. Soc. Rev.* **2014**, *43*, 1660-1733.
- [139] a) R. Noyori, *Angew. Chem. Int. Ed.* **2002**, *41*, 2008-2022; b) C. Valente, S. Çalimsiz, K. H. Hoi, D. Mallik, M. Sayah, M. G. Organ, *Angew. Chem. Int. Ed.* **2012**, *51*, 3314-3332; c) G. Lu, C. Fang, T. Xu, G. Dong, P. Liu, *J. Am. Chem. Soc.* **2015**, *137*, 8274-8283.
- [140] I. Kalvet, K. Deckers, I. Funes-Ardoiz, G. Magnin, T. Sperger, M. Kremer, F. Schoenebeck, *Angew. Chem.* **2020**, *132*, 7795-7799.
- [141] a) Y. Zhao, D. G. Truhlar, *Org. Lett.* **2007**, *9*, 1967-1970; b) J. P. Wagner, P. R. Schreiner, *J. Chem. Theory Comput.* **2016**, *12*, 231-237.
- [142] Y. Xi, B. Su, X. Qi, S. Pedram, P. Liu, J. F. Hartwig, *J. Am. Chem. Soc.* **2020**, *142*, 18213-18222.
- [143] M. Marin-Luna, P. Patschinski, H. Zipse, *Chem. Eur. J.* **2018**, *24*, 15052-15058.
- [144] S. Sakai, A. Fujioka, K. Imai, K. Uchiyama, Y. Shimizu, K. Higashida, M. Sawamura, *Adv. Synth. Catal.* **2022**, *364*, 2333-2339.
- [145] M. C. Schwarzer, A. Fujioka, T. Ishii, H. Ohmiya, S. Mori, M. Sawamura, *Chem. Sci.* **2018**, *9*, 3484-3493.
- [146] a) D. Zell, M. Bursch, V. Müller, S. Grimme, L. Ackermann, *Angew. Chem. Int. Ed.* **2017**, *56*, 10378-10382; b) E. Detmar, V. Müller, D. Zell, L. Ackermann, M. Breugst, *Beilstein J. Org. Chem.* **2018**, *14*, 1537-1545.
- [147] T. H. Meyer, W. Liu, M. Feldt, A. Wuttke, R. A. Mata, L. Ackermann, *Chem. Eur. J.* **2017**, *23*, 5443-5447.
- [148] a) D. Ghorai, V. Müller, H. Keil, D. Stalke, G. Zanon, B. A. Tkachenko, P. R. Schreiner, L. Ackermann, *Adv. Synth. Catal.* **2017**, *359*, 3137-3141; b) K. Reinhardt, S. Koller, P. Klein, C. Lossin, J. Gatzka, P. J. Altmann, A. Pöthig, L. Hintermann, *Organometallics* **2022**, *41*, 1-19.
- [149] T. G. Saint-Denis, N. Y. S. Lam, N. Chekshin, P. F. Richardson, J. S. Chen, J. Ellerass, K. D. Hesp, D. C. Schmitt, Y. Lian, C. W. Huh, J.-Q. Yu, *ACS Catal.* **2021**, *11*, 9738-9753.
- [150] a) A. Changotra, B. Bhaskararao, C. M. Hadad, R. B. Sunoj, *J. Am. Chem. Soc.* **2020**, *142*, 9612-9624; b) H. Xu, B. Li, Z. Liu, Y. Dang, *ACS Catal.* **2021**, *11*, 9008-9021; c) B. Li, H. Xu, Y. Dang, K. N. Houk, *J. Am. Chem. Soc.* **2022**, *144*, 1971-1985.
- [151] S. Meninno, M. Meazza, J. W. Yang, T. Tejero, P. Merino, R. Rios, *Chem. Eur. J.* **2019**, *25*, 7623-7627.

REVIEW

- [152] S. M. Maley, R. Steagall, G. R. Lief, R. M. Buck, Q. Yang, O. L. Sydora, S. M. Bischof, D. H. Ess, *Organometallics* **2022**, *41*, 581-593.
- [153] a) M. Paul, M. Breugst, J.-M. Neudörfl, R. B. Sunoj, A. Berkessel, *J. Am. Chem. Soc.* **2016**, *138*, 5044-5051; b) V. R. Yatham, W. Harnying, D. Kootz, J.-M. Neudörfl, N. E. Schlörer, A. Berkessel, *J. Am. Chem. Soc.* **2016**, *138*, 2670-2677; c) M. Paul, P. Sudkaow, A. Wessels, N. E. Schlörer, J.-M. Neudörfl, A. Berkessel, *Angew. Chem. Int. Ed.* **2018**, *57*, 8310-8315; d) M. Paul, J.-M. Neudörfl, A. Berkessel, *Angew. Chem. Int. Ed.* **2019**, *58*, 10596-10600; e) W. Harnying, J.-M. Neudörfl, A. Berkessel, *Org. Lett.* **2020**, *22*, 386-390; f) W. Harnying, P. Sudkaow, A. Biswas, A. Berkessel, *Angew. Chem. Int. Ed.* **2021**, *60*, 19631-19636.
- [154] L. P. Ho, A. Nasr, P. G. Jones, A. Altun, F. Neese, G. Bistoni, M. Tamm, *Chem. Eur. J.* **2018**, *24*, 18922-18932.
- [155] P. Šliwa, M. P. Mitoraj, F. Sagan, J. Handzlik, *J. Mol. Model.* **2019**, *25*, 331.
- [156] A. Hamza, D. Mook, C. Schlepffhorst, J. Schneidewind, W. Baumann, F. Glorius, *Chem. Sci.* **2022**, *13*, 985-995.
- [157] D. E. Koshland, *P. Natl. Acad. Sci. USA* **1958**, *44*, 98.
- [158] D. Yepes, F. Neese, B. List, G. Bistoni, *J. Am. Chem. Soc.* **2020**, *142*, 3613-3625.
- [159] N. I. Saper, A. Ohgi, D. W. Small, K. Semba, Y. Nakao, J. F. Hartwig, *Nat. Chem.* **2020**, *12*, 276-283.
- [160] D. Baek, H. Ryu, J. Y. Ryu, J. Lee, B. M. Stoltz, S. Hong, *Chem. Sci.* **2020**, *11*, 4602-4607.
- [161] L. R. Andreola, S. E. Wheeler, *Org. Chem. Front.* **2022**, *9*, 3027-3033.

2. Publications

2.1 Hexaphenylditetrels – When Longer Bonds Provide Higher Stability



Abstract:

We present a computational analysis of hexaphenylethane derivatives with heavier tetrels comprising the central bond. In stark contrast to parent hexaphenylethane, the heavier tetrel derivatives can readily be prepared. In order to determine the origin of their apparent thermodynamic stability against dissociation as compared to the carbon case, we employed local energy decomposition analysis (LED) and symmetry-adapted perturbation theory (SAPT) at the DLPNO-CCSD(T)/def2-TZVP and sSAPT0/def2-TZVP levels of theory. We identified London dispersion (LD) interactions as the decisive factor for the molecular stability of heavier tetrel derivatives. This stability is made possible owing to the longer (than C–C) central bonds that move the phenyl groups out of the heavily repulsive regime so they can optimally benefit from LD interactions.

Reference:

Lars Rummel, Jan M. Schümann, and Peter R. Schreiner, *Chem. Eur. J.* **2021**, *27*, 13699-13702. DOI: 10.1002/chem.202102271

Highlight:

When Longer Bonds Provide Higher Stability, *Chemistry Views*, **2021**. (https://www.chemistryviews.org/details/ezone/11318599/When_Longer_Bonds_Provide_Higher_Stability/)

Reproduced with permission from:

© 2021, John Wiley & Sons, Inc.
111 River Street
Hoboken, NJ, 07030-5774
United States of America


Hexaphenylditetrels – When Longer Bonds Provide Higher Stability
Lars Rummel^{+, [a]}, Jan M. Schümann^{+, [a]} and Peter R. Schreiner^{*, [a]}

Abstract: We present a computational analysis of hexaphenylethane derivatives with heavier tetrels comprising the central bond. In stark contrast to parent hexaphenylethane, the heavier tetrel derivatives can readily be prepared. In order to determine the origin of their apparent thermodynamic stability against dissociation as compared to the carbon case, we employed local energy decomposition analysis (LED) and symmetry-adapted perturbation theory (SAPT) at the DLPNO-CCSD(T)/def2-TZVP and sSAPT0/def2-TZVP levels of theory. We identified London dispersion (LD) interactions as the decisive factor for the molecular stability of heavier tetrel derivatives. This stability is made possible owing to the longer (than C–C) central bonds that move the phenyl groups out of the heavily repulsive regime so they can optimally benefit from LD interactions.

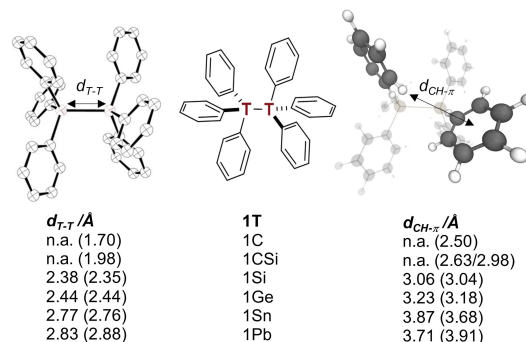


Figure 1. S_6 -symmetric hexaphenylditetrel structure **1T** (center), X-ray structure (left), and corresponding computed hexaphenylditetrel structure with highlighted $d_{CH-\pi}$ contact at B3LYP-D3(BJ)/def2-TZVP (right). First numbers are experimental distances, numbers in parentheses correspond to the computations.

While long sought-after hexaphenylethane^[1] (**1C**, Figure 1, the letter T designates the tetrel) remains elusive^[2] (trityl radicals dimerize in a head-to-tail fashion),^[3] its higher tetrel congeners with T = CSi,^[4] Si,^[5] Ge,^[6] Sn,^[7] and Pb^[8] have been known for a long time. What makes the latter stable under ambient conditions even though the higher tetrel-tetrel single bond energies decrease rapidly as one goes down group 14?

The Pb–Pb bond dissociation energy (BDE) of hexamethyldiplumbane is 22.5 kcal mol^{−1} lower than that of the central C–C bond in “hexamethylethane” (2,2,3,3-tetramethylbutane, BDE = 77.1 ± 1.0 kcal mol^{−1}),^[9] in line with the expectations of bond energies down a group in the periodic table.^[10] The opposite is observed for hexaphenylditetrels **1T** and parent **1C** has not been reported experimentally. Only some highly substituted derivatives utilizing dispersion energy donors^[11] (DED) such as *t*-butyl groups in the all-*meta* positions of **1C** can

be observed,^[2b,12] thereby emphasizing the notion of stabilizing London dispersion (LD) interactions.^[13] As the higher tetrel derivatives do not need additional DED groups to be isolable, but intrinsically have higher T–T BDEs than **1C**, one asks what makes these compounds stable toward central T–T bond dissociation. Note that some derivatives with T=Sn are extraordinarily stable, even up to 235 °C.^[14] The first equilibrium measurement of a **1Sn** derivative was with the phenyl groups equipped with 2,4,6-trimethyl and triethyl substituents. The onset of dissociation as measured through the presence of EPR signals of the “hetero-Gomberg-type” radicals was found at 180 and 100 °C for these derivatives, respectively.^[15]

Even though there is no physical basis, there is a well-accepted principle in organic chemistry that longer bonds are assumed to be weaker and therefore dissociate more easily.^[16] While this simple diatomic model-derived concept has been investigated and confirmed for large series of molecules, it cannot explain the discrepancy in thermodynamic stabilities of the hexaphenylditetrels **1T**. Especially for large structures (i.e., far beyond diatomics), the transferability of this concept is questionable.^[17] Prominent examples are the phosphine-metal dissociation energies of Grubbs catalysts with sterically demanding N-heterocyclic carbene ligands^[18] and 2-(1-diamantyl)-[121]tetramantane with a bond length of 1.71 Å but a sizeable BDE of around +36 kcal mol^{−1}.^[19]

As studies highlight that the noncovalent van-der-Waals benzene dimers are stabilized by LD interactions,^[20] we hypothesized that such interactions may be responsible for the

[a] L. Rummel,⁺ J. M. Schümann,⁺ Prof. Dr. P. R. Schreiner
Institute of Organic Chemistry
Justus Liebig University
Heinrich-Buff-Ring 17, 35392 Giessen (Germany)
E-mail: prs@uni-giessen.de

[*] These authors contributed equally to this work.

Supporting information for this article is available on the WWW under <https://doi.org/10.1002/chem.202102271>



Part of a Special Collection on Noncovalent Interactions.

© 2021 The Authors. Chemistry - A European Journal published by Wiley-VCH GmbH. This is an open access article under the terms of the Creative Commons Attribution License, which permits use, distribution and reproduction in any medium, provided the original work is properly cited.

stabilities of the higher 1T structures as well. But why does this apparently not provide sufficient stabilization for 1C?

We began our computational study with the crystal structure geometries for gas phase optimizations. Following the theoretical treatment of Rösel et al.^[26] we utilized the well-established B3LYP^[21] and M06-2X^[22] functionals for direct comparisons with existing data and because they are commonly employed. Ahlrich's def2-TZVP basis set^[23] was used for all computations. B3LYP was used with the Becke-Johnson (BJ) damped dispersion D3 correction of Grimme et al.^[24] First and foremost, the optimized structures are in good agreement with the experimental structures (Figure 1 and Figures S2–S5, Table S10). All phenyl moieties are arranged in an off-set T-shape manner with CH– π contacts with the opposite trityl group. The computed dimerization energy of the triphenylmethyl radical is endergonic ($\Delta G_{\text{dim}}^{298} = +11.8 \text{ kcal mol}^{-1}$) and agrees with the results of previous studies.^[26] Both the B3LYP-D3(BJ) and M06-2X results show the same trends. Due to a lack of experimental dissociation energies for the unsubstituted 1T, we validated our method by comparing dissociation energies of $\text{H}_3\text{T}-\text{TH}_3$ as well as $\text{Me}_3\text{T}-\text{TMe}_3$ that agree well with experimental values within their error bounds (Tables S1–S3, Figure S1).

Whereas the carbon-based hexaphenylditetrel readily dissociates into its monomers ($\Delta G_{\text{dim}}^{298} > 0$), the higher tetrel derivatives all display $\Delta G_{\text{dim}}^{298} < 0$ up to $-70 \text{ kcal mol}^{-1}$ (Figure 2). The reason behind the dissociation of 1C can only be explained by Pauli (exchange) repulsion that has a very steep distance dependence, outweighing LD interactions, in line with the notion of excessive steric hindrance. Due to close intramolecular contacts of the aromatic moieties, hexaphenylethane 1C cannot persist at 298 K (the computed shortest contact $d_{\text{CH}-\pi}$ in 1C is around 2.5 \AA). However, as higher tetrels display significantly longer central bonds, this leads to an increase of the CH– π contact distances (the computed $d_{\text{CH}-\pi}$ in 1Si is

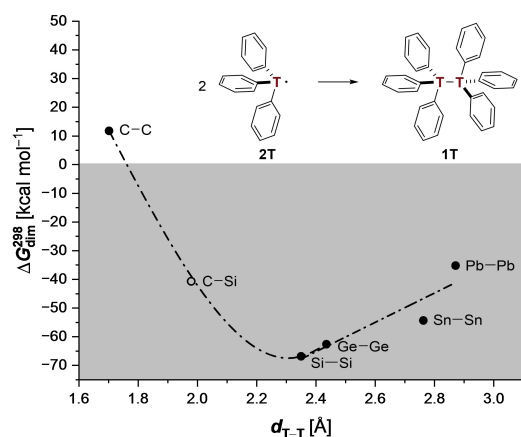


Figure 2. Correlation of distance $d_{\text{T}-\text{T}}$ [Å] of the central tetrel bond with the computed Gibbs free energies $\Delta G_{\text{dim}}^{298}$ [kcal mol⁻¹] for the depicted dimerization reaction. Computations at the B3LYP-D3(BJ)/def2-TZVP level of theory. The dashed line is used to guide the eye.

around 3.1 \AA , Figure 1). In comparison, the CH– π distance in the crystal lattice of benzene at 270 K is around 2.9 \AA .^[25]

To investigate the origin of the somewhat counterintuitive stabilities of the higher tetrel congeners, we visualized all intramolecular interactions using non-covalent interaction plots (NCI plots, Figure 3) for T=C vs. Pb.^[26] Hereby, strongly attractive and repulsive interactions are visualized as blue and red isosurfaces, respectively. Green areas indicate weak molecular contacts predominantly evoked by LD interactions.

A comparison of the NCI-plots reveals strong repulsions (red) and strong attractions (blue) but no “weak” interactions (green) in 1C between the two molecular halves. The opposite is observed for 1Pb (with the same drawing cut-offs) that clearly shows a green isosurface orthogonal to the central bond, emanating from the phenyl substituents.

Another approach for assessing the LD contributions is through splitting the central tetrel bond and analyzing the interactions between the two resulting fragments via a Local Energy Decomposition (LED) analysis^[27] as implemented in ORCA (Version 4.1.2).^[28] As a consequence of this approach, two radical fragments interact at short range, resulting in large electrostatic interactions. Hence, in this analysis we focus only on the magnitude of the LD interactions evoked by three phenyl-phenyl CH– π contacts (Figure 4). According to this analysis, 1C benefits from the highest LD contribution, while all higher congeners are LD-stabilized by a remarkably similar amount around $20 \pm 5 \text{ kcal mol}^{-1}$ for T \neq C. That is, the instability of 1C is not due to an insufficient LD stabilization but must lie in the massive growth of steric repulsion at short distance (see above). Vice versa, the lengthening of the central T–T bonds reduces Pauli repulsion more than dispersion so that an overall stabilization results.

In addition to the LED analysis, we utilized a homodesmotic equation^[29] (Figure 5) to determine the overall relative thermodynamic stabilities of 1T. Thereby, we aimed at isolating the amount of LD due to the three pairwise phenyl-phenyl contacts excluding the central tetrel interactions through calculating $\Delta\Delta E_{\text{disp}} = \Delta G(\text{B3LYP-D3(BJ)}) - \Delta G(\text{B3LYP})$.

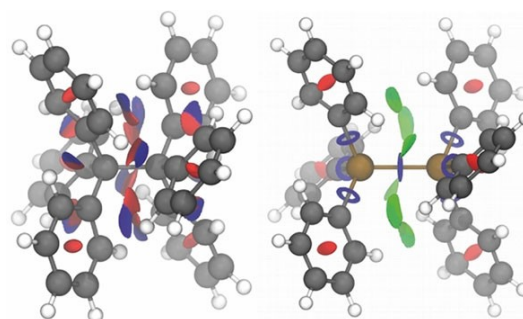


Figure 3. Non-covalent interaction (NCI) plots of hexaphenylethane 1C (left) and the hexaphenyldiplumbane 1Pb compound (right) at the B3LYP-D3(BJ)/def2-TZVP level of theory. Isosurfaces are colored on a blue-green-red scale according to an isovalue $s(\rho)$ of 0.2, ranging from $\rho(r) = -2 \text{ a.u.}$ to $+2 \text{ a.u.}$. Blue indicates strong attractive interactions, green corresponds to weak NCI, and red indicates strong repulsion.

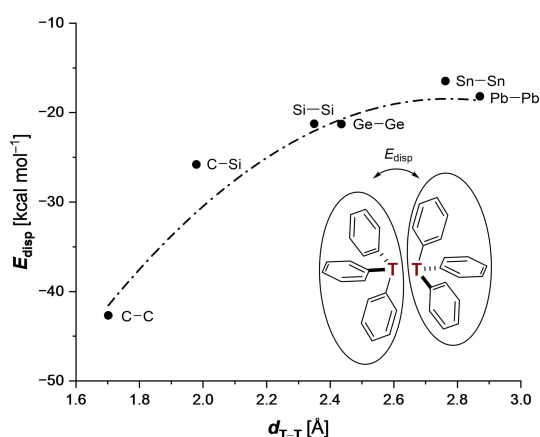


Figure 4. LED analysis of two trityl monomer singlet radicals in their dimer geometry at DLPNO-CCSD(T)/def2-TZVP//B3LYP-D3(BJ)/def2-TZVP. The dashed line is used to guide the eye.

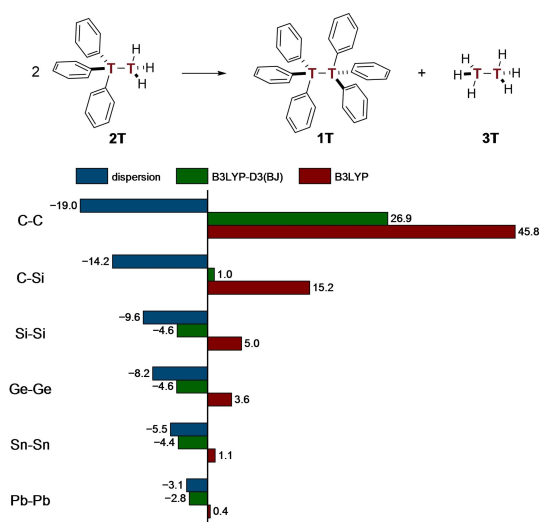


Figure 5. Homodesmotic equation with free energies (ΔG_{298}) given in kcal mol^{-1} at the B3LYP-D3(BJ)/def2-TZVP level of theory.

The DFT computations not including LD suggest that the presence of all six phenyl groups within one molecule (1T) is highly unfavorable relative to distributing them across two triphenylditetrels 2T. This picture would support the widespread notion of the predominance of steric hindrance. The elongation of the central tetrel bond entails a rapid decrease in repulsive energy from $\sim 46 \text{ kcal mol}^{-1}$ in 1C to only $0.4 \text{ kcal mol}^{-1}$ in 1Pb. Additionally, inclusion of LD, estimated from the value of the D3 correction, stabilizes all structures. Even though 1C is stabilized most, LD cannot outbalance the strong repulsions, leading to an overall thermodynamically unstable structure. As repulsion reduces upon central bond

elongation, all other tetrel derivatives beyond 1C are stabilized overall. Whereas mixed 1CSi is thermo-neutral in terms of LD and electron-electron repulsion, higher tetrel derivatives are stable due to LD that falls off less rapidly than Pauli repulsion. Consequently, LD interactions are most effective in the tetrel derivative with the longest bond (1Pb) where the total energy for this equation is comprised of 90% LD interactions.

As most recently demonstrated by Herbert and Carter-Fenk,^[20c] LD interactions and Pauli repulsion are the dominant factor in the noncovalent dimerization process of two benzene molecules, with the electrostatic component essentially being sidelined.^[20a,b,27a,30] Within the series of hexaphenylditetrels the phenyl moieties adopt an off-set T-shaped geometry to optimized these two dominant interactions. This supports our findings since 1Si is the most stable hexaphenylditetrel with an off-set $\text{CH}-\pi$ distance of 3.1 \AA . In order to qualitatively evaluate the dispersion energy deriving from phenyl moieties, we also employed a symmetry-adapted perturbation theory (SAPT) analysis.^[31] The scaled protocol was utilized to improve performance of the SAPT computations according to Parker et al.^[32] Hereby, we focus on the interaction between benzene dimers.^[33] We took the B3LYP-D3(BJ)/def2-TZVP optimized geometries, removed the tetrels, and saturated the resulting phenyl radicals with hydrogen atoms in order to avoid open-shell configurations^[34] (Figure 6). The total interaction energy (black) shows an energy minimum at a central bond distance $d_{\text{Si-Si}}$ of around 2.3 \AA . The carbon derivative with a $d_{\text{C-C}}$ of 1.7 \AA is again the only thermodynamically unstable 1T due to the large Pauli exchange repulsion term (red). All other structures are situated within the attractive part of the diagram. While LD interactions (green) are the main attractive component, electrostatics (blue) as well as induction (brown) also favor the dimerization process.

Our findings utilizing various interaction analyses and a homodesmotic equation are well in line with the conceptually simple but very useful r^{-12} repulsive and r^{-6} LD^[13a] attractive (12,6)-Lennard-Jones type potential of the noncovalent inter-

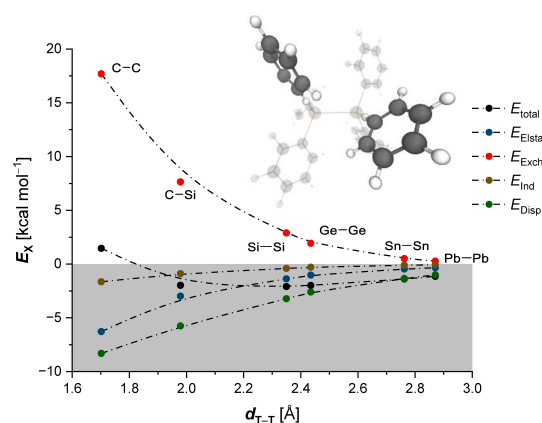


Figure 6. sSAPT analysis of two benzene monomers in geometry of the hexaphenylditetrels, $d_{\text{T-T}}$ corresponds to the central tetrel bond. Computations at the sSAPTO/def2-TZVP level of theory.

action distance. The much steeper repulsive potential may have led to the general notion in structural chemistry that repulsion may be more important overall, which is not true. As a consequence, hexaphenyldisilane (**15i**) is the most stable parent hexaphenylditetrel derivative.

As we demonstrate here, there is a fine interplay of attraction and repulsion in molecular structures; naturally, that is why they are called “equilibrium structures.” As repulsion decreases rapidly with distance, LD is the most important stabilizing factor. The often invoked principle that longer bonds are to be weaker^[16] does not have to be true^[35] in the presence of additional interactions around the bonds in question. In the cases shown here this means that depending on the length of the central tetrel bond the phenyl groups can have a stabilizing or destabilizing effect on the structures. Hence, the high stability of the compounds with longer bonds is made possible through the assistance of LD interactions of the phenyl groups.

Acknowledgments

This work was supported by the priority program “Control of London Dispersion in Molecular Chemistry” (SPP1807) of the Deutsche Forschungsgemeinschaft. We thank Dennis Gerbig for technical assistance and Bastian Bernhardt for fruitful discussions. Open Access funding enabled and organized by Projekt DEAL.

Conflict of Interest

The authors declare no conflict of interest.

Keywords: bond dissociation energy · bond strength · C–H- π -interactions · London dispersion · Pauli repulsion

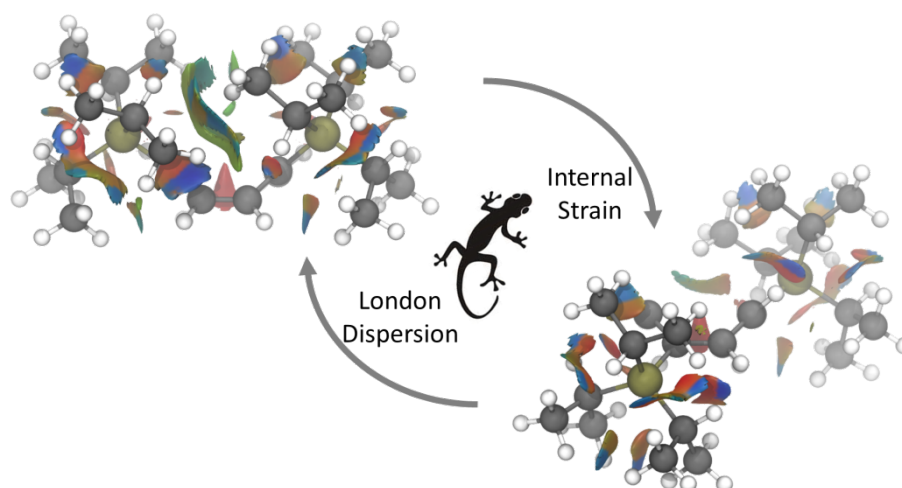
- [1] a) M. Gombert, *Ber. Dtsch. Chem. Ges.* **1900**, *33*, 3150–3163; b) M. Gombert, *J. Am. Chem. Soc.* **1900**, *22*, 757–771.
 [2] a) S. Grimme, P. R. Schreiner, *Angew. Chem. Int. Ed.* **2011**, *50*, 12639–12642; *Angew. Chem.* **2011**, *123*, 12849–12853; b) S. Rösel, C. Balestrieri, P. R. Schreiner, *Chem. Sci.* **2017**, *8*, 405–410.
 [3] a) P. Jacobson, *Ber. Dtsch. Chem. Ges.* **1905**, *38*, 196–199; b) H. Lankamp, W. T. Nauta, C. MacLean, *Tetrahedron Lett.* **1968**, *9*, 249–254.
 [4] A. Brook, H. Gilman, L. Miller, *J. Am. Chem. Soc.* **1953**, *75*, 4759–4765.
 [5] a) W. Schlenk, J. Renning, G. Racky, *Ber. Dtsch. Chem. Ges.* **1911**, *44*, 1178–1182; b) H. Gilman, G. Dunn, *J. Am. Chem. Soc.* **1951**, *73*, 5077–5079; c) T. Bernert, B. Winkler, Y. Krysiak, L. Fink, M. Berger, E. Alig, L. Bayarjargal, V. Milman, L. Ehm, P. W. Stephens, N. Auner, H.-W. Lerner, *Cryst. Growth Des.* **2014**, *14*, 2937–2944.
 [6] a) G. T. Morgan, H. D. K. Drew, *J. Chem. Soc. Trans.* **1925**, *127*, 1760–1768; b) P. Selwood, *J. Am. Chem. Soc.* **1939**, *61*, 3168–3169; c) M. Dräger, L. Ross, *Z. Anorg. Allg. Chem.* **1980**, *460*, 207–216.
 [7] a) E. Krause, R. Becker, *Ber. Dtsch. Chem. Ges.* **1920**, *53*, 173–190; b) H. Morris, W. Byerly, P. Selwood, *J. Am. Chem. Soc.* **1942**, *64*, 1727–1729; c) H. Preut, H. J. Haupt, F. Huber, *Z. Anorg. Allg. Chem.* **1973**, *396*, 81–89; d) H. Piana, U. Kirchgäßner, U. Schubert, *Chem. Ber.* **1991**, *124*, 743–751; e) D. Dakternieks, F. Sheen Kuan, A. Duthie, E. R. T. Tiekink, *Main Group Met. Chem.* **2001**, *24*, 65–66; f) J. O. Bauer, *Main Group Met. Chem.* **2020**, *43*, 1–6.
 [8] a) E. Krause, G. G. Reißaus, *Ber. Dtsch. Chem. Ges.* **1922**, *55*, 888–902; b) R. Preckel, P. Selwood, *J. Am. Chem. Soc.* **1940**, *62*, 2765–2766; c) H.

- Preut, H. Haupt, F. Huber, *Z. Anorg. Allg. Chem.* **1972**, *388*, 165–168; d) H. Preut, F. Huber, *Z. Anorg. Allg. Chem.* **1976**, *419*, 92–96.
 [9] W. M. Haynes, *Handbook of Chemistry and Physics*, 97th ed. CRC Press, Cleveland, Ohio, **2016–2017**, p. 84.
 [10] G. Frenking, S. Shaik, *The Chemical Bond: Chemical Bonding Across the Periodic Table*, Vol. 2, John Wiley & Sons, **2014**.
 [11] S. Grimme, R. Huenerbein, S. Ehrlich, *ChemPhysChem* **2011**, *12*, 1258–1261.
 [12] a) M. Stein, W. Winter, A. Rieker, *Angew. Chem. Int. Ed.* **1978**, *17*, 692–694; *Angew. Chem.* **1978**, *90*, 737–738; b) B. Kahr, D. Van Engen, K. Mislou, *J. Am. Chem. Soc.* **1986**, *108*, 8305–8307; c) S. Rösel, J. Becker, W. D. Allen, P. R. Schreiner, *J. Am. Chem. Soc.* **2018**, *140*, 14421–14432.
 [13] a) F. London, *Z. Phys.* **1930**, *63*, 245–279; b) F. London, *Trans. Faraday Soc.* **1937**, *33*, 8b–26; c) J. P. Wagner, P. R. Schreiner, *Angew. Chem. Int. Ed.* **2015**, *54*, 12274–12296; *Angew. Chem.* **2015**, *127*, 12446–12471; d) D. J. Liptrot, P. P. Power, *Nat. Chem. Rev.* **2017**, *1*, 0004.
 [14] E. J. Bulten, H. A. Budding, J. G. Noltes, *J. Organomet. Chem.* **1970**, *22*, C5–C6.
 [15] a) H. U. Buschhaus, W. P. Neumann, *Angew. Chem. Int. Ed.* **1978**, *17*, 59–59; *Angew. Chem.* **1978**, *90*, 74–74; b) H.-U. Buschhaus, W. P. Neumann, T. Apoussidis, *Liebigs Ann. Chem.* **1981**, *1981*, 1190–1197.
 [16] A. A. Zavitsas, *J. Phys. Chem. A* **2003**, *107*, 897–898.
 [17] P. R. Schreiner, L. V. Chernish, P. A. Gunchenko, E. Y. Tikhonchuk, H. Hausmann, M. Serafin, S. Schlecht, J. E. P. Dahl, R. M. K. Carlson, A. A. Fokin, *Nature* **2011**, *477*, 308–311.
 [18] Y. Zhao, D. G. Truhlar, *Org. Lett.* **2007**, *9*, 1967–1970.
 [19] A. A. Fokin, L. V. Chernish, P. A. Gunchenko, E. Y. Tikhonchuk, H. Hausmann, M. Serafin, J. E. P. Dahl, R. M. K. Carlson, P. R. Schreiner, *J. Am. Chem. Soc.* **2012**, *134*, 13641–13650.
 [20] a) M. O. Sinnokrot, C. D. Sherrill, *J. Phys. Chem. A* **2006**, *110*, 10656–10668; b) S. E. Wheeler, *J. Am. Chem. Soc.* **2011**, *133*, 10262–10274; c) K. Carter-Fenk, J. M. Herbert, *Chem. Sci.* **2020**, *11*, 6758–6765.
 [21] a) A. D. Becke, *J. Chem. Phys.* **1993**, *98*, 5648–5652; b) C. Lee, W. Yang, R. Parr, *Phys. Rev. B* **1988**, *37*, 785–789.
 [22] a) Y. Zhao, D. G. Truhlar, *Theor. Chem. Acc.* **2008**, *120*, 215–241; b) D. Josa, J. Rodríguez-Otero, E. M. Cabaleiro-Lago, M. Rellán-Piñeiro, *Chem. Phys. Lett.* **2013**, *557*, 170–175.
 [23] A. Schäfer, C. Huber, R. Ahlrichs, *J. Chem. Phys.* **1994**, *100*, 5829–5835.
 [24] a) S. Grimme, J. Antony, S. Ehrlich, H. Krieg, *J. Chem. Phys.* **2010**, *132*, 154104; b) S. Grimme, S. Ehrlich, L. Goerigk, *J. Comput. Chem.* **2011**, *32*, 1456–1465.
 [25] a) E. G. Cox, J. A. S. Smith, *Nature* **1954**, *173*, 75–75; b) E. G. Cox, D. W. J. Cruickshank, J. A. S. Smith, *Proc. R. Soc. London Ser. A* **1958**, *247*, 1–21.
 [26] a) E. R. Johnson, S. Keinan, P. Mori-Sánchez, J. Contreras-García, A. J. Cohen, W. Yang, *J. Am. Chem. Soc.* **2010**, *132*, 6498–6506; b) J. Contreras-García, E. R. Johnson, S. Keinan, R. Chaudret, J.-P. Piquemal, D. N. Beratan, W. Yang, *J. Chem. Theory Comput.* **2011**, *7*, 625–632.
 [27] a) W. B. Schneider, G. Bistoni, M. Sparta, M. Saitow, C. Riplinger, A. A. Auer, F. Neese, *J. Chem. Theory Comput.* **2016**, *12*, 4778–4792; b) A. Altun, F. Neese, G. Bistoni, *J. Chem. Theory Comput.* **2018**, *15*, 215–228; c) A. Altun, M. Saitow, F. Neese, G. Bistoni, *J. Chem. Theory Comput.* **2019**, *15*, 1616–1632.
 [28] a) F. Neese, *WIREs Comput. Mol. Sci.* **2012**, *2*, 73–78; b) F. Neese, *WIREs Comput. Mol. Sci.* **2018**, *8*, e1327.
 [29] a) S. E. Wheeler, K. N. Houk, P. v. R. Schleyer, W. D. Allen, *J. Am. Chem. Soc.* **2009**, *131*, 2547–2560; b) J. P. Wagner, P. R. Schreiner, *J. Chem. Theory Comput.* **2016**, *12*, 231–237.
 [30] M. Linnemannstöns, J. Schwabedissen, A. A. Schultz, B. Neumann, H.-G. Stämmler, R. J. F. Berger, N. W. Mitzel, *Chem. Commun.* **2020**, *56*, 2252–2255.
 [31] K. Szalewicz, *WIREs Comput. Mol. Sci.* **2012**, *2*, 254–272.
 [32] T. M. Parker, L. A. Burns, R. M. Parrish, A. G. Ryno, C. D. Sherrill, *J. Chem. Phys.* **2014**, *140*, 094106.
 [33] C. D. Sherrill, *Acc. Chem. Res.* **2013**, *46*, 1020–1028.
 [34] J. Hwang, P. Li, M. D. Smith, C. E. Warden, D. A. Sirianni, E. C. Vik, J. M. Maier, C. J. Yehl, C. D. Sherrill, K. D. Shimizu, *J. Am. Chem. Soc.* **2018**, *140*, 13301–13307.
 [35] M. Kaupp, B. Metz, H. Stoll, *Angew. Chem. Int. Ed.* **2000**, *39*, 4607–4609; *Angew. Chem.* **2000**, *112*, 4780–4782.

Manuscript received: June 25, 2021

Version of record online: August 6, 2021

2.2 Gauging the Steric Effects of Silyl Groups with a Molecular Balance



Abstract:

We present an experimental and computational study of a cyclooctatetraene (COT)-based molecular balance disubstituted with commonly used silyl groups. Such groups often serve as protecting groups and are typically considered innocent bystanders. Our motivation here is to determine the actual steric effects of such groups by employing a molecular balance. While in the unfolded 1,4-valence isomer the silyl groups are far apart ($d_{\sigma-\sigma} \geq 5.15 \text{ \AA}$), the folded 1,6-isomer is affected greatly by noncovalent interactions due to close $\sigma-\sigma$ contacts ($d_{\sigma-\sigma} \leq 2.58 \text{ \AA}$). In order to investigate the thermodynamic equilibrium between the 1,6- and 1,4-valence isomers, we employed temperature-dependent nuclear magnetic resonance measurements. Additionally, we assessed the nature of attractive and repulsive interactions in 1,6-disilyl-COT derivatives *via* a combination of local energy decomposition analysis (LED) and symmetry-adapted perturbation theory (SAPT) at the DLPNO-CCSD(T)/def2-TZVP and sSAPT0/aug-cc-pVDZ levels of theory. We identified London dispersion interactions as the main contributor to the molecular stability of the folded states, whereas Pauli exchange repulsion and a resulting internal strain favor the unfolded diastereomer.

Reference:

Henrik F. König, Lars Rummel, Heike Hausmann, Jonathan Becker, Jan M. Schümann, and Peter R. Schreiner, *J. Org. Chem.* **2022**, *87*, 7, 4670–4679. DOI: 10.1021/acs.joc.1c03103

Reproduced with permission from:

© 2022, American Chemical Society
1155 16th Street NW
Washington, DC, 20036
United States of America

Gauging the Steric Effects of Silyl Groups with a Molecular Balance

Henrik F. König,[§] Lars Rummel,[§] Heike Hausmann, Jonathan Becker, Jan M. Schümann, and Peter R. Schreiner*

Cite This: *J. Org. Chem.* 2022, 87, 4670–4679

Read Online

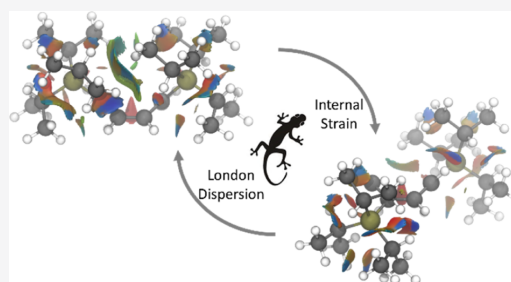
ACCESS |

Metrics & More

Article Recommendations

Supporting Information

ABSTRACT: We present an experimental and computational study of a cyclooctatetraene (COT)-based molecular balance disubstituted with commonly used silyl groups. Such groups often serve as protecting groups and are typically considered innocent bystanders. Our motivation here is to determine the actual steric effects of such groups by employing a molecular balance. While in the unfolded 1,4-valence isomer the silyl groups are far apart ($d_{\sigma-\sigma} \geq 5.15$ Å), the folded 1,6-isomer is affected greatly by noncovalent interactions due to close $\sigma-\sigma$ contacts ($d_{\sigma-\sigma} \leq 2.58$ Å). In order to investigate the thermodynamic equilibrium between the 1,6- and 1,4-valence isomers, we employed temperature-dependent nuclear magnetic resonance measurements. Additionally, we assessed the nature of attractive and repulsive interactions in 1,6-disilyl-COT derivatives via a combination of local energy decomposition analysis (LED) and symmetry-adapted perturbation theory (SAPT) at the DLPNO-CCSD(T)/def2-TZVP and sSAPT0/aug-cc-pVDZ levels of theory. We identified London dispersion interactions as the main contributor to the molecular stability of the folded states, whereas Pauli exchange repulsion and a resulting internal strain favor the unfolded diastereomer.



INTRODUCTION

Silyl groups often are conveniently employed to transform, for example, “reactive” hydroxyl groups to “unreactive” silyl ethers.^{1,2} These groups enjoy great popularity due to their commercial availability, simple attachment, as well as mild and selective detachment procedures. Such silyl-protecting groups are commonly chosen on the basis of their stability under typically neutral or basic reaction conditions. The bulkiness of silyl-protecting groups is mostly considered only with regards to selective cleavability.³ The use of abbreviations such as TPS (triphenylsilyl) further obfuscates the spatial demand of such groups. However, attaching bulky silyl-protecting groups to a flexible backbone can significantly alter conformational preferences and hence the stereoelectronic properties of a system. This is highlighted by so-called “super-armed” glycosyl donors, for which exclusive protection with bulky silyl ethers enforces an all-axial conformation.^{4,5} As a consequence, this results in a reactivity increase by more than an order of magnitude in comparison to the benzylated derivatives.^{4,5} Clearly, bulkiness is an important feature of the most frequently utilized silyl-protecting groups, but this fact is often not given much attention. Consequently, only a few efforts have been made to quantify the steric demand of such groups.^{6–8}

In recent years, the role of London dispersion (LD) interactions^{9–12} as a decisive structural factor for conformational preferences and transition structures emerged in a variety of molecular systems.^{13–19} Because LD interactions are

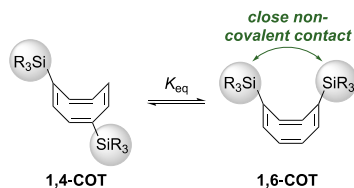
approximately additive pairwise interactions, it is clear that large alkyl and silyl groups must be more than just providers of steric bulk. While LD interactions between alkyl groups, allegedly, are capable of facilitating labile compounds such as hexaphenylethane^{20–23} or coupled diamondoids²⁴ by offering intramolecular stabilization, the effects of commonly utilized silyl groups have not been studied in detail. Apart from intramolecular noncovalent interactions, intermolecular stabilization via silyl groups, that is, in transition structures, can be of great importance. Hartwig et al.²⁵ already demonstrated the impact of trimethylsilyl (TMS) as a dispersion energy donor group²⁶ (DED^{11,27}) in hydroboration reactions. Here, the TMS groups increased reaction rates by binding the substrate more efficiently. With the aim to utilize silyl groups as variable steric directing groups, we chose a cyclooctatetraene (COT)-based molecular balance to gauge the size and potential of commonly used silyl groups to act as DEDs.

A systematic study of the di-*tert*-butyl-substituted COT molecular balance in various solvents highlighted the attractive nature of LD interactions.²⁸ The disubstituted COT system, initially presented by Streitwieser et al.²⁹ using di-*tert*-butyl

Received: December 22, 2021

Published: March 16, 2022



Scheme 1. Equilibrium of 1,4- and 1,6-Disilyl Substituted Cyclooctatetraene

substituents and its folding mechanism (a double-bond valence shift and ring inversion^{30,31}), has been studied both experimentally^{32–34} and computationally.^{35,36} All studies confirmed the sterically more hindered 1,6-di-*tert*-butyl COT to be the preferred valence isomer in solution and in the gas phase.

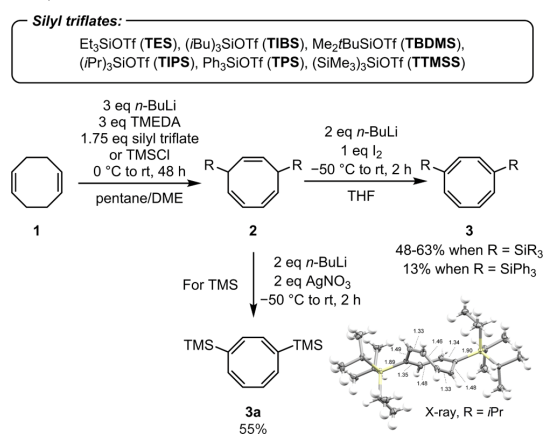
We chose the COT system to enforce close σ – σ contacts in the 1,6-disilyl-COT (Scheme 1) valence isomer. On the other hand, the 1,4-disilyl-COT does not display close contacts between the silyl groups. An analysis of the equilibrium between 1,6- and 1,4-disilyl-COT should offer insights into the attractive and repulsive nature between the silyl groups. While di-*tert*-butyl substituted COT prefers the folded isomer independent of the solvent, bulky silyl groups are expected to disfavor this valence isomer due to an increasing number of repulsive contacts.²⁸ Therefore, our system is suitable to gauge the relative bulkiness of various silyl groups.

RESULTS AND DISCUSSION

We utilized the COT molecular balance substituted with trimethylsilyl³⁷ (TMS), triethylsilyl (TES), *tert*-butyldimethylsilyl³⁸ (TBDMS), tri-*iso*-propylsilyl³⁹ (TIPS), tri-*iso*-butylsilyl (TIBS), tris(trimethylsilyl)silyl (TTMSS), and triphenylsilyl^{40,41} (TPS).

We adopted modified literature procedures^{37–41} to synthesize the disilyl COT derivatives (Scheme 2). We gathered

Scheme 2. Synthetic Procedure for the Preparation of Disilyl COT Derivatives (Left) and Single Crystal X-ray Structure of di-TIPS COT (Bottom Right, Bond Distances in Å)^a



^aThermal ellipsoid plot of the molecular structure obtained by single-crystal X-ray diffraction was drawn at 50% probability level.

single-crystal X-ray structural data for di-TIPS-COT (Scheme 2) and di-TMSS-COT (see Supporting Information). Both compounds crystallize in the unfolded valence isomer form, thereby maximizing intermolecular alkyl–alkyl interactions. In solution, di-TIPS-COT equilibrates between both diastereomers. The thermodynamic equilibria were subjected to van't Hoff analyses utilizing temperature-dependent nuclear magnetic resonance (NMR) measurements to dissect the isomerization enthalpies (ΔH_{eq}) and entropies (ΔS_{eq}).

NMR samples were equilibrated for 16 h at 40 °C prior to the experiment (Figure 1) and measured in the temperature range of 313–373 K (steps of 10 K; for details, see Supporting Information). All COT balances show linear regressions with $R^2 > 0.97$. As the folding equilibrium of di-*tert*-butyl substituted COT varies with the NMR solvent in a range from $K_{\text{eq}} = 1.18$ –2.13, toluene was chosen for temperature-dependent measurements, as it lies in the middle of the solvent bias range ($K_{\text{eq}} = 1.55$).²⁸

We also analyzed the noncovalent interactions between the silyl groups computationally utilizing the well-established B3LYP^{42,43} functional excluding and including LD interactions with the Becke–Johnson (BJ) damped dispersion D3 correction of Grimme et al.^{27,44} This provides an estimate of the LD correction. To validate this method, we compared our results with those computed using the M06-2X⁴⁵ and ω B97X-D⁴⁶ functional combinations. Ahlrich's def2-TZVPP basis set⁴⁷ was used for all computations. Because all methods show the same trend, the B3LYP-D3(BJ)/def2-TZVPP-optimized geometries were utilized as the basis for DLPNO-CCSD(T)/def2-TZVPP single-point energy computations^{48,49} (see Supporting Information). This approach has demonstrated good agreement with experimental data for COT molecular balances.²⁸ The rate-determining double-bond valence shift barrier was computationally estimated to be around 24 kcal mol⁻¹ for alkyl-substituted silyl groups, which is similar to that of di-*tert*-butyl COT.²⁸ In contrast, the activation barrier for di-TIPS-COT was estimated to be around 35 kcal mol⁻¹, that is, thermally out of reach for our experimental parameters (see Supporting Information).

While the silyl groups are even more demanding in size than a *tert*-butyl substituent (with van der Waals Volume of around 101 Å³, Scheme 3 and Supporting Information), the equilibria between 1,6- and 1,4-disilyl-COT were assumed to shift markedly toward the unfolded balance. Figure 2 displays the experimental enthalpies ΔH_{eq} (black markings) and the computed values (red markings). While computations suggest that the di-TMS-COT is nearly thermoneutral ($\Delta H_{\text{eq}} \approx 0$ kcal mol⁻¹), larger silyl groups shift the equilibrium toward 1,4-disilyl-COT. The computed increase in energy for the equilibrium depicted in Figure 2 between di-TBDMS-, di-TES-, di-TIPS-, and di-TMSS-COT ranges from 0.3 to 1.4 kcal mol⁻¹, favoring 1,4-disilyl-COT. The computational assessment and the experimental data agree within ± 0.6 kcal mol⁻¹ with an experimental error smaller than 0.13 kcal mol⁻¹. The experimentally determined enthalpy value for di-TMS-COT is with $\Delta H_{\text{eq}} = -0.6$, only 0.1 kcal mol⁻¹ higher in energy than the di-*tert*-butyl substituted COT.²⁸ While di-TMSS-COT is completely in favor of 1,4-disilyl-COT and therefore cannot be measured, the di-TIPS-COT equilibrium shows the highest enthalpy ($\Delta H_{\text{eq}} = 1.7$ kcal mol⁻¹). Interestingly, di-TIBS-COT does not follow the expected pattern that a larger van der Waals surface or volume introduces more steric hindrance into the system. Both the computational and

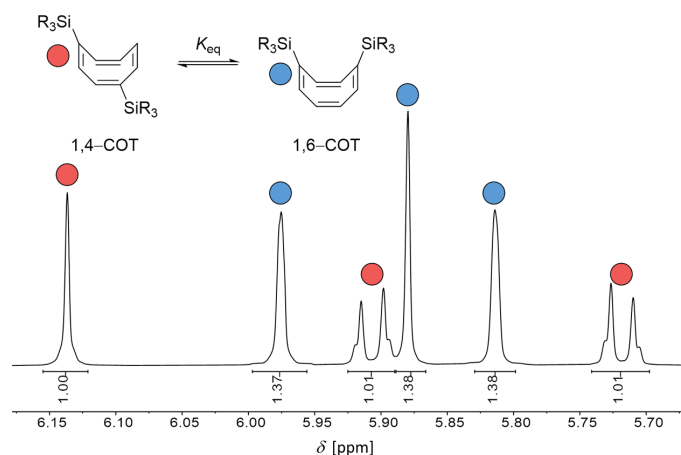
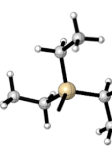
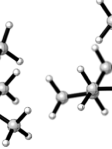
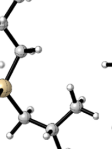


Figure 1. ^1H NMR spectra (600 MHz) and signal assignment of the equilibrium between 1,4- (red) and 1,6-di-TMS (blue) COT at 40 °C.

Scheme 3. Comparison of van der Waals Surfaces and Volumes of Tri-substituted Silyl Groups (Optimized with the Silane Geometry) at the B3LYP-D3/def2-TZVPP Level of Theory

Structure						
Abbreviation	TMS	TBDMS	TES	TIPS	TIBS	TTMSS
Van der Waals Surface [\AA^2]	127.8	171.1	173.3	219.2	295.7	340.2
Van der Waals Volume [\AA^3]	109.2	155.5	151.5	199.6	285.2	328.8

experimental values give a ΔH_{eq} as high as di-TBDMS- and di-TES-COT ($\Delta H_{\text{eq}} \approx 0.8 \text{ kcal mol}^{-1}$). Therefore, an additional source of stabilization must be present.

Three questions arise from the data collected:

1. What is the origin of the stabilization of the folded di-TMS-COT?
2. Why do larger silyl groups not show similar behavior?
3. Why does di-TIBS-COT not follow that trend?

To answer the first question, we focused on the noncovalent interactions between the interacting groups. By utilizing homodesmotic equations,^{50,51} we extracted the magnitude of the LD interactions due to close σ - σ contacts between the silyl groups in 1,6-disilyl-COT. Including and excluding LD interactions via Grimme's D3(BJ) correction results in an LD correction estimate, which we take, in a first approximation, as a measure of the dispersion energy. This seems reasonable, as we are comparing similar groups in the same molecular system where absolute magnitudes are less important than relative measures for comparison.

The analysis reveals large LD contributions between the silyl groups (Figure 3). Whereas the DFT computations excluding LD (red bars) demonstrate the general assumption that large substituents repel each other due to steric hindrance, including LD (blue bars) suggests the opposite trend. The magnitude of LD interactions (green bars) increases with the size of the silyl

groups. Therefore, the largest alkyl substituent (TTMSS) stabilizes 1,6-disilyl-COT by around $\Delta E_{\text{disp}} = -5.0 \text{ kcal mol}^{-1}$. Only di-TIBS-COT deviates from the general trend observed.

For better energy estimates of the intramolecular LD interactions, we performed local energy decomposition⁵²⁻⁵⁴ (LED) analyses as implemented in ORCA.⁵⁵ Thereby, we separated each balance into three molecular fragments (F1, F2, and F3) according to Figure 4 and dissected the interaction energy into its main parts. Because this process involves bond splitting, the resulting radical fragment interactions involve large electrostatic interactions. As a consequence, we can only isolate an energy term for LD interactions between F2 and F3.

Apart from di-TIBS substituted COT, the results of this analysis (Figure 4) fit qualitatively to the results of the homodesmotic equation (Figure 3). While in both cases the magnitude of intramolecular LD interactions increases from di-TMS- to di-TTMSS-COT, di-TIBS-COT is the strongest dispersion energy donor (DED) group within the LED analysis. On the other hand, di-TMS-COT benefits the least from stabilizing LD interactions. Nevertheless, it is the only case favoring 1,6-disilyl-COT. Counteracting repulsive interactions do not outweigh the LD stabilization in di-TMS-COT. The strong stabilizing contacts between two TIBS groups translate into a measurable shift in the equilibrium as well. In comparison to di-TMS-COT, the interaction is not prominent

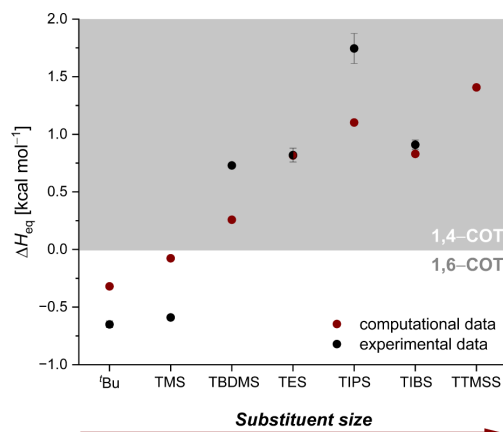


Figure 2. Enthalpies for the equilibrium of 1,4- and 1,6-disilyl substituted cyclooctatetraene. Experimental data (black markings) were derived from van't Hoff analyses. Computations (red markings) at the DLPNO-CCSD(T)/def2-TZVP//B3LYP-D3/def2-TZVP level of theory. The silyl groups were ordered according to increasing van der Waals surface. All datapoints within the shaded area favor 1,4-disilyl-COT. Data for 'Bu was extracted from the work of Schümann et al.²⁸

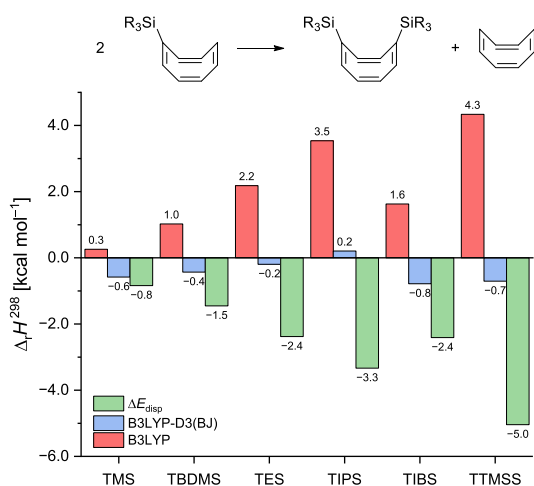


Figure 3. Homodesmotic equation and reaction enthalpies ($\Delta_r H^{298}$) in kcal mol⁻¹ at B3LYP(D3(BJ))/def2-TZVP.

enough to favor 1,6-disilyl-COT. Because larger groups favor 1,4-disilyl-COT, destabilizing interactions must counteract LD.

To answer the second question, we aimed at isolating the contributions of Pauli repulsion for 1,4- and 1,6-disilyl-COT. We employed symmetry-adapted perturbation theory⁵⁶ (SAPT) at the sSAPT0/aug-cc-pVDZ level of theory utilizing a scaled protocol according to Parker et al.⁵⁷ To isolate interactions between the silyl groups, we employed B3LYP-D3/def2-TZVP optimized structures, removed the COT backbone, and saturated the radical sites.⁵⁸ The total interaction energy E_{tot} can then be decomposed into its main components (Figure 5). Whereas the inductive energy E_{ind} (yellow markings) and the electrostatic energy E_{elst} (blue markings) terms marginally stabilize 1,6-disilyl-COT, the main

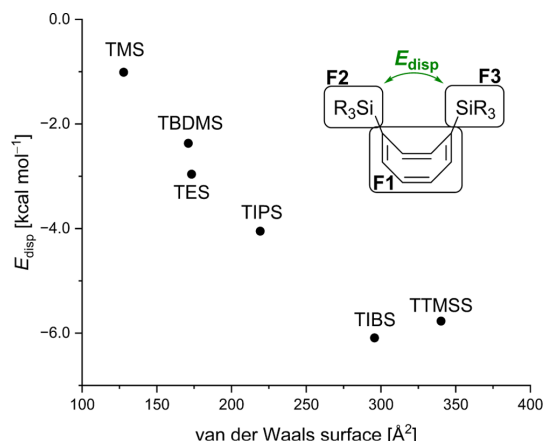


Figure 4. LED analysis of two silyl groups in their 1,6-disilyl-substituted cyclooctatetraene geometry at DLPNO-CCSD(T)/def2-TZVP//B3LYP-D3(BJ)/def2-TZVP.

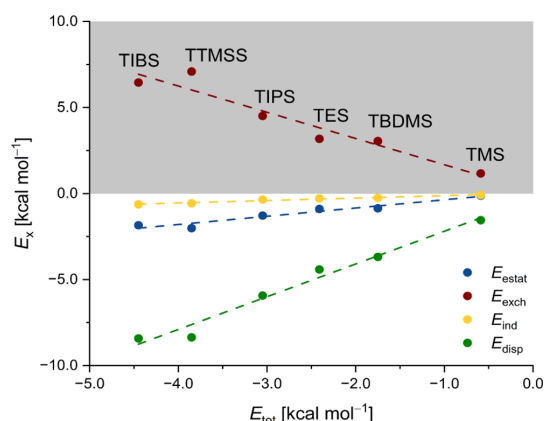


Figure 5. sSAPT analysis of two silyl groups in geometries of the respective 1,6-COT derivative at sSAPT0/aug-cc-pVDZ. The dashed lines are used as a guide to the eye.

contributors to the total interaction energy are LD interactions E_{disp} (green markings) and Pauli exchange repulsion E_{exch} (red markings). While 1,4-disilyl-COT is hardly influenced by repulsive interactions, the close σ - σ contacts in 1,6-disilyl-COT result in significant Pauli repulsion (Figure 5). The latter is, however, largely offset by LD interactions for all studied derivatives and hence cannot be the decisive factor for the shift in folding equilibria. In particular, di-TIBS-COT benefits from stabilizing LD interactions coupled with fewer steric constraints than di-TTMSS-COT. Therefore, flexible alkyl groups align more efficiently and optimize the balance between attractive and repulsive contacts.

The SAPT analysis does not directly yield an explanation for our findings, and the origin of increasing destabilization must lie elsewhere. When assessing optimized 1,6-disilyl-COT structures, we noticed significant deviations in the geometric parameters of the respective COT backbone with differing silyl groups, that is, the dihedral angle α (Figure 6). Consequently, we carried out a strain analysis, with the aim of capturing ring strain introduced in both the COT scaffold and the silyl

groups. To account for the ring strain, we utilized the B3LYP-D3/def2-TZVPP optimized structures, split off the substituents attached to Si, and saturated the compound with H to give a strained disilane COT. Next, the single-point energies of these compounds were compared to a disilane COT optimized at the same level of theory. Additionally, we utilized the optimized structures, removed the COT molecular backbone, and saturated the radical sites to give the corresponding strained silanes. Again, the difference in energy between strained silanes and geometry optimized compounds was taken into account (for details, see Supporting Information).

Figure 6 displays the sum of strain energy ΔE_{strain} exerted on the ring due to the substituents of the corresponding di-silyl substituted COT derivative and van der Waals strain introduced in the silyl groups due to repulsive contacts (see Supporting Information for details). While the incorporation of six methyl groups does not affect ΔE_{strain} (0.0 kcal mol⁻¹ for di-TMS-COT), the introduction of bulkier substituents leads to a rise in strain up to 1.9 kcal mol⁻¹ for di-TMSS-COT. For smaller and flexible silyl substituents up to TIBS ΔE_{strain} is mostly comprised of strain from the silyl substituents (see Supporting Information). The influence of ring strain increases significantly for bulkier and rigid substituents (TIPS and TMSS). The strain energy is a result of the attenuation of Pauli repulsion between both silyl groups. By increasing the distance between substituents the release in repulsive interaction energy is directly exerted on the COT molecular backbone. Because LD decreases slower with respect to the distance (r^{-6}) in comparison to Pauli repulsion (r^{-12}), the ratio of both energy components is optimized.^{9,10}

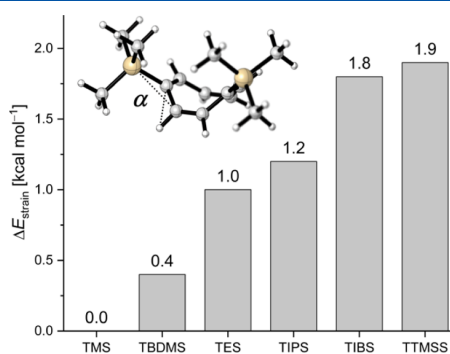


Figure 6. Strain energy ΔE_{strain} for disilyl-substituted cyclooctatetraene. The energy values correspond to the relative strain between 1,4- and 1,6-disilyl-substituted cyclooctatetraene.

By mapping the obtained experimental data to parameters capturing steric bulk, such as A-values,^{7,8,59} solvolysis rates,⁶ and Tolman's steric parameter θ ,^{60,61} the suitability of disilyl COTs to gauge the steric size of silyl groups can be further rationalized. While θ resembles an empirical measure, it is nevertheless often used to assess the steric demand of ligands. Figure 7 showcases the correlation between θ and ΔG_{eq} values of the disilyl COT balances. Because of the strong correlation observed, it is possible to predict θ from computed or experimental ΔG_{eq} values. For instance, TIBS has recently found use as a protecting group in organic synthesis but has not been characterized within the framework of steric parameters. According to the data collected (Figure 7), we

can determine $\theta = 144^\circ$ for the TIBS group (red marking), which is in accordance with Tolman's parameter for P(^tBu)₃ ($\theta = 143^\circ$).⁶⁰ Similar correlations of ΔG_{eq} to steric parameters such as A-values and solvolysis rates are observed (see Supporting Information).

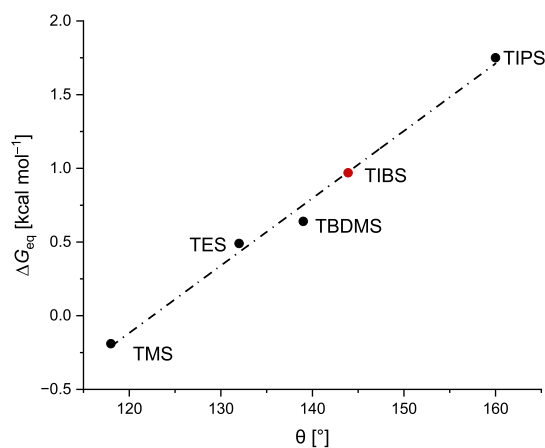


Figure 7. Correlation of experimental free energy values (ΔG_{eq}) of the COT molecular balances and Tolman's steric parameter. The dashed line is derived from linear regression of the black data points. The red marking was calculated according to a linear regression as a guide to the eye.

CONCLUSIONS

We prepared a variety of 1,4- and 1,6-disilyl-substituted cyclooctatetraene structures and conducted temperature-dependent NMR measurements to determine equilibrium parameters. By comparing the thus obtained ΔH_{eq} values to computed thermochemical data ($\Delta_r H^{298}$, and ΔE_{strain}), we were able to pinpoint LD interactions as a key factor affecting the folding equilibria. The main interaction energy component that counteracts LD is Pauli exchange repulsion, while the induced strain is a mechanism to either attenuate repulsion or optimize LD. With the exception of di-TMS-COT, ring strain overcompensates the stabilizing contribution of LD interactions in the folded 1,6-isomer. Hence, the equilibrium shifts toward the unfolded 1,4-isomer as bulkier silyl groups are installed.

Our experimentally determined ΔG_{eq} values correlate well with steric parameters for silyl groups known from the literature. The ring strain observed in the 1,6-valence isomers can be interpreted as a "fingerprint" of the respective group. This renders the COT molecular balance system suitable for gauging the relative bulkiness of silyl and, in the future, other groups.

LD interactions turn out to play a key role in stabilizing the folded 1,6-isomers. This is particularly evident from LED and SAPT analyses (vide infra). Without the LD contributions, the equilibria are predicted to favor the unfolded 1,4-isomer much more strongly than what is observed experimentally.

While the incorporation of bulky substituents directly attached to Si (TMS, TBDMS, TIPS, and TMSS) results in a linear correlation between the actual size (van der Waals surface, Scheme 3) and the apparent relative bulkiness (ΔG_{eq} and ΔH_{eq} , Figure 2) of silyl groups, a remote substitution

pattern as in di-TIBS-COT stabilizes the folded 1,6-valence isomer via LD interactions.

EXPERIMENTAL SECTION

General Information. Thin-layer chromatography was carried out using PolyGram SIL G/UV₂₅₄ plates with detection via UV $\lambda = 254$ nm and by staining with a 10 wt % ethanolic phosphomolybdic acid (PMA) stain solution. All chemicals were commercially obtained from Acros Organics, TCI, and Sigma-Aldrich and used without further purification. Anhydrous solvents were purchased from Acros Organics. Unless otherwise noted, all reactions were carried out under standard Schlenk conditions employing N₂ as the inert gas. Standard NMR spectra were obtained using Bruker Avance II 400 MHz and Bruker Avance III HD 400 MHz (¹³C spectra) spectrometers. Temperature-dependent NMR experiments were carried out with a Bruker Avance III HD 600 MHz spectrometer. High-resolution mass spectra were obtained with a Bruker micrOTOF mass spectrometer. For temperature-dependent measurements, NMR samples were equilibrated for 16 h at 40 °C prior to the experiment utilizing an IKA ICC basic eco 8 immersion circulator.

Temperature-Dependent NMR Experiments. After sample transfer from the thermostat to the NMR spectrometer, equilibration was continued for another hour in the spectrometer before the first spectrum (40 °C) was recorded. Spectra were recorded in 10 °C steps. From 60 °C onward, the equilibration period before measurement was reduced to 30 min.

Synthetic Procedures. *Triphenylsilyl Triflate (4).* Triphenylsilyl triflate was prepared according to a modified literature procedure.⁶² To a stirred suspension of 3.592 g (14 mmol) of AgOTf in 30 mL of DCM was added a solution of 4.428 g (15 mmol) triphenylsilyl chloride in 20 mL of DCM at room temperature. After complete addition, the reaction mixture was stirred under the exclusion of light at room temperature for another 12 h. The mixture was then filtered to remove AgCl, yielding a clear colorless filtrate. The filtrate was then concentrated under reduced pressure to yield 6.032 g of a colorless solid, which was used without further purification in the preparation of di(TPS)cyclooctatetraene **3g**.

Tris(trimethylsilyl)silyl Triflate (5). Tris(trimethylsilyl)silyl silane (4.63 mL, 15 mmol) was diluted with 7 mL of *n*-pentane. Afterward, 1.25 mL (14 mmol, 0.95 equiv) of trifluoromethanesulfonic acid was added dropwise (gas formation) and the resulting mixture was stirred for 1 h at room temperature. The resulting solution was used without further purification in the preparation of di(TTMSS)-cyclooctatetraene **3f**.

Tri(isobutyl)silyl Triflate (6). Triisobutylsilane 3.87 mL (15 mmol) was diluted in 5 mL of *n*-pentane. Afterward, 1.23 mL (14 mmol, 0.95 equiv) of trifluoromethanesulfonic acid was added dropwise (gas formation) and the resulting mixture was stirred for 1 h at room temperature. The resulting solution was used without further purification in the preparation of di(TIBS)cyclooctatetraene **3c**.

5,8-Di(silyl)cycloocta-1,3,6-trienes (2).^{37–41} 5,8-Di(silyl)-cycloocta-1,3,6-trienes were prepared according to the following general procedure: to a stirred solution of 0.98 mL (8.0 mmol) of 1,5-cyclooctadiene in 10 mL of *n*-pentane was added 9.60 mL (24 mmol, 3.0 equiv) of a *n*-butyllithium solution (2.5 M in hexanes) at 0 °C. Afterward, 3.60 mL (24 mmol, 3.0 equiv) of TMEDA was added dropwise and the yellow solution was kept stirring at 0 °C for 15 min. The cooling bath was removed thereafter, and stirring was continued at room temperature for 48 h. To the then orange mixture was added 20 mL of DME, and stirring was continued for another 15 min at room temperature. The mixture was then filtered to yield a deep red filtrate that was cooled to –50 °C and treated with 1.75 equiv of the corresponding silyl triflate or silyl chloride. After 30 min at –50 °C, the reaction mixture was quenched with 20 mL of a saturated aqueous NaHCO₃ solution. Phases were separated, and the aqueous phase was extracted with *n*-hexane (3 × 50 mL). The combined organic phases were dried over anhydrous MgSO₄, filtered, and concentrated under reduced pressure to yield the corresponding crude products as either off-white oils or solids. Purification was carried out by filtering

through a pad of silica eluting with *n*-hexane or a 10:1 mixture of *n*-hexane and ethyl acetate (5,8-di(TPS)cycloocta-1,3,6-triene **2g**). Because of their instability, the 5,8-di(silyl)cycloocta-1,3,6-triene **2** precursors were used immediately in the next synthetic step.

Di(TMS)cyclooctatetraene (3a). 1.264 g (5.0 mmol) of 5,8-di(TMS)cycloocta-1,3,6-triene was dissolved in 20 mL of THF and cooled to –50 °C. While stirring, 4.45 mL (11 mmol, 2.2 equiv) of 2.5 M *n*-butyllithium in hexanes was added dropwise. After stirring for 15 min at –50 °C, the reaction mixture was allowed to reach 0 °C by replacing the liquid nitrogen–acetone cooling bath with an ice-water cooling bath. Stirring of the solution was continued for 2 h at 0 °C. The now deep red solution was brought to –30 °C, and 1.712 g (10 mmol, 2.0 equiv) of silver nitrate was added in small portions. The reaction mixture was stirred for a further 16 h at room temperature before quenching was carried out with 20 mL of water. Phases were separated, and the aqueous phase was extracted with *n*-hexane (3 × 50 mL). The combined organic phases were dried over anhydrous MgSO₄, filtered, and concentrated under reduced pressure to yield the crude product as an off-white solid. The crude product was purified by crystallization using methanol at –25 °C, yielding 1.093 g (4.4 mmol, 55% over two steps) of **3a** as a colorless solid.

¹H NMR (400 MHz, CDCl₃), 1,4-**3a**: δ 6.11 (s, 2H), 5.99–5.84 (m, 2H), 5.73 (q, $J = 2.8$ Hz, 2H), 0.07 (s, 18H).

¹H NMR (400 MHz, CDCl₃), 1,6-**3a**: δ 5.99–5.84 (m, 6H), 0.08 (s, 18H).

¹³C{¹H} NMR (100 MHz, CDCl₃): δ 149.3, 148.8, 139.6, 138.4, 134.2, 132.9, 132.3, 129.3, –1.4, –1.6.

HRMS (APCI-TOF) m/z : [M + H]⁺ calcd for C₁₄H₂₄Si₂, 249.1494; found, 249.1487.

Di(silyl)cyclooctatetraene (3).^{37–41} With the exception of di(trimethylsilyl)cyclooctatetraene **3a**, all cyclooctatetraenes were prepared according to the following general procedure: a 0.25 M solution of the corresponding 5,8-di(silyl)cycloocta-1,3,6-triene **2** in THF was prepared and cooled to –50 °C. While stirring, 2.2 equiv of *n*-butyllithium (2.5 M in hexanes) was added dropwise. After stirring for 15 min at –50 °C, the reaction mixture was allowed to reach 0 °C by replacing the liquid nitrogen–acetone cooling bath with an ice-water cooling bath. Stirring of the deep red solution was continued for 2 h at 0 °C before cooling the solution to –30 °C. Upon complete addition of 1.1 equivalents of elemental iodine at –30 °C in small portions, the color of the solution faded completely. The reaction mixture was stirred for another 15 min before quenching was carried out with 20 mL of a saturated aqueous Na₂SO₃ solution. Phases were separated, and the aqueous phase was extracted with *n*-hexane (3 × 50 mL). The combined organic phases were dried over anhydrous MgSO₄, filtered, and concentrated under reduced pressure to yield the corresponding crude products as either off-white oils or solids. The di(silyl)cyclooctatetraenes were purified either by trituration with cold methanol (–20 °C) or by silica flash column chromatography eluting with *n*-hexane or a 10:1 mixture of *n*-hexane and ethyl acetate (di(TPS)cyclooctatetraene **3g**).

Di(TES)cyclooctatetraene (3b). 3.16 mL (14 mmol, 1.75 equiv) of triethylsilyl triflate was utilized according to the general procedure described above for the preparation of 5,8-di(silyl)cycloocta-1,3,6-trienes (**2**). 1.686 g (5.0 mmol) of 5,8-di(TES)cycloocta-1,3,6-triene **2b** was obtained as a colorless oil. Compound **2b** was dissolved in 20 mL of THF and subsequently treated as in the general procedure for the preparation of di(silyl)cyclooctatetraenes (**3**) described above. 4.43 mL (11 mmol) of 2.5 M *n*-butyllithium in hexanes and 1.404 g (5.5 mmol) of elemental iodine were utilized for the preparation of di(TES)cyclooctatetraene (**3b**). After purification by flash column chromatography, 1.408 g (4.2 mmol, 53%) of **3b** was obtained as a colorless oil.

¹H NMR (400 MHz, CDCl₃), 1,4-**3b**: δ 6.09 (s, 2H), 5.96–5.79 (m, 2H), 5.69 (q, $J = 2.8$ Hz, 2H), 0.98–0.89 (m, 18H), 0.65–0.52 (m, 12H).

¹H NMR (400 MHz, CDCl₃), 1,6-**3b**: δ 5.96–5.79 (m, 6H), 0.98–0.89 (m, 18H), 0.65–0.52 (m, 12H).

¹³C{¹H} NMR (100 MHz, CDCl₃): δ 146.0, 145.2, 141.2, 139.9, 135.0, 132.9, 132.6, 128.8, 7.6, 7.5, 3.1, 3.0.

HRMS (APCI-TOF) m/z : $[M + H]^+$ calcd for $C_{20}H_{36}Si_2$, 333.2434; found, 333.2427.

Di(TIBS)cyclooctatetraene (3c). Tri(isobutyl)silyl triflate (**6**) was utilized according to the general procedure described above for the preparation of 5,8-di(silyl)cycloocta-1,3,6-trienes (**2**). 2.495 g (5.0 mmol) of 5,8-di(TIBS)cycloocta-1,3,6-triene **2c** was obtained as a colorless oil. Compound **2c** was dissolved in 20 mL of THF and subsequently treated as in the general procedure for the preparation of di(silyl)cyclooctatetraenes (**3**) described above. 4.40 mL (11 mmol) of 2.5 M *n*-butyllithium in hexanes and 1.385 g (5.5 mmol) of elemental iodine were utilized for the preparation of di(TES)-cyclooctatetraene (**3b**). After purification by flash column chromatography, 2.085 g (4.2 mmol, 52%) of **3c** was obtained as a colorless oil.

1H NMR (400 MHz, $CDCl_3$), 1,4-**3c**: δ 6.05 (s, 2H), 5.93 (q, J = 2.7 Hz, 2H), 5.65 (q, J = 2.8 Hz, 2H), 1.86–1.74 (m, 6H), 0.96–0.90 (m, 36H), 0.69–0.54 (m, 12H).

1H NMR (400 MHz, $CDCl_3$), 1,6-**3c**: δ 5.99 (s, 2H), 5.85 (s, 2H), 5.84 (s, 2H), 1.86–1.74 (m, 6H), 0.96–0.90 (m, 36H), 0.69–0.54 (m, 12H).

$^{13}C\{^1H\}$ NMR (100 MHz, $CDCl_3$): δ 147.5, 146.6, 141.4, 140.3, 135.3, 132.9, 132.9, 129.2, 26.9, 26.8, 26.8, 26.7, 24.9, 24.9, 24.1, 23.7.

HRMS (APCI-TOF) m/z : $[M + H]^+$ calcd for $C_{32}H_{60}Si_2$, 501.4312; found, 501.4308.

Di(TBDMs)cyclooctatetraene (3d). 3.22 mL (14 mmol) of *tert*-butyldimethylsilyl triflate was utilized according to the general procedure described above for the preparation of 5,8-di(silyl)cycloocta-1,3,6-trienes (**2**). 2.821 g (5.6 mmol) of 5,8-di(TBDMs)-cycloocta-1,3,6-triene **2d** was obtained as a colorless solid. Compound **2d** was dissolved in 22 mL of THF and subsequently treated as in the general procedure for the preparation of di(silyl)cyclooctatetraenes (**3**) described above. 4.93 mL (12 mmol) of 2.5 M *n*-butyllithium in hexanes and 1.570 g (6.2 mmol) of elemental iodine were utilized for the preparation of di(TBDMs)cyclooctatetraene (**3d**). After purification by trituration with cold methanol, 2.523 g (5.0 mmol, 63%) of **3d** was obtained as a colorless solid.

1H NMR (400 MHz, $CDCl_3$), 1,4-**3d**: δ 6.10 (s, 2H), 6.01–5.84 (m, 2H), 5.68 (q, J = 2.8 Hz, 2H), 0.90 (s, 18H), 0.08–0.01 (m, 12H).

1H NMR (400 MHz, $CDCl_3$), 1,6-**3d**: δ 6.01–5.84 (m, 6H), 0.89 (s, 18H), 0.08–0.01 (m, 12H).

$^{13}C\{^1H\}$ NMR (100 MHz, $CDCl_3$): δ 146.6, 145.9, 141.8, 140.9, 136.0, 133.2, 132.9, 128.8, 27.0, 27.0, 17.4, 17.2, –5.6, –5.7, –5.7, –6.2.

HRMS (APCI-TOF) m/z : $[M + H]^+$ calcd for $C_{20}H_{36}Si_2$, 333.2434; found, 333.2428.

Di(TIPS)cyclooctatetraene (3e). 3.76 mL (14 mmol) of triisopropylsilyl triflate was utilized according to the general procedure described above for the preparation of 5,8-di(silyl)cycloocta-1,3,6-trienes (**2**). 2.113 g (5.0 mmol) of 5,8-di(TIPS)-cycloocta-1,3,6-triene **2e** was obtained as a colorless solid. Compound **2e** was dissolved in 20 mL of THF and subsequently treated as in the general procedure for the preparation of di(silyl)cyclooctatetraenes (**3**) described above. 4.43 mL (11 mmol) of 2.5 M *n*-butyllithium in hexanes and 1.412 g (5.5 mmol) of elemental iodine were utilized for the preparation of di(TIPS)cyclooctatetraene (**3e**). After purification by trituration with cold methanol, 1.650 g (4.0 mmol, 50%) of **3e** was obtained as a colorless solid.

1H NMR (400 MHz, $CDCl_3$), 1,4-**3e**: δ 6.11 (s, 2H), 6.03–5.83 (m, 2H), 5.67 (q, J = 2.8 Hz, 2H), 1.15–1.01 (m, 42H).

1H NMR (400 MHz, $CDCl_3$), 1,6-**3e**: δ 6.03–5.83 (m, 6H), 1.15–1.01 (m, 42H).

$^{13}C\{^1H\}$ NMR (100 MHz, $CDCl_3$): δ 144.3, 142.6, 142.2, 141.9, 136.6, 133.5, 132.8, 128.5, 19.0, 19.0, 18.8, 18.7, 11.4, 11.2.

HRMS (APCI-TOF) m/z : $[M + H]^+$ calcd for $C_{26}H_{48}Si_2$, 417.3373; found, 417.3368.

Di(TMSS)cyclooctatetraene (3f). Tris(trimethylsilyl)silyl triflate (**5**) was utilized according to the general procedure described above for the preparation of 5,8-di(silyl)cycloocta-1,3,6-trienes (**2**). 2.872 g (4.8 mmol) of 5,8-di(TMSS)cycloocta-1,3,6-triene **2f** was obtained as a colorless solid. Compound **2f** was dissolved in 19 mL of THF and

subsequently treated as in the general procedure for the preparation of di(silyl)cyclooctatetraenes (**3**) described above. 4.22 mL (10 mmol) of 2.5 M *n*-butyllithium in hexanes and 1.328 g (5.3 mmol) of elemental iodine were utilized for the preparation of di(TMSS)-cyclooctatetraene (**3f**). After purification by trituration with cold methanol, 2.295 g (3.8 mmol, 48%) of **3f** was obtained as a colorless solid.

1H NMR (400 MHz, $CDCl_3$), 1,4-**3f**: δ 6.01 (s, 2H), 5.89 (q, J = 2.8 Hz, 2H), 5.59 (q, J = 2.8 Hz, 2H), 0.21–0.17 (m, 54H).

$^{13}C\{^1H\}$ NMR (100 MHz, $CDCl_3$): δ 142.2, 141.4, 138.2, 126.9, 1.5.

HRMS (APCI-TOF) m/z : $[M + H]^+$ calcd for $C_{26}H_{60}Si_8$, 597.2927; found, 597.2924.

Di(TPS)cyclooctatetraene (3g). Triphenylsilyl triflate (**4**) was utilized according to the general procedure described above for the preparation of 5,8-di(silyl)cycloocta-1,3,6-trienes (**2**). 1.391 g (2.2 mmol) of 5,8-di(TPS)cycloocta-1,3,6-triene **2g** was obtained as a colorless solid. Compound **2g** was dissolved in 9 mL of THF and subsequently treated as in the general procedure for the preparation of di(silyl)cyclooctatetraenes (**3**) described above. 1.96 mL (4.9 mmol) of 2.5 M *n*-butyllithium in hexanes and 0.631 g (2.5 mmol) of elemental iodine were utilized for the preparation of di(TPS)-cyclooctatetraene (**3g**). After purification by flash column chromatography (10:1 *n*-hexane and ethyl acetate), 0.638 g (1.0 mmol, 13%) of **3g** was obtained as a colorless solid.

1H NMR (400 MHz, CD_2Cl_2), 1,4-**3g**: δ 7.61–7.25 (m, 30H), 6.24 (s, 2H), 6.10 (q, J = 2.8 Hz, 2H), 5.91–5.84 (m, 2H).

1H NMR (400 MHz, CD_2Cl_2), 1,6-**3g**: δ 7.61–7.25 (m, 30H), 6.24 (s, 2H), 5.96 (s, 2H), 5.91–5.84 (m, 2H).

$^{13}C\{^1H\}$ NMR (100 MHz, CD_2Cl_2): δ 147.2, 146.2, 143.6, 143.4, 136.7, 136.7, 135.9, 134.3, 134.1, 134.0, 133.6, 130.8, 130.0, 129.9, 128.3, 128.1.

HRMS (APCI-TOF) m/z : $[M + H]^+$ calcd for $C_{44}H_{37}Si_2$, 621.2434; found, 621.2427.

Computational Details. To compute the LD interactions, we utilized multiple tools recognized in the literature. We started our investigation with a conformer search in the gas-phase using the Conformer-Rotamer Ensemble Sampling Tool (crest) developed by Grimme et al.⁶³ The results for 1,6- and 1,4-disilyl-COT (the conformers lowest in energy) were further optimized with Gaussian16⁶⁴ in the gas phase using B3LYP,^{42,43} B3LYP-D3(BJ),^{27,44} M06-2X,⁴⁵ and ω B97X-D⁴⁶ in conjunction with the def2-SVPP and def2-TZVPP basis sets.⁴⁷ Hereby, the highest possible symmetry was employed (C_2 for 1,4-disilyl-COT and C_s/C_1 for 1,6-disilyl-COT). All structures were characterized as minima on the potential energy hypersurface. Additionally, single-point energy computations at the DLPNO-CCSD(T)/def2-TZVPP level of theory^{48,49} were performed on the B3LYP-D3(BJ)/def2-TZVPP optimized geometries. Tables S23–S28 summarize the results of the thermochemical analyses.

Homodesmotic (error-balancing) equations^{50,51} were performed to estimate the strength of the intramolecular LD interactions. As described above, the crest program was utilized to identify all conformers lowest in energy, which were then optimized in the gas phase using B3LYP/def2-TZVPP including (GD3BJ) and excluding LD interactions. The dispersion energy was computed according to the following equation

$$E_{\text{disp}} = \sum E(\text{product}) - D3(\text{BJ}) - \sum E(\text{starting material}) - D3(\text{BJ}) - \sum E(\text{product}) - \sum E(\text{starting material})$$

Figures S13–S18 summarize the results of the homodesmotic equations.

A local energy decomposition^{52–54} (LED) analysis was performed by using the Orca program⁵⁵ version 4.2.1. The B3LYP-D3(BJ)/def2-TZVPP-optimized geometries were utilized, and the molecules were split into fragments (F1–F3), which are defined in detail in the Supporting Information. The LED analysis was performed at DLPNO-CCSD(T)/def2-TZVPP utilizing tight pair natural orbital

(TightPNO) settings. Tables S29–S34 summarize the results of the LED analyses of all silyl COT derivatives.

Finally, a scaled Symmetry-Adapted Perturbation Theory⁵⁶ (sSAPT) analysis was performed using the PSI4 program.^{65,66} In order to isolate the interactions between the silyl groups, the molecular backbone of the COT balance was removed and the groups were saturated with hydrogens. A nonrelaxed dimer scan was performed at the sSAPT0/aug-cc-pVDZ level of theory. The empirical recipe for scaled SAPT0 was utilized in order to improve the performance according to Parker et al.⁵⁷ Tables S35–S40 and Figures S19–S24 summarize the results of the sSAPT analysis.

Visualizations of noncovalent interactions (NCI-plots⁶⁷) were plotted as a reduced density gradient in regions of low electron density. The B3LYP-D3(BJ)/def2-TZVPP-optimized geometries were utilized for the visualization of noncovalent interactions. All plots were generated with NCIPLOT⁶⁸ and visualized with VMD.⁶⁹ The density cut-off of the reduced density gradient ($\rho(r) = -0.2$ to $+0.2$ a.u.) and the color scale data range (-2 to $+2$ a.u.) were kept consistent throughout all NCI plots. Thereby, red isosurfaces indicate strongly repulsive interactions, green isosurfaces correspond to weak noncovalent contacts, and blue isosurfaces indicate strongly attractive interactions. Figures S25–S30 show all visualizations of 1,6- and 1,4-disilyl-COT.

■ ASSOCIATED CONTENT

Supporting Information

The Supporting Information is available free of charge at <https://pubs.acs.org/doi/10.1021/acs.joc.1c03103>.

¹H NMR and ¹³C{¹H} NMR data for all molecular balances; error estimation for experimental data; single-crystal X-ray diffraction data; HRMS data; and computational details (PDF)

XYZ files for 1,6- and 1,4-cyclooctatetraene (ZIP)

Accession Codes

CCDC 2124606–2124607 contain the supplementary crystallographic data for this paper. These data can be obtained free of charge via www.ccdc.cam.ac.uk/data_request/cif, or by emailing data_request@ccdc.cam.ac.uk, or by contacting The Cambridge Crystallographic Data Centre, 12 Union Road, Cambridge CB2 1EZ, UK; fax: +44 1223 336033.

■ AUTHOR INFORMATION

Corresponding Author

Peter R. Schreiner – Institute of Organic Chemistry, Justus Liebig University, 35392 Giessen, Germany; orcid.org/0000-0002-3608-5515; Email: prs@uni-giessen.de

Authors

Henrik F. König – Institute of Organic Chemistry, Justus Liebig University, 35392 Giessen, Germany; orcid.org/0000-0002-4246-6744

Lars Rummel – Institute of Organic Chemistry, Justus Liebig University, 35392 Giessen, Germany; orcid.org/0000-0002-3772-2109

Heike Hausmann – Institute of Organic Chemistry, Justus Liebig University, 35392 Giessen, Germany

Jonathan Becker – Institute of Inorganic and Analytical Chemistry, Justus Liebig University, 35392 Giessen, Germany

Jan M. Schümann – Institute of Organic Chemistry, Justus Liebig University, 35392 Giessen, Germany; orcid.org/0000-0001-7494-5603

Complete contact information is available at: <https://pubs.acs.org/doi/10.1021/acs.joc.1c03103>

Author Contributions

[§]H.F.K. and L.R. contributed equally to this work.

Notes

The authors declare no competing financial interest.

■ ACKNOWLEDGMENTS

This work was supported by the priority program “Control of London Dispersion in Molecular Chemistry” (SPP1807) of the Deutsche Forschungsgemeinschaft.

■ DEDICATION

This paper is dedicated to the memory of Andrew Streitwieser who taught us so much about organic chemistry.

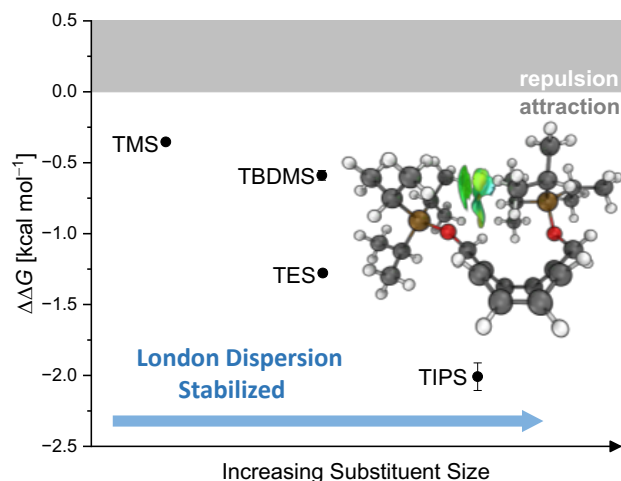
■ REFERENCES

- (1) Greene, T. W.; Wuts, P. G. *Protective Groups in Organic Synthesis*; Wiley, 1991.
- (2) Schelhaas, M.; Waldmann, H. Protecting Group Strategies in Organic Synthesis. *Angew. Chem., Int. Ed.* **1996**, *35*, 2056–2083.
- (3) Nelson, T. D.; Crouch, R. D. Selective Deprotection of Silyl Ethers. *Synthesis* **1996**, *1996*, 1031–1069.
- (4) Pedersen, C. M.; Marinescu, L. G.; Bols, M. Conformationally armed glycosyl donors: reactivity quantification, new donors and one pot reactions. *Chem. Commun.* **2008**, *21*, 2465–2467.
- (5) Bols, M.; Pedersen, C. M. Silyl-protective groups influencing the reactivity and selectivity in glycosylations. *Beilstein J. Org. Chem.* **2017**, *13*, 93–105.
- (6) Shimizu, N.; Naohide, T.; Sigefumi, Y.; Takahiko, I. Prediction of Structural Effects of Trialkylsilyl Groups on Reactivity toward Nucleophilic Displacement at Silicon. *Chem. Lett.* **1993**, *22*, 1807–1810.
- (7) Eliel, E. L.; Satici, H. Conformational analysis of cyclohexyl silyl ethers. *J. Org. Chem.* **1994**, *59*, 688–689.
- (8) Marzabadi, C. H.; Anderson, J. E.; Gonzalez-Outeirino, J.; Gaffney, P. R. J.; White, C. G. H.; Tocher, D. A.; Todaro, L. J. Why Are Silyl Ethers Conformationally Different from Alkyl Ethers? Chair–Chair Conformational Equilibria in Silyloxycyclohexanes and Their Dependence on the Substituents on Silicon. The Wider Roles of Eclipsing, of 1,3-Repulsive Steric Interactions, and of Attractive Steric Interactions. *J. Am. Chem. Soc.* **2003**, *125*, 15163–15173.
- (9) London, F. Zur Theorie und Systematik der Molekularkräfte. *Z. Phys.* **1930**, *63*, 245–279.
- (10) London, F. The General Theory of Molecular Forces. *Trans. Faraday Soc.* **1937**, *33*, 8b–26.
- (11) Wagner, J. P.; Schreiner, P. R. London Dispersion in Molecular Chemistry—Reconsidering Steric Effects. *Angew. Chem., Int. Ed.* **2015**, *54*, 12274–12296.
- (12) Liptrot, D. J.; Power, P. P. London dispersion forces in sterically crowded inorganic and organometallic molecules. *Nat. Chem. Rev.* **2017**, *1*, 0004.
- (13) Schweighauser, L.; Strauss, M. A.; Bellotto, S.; Wegner, H. A. Attraction or Repulsion? London Dispersion Forces Control Azobenzene Switches. *Angew. Chem., Int. Ed.* **2015**, *54*, 13436–13439.
- (14) Procházková, E.; Kolmer, A.; Ilgen, J.; Schwab, M.; Kaltschnee, L.; Fredersdorf, M.; Schmidts, V.; Wende, R. C.; Schreiner, P. R.; Thiele, C. M. Uncovering Key Structural Features of an Enantioselective Peptide-Catalyzed Acylation Utilizing Advanced NMR Techniques. *Angew. Chem., Int. Ed.* **2016**, *55*, 15754–15759.
- (15) Hwang, J.; Li, P.; Smith, M. D.; Shimizu, K. D. Distance-Dependent Attractive and Repulsive Interactions of Bulky Alkyl Groups. *Angew. Chem., Int. Ed.* **2016**, *55*, 8086–8089.
- (16) Lu, G.; Liu, R. Y.; Yang, Y.; Fang, C.; Lambrecht, D. S.; Buchwald, S. L.; Liu, P. Ligand–Substrate Dispersion Facilitates the Copper-Catalyzed Hydroamination of Unactivated Olefins. *J. Am. Chem. Soc.* **2017**, *139*, 16548–16555.

- (17) Pollice, R.; Bot, M.; Kobylanski, I. J.; Shenderovich, I.; Chen, P. Attenuation of London Dispersion in Dichloromethane Solutions. *J. Am. Chem. Soc.* **2017**, *139*, 13126–13140.
- (18) Eschmann, C.; Song, L.; Schreiner, P. R. London Dispersion Interactions Rather than Steric Hindrance Determine the Enantioselectivity of the Corey–Bakshi–Shibata Reduction. *Angew. Chem., Int. Ed.* **2021**, *60*, 4823–4832.
- (19) Singha, S.; Buchsteiner, M.; Bistoni, G.; Goddard, R.; Fürstner, A. A New Ligand Design Based on London Dispersion Empowers Chiral Bismuth–Rhodium Paddlewheel Catalysts. *J. Am. Chem. Soc.* **2021**, *143*, 5666–5673.
- (20) Gomberg, M. Triphenylmethyl, ein Fall von dreierwertigem Kohlenstoff. *Ber. Dtsch. Chem. Ges.* **1900**, *33*, 3150–3163.
- (21) Gomberg, M.; Carbon, A. I. O. T. An Instance of Trivalent Carbon: Triphenylmethyl. *J. Am. Chem. Soc.* **1900**, *22*, 757–771.
- (22) Grimme, S.; Schreiner, P. R. Steric Crowding Can Stabilize a Labile Molecule: Solving the Hexaphenylethane Riddle. *Angew. Chem., Int. Ed.* **2011**, *50*, 12639–12642.
- (23) Rösel, S.; Balestrieri, C.; Schreiner, P. R. Sizing the role of London dispersion in the dissociation of all-meta tert-butyl hexaphenylethane. *Chem. Sci.* **2017**, *8*, 405–410.
- (24) Schreiner, P. R.; Chernish, L. V.; Gunchenko, P. A.; Tikhonchuk, E. Y.; Hausmann, H.; Serafin, M.; Schlecht, S.; Dahl, J. E. P.; Carlson, R. M. K.; Fokin, A. A. Overcoming lability of extremely long alkane carbon–carbon bonds through dispersion forces. *Nature* **2011**, *477*, 308–311.
- (25) Xi, Y.; Su, B.; Qi, X.; Pedram, S.; Liu, P.; Hartwig, J. F. Application of Trimethylgermyl-Substituted Bisphosphine Ligands with Enhanced Dispersion Interactions to Copper-Catalyzed Hydroboration of Disubstituted Alkenes. *J. Am. Chem. Soc.* **2020**, *142*, 18213–18222.
- (26) Grimme, S.; Huenerbein, R.; Ehrlich, S. On the Importance of the Dispersion Energy for the Thermodynamic Stability of Molecules. *ChemPhysChem* **2011**, *12*, 1258–1261.
- (27) Grimme, S.; Ehrlich, S.; Goerigk, L. Effect of the damping function in dispersion corrected density functional theory. *J. Comput. Chem.* **2011**, *32*, 1456–1465.
- (28) Schümann, J. M.; Wagner, J. P.; Eckhardt, A. K.; Quanz, H.; Schreiner, P. R. Intramolecular London Dispersion Interactions Do Not Cancel in Solution. *J. Am. Chem. Soc.* **2021**, *143*, 41–45.
- (29) Miller, M. J.; Lyttle, M. H.; Streitwieser, A., Jr tert-Butyl-substituted cyclooctatetraenes. *J. Org. Chem.* **1981**, *46*, 1977–1984.
- (30) Wenthold, P. G.; Hrovat, D. A.; Borden, W. T.; Lineberger, W. C. Transition-State Spectroscopy of Cyclooctatetraene. *Science* **1996**, *272*, 1456–1459.
- (31) Castaño, O.; Palmeiro, R.; Frutos, L. M.; Luisandrés, J. Role of bifurcation in the bond shifting of cyclooctatetraene. *J. Comput. Chem.* **2002**, *23*, 732–736.
- (32) Lyttle, M. H.; Streitwieser, A., Jr; Kluttz, R. Q. Unusual equilibrium between 1, 4-and 1, 6-di-tert-butylcyclooctatetraenes. *J. Am. Chem. Soc.* **1981**, *103*, 3232–3233.
- (33) Paquette, L. A.; Hefferon, G. J.; Samodral, R.; Hanzawa, Y. Bond fixation in annulenes. 14. Synthesis of and bond shifting equilibrium between 1, 4-and 1, 6-di-tert-butylcyclooctatetraenes. *J. Org. Chem.* **1983**, *48*, 1262–1266.
- (34) Anderson, J. E.; Kirsch, P. A. Structural equilibria determined by attractive steric interactions. 1,6-Dialkylcyclooctatetraenes and their bond-shift and ring inversion investigated by dynamic NMR spectroscopy and molecular mechanics calculations. *J. Chem. Soc., Perkin Trans. 1* **1992**, *2*, 1951–1957.
- (35) Allinger, N. L.; Frierson, M.; Van-Catledge, F. A. The importance of van der Waals attractions in determining the equilibrium between 1, 4-and 1, 6-dialkylcyclooctatetraenes. *J. Am. Chem. Soc.* **1982**, *104*, 4592–4593.
- (36) Tosi, C. A quantum mechanical study of the equilibrium between 1,4- and 1,6-dialkylcyclooctatetraenes. *J. Comput. Chem.* **1984**, *5*, 248–251.
- (37) Burton, N. C.; Cloke, F. G. N.; Joseph, S. C. P.; Karamallakis, H.; Sameh, A. A. Trimethylsilyl derivatives of cyclooctatetraene. *J. Organomet. Chem.* **1993**, *462*, 39–43.
- (38) Parry, J. S.; Coles, S. J.; Hursthouse, M. B. Synthesis and Characterization of the First Sandwich Complex of Trivalent Thorium: A Structural Comparison with the Uranium Analogue. *J. Am. Chem. Soc.* **1999**, *121*, 6867–6871.
- (39) Summerscales, O. T.; Cloke, F. G. N.; Hitchcock, P. B.; Green, J. C.; Hazari, N. Reductive Cyclotetramerization of CO to Squarate by a U(III) Complex: The X-ray Crystal Structure of $[(U(\eta-C_8H_6\{Si^iPr_3-1,4\}_2)(\eta-C_3Me_4H)_2)(\mu-\eta^2-\eta^2-C_4O_4)]$. *J. Am. Chem. Soc.* **2006**, *128*, 9602–9603.
- (40) Lorenz, V.; Schmiede, B. M.; Hrib, C. G.; Ziller, J. W.; Edelmann, A.; Blaurock, S.; Evans, W. J.; Edelmann, F. T. Unprecedented Bending and Rearrangement of f-Element Sandwich Complexes Induced by Superbulky Cyclooctatetraenide Ligands. *J. Am. Chem. Soc.* **2011**, *133*, 1257–1259.
- (41) Lorenz, V.; Liebing, P.; Rausch, J.; Blaurock, S.; Hrib, C. G.; Hilfert, L.; Edelmann, F. T. Preparation and crystal structures of silyl-substituted potassium cyclooctatetraenides. *J. Organomet. Chem.* **2018**, *857*, 38–44.
- (42) Lee, C.; Yang, W.; Parr, R. G. Development of the Colle-Salvetti correlation-energy formula into a functional of the electron density. *Phys. Rev. B: Condens. Matter Mater. Phys.* **1988**, *37*, 785–789.
- (43) Becke, A. D. Density-functional thermochemistry. III. The role of exact exchange. *J. Chem. Phys.* **1993**, *98*, 5648–5652.
- (44) Grimme, S.; Antony, J.; Ehrlich, S.; Krieg, H. A consistent and accurate ab initio parametrization of density functional dispersion correction (DFT-D) for the 94 elements H–Pu. *J. Chem. Phys.* **2010**, *132*, 154104.
- (45) Zhao, Y.; Truhlar, D. G. The M06 suite of density functionals for main group thermochemistry, thermochemical kinetics, non-covalent interactions, excited states, and transition elements: two new functionals and systematic testing of four M06-class functionals and 12 other functionals. *Theor. Chem. Acc.* **2008**, *120*, 215–241.
- (46) Chai, J.-D.; Head-Gordon, M. Long-range corrected hybrid density functionals with damped atom–atom dispersion corrections. *Phys. Chem. Chem. Phys.* **2008**, *10*, 6615–6620.
- (47) Schäfer, A.; Huber, C.; Ahlrichs, R. Fully optimized contracted Gaussian basis sets of triple zeta valence quality for atoms Li to Kr. *J. Chem. Phys.* **1994**, *100*, 5829–5835.
- (48) Riplinger, C.; Neese, F. An efficient and near linear scaling pair natural orbital based local coupled cluster method. *J. Chem. Phys.* **2013**, *138*, 034106.
- (49) Liakos, D. G.; Sparta, M.; Kesharwani, M. K.; Martin, J. M. L.; Neese, F. Exploring the Accuracy Limits of Local Pair Natural Orbital Coupled-Cluster Theory. *J. Chem. Theory Comput.* **2015**, *11*, 1525–1539.
- (50) Wheeler, S. E.; Houk, K. N.; Schleyer, P. v. R.; Allen, W. D. A Hierarchy of Homodesmotic Reactions for Thermochemistry. *J. Am. Chem. Soc.* **2009**, *131*, 2547–2560.
- (51) Wagner, J. P.; Schreiner, P. R. London Dispersion Decisively Contributes to the Thermodynamic Stability of Bulky NHC-Coordinated Main Group Compounds. *J. Chem. Theory Comput.* **2016**, *12*, 231–237.
- (52) Schneider, W. B.; Bistoni, G.; Sparta, M.; Saitow, M.; Riplinger, C.; Auer, A. A.; Neese, F. Decomposition of Intermolecular Interaction Energies within the Local Pair Natural Orbital Coupled Cluster Framework. *J. Chem. Theory Comput.* **2016**, *12*, 4778–4792.
- (53) Altun, A.; Neese, F.; Bistoni, G. Effect of Electron Correlation on Intermolecular Interactions: A Pair Natural Orbitals Coupled Cluster Based Local Energy Decomposition Study. *J. Chem. Theory Comput.* **2019**, *15*, 215–228.
- (54) Altun, A.; Saitow, M.; Neese, F.; Bistoni, G. Local Energy Decomposition of Open-Shell Molecular Systems in the Domain-Based Local Pair Natural Orbital Coupled Cluster Framework. *J. Chem. Theory Comput.* **2019**, *15*, 1616–1632.
- (55) Neese, F. The ORCA program system. *Wiley Interdiscip. Rev.: Comput. Mol. Sci.* **2012**, *2*, 73–78.

- (56) Szalewicz, K. Symmetry-adapted perturbation theory of intermolecular forces. *Wiley Interdiscip. Rev.: Comput. Mol. Sci.* **2012**, *2*, 254–272.
- (57) Parker, T. M.; Burns, L. A.; Parrish, R. M.; Ryno, A. G.; Sherrill, C. D. Levels of symmetry adapted perturbation theory (SAPT). I. Efficiency and performance for interaction energies. *J. Chem. Phys.* **2014**, *140*, 094106.
- (58) Hwang, J.; Li, P.; Smith, M. D.; Warden, C. E.; Sirianni, D. A.; Vik, E. C.; Maier, J. M.; Yehl, C. J.; Sherrill, C. D.; Shimizu, K. D. Tipping the Balance between S- π and O- π Interactions. *J. Am. Chem. Soc.* **2018**, *140*, 13301–13307.
- (59) Solel, E.; Ruth, M.; Schreiner, P. R. London Dispersion Helps Refine Steric A-Values: Dispersion Energy Donor Scales. *J. Am. Chem. Soc.* **2021**, *143*, 20837–20848.
- (60) Tolman, C. A. Steric effects of phosphorus ligands in organometallic chemistry and homogeneous catalysis. *Chem. Rev.* **1977**, *77*, 313–348.
- (61) Panek, J. S.; Prock, A.; Eriks, K.; Giering, W. P. Addition of carbenium ions to allylsilanes: interpretation of kinetic data via the quantitative analysis of ligand effects. *Organometallics* **1990**, *9*, 2175–2176.
- (62) Weicker, S. A.; Stephan, D. W. Activation of Carbon Dioxide by Silyl Triflate-Based Frustrated Lewis Pairs. *Chem.—Eur. J.* **2015**, *21*, 13027–13034.
- (63) Pracht, P.; Bohle, F.; Grimme, S. Automated exploration of the low-energy chemical space with fast quantum chemical methods. *Phys. Chem. Chem. Phys.* **2020**, *22*, 7169–7192.
- (64) Frisch, M. J.; Trucks, G. W.; Schlegel, H. B.; Scuseria, G. E.; Robb, M. A.; Cheeseman, J. R.; Scalmani, G.; Barone, V.; Petersson, G. A.; Nakatsuji, H.; Li, X.; Caricato, M.; Marenich, A. V.; Bloino, J.; Janesko, B. G.; Gomperts, R.; Mennucci, B.; Hratchian, H. P.; Ortiz, J. V.; Izmaylov, A. F.; Sonnenberg, J. L.; Ding, F.; Lipparini, F.; Egidi, F.; Goings, J.; Peng, B.; Petrone, A.; Henderson, T.; Ranasinghe, D.; Zakrzewski, V. G.; Gao, J.; Rega, N.; Zheng, G.; Liang, W.; Hada, M.; Ehara, M.; Toyota, K.; Fukuda, R.; Hasegawa, J.; Ishida, M.; Nakajima, T.; Honda, Y.; Kitao, O.; Nakai, H.; Vreven, T.; Throssell, K.; Montgomery, J. A., Jr.; Peralta, J. E.; Ogliaro, F.; Bearpark, M. J.; Heyd, J. J.; Brothers, E. N.; Kudin, K. N.; Staroverov, V. N.; Keith, T. A.; Kobayashi, R.; Normand, J.; Raghavachari, K.; Rendell, A. P.; Burant, J. C.; Iyengar, S. S.; Tomasi, J.; Cossi, M.; Millam, J. M.; Klene, M.; Adamo, C.; Cammi, R.; Ochterski, J. W.; Martin, R. L.; Morokuma, K.; Farkas, O.; Foresman, J. B.; Fox, D. J. *Gaussian 16*, Rev. C. 01; Wallingford, CT, 2016.
- (65) Turney, J. M.; Simmonett, A. C.; Parrish, R. M.; Hohenstein, E. G.; Evangelista, F. A.; Fermann, J. T.; Mintz, B. J.; Burns, L. A.; Wilke, J. J.; Abrams, M. L.; Russ, N. J.; Leininger, M. L.; Janssen, C. L.; Seidl, E. T.; Allen, W. D.; Schaefer, H. F.; King, R. A.; Valeev, E. F.; Sherrill, C. D.; Crawford, T. D. Psi4: an open-source ab initio electronic structure program. *Wiley Interdiscip. Rev.: Comput. Mol. Sci.* **2012**, *2*, 556–565.
- (66) Parrish, R. M.; Burns, L. A.; Smith, D. G. A.; Simmonett, A. C.; DePrince, A. E.; Hohenstein, E. G.; Bozkaya, U.; Sokolov, A. Y.; Di Remigio, R.; Richard, R. M.; Gonthier, J. F.; James, A. M.; McAlexander, H. R.; Kumar, A.; Saitow, M.; Wang, X.; Pritchard, B. P.; Verma, P.; Schaefer, H. F.; Patkowski, K.; King, R. A.; Valeev, E. F.; Evangelista, F. A.; Turney, J. M.; Crawford, T. D.; Sherrill, C. D. Psi4 1.1: An Open-Source Electronic Structure Program Emphasizing Automation, Advanced Libraries, and Interoperability. *J. Chem. Theory Comput.* **2017**, *13*, 3185–3197.
- (67) Johnson, E. R.; Keinan, S.; Mori-Sánchez, P.; Contreras-García, J.; Cohen, A. J.; Yang, W. Revealing Noncovalent Interactions. *J. Am. Chem. Soc.* **2010**, *132*, 6498–6506.
- (68) Contreras-García, J.; Johnson, E. R.; Keinan, S.; Chaudret, R.; Piquemal, J.-P.; Beratan, D. N.; Yang, W. NCIPLOT: A Program for Plotting Noncovalent Interaction Regions. *J. Chem. Theory Comput.* **2011**, *7*, 625–632.
- (69) Humphrey, W.; Dalke, A.; Schulten, K. VMD: Visual molecular dynamics. *J. Mol. Graph. Model.* **1996**, *14*, 33–38.

2.3 Silyl Groups Are Strong Dispersion Energy Donors



Abstract:

We present an experimental and computational study to investigate noncovalent interactions between silyl groups that are often employed as “innocent” protecting groups. We chose an extended cyclooctatetraene (COT)-based molecular balance comprising unfolded (1,4-disubstituted) and folded (1,6-disubstituted) valence bond isomers that typically display remote and close silyl group contacts, respectively. The thermodynamic equilibria were determined using nuclear magnetic resonance measurements. Additionally, we utilized Boltzmann weighted symmetry-adapted perturbation theory (SAPT) at the sSAPT0/aug-cc-pVDZ level of theory to dissect and quantify noncovalent interactions. Apart from the extremely bulky tris(trimethylsilyl)silyl “supersilyl” group, there is a preference for the folded 1,6-COT valence isomer, with London dispersion interactions being the main stabilizing factor. This makes silyl groups excellent dispersion energy donors, a finding that needs to be taken into account in synthesis planning.

Reference:

Lars Rummel, Henrik F. König, Heike Hausmann, and Peter R. Schreiner, *J. Org. Chem.* **2022**, *87*, 19, 13168–13177. DOI: 10.1021/acs.joc.2c01633

Reproduced with permission from:

© 2022, American Chemical Society
1155 16th Street NW
Washington, DC, 20036
United States of America

Silyl Groups Are Strong Dispersion Energy Donors

Lars Rummel,[#] Henrik F. König,[#] Heike Hausmann, and Peter R. Schreiner^{*}

Cite This: *J. Org. Chem.* 2022, 87, 13168–13177

Read Online

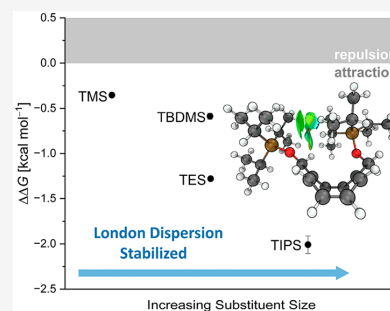
ACCESS |

Metrics & More

Article Recommendations

Supporting Information

ABSTRACT: We present an experimental and computational study to investigate noncovalent interactions between silyl groups that are often employed as “innocent” protecting groups. We chose an extended cyclooctatetraene (COT)-based molecular balance comprising unfolded (1,4-disubstituted) and folded (1,6-disubstituted) valence bond isomers that typically display remote and close silyl group contacts, respectively. The thermodynamic equilibria were determined using nuclear magnetic resonance measurements. Additionally, we utilized Boltzmann weighted symmetry-adapted perturbation theory (SAPT) at the sSAPT0/aug-cc-pVDZ level of theory to dissect and quantify noncovalent interactions. Apart from the extremely bulky tris(trimethylsilyl)silyl “supersilyl” group, there is a preference for the folded 1,6-COT valence isomer, with London dispersion interactions being the main stabilizing factor. This makes silyl groups excellent dispersion energy donors, a finding that needs to be taken into account in synthesis planning.



INTRODUCTION

Bulky substituents, such as *tert*-butyldimethylsilyl (TBDMS) or tri-*iso*-propylsilyl (TIPS), are usually considered to be repulsive, thereby affecting chemical reactions on the basis of their steric bulk.^{1–3} The attractive components of noncovalent interactions (NCIs) of such large and highly polarizable groups are usually not considered. Although similar sterically demanding substituents, for example, *tert*-butyl groups, have amply been demonstrated to interact strongly *via* stabilizing London dispersion (LD) interactions;^{4–7} similar behavior is generally not attributed to silyl groups.

This is surprising because bulky substituents are nowadays incorporated as design elements to increase intramolecular stability or facilitate intermolecular aggregation.^{13–19} Examples include organic compounds such as hexaphenylethane,^{20–24} coupled diamondoids,²⁵ or tetrahedranes,^{8,9} which are substantially stabilized by forming a strongly interacting LD shell around a labile core.^{6,23,26} In this context, tetrakis(trimethylsilyl)tetrahedrane (Figure 1, left) as the most stable tetrahedrane derivative reported thus far is particularly remarkable. Its even greater stability than *tert*-butyl analogue may be attributed to a combination of the “corset effect”, electronic stabilization of the tetrahedrane core, and LD interactions.^{8,9,25} While the “corset effect” is presumed to provide kinetic stabilization through steric inhibition of cage opening, the thermodynamic stability of tetrakis(trimethylsilyl)tetrahedrane is boosted by an increased σ -donor ability of trimethylsilyl (TMS) groups and LD interactions between them. Furthermore, LD interactions have also proven to be relevant in stabilizing exotic organometallic compounds⁷ such as disilanes,^{27,28} carbene analogues^{29,30} (Figure 1, middle), and *meta*-terphenyl

dimers^{10,11} of heavy group 14 elements. Because LD interactions are not only pairwise additive⁴ but also highly distance dependent (with R^{-6}), LD interactions are suited to stabilizing transition structures as well because of their increased polarizability as compared to the ground states.^{16,18} While the silylation of secondary alcohols is greatly assisted by LD^{31,32} (especially for large silyl substituents), their use as dispersion energy donors^{6,33} (DEDs) is currently limited to TMS. Hartwig *et al.*¹² utilized higher tetrel congeners (Si and Ge) of the *tert*-butyl DED to increase catalyst–substrate binding affinities to accelerate reactions (Figure 1, right).

We chose the evaluation of a disubstituted cyclooctatetraene^{34,35} (COT) molecular balance as an appropriate system to determine the strengths of NCIs between several commonly employed silyl groups.³⁶ This molecular balance consists of two distinct valence isomers (Scheme 1) that can equilibrate *via* a double-bond valence bond isomerization.^{37,38} For bulky *tert*-butyl substituents, experimental^{35,36,39,40} and computational^{41,42} studies suggest the “folded” 1,6-isomer to be preferred in solution and in the gas phase. Considering the steric size of commonly utilized silyl groups, it is reasonable to hypothesize about the potential of these groups to serve as DEDs because they are far more polarizable.⁴³ In a recent study, we have addressed the effective size of commonly used silyl groups by utilizing a disubstituted COT molecular balance

Received: July 12, 2022

Published: September 27, 2022



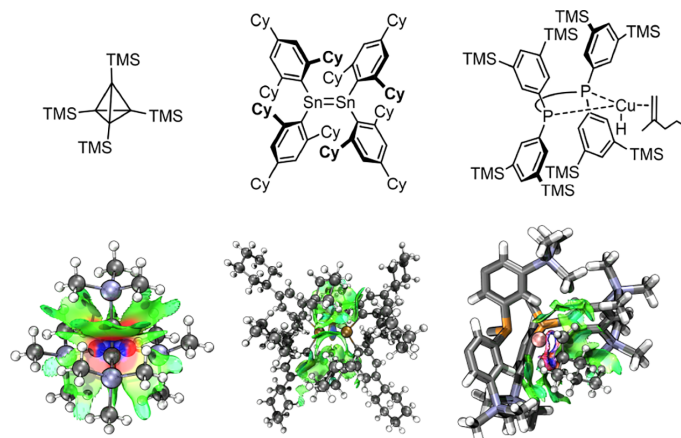
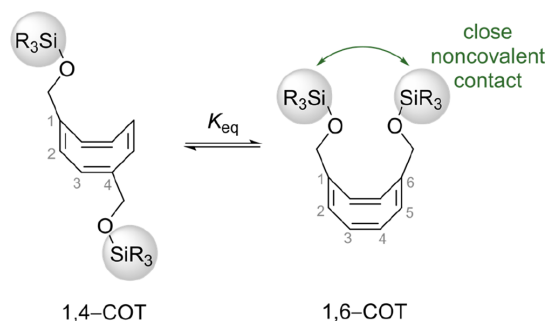


Figure 1. Intramolecular NCI plots of tetrakis(trimethylsilyl)tetrahedrane^{8,9} (left), $\{\text{Sn}(\text{C}_6\text{H}_2\text{-}2,4,6\text{-Cy}_3)_2\}_2$ (Cy = cyclohexyl, middle),^{10,11} and the favored si face hydrocupration transition structure according to Hartwig *et al.*¹² (selected functional groups omitted for clarity). Isosurfaces (isovalue s of 0.5, ranging from $\text{sign}(\lambda_2)\rho = -0.05$ to $+0.05$ a.u.) are color-coded red (indicating strong repulsion), blue (strong attractive interactions), and green (corresponding to weak NCIs).

Scheme 1. Equilibrium of 1,4- and 1,6-Di-*O*-silyl Substituted COT



with silyl groups directly attached in the 1,4-/1,6-position, and we demonstrated that an increase in size from TMS to extremely bulky tris(trimethylsilyl)silyl (TTMSS) leads to destabilizing internal strain on the COT backbone dominating the equilibrium between 1,4- and 1,6-COT.⁴⁴ The extended COT system under consideration here circumvents this problem. Computations suggested a balance between Pauli repulsion (“steric hindrance”) and attractive LD interactions, with the latter being the larger component. We hypothesized that the introduction of a $-\text{CH}_2\text{O}-$ spacer to the system would considerably reduce the internal strain in the 1,6-isomer (Scheme 1), and we demonstrate in the following that this is indeed the case. On the other hand, an increase in flexibility might come at the cost of an entropic penalty for the 1,6-isomer in which rotational degrees of freedom are significantly restrained.^{45,46} Because the investigated silyl groups are often employed as protecting groups for alcohols, another advantage of such a molecular balance lies in the close structural relationship to the common use case.

RESULTS AND DISCUSSION

We chose somewhat of an unusual route to generate the diol precursor (3) starting from dimethyl 1,4-cubanedicarboxylate

(1) that can be rearranged catalytically with rhodium.^{47,48} This choice was made on the basis that other synthetic routes *via* cyclooctatriene or COT toward 2 turned out to be very low-yielding; 1 is commercially available but can also readily be prepared.⁴⁹ Reduction of the COT dimethyl ester (2), 3, and preparation of the targeted silyl ethers (4) was accomplished *via* a standard alcohol protecting procedure⁵⁰ (Figure 2, top) utilizing TMS, triethylsilyl (TES), TBDMS, TIPS, *tert*-butyldiphenylsilyl (TBDPS), and TTMSS groups.

We utilized nuclear magnetic resonance (NMR) measurements to determine the valence isomer equilibrium constants. The allylic CH_2 groups of the spacer in conjunction with characteristic signals in the olefinic region enabled us to quantify the 1,4- and 1,6-isomers (Figure 2, bottom). Due to signal broadening at higher temperatures and resulting signal overlap, the thermodynamic equilibria could not be subjected to van't Hoff analyses to determine the individual ΔH and ΔS contributions. Each NMR sample was equilibrated for 16 h at 40 °C, and the equilibration was monitored *via* NMR. Chloroform was chosen as the solvent to ensure signal separation between the isomers. Figure 3 shows the results of the experiments (black markings) correlated to polarizability values of each silyl group (computed at revDSD-PBEP86-D4/def2-QZVPP//PBEh-3c).

In general, the overall influence of silyl groups on the equilibria is small. Still, $\Delta_r G^{313}$ could be measured very accurately with error bars an order of magnitude below the measured values (see Supporting Information for details). While the di-OTMS-COT equilibrium is essentially thermoneutral ($\Delta_r G^{313} \approx 0$ kcal mol⁻¹), larger silyl groups shift the equilibrium toward more crowded 1,6-COT. Despite their similar size and surface area of around 170 Å² (see Supporting Information), the OTBDMS and OTES substituted systems differ in their behavior as DED groups. With $\Delta_r G^{313} = -0.08 \pm 0.00(4)$ kcal mol⁻¹ for di-OTBDMS-COT, its energy in favor of 1,6-COT is twice as large as that of di-OTES-COT. This can be rationalized by an increasing entropic penalty for the more flexible TES group in 1,6-COT.⁵¹ The most stabilizing effect stems from the interaction of two TIPS groups. The di-OTIPS-COT equilibrium most clearly favors the folded 1,6-COT

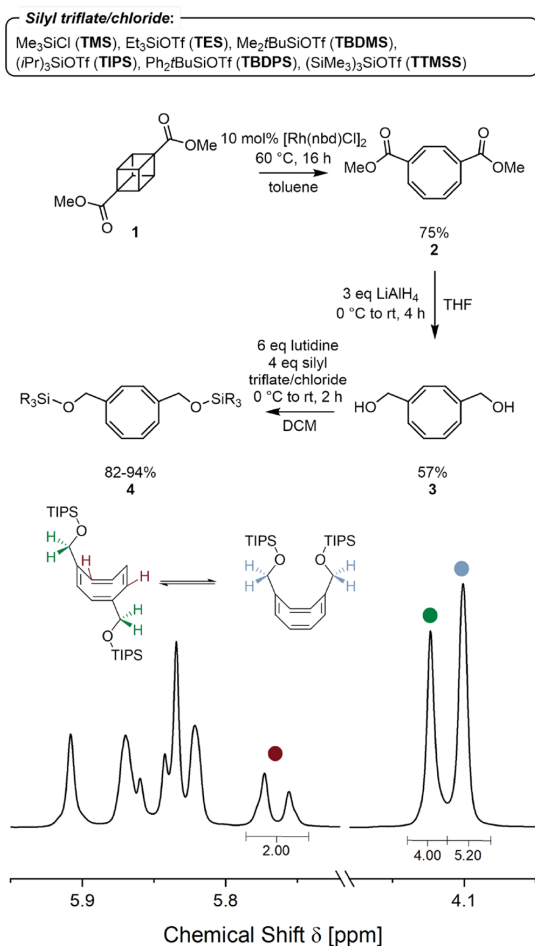


Figure 2. Top: Synthesis of 1,4- and 1,6-di-O-silyl substituted COTs (4); bottom: ¹H NMR spectra (600 MHz) and signal assignment of the equilibrium between 1,4- (green) and 1,6-di-OTIPS (blue) COT at 40 °C in chloroform.

($\Delta_r G^{313} = -0.14 \pm 0.01$ kcal mol⁻¹) isomer. More polarizable groups such as TBDPS and TTMSS appear to be less effective DEDs (vide infra). While TBDPS favors the more crowded 1,6-COT, the di-OTMSS substitution pattern prefers the “unfolded” 1,4-COT by $\Delta_r G^{313} = +0.13 \pm 0.01$ kcal mol⁻¹. While the -CH₂O- spacer reduces internal strain, entropic contributions significantly dampen the effects of attractive NCIs; the conformational entropy penalty due to the spacer group amounts to $\Delta S_{\text{conf}} \approx +1.1$ kcal mol⁻¹ at 40 °C computed according to Grimme and co-workers.^{52,53} Still, such small $\Delta_r G^{313}$ values are quite relevant for transition structures, where even small effects lead to large changes in rates and/or selectivities.

Apart from experimental investigations, we also examined the equilibria computationally, notwithstanding the challenges associated with recovering such small ΔG values. While the inclusion of a spacer group and the utility of flexible silyls (such as TES) increases the number of possible conformers per valence isomer significantly, the identification of a single

most prominent structure can prove to be ineffective.⁵⁴ The computational error due to conformational complexity was shown by Lledós *et al.*⁵⁵ to surmount up to 10 kcal mol⁻¹ for bulky and flexible ligands. To account for a larger conformational space,^{52,56} multiple conformers must be included in thermochemical investigations⁵⁷ as well as spectral predictions.^{58,59} Recently, the necessity of a conformational analysis has been demonstrated by Chen *et al.*⁶⁰ to rationalize the interplay of bulky DEDs with cation- π interactions. We utilized the conformer-rotamer ensemble sampling tool (CREST)⁶¹ to identify the conformers lowest in energy. The resulting structures were further optimized using the PBEh-3c⁶²⁻⁶⁶ method due to its efficient performance to give accurate geometries for large molecular systems.⁶⁶ With the aim to qualitatively sort and weigh conformers, all PBEh-3c optimized structures were utilized in a Boltzmann distribution and their probability was calculated at 313.15 K. To reduce the number of conformers, only molecules with a Boltzmann probability > 1% were used for single point computations at the revDSD-PBEP86-D4/def2-QZVPP⁶⁷⁻⁷² level of theory, including solvation effects (chloroform) *via* the PCM^{73,74} model. Accordingly, all conformers that do not play a dominant role at 315.15 K were omitted from the analysis. The Boltzmann weighted Gibbs free energies are also depicted in Figure 3 (green makings), and we are pleased that the qualitative agreement is very good: the relative energies are significantly shifted toward the more crowded 1,6-COT structures. However, the computed absolute values are significantly overestimated. This may be due to errors in the computations (for the chosen functional and basis set, errors are estimated around ± 2 kcal mol⁻¹ of absolute weighted mean average deviation according to Martin *et al.*⁷¹) and possibly incomplete inclusion of solvation effects with the simple continuum model.^{17,36,75} Furthermore, incorporation of the -CH₂O- spacer promotes free rotation of the silyl groups, hence leading to very flat conformational hypersurfaces. To include the most relevant conformers of a conformer ensemble in the thermodynamic analysis, a Boltzmann distribution analysis was performed. As a result, the entropy error could be minimized and the relative difference in energies be reproduced.⁵² The strongest effect is observed for di-OTIPS-COT, which favors the folded over the unfolded isomer by around -2.7 kcal mol⁻¹. The bulkiest but most polarizable substituent (TTMSS) is the only group favoring 1,4-COT by around 0.3 kcal mol⁻¹.

To quantify intramolecular LD stabilization, we utilized symmetry-adapted perturbation theory⁷⁶ (SAPT) at the sSAPT0/aug-cc-pVDZ level of theory in conjunction with the PBEh-3c optimized structures. The scaled protocol was employed according to Parker *et al.*⁷⁷ to increase performance. Because we did not identify a single conformer for each isomer but rather studied an ensemble to address structural flexibility, we applied a Boltzmann distribution analysis for the energy decomposition method as well. Consequently, all conformers utilized for single point energy computations were taken into account in the scaled SAPT (sSAPT) analysis. To assess the interaction energy between two silyl groups, the molecular backbone and the spacer groups were removed, and the resulting radicals were saturated (*cf.* Scheme S1 in the Supporting Information).⁷⁸ The resulting energies were applied against the probability that each conformer is occupied at 298 K according to the revDSD-PBEP86-D4/def2-QZVPP single point energy computations. Figure 4 depicts the relative

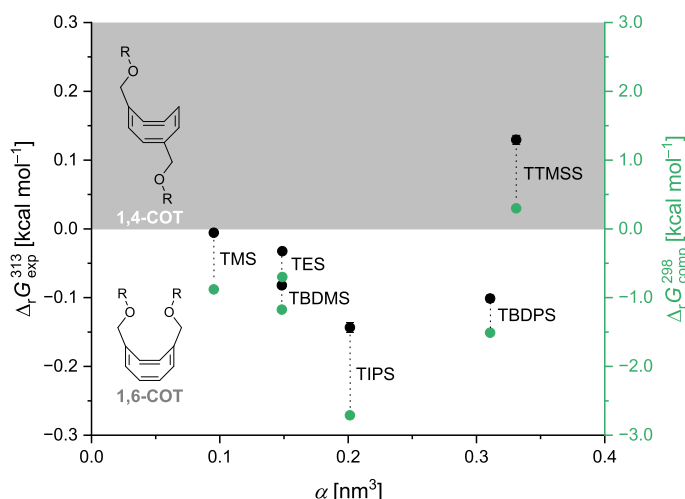


Figure 3. Correlation of the Gibbs free energies for the equilibrium of 1,4- and 1,6-di-O-silyl substituted COT in chloroform. The experimental data (black markings) were derived from NMR measurements at 40 °C. The computational data (green markings) were derived from Boltzmann distribution analysis at PCM(chloroform)-revDSD-PBEP86-D4/def2-QZVPP//PBEh-3c. All data points in the white area favor 1,6-disilyl-COT.

energy differences (ΔE_x) between the folded and unfolded isomers.

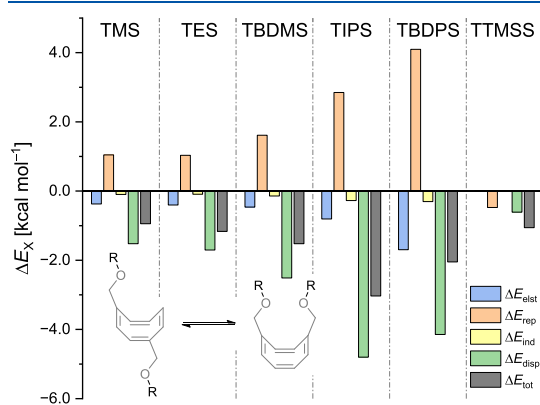


Figure 4. Relative energies between the folded and unfolded isomers of a Boltzmann weighted sSAPT analysis of silyl groups of all relevant conformers according to the conformer ensemble of each isomer. Computations were performed at the sSAPT0/aug-cc-pVDZ level of theory.

The sSAPT analysis dissects the relative total interaction energy ΔE_{tot} (gray bars) into its main components (for absolute energy values, see the Supporting Information). While inductive effects ΔE_{ind} (yellow bars) play only a minor role throughout all conformers, relative electrostatic interactions ΔE_{elst} (blue bars) can contribute to the stability of the folded isomer by up to $-1.7 \text{ kcal mol}^{-1}$ (TBDPS dimer). Nevertheless, electrostatic contributions are not important for the dimerization of alkylsilanes. Here, ΔE_{elst} does not exceed $-0.8 \text{ kcal mol}^{-1}$ (TIPS dimer). For TTMSS dimers, electrostatic and inductive effects cancel and do not contribute to the relative total interaction energy. The most prominent effects governing the dimerization of silanes are attractive LD

interactions ΔE_{disp} (green bars) and Pauli (exchange) repulsion ΔE_{rep} (orange bars). While the latter increases with the size of silyl groups from TMS to TBDPS, the largest substituent slightly favors the folded over the unfolded isomer with respect to repulsive interactions. This hints to similar distances of the TTMSS groups in the folded ($d_{\sigma-\sigma} \approx 2.53 \text{ \AA}$) and unfolded ($d_{\sigma-\sigma} \approx 2.64 \text{ \AA}$) isomers, implying a rotation of the spacer group to minimize repulsive interactions in the folded isomer. The largest ΔE_{rep} is observed for the TBDPS dimer, with $\Delta E_{\text{rep}} = 4.1 \text{ kcal mol}^{-1}$ destabilizing the folded isomer. Nevertheless, the steric repulsion due to close silyl contacts is insufficient to rationalize the observed experimental and computational data (Figure 3). The largest interaction counteracting Pauli (exchange) repulsion is LD. As a matter of fact, ΔE_{disp} is the largest contributor to ΔE_{tot} for all dimers. The TIPS system benefits the most from LD interactions of around $-4.8 \text{ kcal mol}^{-1}$. Both TBDPS and TTMSS show lower ΔE_{disp} and, therefore, appear to be weaker DEDs than TIPS. Nevertheless, the relative total interaction energy ΔE_{tot} and ΔE_{disp} can be directly correlated to the overall observed and computed Gibbs free energies (Figure 3). The similar trend of both energies and experimental Gibbs free energies confirms that the observed effects stem from NCIs of the silyl groups, with LD as the main contributor for all systems studied.

While the results of TMS, TES, TBDMS, and TIPS fit qualitatively to the logical series of size and polarizability, those of TBDPS and TTMSS do not. To shed more light on this, we analyzed the conformer ensemble of each isomer. Contrary to expectations, the unfolded 1,4-disubstituted COT displays stabilizing intramolecular interactions similar to those of the folded isomer. Accordingly, the spacer group allows the silyl groups to bend around the 1,4-COT moiety to enable close intramolecular interactions. We depicted the most prominent conformer of the folded and unfolded TIPS and TBDPS system for comparison *via* an intramolecular NCI plot,^{79,80} highlighting only NCIs between the silyl groups (Figure 5). Therefore, we plotted the reduced density gradient in regions of low electron density between the silyl groups. The resulting

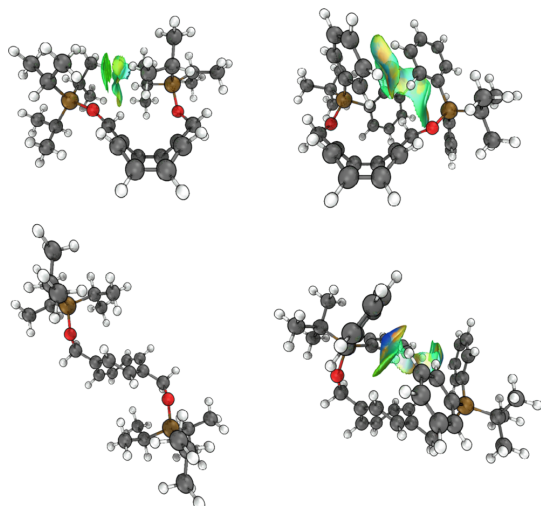


Figure 5. Intramolecular NCI plot of the folded 1,6-COT with TIPS (top, left) and TBDPS (top, right) and the unfolded 1,4-COT with TIPS (bottom, left) and TBDPS (bottom, right) at PBEh-3c. The most stable conformers were chosen according to the Boltzmann analysis. Isosurfaces (isovalue s of 0.5, ranging from $\text{sign}(\lambda_2)\rho = -0.05$ to $+0.05$ a.u.) are color coded red (indicating strong repulsion), blue (strong attractive interactions), and green (corresponding to weak NCIs).

isosurfaces are color coded in red, blue, and green. Whereas the first two correspond to strongly repulsive and attractive interactions, respectively, the latter can be described as weakly noncovalent, that is, LD, interactions.

Both experimental and computational data suggest the TIPS group to be the strongest DED group in the system studied. In accordance with the concept of molecular balances, the folded isomer (Figure 5, top, left) consists of close σ - σ contacts ($d_{\sigma-\sigma} \approx 2.33$ Å as shortest contact) between both silyl groups. Therefore, the NCI plot shows a green isosurface, indicating LD interactions. According to the SAPT analysis, these interactions correspond to $E_{\text{disp}} = -5.1$ kcal mol⁻¹ for the entire ensemble of LD interactions. On the other hand, the unfolded isomer (Figure 5, bottom, left) shows no interaction in the NCI plot due to the LD distance dependence. Nevertheless, SAPT suggests a small contribution of $E_{\text{disp}} = -0.3$ kcal mol⁻¹ for 1,4-COT. As a result, the relative energy $\Delta E_{\text{disp}} = -4.8$ kcal mol⁻¹ (Figure 4) strongly favors the folded isomer. While experimental data suggest fewer stabilizing interactions for TBDPS in the folded 1,6-COT (Figure 3), the NCI plot does not agree. The folded 1,6-disubstituted system shows larger isosurfaces between the phenyl moieties than for the σ -contacts in the TIPS system. The absolute value for the LD interactions for the folded TBDPS-COT rises up to $E_{\text{disp}} = -15.7$ kcal mol⁻¹ for the entire Boltzmann-weighted ensemble. The origin of stabilization lies in two offset T-shaped phenyl contacts ($d_{\text{CH}-\pi} \approx 2.33$ Å). While this classifies TBDPS as a strong DED, the overall effect is smaller than for TIPS. The observed ratio can be rationalized with an analysis of the unfolded isomer. Due to the flexibility of the spacer group, TBDPS twists around to form two T-shaped phenyl contacts ($d_{\text{CH}-\pi} \approx 2.56$ Å) in the unfolded 1,4-COT as well. According to SAPT, the interaction stabilizes the unfolded isomer by

around $E_{\text{disp}} = -11.5$ kcal mol⁻¹. A similar but weaker effect can be observed for TTMSS ($E_{\text{disp}} = -4.0$ kcal mol⁻¹ for the entire Boltzmann-weighted ensemble of the folded isomer).

While the measured absolute values with the di-*O*-silyl substituted COT are small (Figure 3), the impact of the spacer group becomes apparent by comparing the computed data with experimental measurements.⁴⁴ Note that the di-silyl substituted COTs were investigated in toluene, while the di-*O*-silyl substituted COTs were investigated in chloroform due to an incomplete signal separation of the latter in toluene. The ΔG difference due to solvation can be estimated to be around -0.1 kcal mol⁻¹ for the COT system going from toluene to chloroform.³⁶ While direct attachment of silyl groups at COT suffers from strain (ΔE_{strain}), the incorporation of a spacer group increases the flexibility, resulting in an entropic penalty in favor of the unfolded balance (ΔS). As already mentioned, di-*O*-TMS-COT does not benefit from the incorporation of $-\text{CH}_2\text{O}-$ groups but suffers from an entropic penalty⁵¹ due to increasing flexibility without additional stabilization due to LD. Figure 6 shows the total energy differences $\Delta\Delta E$ of the relative

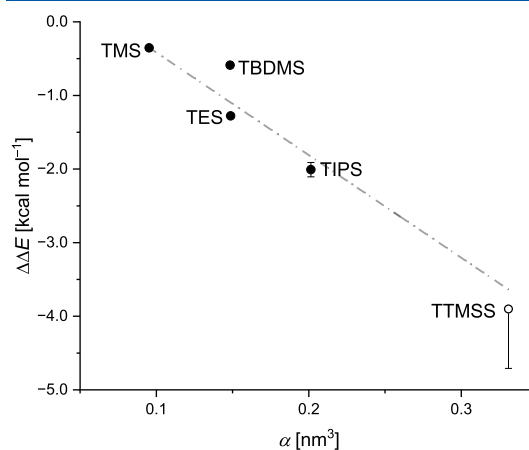


Figure 6. Correlating the total energy difference $\Delta\Delta E$ between di-*O*-silyl COT and di-silyl-COT with polarizabilities excluding strain energy (ΔE_{strain}) and entropic penalties (ΔS). Negative energy values correspond to attractive interactions. For TTMSS, the smallest energy difference was approximated.

Gibbs free energy values $\Delta\Delta G$ with $\Delta\Delta G = \Delta G_{\text{di-O-Si-COT}} - \Delta G_{\text{di-Si-COT}}$. Additionally, ΔE_{strain} and ΔS were considered computationally to exclude them from the analysis. Consequently, $\Delta\Delta E$ was calculated according to the following equation:

$$\Delta\Delta E = \Delta\Delta G - \Delta E_{\text{strain}} - \Delta S$$

$\Delta\Delta E$ corresponds to the total energy gain (negative energy values in Figure 6) arising from close silyl group contacts, excluding entropic penalties and energy gain due to strain release. In combination with the SAPT results (Figure 4) and NCI plots (Figure 5), most of the interactions can be assigned to LD. The largest energy change was observed for the TTMSS group ($\Delta\Delta E = -3.9$ kcal mol⁻¹). Because only the 1,4-di-TTMSS-COT could be reported in the earlier study, the $\Delta\Delta G$ for TTMSS (unfilled circle) represents the minimal shift in energy toward the folded isomer. The exact energy gap is larger but could not be determined. Accordingly, the TIPS group

shows the highest stabilizing interaction energy detected for both molecular balances ($\Delta\Delta E = -2.0$ kcal mol⁻¹).

CONCLUSIONS

We report on our approach to quantifying NCIs between silyl groups in a molecular balance based on a COT motif. By including a $-\text{CH}_2\text{O}-$ spacer group between the COT molecular balance and the silyl groups, we measured the equilibria between 1,4- and 1,6-di-*O*-silyl substituted COT, identifying attractive interactions due to $\sigma-\sigma$ or $\text{CH}-\pi$ contacts. Counterintuitively, NMR measurements reveal that the bulky TIPS group shifts the equilibrium between 1,4- and 1,6-di-*O*-silyl substituted COT furthest toward the folded and more crowded valence isomer. Computational thermochemical data underscore this trend.

An SAPT analysis identifies LD interactions as the key NCIs between the silyl groups. The incorporation of a flexible $-\text{CH}_2\text{O}-$ spacer group allowed the silyl groups to maximize these stabilizing interactions. However, flexibility comes at the cost of an unfavorable folding entropy, and the SAPT analysis furthermore revealed 1,4-isomers of balances substituted with very bulky silyl groups to be significantly stabilized by LD interactions as well. These two effects work in opposite ways but still favor the 1,6-isomer. On the other hand, comparison of the current more flexible molecular balance with previously studied di-silyl substituted COTs (lacking a $-\text{CH}_2\text{O}-$ spacer) highlights how a system governed by repulsion may be modified to profit from bulky DED substituents.

Our results demonstrate that silyl groups are more than just providers of steric bulk and can counterintuitively affect conformational preferences *via* their actions as good DEDs.

EXPERIMENTAL SECTION

Thin layer chromatography was carried out using Polygram SIL G/UV₂₅₄ plates with detection *via* UV $\lambda = 254$ nm and by staining with a 10 wt % ethanolic phosphomolybdic acid stain solution. All chemicals were commercially obtained from Acros Organics, TCI, Boron Molecular, and Sigma-Aldrich and were used without further purification. Anhydrous solvents were purchased from Acros Organics. Unless otherwise noted, all reactions were carried out under standard Schlenk conditions employing N₂ as inert gas. Standard NMR spectra were obtained using Bruker AVANCE II 400 MHz and Bruker AVANCE III HD 400 MHz (¹³C spectra) spectrometers. Elevated temperature NMR experiments were carried out with a Bruker AVANCE III HD 600 MHz spectrometer. High resolution mass spectra were obtained with a Bruker micrOTOF mass spectrometer. For elevated temperature measurements, NMR samples were equilibrated for 16 h at 40 °C prior to the experiment, utilizing an IKA ICC basic eco 8 immersion circulator.

Elevated Temperature NMR Experiments. After sample transfer from the thermostat to the NMR spectrometer, equilibration was continued for another hour in the spectrometer before the spectra were recorded at 40 °C.

Solutions of tri(*isobutyl*)silyl triflate and TTMSS triflate were prepared according to a modified literature procedure and were used without further purification.⁸¹

Dimethyl-cyclooctatetraene-1,4/1,6-dicarboxylate (2). Compound 2 was prepared according to a literature procedure⁴⁸ from commercially obtained 1 (Boron Molecular). 1.160 g (5.27 mmol) of 1 and 242.8 mg (0.53 mmol, 0.10 equiv) of [Rh(nbd)Cl]₂ were dissolved in 80 mL of anhydrous toluene. The reaction mixture was subsequently heated to 60 °C for 16 h utilizing an oil bath. Afterward, the solvent was removed under reduced pressure and purification of the crude product *via* silica flash column chromatography (2:1 mixture of *n*-hexane and ethyl acetate) yielded 870.5 mg (3.95 mmol, 75%) of 2 as a yellow solid.

¹H NMR (400 MHz, CDCl₃), 1,4-2: δ 7.09 (s, 2H), 6.07 (q, $J = 2.8$ Hz, 2H), 5.99 (q, $J = 2.8$ Hz, 2H), and 3.77 (s, 6H); ¹H NMR (400 MHz, CDCl₃), 1,6-2: δ 7.03 (s, 2H), 6.16 (s, 2H), 6.03 (s, 2H), and 3.75 (s, 6H); ¹³C{¹H} NMR (100 MHz, CDCl₃): δ 166.0, 165.9, 141.8, 140.0, 135.1, 133.8, 133.2, 132.3, 130.7, 129.4, 52.4, and 52.2; HRMS (ESI-TOF) m/z : [M + Na]⁺ calcd for C₁₂H₁₂O₄Na, 243.0633; found, 243.0628.

This is in agreement with previously published data.⁴⁸

Cyclooctatetraene-1,4/1,6-dimethanol (3). To a solution of 821.2 mg (3.73 mmol) of 2 in 90 mL of anhydrous tetrahydrofuran was added 426.3 mg (11.2 mmol, 3 equiv) of LiAlH₄ in small portions at 0 °C. After complete addition (approx. 30 min), the reaction mixture was allowed to reach room temperature and was left stirring for another 3 h and 30 min. The reaction mixture was then carefully quenched with 20 mL of saturated aqueous Na₂SO₄ solution. The obtained mixture was then transferred to a separatory funnel and extracted with ethyl acetate (3 × 100 mL). The combined organic phases were dried over anhydrous MgSO₄, and the solvent was evaporated under reduced pressure, yielding the crude product as an orange oil. After purification *via* silica flash column chromatography (ethyl acetate), 350.1 mg (2.13 mmol, 57%) of 3 was obtained as a slightly yellow oil.

¹H NMR (400 MHz, DCM-*d*₂), 1,4-3: δ 5.96–5.76 (m, 6H) and 4.00 (s, 4H); 1.97 (s, 2H); ¹H NMR (400 MHz, DCM-*d*₂), 1,6-3: δ 5.96–5.76 (m, 6H) and 3.99 (s, 4H); 1.97 (s, 2H); ¹³C{¹H} NMR (100 MHz, DCM-*d*₂): δ 144.0, 143.8, 133.4, 133.3, 131.9, 131.7, 127.7, 127.0, and 66.5; HRMS (ESI-TOF) m/z : [M + Na]⁺ calcd for C₁₀H₁₂O₂Na, 187.0733; found, 187.0735.

1,4-/1,6-Di-*O*-silyl Cyclooctatetraenes (4a–g). Di-*O*-silyl cyclooctatetraenes 4a–g were prepared according to the following general procedure: compound 3 (~30 mg) was dissolved in 8 mL of anhydrous dichloromethane (DCM) while stirring. 6 equiv of 2,6-lutidine was added at room temperature, and the reaction mixture was cooled to 0 °C. 4 equiv of the corresponding silyl triflate or silyl chloride was then added, and the reaction mixture was allowed to reach room temperature. After 2 h at room temperature, the reaction was quenched by addition of 3 mL of deionized water. After extraction with DCM (3 × 10 mL), the combined organic phases were dried over MgSO₄ and concentrated under reduced pressure. The crude products were purified *via* silica column chromatography (2:1 mixture of *n*-hexane and DCM), yielding compounds 4a–g as colorless oils.

1,4-/1,6-Di-*O*-TMS-COT (4a). 31.4 mg (0.19 mmol) of 3, 0.13 mL (1.12 mmol, 6 equiv) of 2,6-lutidine, and 0.10 mL (0.79 mmol, 4 equiv) of TMSCl were mixed. After purification *via* silica column chromatography (2:1 mixture of *n*-hexane and DCM), 53.8 mg (0.17 mmol, 90%) of 4a was obtained as a colorless oil.

¹H NMR (400 MHz, CDCl₃), 1,4-4a: δ 5.89–5.72 (m, 6H) and 4.01 (s, 4H); 0.12 (s, 18H); ¹H NMR (400 MHz, CDCl₃), 1,6-4a: δ 5.89–5.72 (m, 6H) and 3.99 (s, 4H); 0.12 (s, 18H); ¹³C{¹H} NMR (100 MHz, CDCl₃): δ 142.8, 142.4, 132.6, 132.3, 131.7, 131.3, 126.3, 126.1, 65.9, 65.8, –0.2, and 0.3; HRMS (ESI-TOF) m/z : [M + Na]⁺ calcd for C₁₆H₂₈O₂Si₂Na, 331.1526; found, 331.1521.

1,4-/1,6-Di-*O*-TES-COT (4b). 28.7 mg (0.17 mmol) of 3, 0.12 mL (1.04 mmol, 6 equiv) of 2,6-lutidine, and 0.16 mL (0.71 mmol, 4 equiv) of TESOTf were mixed. After purification *via* silica column chromatography (2:1 mixture of *n*-hexane and DCM), 60.1 mg (0.15 mmol, 87%) of 4b was obtained as a colorless oil.

¹H NMR (400 MHz, CDCl₃), 1,4-4b: δ 5.89–5.70 (m, 6H), 4.04 (s, 4H); 0.96 (t, $J = 7.9$ Hz, 18H) and 0.65–0.57 (m, 12H); ¹H NMR (400 MHz, CDCl₃), 1,6-4b: δ 5.87–5.70 (m, 6H) and 4.03 (s, 4H); 0.96 (t, $J = 7.9$ Hz, 18H) and 0.65–0.57 (m, 12H); ¹³C{¹H} NMR (100 MHz, CDCl₃): δ 143.0, 142.4, 132.5, 132.2, 131.7, 131.3, 126.0, 125.7, 66.0, 65.8, 6.9, 4.6 and 4.6; HRMS (ESI-TOF) m/z : [M + Na]⁺ calcd for C₂₂H₄₀O₂Si₂Na, 415.2464; found, 415.2458.

1,4-/1,6-Di-*O*-TBDMS-COT (4c). 30.1 mg (0.18 mmol) of 3, 0.13 mL (1.12 mmol, 6 equiv) of 2,6-lutidine, and 0.17 mL (0.74 mmol, 4 equiv) of TBDMSOTf were mixed. After purification *via* silica column chromatography (2:1 mixture of *n*-hexane and DCM), 67.7 mg (0.17 mmol, 94%) of 4c was obtained as a colorless oil. Preparation of 4c

was also carried out on a larger scale, applying the reaction conditions outlined above. 40 mL of anhydrous DCM as the solvent, 145.8 mg (0.89 mmol) of **3**, 0.62 mL (5.34 mmol, 6 equiv) of 2,6-lutidine, and 0.82 mL (3.57 mmol, 4 equiv) of TBDMSOTf were utilized. The reaction mixture was quenched with 15 mL of deionized water and extracted with DCM (3 × 40 mL). Purification *via* silica column chromatography (2:1 mixture of *n*-hexane and DCM) yielded 319.3 mg (0.81 mmol, 91%) of **4c** as a colorless oil.

¹H NMR (400 MHz, CDCl₃), **1,4-4c**: δ 5.89–5.71 (m, 6H) and 4.04 (s, 4H); 0.91 (s, 18H) and 0.07 (s, 12H); ¹H NMR (400 MHz, CDCl₃), **1,6-4c**: δ 5.89–5.71 (m, 6H) and 4.01 (s, 4H); 0.91 (s, 18H) and 0.07 (s, 12H); ¹³C{¹H} NMR (100 MHz, CDCl₃): δ 143.0, 142.5, 132.5, 132.2, 131.7, 131.3, 125.8, 125.6, 66.3, 66.1, 26.1, 18.6, –5.1, and –5.2; HRMS (ESI-TOF) *m/z*: [M + Na]⁺ calcd for C₂₂H₄₀O₂Si₂Na, 415.2464; found, 415.2460.

1,4-/1,6-Di-O-TIBS-COT (4d). 32.5 mg (0.18 mmol) of **3**, 0.14 mL (1.21 mmol, 6 equiv) of 2,6-lutidine, and an *n*-pentane solution (0.79 mmol, 4 equiv) of TIBSOTf (0.22 mL [0.84 mmol]) of triisobutyl silane and 0.07 mL [0.79 mmol] of trifluoromethanesulfonic acid in 2 mL of *n*-pentane were mixed. After purification *via* silica column chromatography (2:1 mixture of *n*-hexane and DCM), 66.3 mg (0.17 mmol, 85%) of **4d** was obtained as a colorless oil.

¹H NMR (400 MHz, CDCl₃), **1,4-4d**: δ 5.87–5.70 (m, 6H) and 4.01 (s, 4H); 1.90–1.76 (m, 6H), 0.96 (s, 36H) and 0.66–0.58 (m, 12H); ¹H NMR (400 MHz, CDCl₃), **1,6-4d**: δ 5.87–5.70 (m, 6H), 3.98 (s, 4H); 1.90–1.76 (m, 6H), 0.94 (s, 36H) and 0.66–0.58 (m, 12H); ¹³C{¹H} NMR (100 MHz, CDCl₃): δ 142.8, 142.2, 132.4, 132.2, 131.7, 131.3, 125.9, 125.4, 65.7, 65.5, 26.6, 25.5, 25.4 and 24.4; HRMS (ESI-TOF) *m/z*: [M + Na]⁺ calcd for C₃₄H₆₄O₂Si₂Na, 583.4342; found, 583.4341.

1,4-/1,6-Di-O-TIPS-COT (4e). 29.6 mg (0.18 mmol) of **3**, 0.13 mL (1.12 mmol, 6 equiv) of 2,6-lutidine, and 0.19 mL (0.71 mmol, 4 equiv) of TIPSOTf were mixed. After purification *via* silica column chromatography (2:1 mixture of *n*-hexane and DCM), 77.5 mg (0.16 mmol, 90%) of **4e** was obtained as a colorless oil.

¹H NMR (400 MHz, CDCl₃), **1,4-4e**: δ 5.95–5.71 (m, 6H) and 4.12 (s, 4H); 1.01–1.16 (m, 42H); ¹H NMR (400 MHz, CDCl₃), **1,6-4e**: δ 5.95–5.71 (m, 6H) and 4.09 (s, 4H); 1.01–1.16 (m, 42H); ¹³C{¹H} NMR (100 MHz, CDCl₃): δ 143.1, 142.3, 132.4, 132.2, 131.7, 131.3, 125.5, 125.2, 66.3, 66.2, 18.2 and 12.2; HRMS (ESI-TOF) *m/z*: [M + Na]⁺ calcd for C₂₈H₅₂O₂Si₂Na, 499.3404; found, 499.3397.

1,4-/1,6-Di-O-TBDPS-COT (4f). 30.3 mg (0.18 mmol) of **3**, 0.13 mL (1.12 mmol, 6 equiv) of 2,6-lutidine, and 0.22 mL (0.74 mmol, 4 equiv) of TBDPSOTf were mixed. After purification *via* silica column chromatography (2:1 mixture of *n*-hexane and DCM), 109.4 mg (0.17 mmol, 92%) of **4f** was obtained as a colorless oil.

¹H NMR (400 MHz, CDCl₃), **1,4-4f**: δ 7.75–7.64 (m, 8H), 7.45–7.34 (m, 12H), 6.01–5.70 (m, 6H) and 4.10 (s, 4H); 1.08 (s, 18H); ¹H NMR (400 MHz, CDCl₃), **1,6-4f**: δ 7.75–7.64 (m, 8H), 7.45–7.34 (m, 12H), 6.01–5.70 (m, 6H) and 4.05 (s, 4H); 1.06 (s, 18H); ¹³C{¹H} NMR (100 MHz, CDCl₃): δ 142.7, 142.0, 135.7, 135.6, 133.8, 133.7, 132.6, 132.2, 131.5, 131.3, 129.8, 129.8, 127.8, 127.8, 125.9, 125.4, 66.8, 66.5, 27.0, 26.9 and 19.4; HRMS (ESI-TOF) *m/z*: [M + Na]⁺ calcd for C₄₂H₄₈O₂Si₂Na, 663.3091; found, 663.3080.

1,4-/1,6-Di-O-TTMSS-COT (4g). 34.0 mg (0.21 mmol) of **3**, 0.14 mL (1.21 mmol, 6 equiv) of 2,6-lutidine, and an *n*-pentane solution (0.79 mmol, 4 equiv) of TTMSSOTf (0.26 mL [0.84 mmol]) of tris(trimethylsilyl) silane and 0.07 mL [0.79 mmol] of trifluoromethanesulfonic acid in 2 mL of *n*-pentane were mixed. After purification *via* silica column chromatography (2:1 mixture of *n*-hexane and DCM), 111.5 mg (0.17 mmol, 82%) of **4g** was obtained as a colorless oil.

¹H NMR (400 MHz, CDCl₃), **1,4-4g**: δ 5.85–5.61 (m, 6H) and 3.88 (s, 4H); 0.19 (s, 54H); ¹H NMR (400 MHz, CDCl₃), **1,6-4g**: δ 5.85–5.61 (m, 6H) and 3.86 (s, 4H); 0.19 (s, 54H); ¹³C{¹H} NMR (100 MHz, CDCl₃): δ 143.0, 142.2, 132.6, 132.0, 131.3, 131.2, 125.2, 125.0, 70.5, 70.4 and 0.49; HRMS (ESI-TOF) *m/z*: [M + Na]⁺ calcd for C₂₈H₆₄O₂Si₈Na, 679.2958; found, 679.2950.

Computational Details. We utilized the CREST developed by Grimme *et al.*⁶¹ to identify conformers lowest in energy. Due to the flexibility of the system, CREST located hundreds of conformers for each isomer within 6 kcal mol⁻¹ energy margin. We reduced the number of conformers by focusing only on molecules in a 1 kcal mol⁻¹ energy margin. The identified structures were optimized using the PBEh-3c functional.^{62–66} All structures located on energy minima of the hypersurface were utilized in a Boltzmann distribution, and their probability was calculated at 298 K. Conformers with a probability > 1% were used for single point computations at the revDSD-PBEP86-D4/def2-QZVPP^{67–72} level of theory including solvation effects (chloroform) *via* the PCM^{73,74} model. All optimizations and energy computations were performed using the ORCA program version 5.0.^{82,83}

For the energy decomposition analysis, we used an sSAPT⁷⁶ analysis as implemented in the PSI4 program.^{84,85} As a starting point, we utilized all conformers identified previously to be relevant for the conformer ensemble with a probability > 1%. The geometries are based on PBEh-3c. In the analysis, we focused on the interaction between silyl groups. Therefore, the molecular backbone (COT) and space group were removed, and the resulting silyl radicals were saturated with hydrogens. The sSAPT analysis was performed at the sSAPT0/aug-cc-pVDZ level of theory. The scaled protocol was utilized according to Parker *et al.*⁷⁷

The NCI plots⁷⁹ were plotted as a reduced density gradient in regions of low electron density. The resulting isosurfaces are color-coded in red, blue, and green. Whereas the first two correspond to strongly repulsive and attractive interactions, respectively, the latter can be described as weak noncovalent, that is, LD, interactions. The density cut-off of the reduced density gradient (isovalue *s* of 0.5, ranging from sign(λ_2) $\rho = -0.05$ to +0.05 a.u.) and the color scale data range were kept consistent throughout all NCI plots. We utilized the most probable conformer according to the Boltzmann analysis based on PCM(chloroform)-revDSD-PBEP86-D4/def2-QZVPP//PBEh-3c for depiction. All plots were generated with NCIPLOT⁸⁰ and visualized with VMD.⁸⁶

■ ASSOCIATED CONTENT

Supporting Information

The Supporting Information is available free of charge at <https://pubs.acs.org/doi/10.1021/acs.joc.2c01633>.

All experimental (NMR spectra) and computational details (PDF)

■ AUTHOR INFORMATION

Corresponding Author

Peter R. Schreiner – *Institute of Organic Chemistry, Justus Liebig University, 35392 Giessen, Germany*; orcid.org/0000-0002-3608-5515; Email: prs@uni-giessen.de, prsgroup@jlu

Authors

Lars Rummel – *Institute of Organic Chemistry, Justus Liebig University, 35392 Giessen, Germany*; orcid.org/0000-0002-3772-2109

Henrik F. König – *Institute of Organic Chemistry, Justus Liebig University, 35392 Giessen, Germany*; orcid.org/0000-0002-4246-6744

Heike Hausmann – *Institute of Organic Chemistry, Justus Liebig University, 35392 Giessen, Germany*; orcid.org/0000-0003-0347-9064

Complete contact information is available at: <https://pubs.acs.org/doi/10.1021/acs.joc.2c01633>

Author Contributions

[#]L.R. and H.F.K. contributed equally to this work.

Notes

The authors declare no competing financial interest.

ACKNOWLEDGMENTS

We dedicate this contribution to Prof. Günther Maier on the occasion of his 90th birthday. This work was supported by the priority program "Control of London Dispersion in Molecular Chemistry" (SPP1807; SCHR 597/27-2) of the Deutsche Forschungsgemeinschaft. We thank Jan M. Schumann for fruitful discussions.

REFERENCES

- (1) Shimizu, N.; Takesue, N.; Yasuhara, S.; Inazu, T. Prediction of Structural Effects of Trialkylsilyl Groups on Reactivity toward Nucleophilic Displacement at Silicon. *Chem. Lett.* **1993**, *22*, 1807–1810.
- (2) Eliel, E. L.; Satici, H. Conformational analysis of cyclohexyl silyl ethers. *J. Org. Chem.* **1994**, *59*, 688–689.
- (3) Marzabadi, C. H.; Anderson, J. E.; Gonzalez-Outeirino, J.; Gaffney, P. R. J.; White, C. G. H.; Tocher, D. A.; Todaro, L. J. Why Are Silyl Ethers Conformationally Different from Alkyl Ethers? Chair–Chair Conformational Equilibria in Silyloxycyclohexanes and Their Dependence on the Substituents on Silicon. The Wider Roles of Eclipsing, of 1,3-Repulsive Steric Interactions, and of Attractive Steric Interactions. *J. Am. Chem. Soc.* **2003**, *125*, 15163–15173.
- (4) London, F. Zur Theorie und Systematik der Molekularkräfte. *Z. Phys.* **1930**, *63*, 245–279.
- (5) London, F. The General Theory of Molecular Forces. *Trans. Faraday Soc.* **1937**, *33*, 8b–26b.
- (6) Wagner, J. P.; Schreiner, P. R. London Dispersion in Molecular Chemistry-Reconsidering Steric Effects. *Angew. Chem., Int. Ed.* **2015**, *54*, 12274–12296.
- (7) Liptrot, D. J.; Power, P. P. London dispersion forces in sterically crowded inorganic and organometallic molecules. *Nat. Rev. Chem.* **2017**, *1*, 0004.
- (8) Maier, G.; Pfiem, S.; Schäfer, U.; Matusch, R. Tetra-tert-butyltetrahedrane. *Angew. Chem., Int. Ed.* **1978**, *17*, 520–521.
- (9) Maier, G.; Neudert, J.; Wolf, O.; Pappusch, D.; Sekiguchi, A.; Tanaka, M.; Matsuo, T. Tetrakis(trimethylsilyl)tetrahedrane. *J. Am. Chem. Soc.* **2002**, *124*, 13819–13826.
- (10) Ndambuki, S.; Ziegler, T. Analysis of the Putative Cr–Cr Quintuple Bond in Ar'CrCrAr' (Ar' = C₆H₅-2,6-(C₆H₃-2,6-Pr^t)₂) Based on the Combined Natural Orbitals for Chemical Valence and Extended Transition State Method. *Inorg. Chem.* **2012**, *51*, 7794–7800.
- (11) Seidu, I.; Seth, M.; Ziegler, T. Role Played by Isopropyl Substituents in Stabilizing the Putative Triple Bond in Ar'EEAr' [E = Si, Ge, Sn; Ar' = C₆H₃-2,6-(C₆H₃-2,6-Pr^t)₂] and Ar'*PbPbAr'* [Ar'* = C₆H₃-2,6-(C₆H₂-2,4,6-Pr^t)₂]. *Inorg. Chem.* **2013**, *52*, 8378–8388.
- (12) Xi, Y.; Su, B.; Qi, X.; Pedram, S.; Liu, P.; Hartwig, J. F. Application of Trimethylgermyl-Substituted Bisphosphine Ligands with Enhanced Dispersion Interactions to Copper-Catalyzed Hydroboration of Disubstituted Alkenes. *J. Am. Chem. Soc.* **2020**, *142*, 18213–18222.
- (13) Schweighauser, L.; Strauss, M. A.; Bellotto, S.; Wegner, H. A. Attraction or Repulsion? London Dispersion Forces Control Azobenzene Switches. *Angew. Chem., Int. Ed.* **2015**, *54*, 13436–13439.
- (14) Procházková, E.; Kolmer, A.; Ilgen, J.; Schwab, M.; Kaltschnee, L.; Fredersdorf, M.; Schmidts, V.; Wende, R. C.; Schreiner, P. R.; Thiele, C. M. Uncovering Key Structural Features of an Enantioselective Peptide-Catalyzed Acylation Utilizing Advanced NMR Techniques. *Angew. Chem., Int. Ed.* **2016**, *55*, 15754–15759.
- (15) Hwang, J.; Li, P.; Smith, M. D.; Shimizu, K. D. Distance-Dependent Attractive and Repulsive Interactions of Bulky Alkyl Groups. *Angew. Chem., Int. Ed.* **2016**, *55*, 8086–8089.
- (16) Lu, G.; Liu, R. Y.; Yang, Y.; Fang, C.; Lambrecht, D. S.; Buchwald, S. L.; Liu, P. Ligand-Substrate Dispersion Facilitates the

Copper-Catalyzed Hydroamination of Unactivated Olefins. *J. Am. Chem. Soc.* **2017**, *139*, 16548–16555.

(17) Pollice, R.; Bot, M.; Kobylanski, I. J.; Shenderovich, I.; Chen, P. Attenuation of London Dispersion in Dichloromethane Solutions. *J. Am. Chem. Soc.* **2017**, *139*, 13126–13140.

(18) Eschmann, C.; Song, L.; Schreiner, P. R. London Dispersion Interactions Rather than Steric Hindrance Determine the Enantioselectivity of the Corey-Bakshi-Shibata Reduction. *Angew. Chem., Int. Ed.* **2021**, *60*, 4823–4832.

(19) Singha, S.; Buchsteiner, M.; Bistoni, G.; Goddard, R.; Fürstner, A. A New Ligand Design Based on London Dispersion Empowers Chiral Bismuth-Rhodum Paddlewheel Catalysts. *J. Am. Chem. Soc.* **2021**, *143*, 5666–5673.

(20) Gomberg, M. Triphenylmethyl, ein Fall von dreierwertigem Kohlenstoff. *Ber. Dtsch. Chem. Ges.* **1900**, *33*, 3150–3163.

(21) Gomberg, M.; Carbon, A. I. O. T. An Instance of Trivalent Carbon: Triphenylmethyl. *J. Am. Chem. Soc.* **1900**, *22*, 757–771.

(22) Grimme, S.; Schreiner, P. R. Steric Crowding Can Stabilize a Labile Molecule: Solving the Hexaphenylethane Riddle. *Angew. Chem., Int. Ed.* **2011**, *50*, 12639–12642.

(23) Rösel, S.; Balestrieri, C.; Schreiner, P. R. Sizing the role of London dispersion in the dissociation of all-*meta* tert-butyl hexaphenylethane. *Chem. Sci.* **2017**, *8*, 405–410.

(24) Rummel, L.; Schumann, J. M.; Schreiner, P. R. Hexaphenylditetrals - When Longer Bonds Provide Higher Stability. *Chem.—Eur. J.* **2021**, *27*, 13699–13702.

(25) Schreiner, P. R.; Chernish, L. V.; Gunchenko, P. A.; Tikhonchuk, E. Y.; Hausmann, H.; Serafin, M.; Schlecht, S.; Dahl, J. E. P.; Carlson, R. M. K.; Fokin, A. A. Overcoming lability of extremely long alkane carbon-carbon bonds through dispersion forces. *Nature* **2011**, *477*, 308–311.

(26) Ghotra, J. S.; Hursthouse, M. B.; Welch, A. J. Three-co-ordinate scandium(III) and europium(III); crystal and molecular structures of their tris(2,2,6,6-tetramethylpiperidin-1-yl)ethanimides. *J. Chem. Soc., Chem. Commun.* **1973**, 669–670.

(27) Linnemannstons, M.; Schwabedissen, J.; Schultz, A. A.; Neumann, B.; Stammler, H.-G.; Berger, R. J. F.; Mitzel, N. W. London dispersion-driven hetero-aryl-aryl interactions in 1,2-diaryldisilanes. *Chem. Commun.* **2020**, *56*, 2252–2255.

(28) Linnemannstons, M.; Schwabedissen, J.; Neumann, B.; Stammler, H.-G.; Berger, R. J. F.; Mitzel, N. W. Aryl-Aryl Interactions in (Aryl-Perhalogenated) 1,2-Diaryldisilanes. *Chem.—Eur. J.* **2020**, *26*, 2169–2173.

(29) Guo, J.-D.; Liptrot, D. J.; Nagase, S.; Power, P. P. The multiple bonding in heavier group 14 element alkene analogues is stabilized mainly by dispersion force effects. *Chem. Sci.* **2015**, *6*, 6235–6244.

(30) Stennett, C. R.; Bursch, M.; Fettinger, J. C.; Grimme, S.; Power, P. P. Designing a Solution-Stable Distannene: The Decisive Role of London Dispersion Effects in the Structure and Properties of {Sn(C₆H₂-2,4,6-Cy₃)₂}₂ (Cy = Cyclohexyl). *J. Am. Chem. Soc.* **2021**, *143*, 21478–21483.

(31) Marin-Luna, M.; Pölloth, B.; Zott, F.; Zipse, H. Size-dependent rate acceleration in the silylation of secondary alcohols: the bigger the faster. *Chem. Sci.* **2018**, *9*, 6509–6515.

(32) Marin-Luna, M.; Patschinski, P.; Zipse, H. Substituent Effects in the Silylation of Secondary Alcohols: A Mechanistic Study. *Chem.—Eur. J.* **2018**, *24*, 15052–15058.

(33) Grimme, S.; Huenerbein, R.; Ehrlich, S. On the Importance of the Dispersion Energy for the Thermodynamic Stability of Molecules. *ChemPhysChem* **2011**, *12*, 1258–1261.

(34) Miller, M. J.; Lyttle, M. H.; Streitwieser, A., Jr. tert-Butyl-substituted cyclooctatetraenes. *J. Org. Chem.* **1981**, *46*, 1977–1984.

(35) Lyttle, M. H.; Streitwieser, A., Jr.; Kluttz, R. Q. Unusual equilibrium between 1,4- and 1,6-di-tert-butylcyclooctatetraenes. *J. Am. Chem. Soc.* **1981**, *103*, 3232–3233.

(36) Schumann, J. M.; Wagner, J. P.; Eckhardt, A. K.; Quanz, H.; Schreiner, P. R. Intramolecular London Dispersion Interactions Do Not Cancel in Solution. *J. Am. Chem. Soc.* **2021**, *143*, 41–45.

- (37) Wenthold, P. G.; Hrovat, D. A.; Borden, W. T.; Lineberger, W. C. Transition-State Spectroscopy of Cyclooctatetraene. *Science* **1996**, *272*, 1456–1459.
- (38) Castaño, O.; Palmeiro, R.; Frutos, L. M.; Luisandrés, J. Role of bifurcation in the bond shifting of cyclooctatetraene. *J. Comput. Chem.* **2002**, *23*, 732–736.
- (39) Paquette, L. A.; Hefferon, G. J.; Samodral, R.; Hanzawa, Y. Bond fixation in annulenes. 14. Synthesis of and bond shifting equilibrium between 1,4- and 1,6-di-tert-butylcyclooctatetraenes. *J. Org. Chem.* **1983**, *48*, 1262–1266.
- (40) Anderson, J. E.; Kirsch, P. A. Structural equilibria determined by attractive steric interactions. 1,6-Dialkylcyclooctatetraenes and their bond-shift and ring inversion investigated by dynamic NMR spectroscopy and molecular mechanics calculations. *J. Chem. Soc., Perkin Trans. 2* **1992**, 1951–1957.
- (41) Allinger, N.; Frierson, M.; Van-Catledge, F. The importance of van der Waals attractions in determining the equilibrium between 1,4- and 1,6-dialkylcyclooctatetraenes. *J. Am. Chem. Soc.* **1982**, *104*, 4592–4593.
- (42) Tosi, C. A quantum mechanical study of the equilibrium between 1,4- and 1,6-dialkylcyclooctatetraenes. *J. Comput. Chem.* **1984**, *5*, 248–251.
- (43) Solel, E.; Ruth, M.; Schreiner, P. R. London Dispersion Helps Refine Steric A-Values: Dispersion Energy Donor Scales. *J. Am. Chem. Soc.* **2021**, *143*, 20837–20848.
- (44) König, H. F.; Rummel, L.; Hausmann, H.; Becker, J.; Schumann, J. M.; Schreiner, P. R. Gauging the Steric Effects of Silyl Groups with a Molecular Balance. *J. Org. Chem.* **2022**, *87*, 4670–4679.
- (45) Van Craen, D.; Rath, W. H.; Huth, M.; Kemp, L.; Räuber, C.; Wollschläger, J. M.; Schalley, C. A.; Valkonen, A.; Rissanen, K.; Albrecht, M. Chasing Weak Forces: Hierarchically Assembled Helicates as a Probe for the Evaluation of the Energetics of Weak Interactions. *J. Am. Chem. Soc.* **2017**, *139*, 16959–16966.
- (46) Strauss, M. A.; Wegner, H. A. Exploring London Dispersion and Solvent Interactions at Alkyl-Alkyl Interfaces Using Azobenzene Switches. *Angew. Chem., Int. Ed.* **2019**, *58*, 18552–18556.
- (47) Cassar, L.; Eaton, P. E.; Halpern, J. Catalysis of symmetry-restricted reactions by transition metal compounds. Valence isomerization of cubane. *J. Am. Chem. Soc.* **1970**, *92*, 3515–3518.
- (48) Houston, S. D.; Xing, H.; Bernhardt, P. V.; Vanden Berg, T. J.; Tsanaktsidis, J.; Savage, G. P.; Williams, C. M. Cyclooctatetraenes through Valence Isomerization of Cubanes: Scope and Limitations. *Chem.—Eur. J.* **2019**, *25*, 2735–2739.
- (49) Falkiner, M. J.; Littler, S. W.; McRae, K. J.; Savage, G. P.; Tsanaktsidis, J. Pilot-Scale Production of Dimethyl 1,4-Cubane-dicarboxylate. *Org. Process Res. Dev.* **2013**, *17*, 1503–1509.
- (50) Greene, T. W.; Wuts, P. G. *Protective Groups in Organic Synthesis*; Wiley, 1991.
- (51) Strauss, M. A.; Wegner, H. A. Molecular Systems for the Quantification of London Dispersion Interactions. *Eur. J. Org. Chem.* **2019**, *2019*, 295–302.
- (52) Pracht, P.; Grimme, S. Calculation of absolute molecular entropies and heat capacities made simple. *Chem. Sci.* **2021**, *12*, 6551–6568.
- (53) Gorges, J.; Grimme, S.; Hansen, A.; Pracht, P. Towards understanding solvation effects on the conformational entropy of non-rigid molecules. *Phys. Chem. Chem. Phys.* **2022**, *24*, 12249–12259.
- (54) Harvey, J. N.; Himo, F.; Maseras, F.; Perrin, L. Scope and Challenge of Computational Methods for Studying Mechanism and Reactivity in Homogeneous Catalysis. *ACS Catal.* **2019**, *9*, 6803–6813.
- (55) Besora, M.; Braga, A. A. C.; Ujaque, G.; Maseras, F.; Lledós, A. The importance of conformational search: a test case on the catalytic cycle of the Suzuki–Miyaura cross-coupling. *Theor. Chem. Acc.* **2011**, *128*, 639–646.
- (56) Wales, D. J. *Energy Landscapes*; Cambridge University Press: Cambridge, UK, 2003.
- (57) Drudis-Solé, G.; Ujaque, G.; Maseras, F.; Lledós, A. A QM/MM Study of the Asymmetric Dihydroxylation of Terminal Aliphatic-Alkenes with OsO₄-(DHQD)₂PDZ: Enantioselectivity as a Function of Chain Length. *Chem.—Eur. J.* **2005**, *11*, 1017–1029.
- (58) Barone, G.; Duca, D.; Silvestri, A.; Gomez-Paloma, L.; Riccio, R.; Bifulco, G. Determination of the Relative Stereochemistry of Flexible Organic Compounds by Ab Initio Methods: Conformational Analysis and Boltzmann-Averaged GIAO ¹³C NMR Chemical Shifts GIAO=gauge including atomic orbitals. *Chem.—Eur. J.* **2002**, *8*, 3240–3245.
- (59) Zanardi, M. M.; Marcarino, M. O.; Sarotti, A. M. Redefining the Impact of Boltzmann Analysis in the Stereochemical Assignment of Polar and Flexible Molecules by NMR Calculations. *Org. Lett.* **2020**, *22*, 52–56.
- (60) Gorbachev, V.; Tsybizova, A.; Miloglyadova, L.; Chen, P. Increasing Complexity in a Conformer Space Step-by-Step: Weighing London Dispersion against Cation- π Interactions. *J. Am. Chem. Soc.* **2022**, *144*, 9007–9022.
- (61) Pracht, P.; Bohle, F.; Grimme, S. Automated exploration of the low-energy chemical space with fast quantum chemical methods. *Phys. Chem. Chem. Phys.* **2020**, *22*, 7169–7192.
- (62) Weigend, F. Accurate Coulomb-fitting basis sets for H to Rn. *Phys. Chem. Chem. Phys.* **2006**, *8*, 1057–1065.
- (63) Grimme, S.; Antony, J.; Ehrlich, S.; Krieg, H. A consistent and accurate ab initio parametrization of density functional dispersion correction (DFT-D) for the 94 elements H–Pu. *J. Chem. Phys.* **2010**, *132*, 154104.
- (64) Grimme, S.; Ehrlich, S.; Goerigk, L. Effect of the damping function in dispersion corrected density functional theory. *J. Comput. Chem.* **2011**, *32*, 1456–1465.
- (65) Kruse, H.; Grimme, S. A geometrical correction for the inter- and intra-molecular basis set superposition error in Hartree-Fock and density functional theory calculations for large systems. *J. Chem. Phys.* **2012**, *136*, 154101.
- (66) Grimme, S.; Brandenburg, J. G.; Bannwarth, C.; Hansen, A. Consistent structures and interactions by density functional theory with small atomic orbital basis sets. *J. Chem. Phys.* **2015**, *143*, 054107.
- (67) Weigend, F.; Ahlrichs, R. Balanced basis sets of split valence, triple zeta valence and quadruple zeta valence quality for H to Rn: Design and assessment of accuracy. *Phys. Chem. Chem. Phys.* **2005**, *7*, 3297–3305.
- (68) Hellweg, A.; Hättig, C.; Höfener, S.; Klopper, W. Optimized accurate auxiliary basis sets for RI-MP2 and RI-CC2 calculations for the atoms Rb to Rn. *Theor. Chem. Acc.* **2007**, *117*, 587–597.
- (69) Weigend, F. Hartree-Fock exchange fitting basis sets for H to Rn. *J. Comput. Chem.* **2008**, *29*, 167–175.
- (70) Caldeweyher, E.; Bannwarth, C.; Grimme, S. Extension of the D3 dispersion coefficient model. *J. Chem. Phys.* **2017**, *147*, 034112.
- (71) Santra, G.; Sylvetsky, N.; Martin, J. M. L. Minimally Empirical Double-Hybrid Functionals Trained against the GMTKN55 Database: revDSD-PBEP86-D4, revDOD-PBE-D4, and DOD-SCAN-D4. *J. Phys. Chem. A* **2019**, *123*, 5129–5143.
- (72) Caldeweyher, E.; Ehlert, S.; Hansen, A.; Neugebauer, H.; Spicher, S.; Bannwarth, C.; Grimme, S. A generally applicable atomic-charge dependent London dispersion correction. *J. Chem. Phys.* **2019**, *150*, 154122.
- (73) Miertuš, S.; Scrocco, E.; Tomasi, J. Electrostatic interaction of a solute with a continuum. A direct utilization of ab initio molecular potentials for the prevision of solvent effects. *Chem. Phys.* **1981**, *55*, 117–129.
- (74) Tomasi, J.; Mennucci, B.; Cammi, R. Quantum Mechanical Continuum Solvation Models. *Chem. Rev.* **2005**, *105*, 2999–3094.
- (75) Pollice, R.; Fleckenstein, F.; Shenderovich, I.; Chen, P. Compensation of London Dispersion in the Gas Phase and in Aprotic Solvents. *Angew. Chem., Int. Ed.* **2019**, *58*, 14281–14288.
- (76) Szalewicz, K. Symmetry-adapted perturbation theory of intermolecular forces. *WIREs Comput. Mol. Sci.* **2012**, *2*, 254–272.
- (77) Parker, T. M.; Burns, L. A.; Parrish, R. M.; Ryno, A. G.; Sherrill, C. D. Levels of symmetry adapted perturbation theory (SAPT). I.

Efficiency and performance for interaction energies. *J. Chem. Phys.* **2014**, *140*, 094106.

(78) Hwang, J.; Li, P.; Smith, M. D.; Warden, C. E.; Sirianni, D. A.; Vik, E. C.; Maier, J. M.; Yehl, C. J.; Sherrill, C. D.; Shimizu, K. D. Tipping the Balance between S- π and O- π Interactions. *J. Am. Chem. Soc.* **2018**, *140*, 13301–13307.

(79) Johnson, E. R.; Keinan, S.; Mori-Sánchez, P.; Contreras-García, J.; Cohen, A. J.; Yang, W. Revealing Noncovalent Interactions. *J. Am. Chem. Soc.* **2010**, *132*, 6498–6506.

(80) Contreras-García, J.; Johnson, E. R.; Keinan, S.; Chaudret, R.; Piquemal, J.-P.; Beratan, D. N.; Yang, W. NCIPLLOT: A Program for Plotting Noncovalent Interaction Regions. *J. Chem. Theory Comput.* **2011**, *7*, 625–632.

(81) Cianfanelli, M.; Olivo, G.; Milan, M.; Klein Gebbink, R. J. M.; Ribas, X.; Bietti, M.; Costas, M. Enantioselective C-H Lactonization of Unactivated Methylenes Directed by Carboxylic Acids. *J. Am. Chem. Soc.* **2020**, *142*, 1584–1593.

(82) Neese, F. Software update: the ORCA program system, version 4.0. *WIREs Comput. Mol. Sci.* **2018**, *8*, No. e1327.

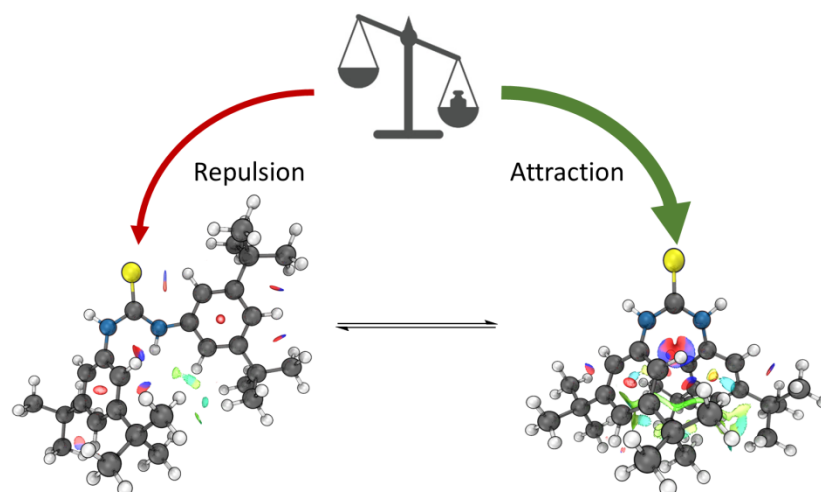
(83) Neese, F. Software update: The ORCA program system—Version 5.0. *WIREs Comput. Mol. Sci.* **2022**, *12*, No. e1606.

(84) Turney, J. M.; Simmonett, A. C.; Parrish, R. M.; Hohenstein, E. G.; Evangelista, F. A.; Fermann, J. T.; Mintz, B. J.; Burns, L. A.; Wilke, J. J.; Abrams, M. L.; Russ, N. J.; Leininger, M. L.; Janssen, C. L.; Seidl, E. T.; Allen, W. D.; Schaefer, H. F.; King, R. A.; Valeev, E. F.; Sherrill, C. D.; Crawford, T. D. Psi4: an open-source ab initio electronic structure program. *WIREs Comput. Mol. Sci.* **2012**, *2*, 556–565.

(85) Parrish, R. M.; Burns, L. A.; Smith, D. G. A.; Simmonett, A. C.; DePrince, A. E.; Hohenstein, E. G.; Bozkaya, U.; Sokolov, A. Y.; Di Remigio, R.; Richard, R. M.; Gonthier, J. F.; James, A. M.; McAlexander, H. R.; Kumar, A.; Saitow, M.; Wang, X.; Pritchard, B. P.; Verma, P.; Schaefer, H. F.; Patkowski, K.; King, R. A.; Valeev, E. F.; Evangelista, F. A.; Turney, J. M.; Crawford, T. D.; Sherrill, C. D. Psi4 1.1: An Open-Source Electronic Structure Program Emphasizing Automation, Advanced Libraries, and Interoperability. *J. Chem. Theory Comput.* **2017**, *13*, 3185–3197.

(86) Humphrey, W.; Dalke, A.; Schulten, K. VMD: Visual molecular dynamics. *J. Mol. Graphics Modell.* **1996**, *14*, 33–38.

2.4 London Dispersion Favors Sterically Hindered Diarylthiourea Conformers in Solution



Abstract:

We present an experimental and computational study on the conformers of *N,N'*-diphenylthiourea substituted with different dispersion energy donor (DED) groups. While the unfolded *anti-anti* conformer is the most relevant for thiourea catalysis, intramolecular non-covalent interactions counterintuitively favor the folded *syn-syn* conformer, as evident from a combination of low-temperature nuclear magnetic resonance measurements and computations. In order to quantify the noncovalent interactions, we utilized local energy decomposition analysis and symmetry-adapted perturbation theory at the DLPNO-CCSD(T)/def2-TZVPP and sSAPT0/6-311G(d,p) levels of theory. Additionally, we applied a double-mutant cycle to experimentally study the effects of bulky substituents on the equilibria. We determined London dispersion as the key interaction that shifts the equilibria towards the *syn-syn* conformers. This preference is likely a factor why such thiourea derivatives can be poor catalysts.

Reference:

Lars Rummel, Marvin H. J. Domanski, Heike Hausmann, Jonathan Becker, and Peter R. Schreiner, *Angew. Chem. Int. Ed.* **2022**, *61*, e202204393; *Angew. Chem.* **2022**, *134*, e202204393. DOI: 10.1002/anie.202204393

Reproduced with permission from:

© 2022, John Wiley & Sons, Inc.
111 River Street
Hoboken, NJ, 07030-5774
United States of America



Noncovalent Interactions Hot Paper

 How to cite: *Angew. Chem. Int. Ed.* **2022**, *61*, e202204393
 International Edition: doi.org/10.1002/anie.202204393
 German Edition: doi.org/10.1002/ange.202204393

London Dispersion Favors Sterically Hindered Diarylthiourea Conformers in Solution

 Lars Rummel[†], Marvin H. J. Domanski[†], Heike Hausmann, Jonathan Becker, and Peter R. Schreiner*

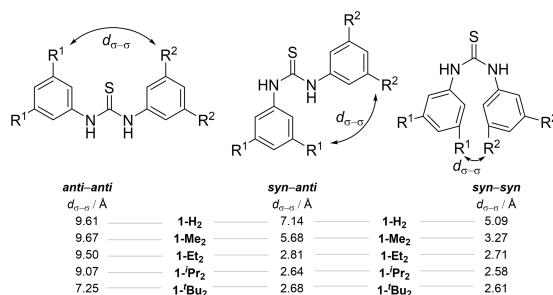
Abstract: We present an experimental and computational study on the conformers of *N,N'*-diphenylthiourea substituted with different dispersion energy donor (DED) groups. While the unfolded *anti-anti* conformer is the most relevant for thiourea catalysis, intramolecular noncovalent interactions counterintuitively favor the folded *syn-syn* conformer, as evident from a combination of low-temperature nuclear magnetic resonance measurements and computations. In order to quantify the noncovalent interactions, we utilized local energy decomposition analysis and symmetry-adapted perturbation theory at the DLPNO-CCSD(T)/def2-TZVPP and sSAPT0/6-311G(d,p) levels of theory. Additionally, we applied a double-mutant cycle to experimentally study the effects of bulky substituents on the equilibria. We determined London dispersion as the key interaction that shifts the equilibria towards the *syn-syn* conformers. This preference is likely a factor why such thiourea derivatives can be poor catalysts.

Introduction

In the field of enzyme catalysis, Fischer's "key and lock" hypothesis^[1] or the more sophisticated "induced fit" model by Koshland^[2] perennially highlight the importance of conformational flexibility and catalytic activity. The structural dynamics of peptides allow enzymes to bind and to recognize substrates effectively and convert them into products. Thus, a specific conformer of the catalyst is needed to exploit transition state stabilization and energetic differ-

entiation among a series of possible transition state geometries. Conformational structure–property relationships can be probed with small molecules as well. The restricted bond rotation within the thioamide functional group offers three differently populated conformers (Scheme 1).^[3] While the mechanism for anion recognition or catalytic activation of a substrate due to hydrogen-bonding is most effective via the open *anti-anti* conformer, an analysis of the conformational landscape of thiourea derivatives is an essential part to understand the origin of their catalytic activity and any limitations thereof.^[3] Here, we present a study of *all-meta*-disubstituted diphenylthiourea^[4] derivatives to elucidate the conformational preferences dependent on noncovalent interactions including London dispersion (LD).^[5] Since the compounds discussed in this work both are less catalytically active than commonly exploited thiourea catalysts^[4c] and poor anion receptors,^[4b,6] we hypothesize this is in part due to the population of a conformer that does not allow double N–H bonding to Lewis-basic atoms or groups in the substrate.^[3]

In recent years, a number of studies demonstrated that the catalytically active *anti-anti* diphenyl(thio)urea conformer is not necessarily the predominant conformer in the gas phase and in solution.^[3,6a,7] Infrared and temperature-dependent NMR measurements in different solvents demonstrated the presence of multiple conformers for diarylthiourea derivatives.^[7] An exception to this conformational flexibility is the well-known *N,N'*-bis[3,5-bis(trifluoromethyl)phenyl]thiourea catalyst with the *anti-anti* conformer being predominant in, for example, tetrahydrofuran (THF)



Scheme 1. Lowest energy conformers of diphenylthiourea derivatives with the *anti-anti* (left), *syn-anti* (center), and *syn-syn* (right) conformers. The shown values correspond to the shortest σ – σ distance $d_{\sigma-\sigma}$ contact for each conformer of 1-*R*¹-*R*² computed at B3LYP-D3(BJ)/def2-TZVPP.

[*] L. Rummel,[†] M. H. J. Domanski,[†] H. Hausmann, P. R. Schreiner
 Institute of Organic Chemistry, Justus Liebig University
 Heinrich-Buff-Ring 17, 35392 Giessen (Germany)
 E-mail: prs@uni-giessen.de

J. Becker
 Institute of Inorganic and Analytical Chemistry, Justus Liebig
 University
 Heinrich-Buff-Ring 17, 35392 Giessen (Germany)

[†] These authors contributed equally to this work.

© 2022 The Authors. Angewandte Chemie International Edition published by Wiley-VCH GmbH. This is an open access article under the terms of the Creative Commons Attribution Non-Commercial NoDerivs License, which permits use and distribution in any medium, provided the original work is properly cited, the use is non-commercial and no modifications or adaptations are made.

at elevated temperatures.^[3] While the experimental evidence points to the fact that the *anti-anti* conformer of this thiourea catalyst is catalytically most active, other substitution patterns are likely to display a different conformational landscape, which, in turn, is likely to result in reduced catalytic activity.

Most recently, Sandler et al.^[6a] highlighted the relationship of conformational effects and the anion binding affinity of receptor molecules such as diphenylthiourea.^[4h,6b] Whereas urea and squaramide derivatives prefer the *anti-anti* conformer due to intramolecular CH-carbonyl hydrogen bonding, diphenylthiourea does not benefit as strongly from this stabilization since its phenyl moieties are twisted out of plane.^[4c] Consequently, diphenylthiourea populates the *syn-anti* and *syn-syn* conformers, thereby lowering its anion binding affinity.^[6a] To explain the enantioselectivity of an asymmetric Henry reaction, Heshmat proposed cinchonathiourea catalyst substrate activation via the *syn-anti* conformer.^[6f] Experimental data suggest a similar trend. In an extensive study of crystal structures of urea and thiourea derivatives, Luchini et al.^[9] showed that around 60% of all thiourea motifs crystallize in a *syn-syn* or *syn-anti* fashion. On the other hand, 98% of urea derivatives are reported to have an *anti-anti* conformation in the solid state.^[9] Solid state and gas phase IR^[10] and NMR^[11] studies in solution support this trend for urea derivatives as well. For diarylthiourea derivatives, IR measurements suggest a significant shift to the *syn-syn* conformer in solution^[7] but a systematic NMR study determining the role and the apparent intramolecular stabilization of the *syn-syn* conformer has not been reported.

In order to investigate the equilibria depicted in Scheme 1, we treated the *N,N'*-diphenylthiourea derivatives as molecular balances.^[12] By increasing the size of the *all-meta*-substituted aryl dispersion energy donors (DEDs),^[5,13] we observed a systematic and counterintuitive shift of the equilibrium toward the folded and more crowded *syn-syn* conformer. The increasing number of close $\sigma-\sigma$ contacts is indicative of the prevalence of attractive LD^[14] interactions rather than Pauli (exchange) repulsion. This effect was recently emphasized in a study of the equilibria of 1,4- and 1,6-di-*tert*-butyl cyclooctatetraene in a large series of solvents of very different polarities showing that intramolecular LD interactions do not cancel in solution.^[15]

Results and Discussion

To dissect the influence of each DED, we synthesized a logical series of diphenylthiourea derivatives with methyl (Me), ethyl (Et), *iso*-propyl (Pr), and *tert*-butyl (Bu) substituents. In brief, the *all-meta*-substituted *N,N'*-diphenylthioureas were synthesized via a two-step addition of aniline precursors to thiophosgene.^[3] Prior, the *all-meta*-substituted aniline precursors were generated via bromination and de-diazotization reaction of 2,6-disubstituted aniline derivatives (for details, see Supporting Information).^[16] To gather as much information as possible, we generated all R¹ and R² combinations of these groups and measured

¹H NMR spectra in THF. The choice of solvent was based on its physical properties (i.e., low melting point) and the fact that all diphenylthiourea derivatives remained soluble during the low-temperature NMR measurements.

The restricted bond rotation of all *N,N'*-diphenylthiourea derivatives required low-temperature NMR measurements (performed at 193 K) in order to freeze the C–N bond rotation. The lowest temperature possible to hold up over a longer period of time in the NMR was 193 K. Intrinsic reaction coordinate (IRC) computations suggest activation barriers of 10.3 kcal mol⁻¹ (corresponding to a rate constant of 4.0 × 10⁻³ s⁻¹) and 9.0 kcal mol⁻¹ (1.3 s⁻¹) for unsubstituted diphenylthiourea.^[3] We first tested our approach with *N,N'*-bis(3,5-di-*tert*-butylphenyl)thiourea **1-Bu₂** (**1-R¹R²**) and the parent *N,N'*-diphenylthiourea **1-H₂**. For both derivatives the singlet N–H signal splits into three separate signals upon cooling, two of which belong to the same conformer (blue marking, Figure 1). Additionally, the aromatic signals (Figure 2) split into four, and the aliphatic *tert*-butyl signals into two separate NMR peaks.

Accordingly, these signals were assigned to the *syn-anti* conformer since it is the only structure with inequivalent N–H, aromatic, and *tert*-butyl protons. While the parent **1-H₂** (purple NMR, Figure 1) considerably favors the *syn-anti* conformer by around 2.3 ± 0.1 kcal mol⁻¹ (all energies were determined via K_{eq} at 193 K), the NMR of **1-Bu₂**

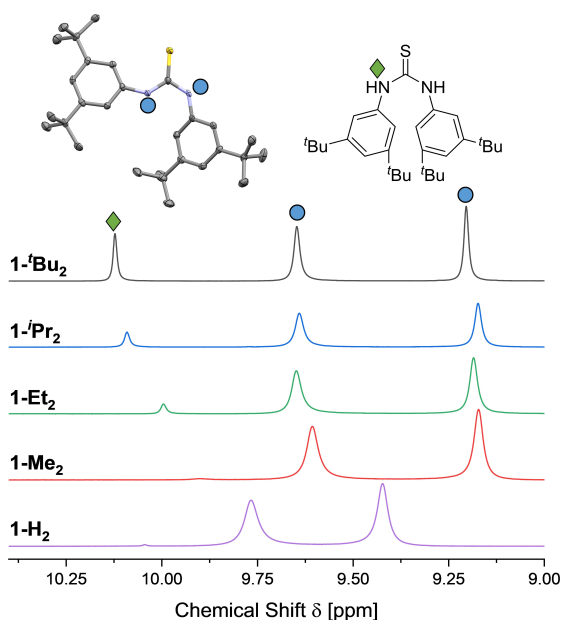


Figure 1. NMR measurements at 193 K of symmetrically substituted *N,N'*-diphenylthiourea derivatives **1-R¹R²** in THF and molecular structure of **1-Bu₂**. For simplicity, the NH signals of symmetric **1-R¹R²** are depicted only. Thermal ellipsoid plot of the molecular structure obtained by single-crystal X-ray diffraction was drawn at 50% probability level. The blue markings correspond to the NH signals of the *syn-anti* and the green markings to the *syn-syn* conformer. Note that the *anti-anti* conformer is not populated and has therefore been omitted.

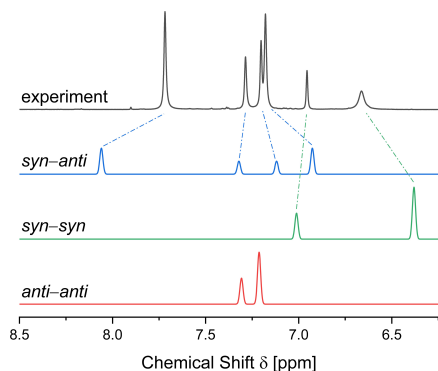


Figure 2. NMR measurements at 193 K of the aromatic signals of **1-Bu₂** (grey) and computed spectra for the *syn-anti* (blue), *syn-syn* (green), and *anti-anti* (red) conformers in THF (SMD solvent model) at the B3LYP-D3(BJ)/def2-TZVPP level of theory. For the full spectral data see the Supporting Information.

(black NMR, Figure 1) shows a distinct symmetric conformer. Nevertheless, **1-Bu₂** favors the *syn-anti* conformer by around $0.5 \pm 0.0(3)$ kcal mol⁻¹. The computed NMR signals (Figure 2) suggest that the new signals belong to the *syn-syn* conformer (green spectrum), which also helped us assign the *syn-anti* (blue spectrum) and disregard the *anti-anti* (red spectrum) conformer. Whereas the N–H proton shift is difficult to determine by NMR computations,^[17] the aromatic and aliphatic C–H signals were assigned to the *syn-syn* conformer.

Concentration dependent measurements showed no change in signal ratios with the lowest concentration being 15.5 mM (0.01 mmol). This is in line with NMR measurements investigating the complexation of thiourea catalyst with lactones, where it was found that the *anti-anti* conformer is catalytically most active.^[3] Consequently, aggregation in solution was deemed to be unimportant. To ensure that equilibrium had been reached, we equilibrated each NMR sample for one hour at 193 K. Since the barrier height for rotation around the thioamide bond is around 10 kcal mol⁻¹, equilibrium was reached after around 5 min (see Supporting Information for details). After transferring the samples to the NMR spectrometer, they were further equilibrated until the temperature stabilized at 193 K. Figure 1 displays the N–H proton splitting for symmetric **1-R¹R²**. While **1-H₂** shows only low concentrations of a second conformer, bulky substituents such as those with *tert*-butyl groups clearly affect the conformer distributions.

Figure 3 displays a summary of the experimentally determined $\Delta G_{R^1R^2-HH}$ values of the equilibrium between *syn-syn* and *syn-anti* **1-R¹R²** relative to parent *N,N'*-diphenylthiourea **1-H₂**. Consequently, **1-H₂** is depicted as $\Delta G_{R^1R^2-HH} = 0.0 \pm 0.2$ kcal mol⁻¹ in Figure 3 (rightmost data point). While **1-H₂** favors the *syn-anti* conformer by around 2.3 ± 0.1 kcal mol⁻¹ (see Supporting Information for absolute energy values), substituents in all-*meta* position shift the equilibrium towards the *syn-syn* conformer ($\Delta G < 0$). In contrast to the often encountered view that large groups

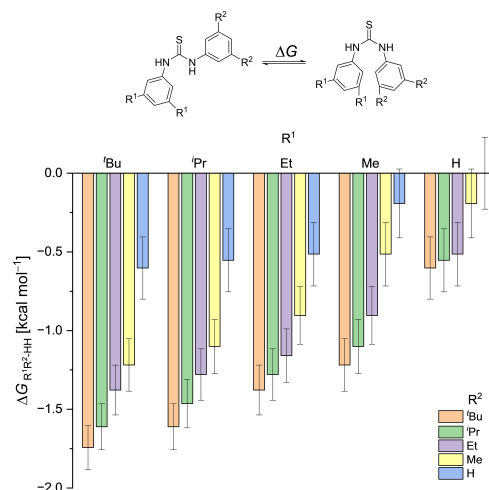


Figure 3. Experimentally determined Gibbs free energy values $\Delta G_{R^1R^2-HH}$ for the equilibrium between *syn-syn* and *syn-anti* **1-R¹R²** at 193 K. Gray lines indicate error bars. $\Delta G < 0$ corresponds to a shift towards the *syn-syn* conformer: The lower and more negative the ΔG expressed, the more favored the *syn-syn* conformer. Note that the supposedly catalytically active *anti-anti* conformation is not populated at all.

repel each other, Figure 3 illustrates that bulky groups favor the conformer that displays close alkyl–alkyl contacts ($d_{\sigma,\sigma} = 2.61$ Å for **1-Bu₂**). The *unsymmetric* functionalization in **1-R¹H** (blue bars) and **1-HR²** (rightmost block of columns) only has a small effect on the equilibrium position (up to $\Delta G_{BuH-HH} = -0.6 \pm 0.2$ kcal mol⁻¹). The shift in energy towards the *syn-syn* conformer can be rationalized by attractive $\sigma-\pi$ interactions between substituents and opposing phenyl moiety. Thereby, a decrease in distance between substituent and phenyl moiety systematically increases the stabilizing $\sigma-\pi$ interactions. A similar effect was already observed and quantified by Shimizu et al. for a *para* substitution pattern utilizing molecular torsion balance.^[18] Here, distance dependence of $\sigma-\pi$ interactions was documented for a *para* substitution pattern with the largest and bulkiest alkyl groups forming the strongest stabilizing interactions. These observations are consistent with the recent concept of DEDs in which bulky alkyl groups form stabilizing dispersion interactions.^[5,13]

By systematically increasing the substituent size on both phenyl moieties, the equilibrium shifts further to the more crowded *syn-syn* structure. The introduction of additional CH₃ groups increases the number of close intramolecular alkyl–alkyl contacts in the *syn-syn* conformer, thereby reducing the distance between substituents (Scheme 1). An increasing number of noncovalent contacts at distances of around 2.5 Å has proven to be effective in stabilizing labile compounds such as hexaphenylethane^[19] or rationalizing isomerization energies of linear and branched alkanes.^[20] The largest difference in energy due to incorporation of a methyl substituent can be observed from **1-BuH** (ΔG

${}^t\text{BuH-HH} = -0.6 \pm 0.2 \text{ kcal mol}^{-1}$) to **1-BuMe** ($\Delta G_{\text{BuMe-HH}} = -1.2 \pm 0.2 \text{ kcal mol}^{-1}$) with around $-0.6 \text{ kcal mol}^{-1}$ stabilization due to σ - σ contacts.^[21] Additional methyl groups shift the equilibrium further towards the *syn-syn* conformer by around $-0.1 \text{ kcal mol}^{-1}$. Consequently, the most prominent effects can be observed for **1-R¹Bu** derivatives (orange bars), which shift the equilibria significantly towards the *syn-syn* conformer (up to $\Delta G_{\text{Bu-HH}} = -1.7 \pm 0.1 \text{ kcal mol}^{-1}$). Hence, the experimental data suggest that increasingly larger alkyl substituents act as stabilizing DEDs rather than as repulsive steric bulk.^[5,19, 22] Correlations of our experimental findings with the molecular volume or in the total molecular dipole moment of each conformer are insufficient to rationalize the trends observed (see Supporting Information).

To support these findings, we performed a computational study focusing on the role of intramolecular non-covalent interactions. To be able to switch dispersion corrections on and off, we utilized density functional theory (DFT) to investigate the equilibria depicted in Scheme 1. After an initial conformer analysis using the Conformer-Rotamer Ensemble Sampling Tool^[23] (crest) program, the lowest conformers were further optimized with Ahlrich's def2-TZVPP^[24] basis set. The B3LYP^[25] functional was utilized with and without (Supporting Information) Grimme's D3^[26] correction including Becke-Johnson^[27] (BJ) damping. All geometry optimizations were performed in the gas phase under standard conditions. The gas phase structures were utilized for single-point energy computations to account for solvation effects and entropy at 193 K. The polarizable continuum model (PCM)^[28] was used with THF as solvent and thermal corrections added from DFT (gas phase) frequency computations. Additionally, the B3LYP-D3(BJ) (gas phase) optimized structures were utilized for single-point energy computations at the DLPNO-CCSD(T)/def2-TZVPP level of theory.^[29] This analysis follows that of Sandler et al. (Supporting Information)^[6a] who demonstrated that the B3LYP functional in conjunction with medium-sized basis sets is an appropriate approach for geometry optimizations of thiourea derivatives and, that DLPNO-CCSD(T)/large basis set is an excellent approximation to its canonical counterpart. Since LD interactions are in a first approximation temperature independent, the results of the thermochemical analysis of the equilibrium fit qualitatively to gas phase computations (see Supporting Information).^[14] The thermochemical results (ΔG_{eq}) for the symmetric and unsymmetric *N,N'*-diphenylthiourea molecular balances are depicted in Figure 4. While the *anti-anti* conformer is highest in energy (red markings) for all systems and cannot be observed by NMR, the *syn-syn* (green markings) conformers are generally favored. Computations on B3LYP/def2-TZVPP excluding the LD corrections predict the *syn-anti/anti-syn* conformers to be favored by around 3–4 kcal mol⁻¹. Including LD, the unsubstituted balance already slightly favors the *syn-syn* conformer ($\Delta G_{\text{eq}} \approx -0.3 \text{ kcal mol}^{-1}$). Increasing alkyl substitution shifts the global energy minimum further from the *syn-anti* towards the *syn-syn* conformer. The largest effect can be observed for **1-Bu₂** ($\Delta G_{\text{eq}} \approx -2.8 \text{ kcal mol}^{-1}$). These results

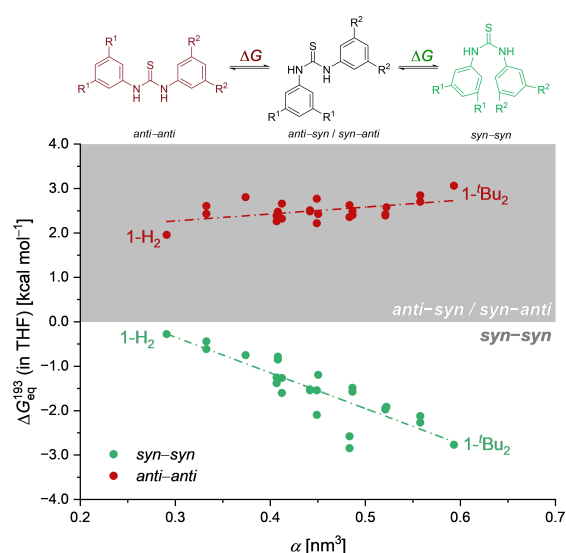


Figure 4. Gibbs free energies at 193 K for the equilibrium of the *syn-syn* (green markings) and *anti-anti* (red markings) conformers relative to the *syn-anti/anti-syn* conformers of **1-R¹R²** at the DLPNO-CCSD(T)/def2-TZVPP//B3LYP-D3(BJ)/def2-TZVPP level of theory including a solvent correction (THF) at the B3LYP-D3(BJ)/def2-TZVPP utilizing the PCM model. Thermal corrections were added from DFT optimizations at 193 K. **1-H₂** and **1-Bu₂** are highlighted for clarity.

fit qualitatively well to our experimental data, albeit the attenuation of the attractive interactions due to solvent effects is higher than predicted by the computations.^[30]

To assess these counterintuitive results, we visualized the intramolecular noncovalent contacts (Figure 5) utilizing non-covalent interaction (NCI) plots^[31] to highlight the main source of thermodynamic stability of **1-Bu₂** by depicting the reduced density gradient in regions of low electron density. While strongly attractive and repulsive interactions are color-coded in blue and red, respectively, green isosurfaces can be assigned to weak NCIs. The *anti-anti* conformer of **1-Bu₂** features a mixture of red and blue isosurfaces due to the substitution pattern and a CH...S contact^[4c] a green contact area is not visible. On the other hand, the *syn-anti* conformer already shows small green areas between bulky ^tBu substituents and the opposing phenyl group. Finally, the *syn-syn* conformer shows large green isosurfaces implying significant intramolecular NCIs. An incorporation of bulky alkyl groups increases the number of noncovalent contacts via close σ - σ (i.e., ^tBu-^tBu in Figure 5) and σ - π (^tBu- π) contacts of both substituents. This analysis qualitatively supports experimental and computational findings.

To quantify the amount of LD interactions between each substituent, we dissected the energy values $\Delta\Delta G_{\text{R}^1\text{R}^2}$ from singly substituted molecular balances.^[32] Hereby, two substituents R¹ and R² are mutated separately to investigate the impact of each substituent on the thiourea molecular backbone. According to the following equation the inter-

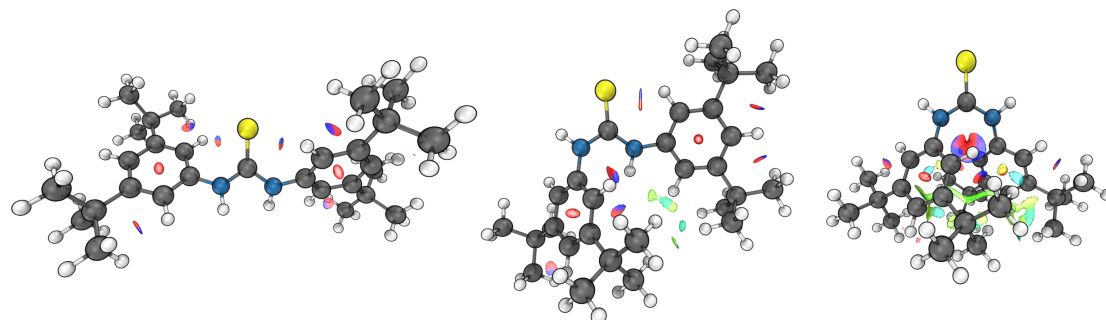


Figure 5. Noncovalent interaction (NCI) plots of the *anti-anti* (left), *syn-anti* (center), and *syn-syn* (right) conformers of **1-tBu₂** at B3LYP-D3(BJ)/def2-TZVPP. Isosurfaces (isovalue s of 0.2, ranging from $\text{sign}(\lambda_2)\rho = -0.05$ a.u. to $+0.05$ a.u.) are color-coded red (indicating strong repulsion), blue (strong attractive interactions), and green (corresponding to weak NCI).

action energy $\Delta\Delta G_{R^1R^2}$ between two substituents can be determined as follows:

$$\Delta\Delta G_{R^1R^2} = \Delta G_{R^1R^2} - \Delta G_{R^1H} - \Delta G_{HR^2} + \Delta G_{HH} \quad (1)$$

While this application of Hess's law (also referred to as double mutant cycle) gives an experimental estimate of the role each DED plays, the results have to be treated with caution due to a large error estimate (see Supporting Information for details). Nevertheless, Figure 6 qualitatively supports our findings that sterically hindered diphenylthiourea derivatives favor the *syn-syn* conformer. In general, all calculated energies are negative implying a stabilizing effect between the alkyl groups. Especially for large moieties, a stabilization of the *syn-syn* conformer can be observed ($\Delta\Delta G_{tBu^2} = -0.5 \pm 0.3$ kcal mol⁻¹). Therefore, around 30% of the observed Gibbs free energy values ($\Delta\Delta G_{tBu^2} - \Delta\Delta G_{HH} = -1.7 \pm 0.1$ kcal mol⁻¹) can be assigned to stabilizing alkyl-alkyl contacts. The remaining 70% consists of σ - π interactions between *t*Bu and the opposing phenyl moiety.^[21] The smallest effect was measured for the **1-Me₂** molecular balance ($\Delta\Delta G_{MeMe} = -0.1 \pm 0.4$ kcal mol⁻¹). In comparison to $\Delta\Delta G_{R^1Me}$ (yellow bars), $\Delta\Delta G_{R^1Et}$ (purple bars) does not profit from an additional CH₃ group. This can be rationalized with an entropic penalty^[33] due to increasing flexibility of the ethyl substituent.

With the aim to dissect the intramolecular interaction energy into its main contributors, we employed symmetry-adapted-perturbation theory^[34] (SAPT) analysis as implemented in PSI4.^[35] The scaled version was used according to Sherrill et al.^[36] to improve the performance of the decomposition method. We focused solely on the interaction between the two substituted phenyl moieties. As a starting point, we took the B3LYP-D3(BJ)/def2-TZVPP optimized geometries and removed the thiourea moiety. The resulting phenyl radicals were saturated with hydrogen yielding a benzene dimer in geometry of the *syn-syn*, *syn-anti* and *anti-anti* conformer. This approach allows us to transfer the intramolecular into intermolecular interactions between two substituted benzene molecules. While the electronic constitution of benzene varies from the electronic structure

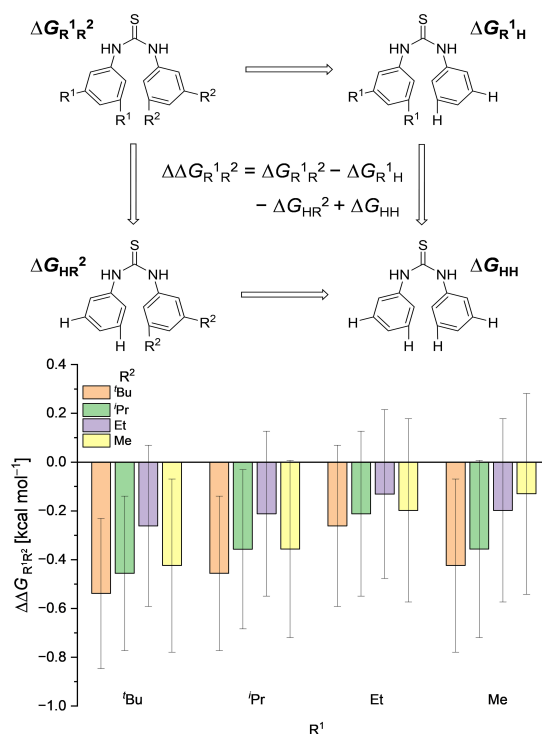


Figure 6. Double mutant cycle (top) to dissect the interaction energy $\Delta\Delta G_{R^1R^2}$ and results of the analysis (bottom); gray lines indicate error bars. $\Delta\Delta G_{R^1R^2}$ describes the relative interaction energies of R^1 - R^2 contacts of the *syn-anti* and *syn-syn* equilibrium at 193 K. Negative energies correspond to stabilizing interactions between both groups.

within diphenylthiourea, this method was solely used to identify the main source of thermodynamic stability. Figure 7 displays the energy decomposition of the total interaction energy (E_{tot}) between two di-substituted benzene molecules based on their geometry in the *syn-syn* conformer (for other conformers see Supporting Information). While inductive effects (E_{ind} , blue markings) only play a minor role

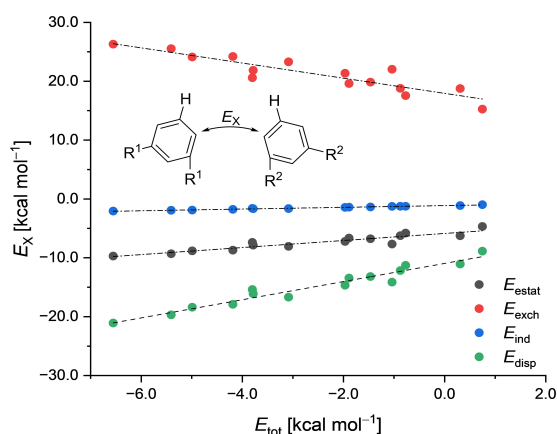


Figure 7. sSAPT analysis of two 1,3-disubstituted benzene molecules in the geometry of the *syn-syn* thiourea conformers at sSAPT0/6-311G(d,p) at 298 K. The dashed lines are used to guide the eye.

in the dimerization of substituted benzene, electrostatic (E_{estat} , grey markings) as well as LD interaction (E_{disp} , green markings) are essential to understand the interaction energy between two benzene molecules. Both energies, E_{estat} and E_{disp} , stabilize the benzene dimer due to alkyl substitution with LD interactions as the major component (up to $E_{\text{disp}} = -21.1 \text{ kcal mol}^{-1}$ for **1-Bu₂**). Nevertheless, only a combination of both energies overcompensates the destabilizing contributions of Pauli exchange repulsion (E_{exch} , red markings). Especially for **1-H₂**, repulsive interactions ($E_{\text{exch}} = +15.3 \text{ kcal mol}^{-1}$) disfavor the aggregation of benzene and override all stabilizing effects ($E_{\text{tot}} = +0.7 \text{ kcal mol}^{-1}$). While Herbert et al.^[37] identified LD as the main attractive component in cofacial π -stacking (via σ - π contacts) of benzene, this effect alone is not strong enough to stabilize **1-H₂**. The geometry of close benzene dimers enforced through the thiourea molecular backbone is therefore not ideal to afford the perfect balance between attractive and repulsive contacts. With increasing substituent bulkiness repulsive interactions increase (up to $E_{\text{exch}} = +26.3 \text{ kcal mol}^{-1}$ for **1-Bu₂**) but do not overcompensate the attractive interactions.

After establishing that LD interactions are the major factor for the conformational preference of diphenylthiourea derivatives, we set out to quantify the magnitude of LD interactions between the aromatic moieties without changing the electronic structure of *N,N'*-diphenylthiourea. While the double mutant cycle (Figure 6) represents the total interaction energy (sum of all attractive and repulsive components) between DED groups attached, the overall energy gain due to LD interactions was dissected using a Local Energy Decomposition (LED) analysis^[38] as implemented in ORCA.^[39] Therefore, we fragmented every *N,N'*-diphenylthiourea molecular balance into three parts (F1, F2, and F3). During this process all bonds are cleaved homolytically resulting in large electrostatic interactions between all fragments. Consequently, we investigated only the gain in

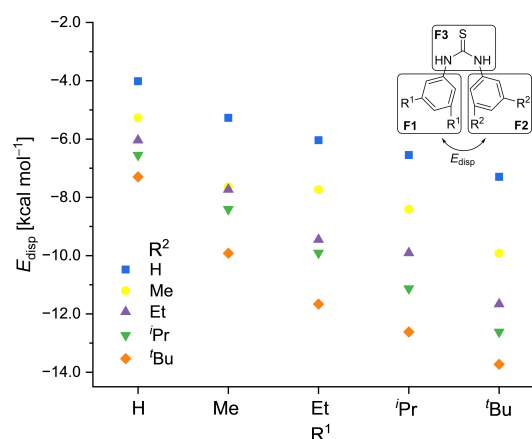


Figure 8. LD interaction energies derived from LED analysis of two **1-R¹R²** substituted phenyl moieties in *syn-syn* conformer at DLPNO-CCSD(T)/def-TZVP//B3LYP-D3(BJ)/def2-TZVPP at 298 K.

energy due to LD interactions between F1 and F2. Figure 8 shows the results of the analysis for the *syn-syn* conformers (see Supporting Information for other conformers).

The LED analysis fits qualitatively to the results of computational and experimental data very well. In comparison to the SAPT analysis, LED suggests lower LD contributions (around 6 kcal mol^{-1}), but this is due to the different models used. Accordingly, **1-H₂** and the semi-substituted **1-HR²** series benefit the least from LD interactions (between -4.0 to $-7.3 \text{ kcal mol}^{-1}$). On the other hand, substitution on both phenyl moieties results in higher LD interaction energies up to $E_{\text{disp}} = -13.7 \text{ kcal mol}^{-1}$ for **1-Bu₂**. This effect is most prominent in the *syn-syn* conformer. All methods utilized to quantify noncovalent interactions demonstrate the role of LD on the conformational preference of *N,N'*-diphenylthiourea derivatives. The experimental and computational data suggest simple additivity of the DED strength due to an increasing preference of the *syn-syn* conformer with growing steric bulk. The double mutant cycle highlights both, σ - σ and σ - π contacts as the origin of stabilization.

Conclusion

We performed a systematic experimental-computational study on the folding equilibria of all-*meta* substituted diphenylthiourea derivatives investigating the impact of steric bulk on the conformer preferences. In stark contrast to the broadly accepted dominance of Pauli repulsion dictating conformations, we identified LD interactions as the main contributor that counterintuitively stabilizes the *syn-syn* conformers. Therefore, LD proves to be a powerful interaction to shift equilibria towards apparently *more crowded* conformers.

A double-mutant cycle allowed us to quantify and differentiate between attractive σ - σ and σ - π contacts as

origin of stabilization. The most prominent shift towards the folded *syn-syn* conformer was observed when attaching bulky *tert*-butyl substituents to diphenylthiourea. An SAPT analysis reveals a combination of electrostatic and LD interactions counteracting Pauli repulsion. The LED analysis helped quantify intramolecular LD interactions and confirmed *tert*-butyl substituents to be highly effective DEDs.

Acknowledgements

This work was supported by the priority program “Control of London Dispersion in Molecular Chemistry” (SPP1807) of the Deutsche Forschungsgemeinschaft. We thank Jan M. Schümann for fruitful discussions. Open Access funding enabled and organized by Projekt DEAL.

Conflict of Interest

The authors declare no conflict of interest.

Data Availability Statement

The data that support the findings of this study are available in the Supporting Information of this article.

Keywords: Conformational Analysis · Local Energy Decomposition · Pauli Repulsion · Symmetry-Adapted-Perturbation Theory · σ - σ Interactions

- [1] E. Fischer, *Ber. Dtsch. Chem. Ges.* **1894**, 27, 2985–2993.
 [2] D. E. Koshland, *Proc. Natl. Acad. Sci. USA* **1958**, 44, 98.
 [3] K. M. Lippert, K. Hof, D. Gerbig, D. Ley, H. Hausmann, S. Guenther, P. R. Schreiner, *Eur. J. Org. Chem.* **2012**, 5919–5927.
 [4] a) P. R. Schreiner, A. Wittkopp, *Org. Lett.* **2002**, 4, 217–220; b) P. R. Schreiner, *Chem. Soc. Rev.* **2003**, 32, 289–296; c) A. Wittkopp, P. R. Schreiner, *Chem. Eur. J.* **2003**, 9, 407–414; d) Y. Takemoto, *Org. Biomol. Chem.* **2005**, 3, 4299–4306; e) S. J. Connon, *Chem. Eur. J.* **2006**, 12, 5418–5427; f) M. S. Taylor, E. N. Jacobsen, *Angew. Chem. Int. Ed.* **2006**, 45, 1520–1543; *Angew. Chem.* **2006**, 118, 1550–1573; g) A. G. Doyle, E. N. Jacobsen, *Chem. Rev.* **2007**, 107, 5713–5743; h) Z. Zhang, P. R. Schreiner, *Chem. Soc. Rev.* **2009**, 38, 1187–1198.
 [5] J. P. Wagner, P. R. Schreiner, *Angew. Chem. Int. Ed.* **2015**, 54, 12274–12296; *Angew. Chem.* **2015**, 127, 12446–12471.
 [6] a) I. Sandler, F. A. Larik, N. Mallo, J. E. Beves, J. Ho, *J. Org. Chem.* **2020**, 85, 8074–8084; b) F. Dressler, P. R. Schreiner in *Anion–Binding Catalysis* (Ed.: O. G. Mancheño), Wiley-VCH, Weinheim, **2022**, pp. 1–77.
 [7] B. Galabov, G. Vassilev, N. Neykova, A. Galabov, *J. Mol. Struct.* **1978**, 44, 15–21.
 [8] M. Heshmat, *J. Phys. Chem. A* **2018**, 122, 7974–7982.
 [9] G. Luchini, D. M. H. Ascough, J. V. Alegre-Requena, V. Gouverneur, R. S. Paton, *Tetrahedron* **2019**, 75, 697–702.
 [10] a) R. Emery, N. A. Macleod, L. C. Snoek, J. P. Simons, *Phys. Chem. Chem. Phys.* **2004**, 6, 2816–2820; b) H. M. Badawi, W. Förner, *Spectrochim. Acta Part A* **2012**, 95, 435–441.
 [11] L. V. Sudha, D. N. Sathyanarayana, S. N. Bharati, *Magn. Reson. Chem.* **1987**, 25, 474–479.
 [12] a) S. Paliwal, S. Geib, C. S. Wilcox, *J. Am. Chem. Soc.* **1994**, 116, 4497–4498; b) I. K. Mati, S. L. Cockroft, *Chem. Soc. Rev.* **2010**, 39, 4195–4205; c) M. A. Strauss, H. A. Wegner, *Eur. J. Org. Chem.* **2019**, 295–302.
 [13] S. Grimme, R. Huenerbein, S. Ehrlich, *ChemPhysChem* **2011**, 12, 1258–1261.
 [14] a) F. London, *Z. Phys.* **1930**, 63, 245–279; b) F. London, *Trans. Faraday Soc.* **1937**, 33, 8b–26.
 [15] J. M. Schümann, J. P. Wagner, A. K. Eckhardt, H. Quanz, P. R. Schreiner, *J. Am. Chem. Soc.* **2021**, 143, 41–45.
 [16] C. Eschmann, L. Song, P. R. Schreiner, *Angew. Chem. Int. Ed.* **2021**, 60, 4823–4832; *Angew. Chem.* **2021**, 133, 4873–4882.
 [17] H. C. Da Silva, W. B. De Almeida, *Chem. Phys.* **2020**, 528, 110479.
 [18] J. Hwang, P. Li, M. D. Smith, K. D. Shimizu, *Angew. Chem. Int. Ed.* **2016**, 55, 8086–8089; *Angew. Chem.* **2016**, 128, 8218–8221.
 [19] S. Rösel, C. Balestrieri, P. R. Schreiner, *Chem. Sci.* **2017**, 8, 405–410.
 [20] a) K. S. Pitzer, *J. Chem. Phys.* **1955**, 23, 1735–1735; b) K. S. Pitzer, E. Catalano, *J. Am. Chem. Soc.* **1956**, 78, 4844–4846.
 [21] a) M. Alonso, T. Woller, F. J. Martín-Martínez, J. Contreras-García, P. Geerlings, F. De Proft, *Chem. Eur. J.* **2014**, 20, 4931–4941; b) A. A. Fokin, D. Gerbig, P. R. Schreiner, *J. Am. Chem. Soc.* **2011**, 133, 20036–20039.
 [22] a) L. Schweighauser, M. A. Strauss, S. Bellotto, H. A. Wegner, *Angew. Chem. Int. Ed.* **2015**, 54, 13436–13439; *Angew. Chem.* **2015**, 127, 13636–13639; b) G. Lu, R. Y. Liu, Y. Yang, C. Fang, D. S. Lambrecht, S. L. Buchwald, P. Liu, *J. Am. Chem. Soc.* **2017**, 139, 16548–16555.
 [23] P. Pracht, F. Bohle, S. Grimme, *Phys. Chem. Chem. Phys.* **2020**, 22, 7169–7192.
 [24] A. Schäfer, C. Huber, R. Ahlrichs, *J. Chem. Phys.* **1994**, 100, 5829–5835.
 [25] a) C. Lee, W. Yang, R. G. Parr, *Phys. Rev. B* **1988**, 37, 785–789; b) A. D. Becke, *J. Chem. Phys.* **1993**, 98, 5648–5652.
 [26] S. Grimme, J. Antony, S. Ehrlich, H. Krieg, *J. Chem. Phys.* **2010**, 132, 154104.
 [27] S. Grimme, S. Ehrlich, L. Goerigk, *J. Comput. Chem.* **2011**, 32, 1456–1465.
 [28] a) S. Miertuš, E. Scrocco, J. Tomasi, *Chem. Phys.* **1981**, 55, 117–129; b) J. Tomasi, B. Mennucci, R. Cammi, *Chem. Rev.* **2005**, 105, 2999–3094.
 [29] a) C. Riplinger, F. Neese, *J. Chem. Phys.* **2013**, 138, 034106; b) D. G. Liakos, M. Sparta, M. K. Kesharwani, J. M. L. Martin, F. Neese, *J. Chem. Theory Comput.* **2015**, 11, 1525–1539.
 [30] a) L. Yang, C. Adam, G. S. Nichol, S. L. Cockroft, *Nat. Chem.* **2013**, 5, 1006–1010; b) R. Pollice, M. Bot, I. J. Kobylianskii, I. Shenderovich, P. Chen, *J. Am. Chem. Soc.* **2017**, 139, 13126–13140.
 [31] a) E. R. Johnson, S. Keinan, P. Mori-Sánchez, J. Contreras-García, A. J. Cohen, W. Yang, *J. Am. Chem. Soc.* **2010**, 132, 6498–6506; b) J. Contreras-García, E. R. Johnson, S. Keinan, R. Chaudret, J.-P. Piquemal, D. N. Beratan, W. Yang, *J. Chem. Theory Comput.* **2011**, 7, 625–632.
 [32] a) P. J. Carter, G. Winter, A. J. Wilkinson, A. R. Fersht, *Cell* **1984**, 38, 835–840; b) H. Adams, F. J. Carver, C. A. Hunter, J. C. Morales, E. M. Seward, *Angew. Chem. Int. Ed. Engl.* **1996**, 35, 1542–1544; *Angew. Chem.* **1996**, 108, 1628–1631.
 [33] a) D. Van Craen, W. H. Rath, M. Huth, L. Kemp, C. Räuber, J. M. Wollschläger, C. A. Schalley, A. Valkonen, K. Rissanen, M. Albrecht, *J. Am. Chem. Soc.* **2017**, 139, 16959–16966; b) M. A. Strauss, H. A. Wegner, *Angew. Chem. Int. Ed.* **2019**, 58, 18552–18556; *Angew. Chem.* **2019**, 131, 18724–18729.
 [34] K. Szalewicz, *WIREs Comput. Mol. Sci.* **2012**, 2, 254–272.

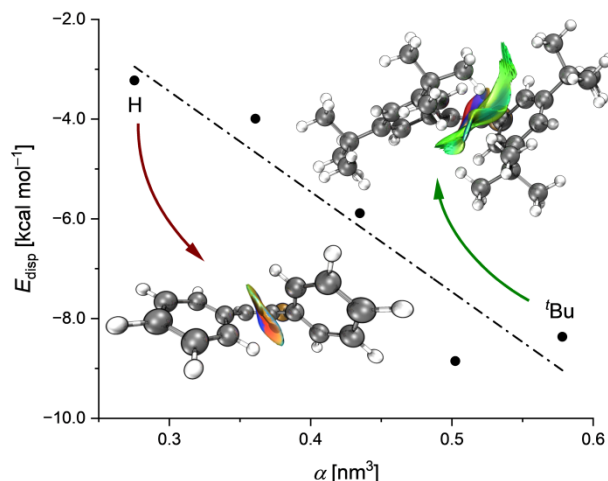
- [35] a) J. M. Turney, A. C. Simmonett, R. M. Parrish, E. G. Hohenstein, F. A. Evangelista, J. T. Fermann, B. J. Mintz, L. A. Burns, J. J. Wilke, M. L. Abrams, N. J. Russ, M. L. Leininger, C. L. Janssen, E. T. Seidl, W. D. Allen, H. F. Schaefer, R. A. King, E. F. Valeev, C. D. Sherrill, T. D. Crawford, *WIREs Comput. Mol. Sci.* **2012**, *2*, 556–565; b) R. M. Parrish, L. A. Burns, D. G. A. Smith, A. C. Simmonett, A. E. DePrince, E. G. Hohenstein, U. Bozkaya, A. Y. Sokolov, R. Di Remigio, R. M. Richard, J. F. Gonthier, A. M. James, H. R. McAlexander, A. Kumar, M. Saitow, X. Wang, B. P. Pritchard, P. Verma, H. F. Schaefer, K. Patkowski, R. A. King, E. F. Valeev, F. A. Evangelista, J. M. Turney, T. D. Crawford, C. D. Sherrill, *J. Chem. Theory Comput.* **2017**, *13*, 3185–3197.
- [36] T. M. Parker, L. A. Burns, R. M. Parrish, A. G. Ryno, C. D. Sherrill, *J. Chem. Phys.* **2014**, *140*, 094106.
- [37] a) K. Carter-Fenk, J. M. Herbert, *Chem. Sci.* **2020**, *11*, 6758–6765; b) K. Carter-Fenk, J. M. Herbert, *Phys. Chem. Chem. Phys.* **2020**, *22*, 24870–24886.
- [38] a) W. B. Schneider, G. Bistoni, M. Sparta, M. Saitow, C. Riplinger, A. A. Auer, F. Neese, *J. Chem. Theory Comput.* **2016**, *12*, 4778–4792; b) A. Altun, M. Saitow, F. Neese, G. Bistoni, *J. Chem. Theory Comput.* **2019**, *15*, 1616–1632; c) A. Altun, F. Neese, G. Bistoni, *J. Chem. Theory Comput.* **2019**, *15*, 215–228.
- [39] F. Neese, *WIREs Comput. Mol. Sci.* **2018**, *8*, e1327.

Manuscript received: March 24, 2022

Accepted manuscript online: May 11, 2022

Version of record online: June 14, 2022

2.5 London Dispersion Stabilizes Chloro-Substituted *cis*-Double Bonds



Abstract:

We present a combined experimental and computational study on the thermodynamic stability of *cis*- and *trans*-alkenes substituted with dispersion energy donor (DED) groups. To investigate the role of noncovalent interactions on equilibrium of *cis*- and *trans*-alkenes we utilized hydrochlorination reactions. While the general assumption is that increasing steric bulk favors the *trans*-alkene, we observe an equilibrium shift towards the more crowded *cis*-alkene with increasing substituent size. With the aim to quantify noncovalent interactions, we performed a double mutant cycle to experimentally gauge the attractive potential of bulky substituents. Additionally, we utilized local energy decomposition analysis at the DLPNO-CCSD(T)/def2-TZVP level of theory. We found LD interactions and Pauli exchange repulsion to be the most dominant components to influence *cis*- and *trans*-alkene equilibria.

Reference:

Lars Rummel, Kai Hanke, Jonathan Becker, and Peter R. Schreiner, *Synlett*, **2022**, 33, A-F.

DOI: 10.1055/a-1928-2473

Reproduced with permission from:

© 2022, Georg Thieme Verlag KG
Rüdigerstraße 14
70469 Stuttgart
Deutschland

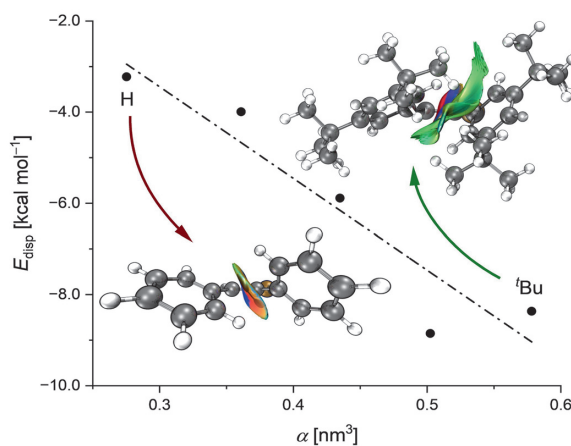
London Dispersion Stabilizes Chloro-Substituted *cis*-Double Bonds

Lars Rummel^a Kai Hanke^a Jonathan Becker^b Peter R. Schreiner^{*a} 

^aInstitute of Organic Chemistry, Justus Liebig University, Heinrich-Buff-Ring 17, 35392 Giessen, Germany
prs@uni-giessen.de

^bInstitute of Inorganic and Analytical Chemistry, Justus Liebig University, Heinrich-Buff-Ring 17, 35392 Giessen, Germany

Published as part of the Cluster
Dispersion Effects



Received: 07.07.2022

Accepted after revision: 19.08.2022

Published online: 19.08.2022 (Accepted Manuscript),
30.09.2022 (Version of Record)

DOI: 10.1055/a-1928-2473; Art ID: ST-2022-07-0314-C



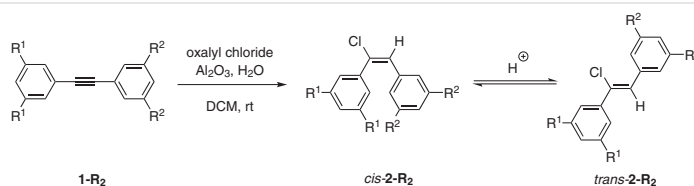
Abstract We present a combined experimental and computational study on the thermodynamic stability of *cis*- and *trans*-alkenes substituted with dispersion energy donor (DED) groups. To investigate the role of noncovalent interactions on equilibrium of *cis*- and *trans*-alkenes we utilized hydrochlorination reactions. While the general assumption is that increasing steric bulk favors the *trans*-alkene, we observe an equilibrium shift towards the more crowded *cis*-alkene with increasing substituent size. With the aim to quantify noncovalent interactions, we performed a double mutant cycle to experimentally gauge the attractive potential of bulky substituents. Additionally, we utilized local energy decomposition analysis at the DLPNO-CCSD(T)/def2-TZVP level of theory. We found LD interactions and Pauli exchange repulsion to be the most dominant components to influence *cis*- and *trans*-alkene equilibria.

Key words double mutant cycle, equilibrium, hydrohalogenation, London dispersion, Pauli repulsion

It is an accepted view in organic chemistry that *trans* double bonds are more stable than their *cis* analogues.¹ Based on the hard-sphere model, intramolecular steric hindrance is believed to alter the stability of the *cis*-isomer more significantly with increasing size of attached alkyl groups than for the 'unfolded' *trans* isomer. The notion of steric hindrance has a firm place in strain analyses, such as allylic,² *syn*-pentane,³ and 1,3-diaxial⁴ strain and is solely based on repulsive interactions due to close alkyl contacts. For instance, the A values are considered to be a direct mea-

sure of steric bulk.⁴ However, recent studies demonstrated that London dispersion (LD) interactions⁵ have to be taken into account as a key counterpart to steric repulsion.⁶ That is, bulky alkyl groups can provide considerable stabilization due to LD. LD interactions were successfully utilized to stabilize weak bonds such as in hexaphenylethane derivatives⁷ or cause molecules to dimerize by forming very close H...H contacts.⁸ As well as carbon double bond, the nitrogen congeners usually favor the unfolded *trans* conformation.⁹ For instance, Wegner et al.¹⁰ demonstrated the importance of LD on the thermal isomerization reaction from *trans*- to *cis*-azobenzene by attaching bulky dispersion energy donor (DED) groups¹¹ in all-*meta* positions. Herein, we investigate the relative thermodynamic stability of *trans*- and *cis*-alkenes by utilizing a hydrohalogenation¹² reaction (Scheme 1) and take into consideration the role LD plays in stabilizing the diastereomers.

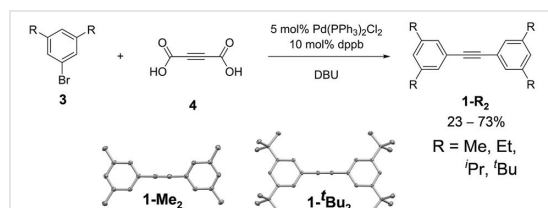
The surface-mediated *syn* addition of HCl generated in situ from the reaction of oxalyl chloride with water first gives the kinetically favored *cis*-alkene. Under acidic conditions the double bond isomerizes via a protonation-deprotonation mechanism. Kropp et al.¹² demonstrated that alkyl groups directly attached to the double bond favor the *trans*-alkene. However, a systematic study on the role of noncovalent intramolecular interactions has not been reported. Herein, we focus on stilbene derivatives using DEDs in all-*meta* positions. While parent stilbene favors the unfolded *trans* form^{1,13} (the enthalpy difference is 5.7 kcal mol⁻¹ derived from heats of hydrogenation,¹⁴ 3.8 kcal mol⁻¹ from heats of combustion,¹⁵ and 2.3 kcal mol⁻¹ from tempera-



Scheme 1 Hydrochlorination reaction of all-*meta*-substituted diphenylalkynes **1-R₂**. The reaction proceeds via a *syn* addition of HCl and forms a mixture of *cis*- and *trans*-alkenes (**2-R₂**), which can equilibrate.

ture-dependent measurement of the iodine-catalyzed isomerization reaction¹⁵) over the more crowded 'folded' *cis*-stilbene due to conjugation of the planar *trans*-stilbene and intramolecular steric hindrance in *cis*-**2-R₂**.¹⁶ The inclusion of chlorine disrupts planarity (dihedral angle $\alpha = \text{ca. } 36^\circ$) of the *trans* isomer and therefore lowers the energy gain due to conjugation by around 2.5 kcal mol⁻¹ (see the Supporting Information (SI) for details). Nevertheless, repulsive steric interactions in *cis*-**2-R₂** are not affected much by chlorine incorporation.

To measure the effects of DEDs on the thermodynamic stability of stilbene derivatives, we synthesized all-*meta*-substituted diphenylalkynes¹⁷ **1-R₂** with methyl (Me), ethyl (Et), *iso*-propyl (^{*i*}Pr), and *tert*-butyl (^{*t*}Bu) groups attached. We generated the 1-bromo-3,5-disubstituted benzene derivatives via literature procedures^{7a,18} and utilized a Pd-catalyzed decarboxylative coupling reaction¹⁹ with 2-butyne-dioic acid to give all-*meta*-substituted diphenylalkynes **1-R₂** (Scheme 2). Unsymmetrical diphenylalkynes were synthesized in a coupling reaction with phenylpropionic acid.



Scheme 2 Synthetic procedure for the preparation of all-*meta*-substituted diphenylalkynes and molecular structures derived from single-crystal X-ray diffraction of **1-Me₂** and **1-^{*t*}Bu₂**. Thermal ellipsoids drawn at 50% probability level.

To test the suitability of the hydrochlorination and to gather information on thermodynamic equilibria of the stilbene derivatives, we chose 1,2-bis(3,5-dimethylphenyl)ethyne (**1-Me₂**) as a model system.²⁰ We adopted the procedure of Kropp et al.¹² utilizing alumina for surface activation. The hydrolysis of oxalyl chloride was used to generate HCl in situ. The reaction was monitored via gas chromatography (GC-MS). After adding oxalyl chloride to a suspension of alkyne and alumina in DCM the starting material was consumed after around 20 min. Alumina adsorbs HCl in

DCM solution, thereby enhancing its acidity and reactivity towards alkynes.^{12b} The *syn* addition of HCl with the alkyne gives *cis*-**2-Me₂**. With an excess of reagent, the system equilibrates between the two diastereomers resulting in *trans*-**2-Me₂** as the main product. While equilibrium was reached after around 2 h, the mixture was allowed to react for 4 h in total. Figure 1 shows the composition of the reaction mixture with *cis*-alkene (red markings) as the kinetic and *trans*-alkene (blue markings) as the thermodynamic product. The starting material (grey markings) is consumed quickly. While the equilibrium shifts towards the unfolded *trans*-**2-Me₂**, the ratio and therefore energy difference between both conformers can be determined. Accordingly, the hydrochlorination is a means to an end to equilibrate the stilbene isomers.

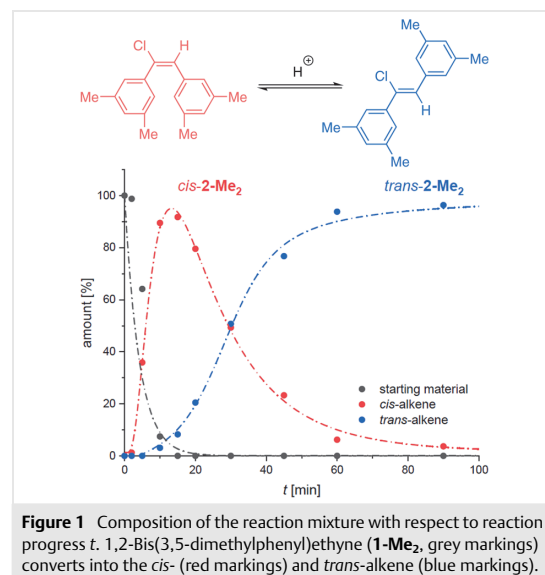


Figure 1 Composition of the reaction mixture with respect to reaction progress *t*. 1,2-Bis(3,5-dimethylphenyl)ethyne (**1-Me₂**, grey markings) converts into the *cis*- (red markings) and *trans*-alkene (blue markings).

The thermochemical results ($\Delta G_{\text{R-R}} - \Delta G_{\text{H-H}}$) of the computational and experimental study are depicted in Figure 2. By representing the relative Gibbs free energies of the substituted and unsubstituted system, the trend already highlights the role DEDs play in the equilibrium (for absolute

values, see the SI). While negative energy values correspond to a shift towards the more crowded *cis* diastereomer, positive values denote a shift to the *trans* isomer. Accordingly, the experimental data (Figure 2, blue markings) show a shift to the *cis* isomer with increasing polarizability of the substituents, although the absolute energies shows a preference of the *trans* isomer for all derivatives (for absolute values, see the SI). While Me substituents do not affect the equilibrium in comparison to the parent system ($\Delta G_{\text{Me-Me}} - \Delta G_{\text{H-H}} = -0.1 \pm 0.2 \text{ kcal mol}^{-1}$), bulkier substituents *all* favor the folded isomer (negative energy values). This trend correlates well with polarizability α and therefore can be traced back to the substituents acting as DEDs.⁵ Hence, the largest effect can be observed with *tert*-butyl substitution ($\Delta G_{\text{tBu-tBu}} - \Delta G_{\text{H-H}} = -0.7 \pm 0.2 \text{ kcal mol}^{-1}$). While bulkier DEDs shift the equilibrium to the more crowded *cis*-stilbene derivative, the chlorine atom appears to have a minor impact on the equilibrium. With its high polarizability chlorine can compete with alkyl substituents and diminishes the energetic preference for the *cis* derivative.²¹

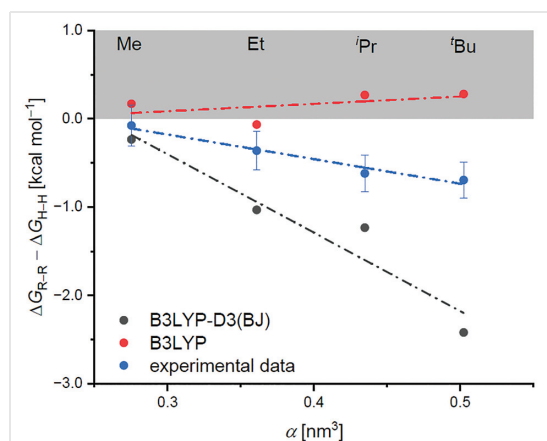


Figure 2 Gibbs free energies for the equilibrium of all-*meta*-substituted diphenyl *cis*- and *trans*-alkenes relative to the unsubstituted alkenes plotted vs. the polarizability α . Blue markings correspond to experimental values. Computations were performed at the B3LYP-D3(BJ)/def2-TZVPP (grey markings) and B3LYP/def2-TZVPP (red markings) level of theory. The PCM solvent model (DCM) was utilized for single-point energy computations with thermal corrections added from DFT frequency computations. Data points in the shaded area correspond to repulsive interactions.

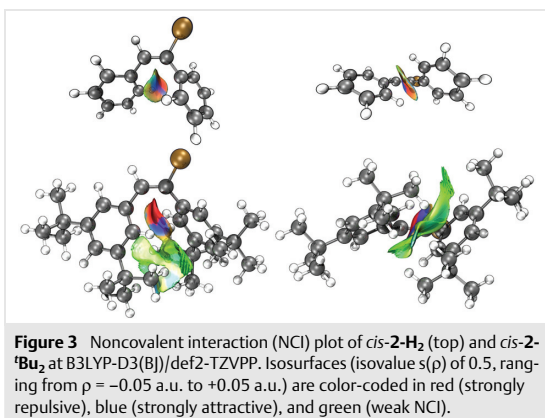
We also performed a computational study on the thermodynamic stability of stilbene derivatives to assess the *cis* and *trans* diastereomer equilibrium. We utilized the Conformer-Rotamer Ensemble Sampling Tool²² (crest) to identify conformers lowest in energy for the *cis*- and *trans*-alkenes. The preoptimized diastereomers were further optimized in the gas phase with Gaussian16.²³ We chose the B3LYP²⁴ functional including and excluding Grimme's D3(BJ) correction²⁵ in conjunction with Ahlrich's def2-TZ-

VPP²⁶ basis set. To address solvent effects, single-point energy computations were performed utilizing the PCM model²⁷ with DCM as solvent. We verified these results using ω B97X-D²⁸ and higher-level computations such as single-point energies at the DLPNO-CCSD(T)/def2-TZVP²⁹ level of theory (see the SI for details).

The exclusion of LD interactions by utilizing the B3LYP functional without dispersion correction (red markings) predicts the *trans*-alkene to be lowest in energy for all compounds studied. Additionally, an incorporation of bulky substituents, such as *iso*-propyl or *tert*-butyl groups in all-*meta* position, results in positive energy values (up to +0.3 kcal mol⁻¹). This would imply the intuitively often preferred repulsive nature of the intramolecular interactions in the *cis*-alkene. On the contrary, the inclusion of Grimme's D3(BJ) correction (grey markings) leads to a significant stabilization in favor of the *cis* diastereomer. While the parent *trans*-stilbene is computationally favored by $\Delta G_{\text{eq}} = +0.4 \text{ kcal mol}^{-1}$, bulky substituents shift the equilibrium towards the *cis*-alkene. The largest effect is associated with the most polarizable *tert*-butyl groups with $\Delta G_{\text{tBu-tBu}} - \Delta G_{\text{H-H}} = -2.4 \text{ kcal mol}^{-1}$ (for absolute values, see the SI). The close correlation with the polarizability α (Figure 2) hints to attractive interactions relating to LD. By comparing computed with experimental data (blue markings), it is apparent that only the inclusion of dispersion corrections can help rationalize the observed trends. While computed energies arising from B3LYP/def2-TZVPP are not affected by the attached substituents, the B3LYP-D3(BJ)/def2-TZVPP level of theory is in line with the relative experimental energies. Both linear regressions (blue and grey markings) show the same sign and shift the equilibrium towards to more sterically hindered alkene. Nevertheless, the computed energetic preference due to the all-*meta* substitution pattern is around 70% more pronounced than our experimental findings suggest.³⁰ The highest shift towards the *cis*-alkene was observed with *tert*-butyl substitution ($\Delta G_{\text{tBu-tBu}} - \Delta G_{\text{H-H}} = -0.7 \pm 0.2 \text{ kcal mol}^{-1}$). While the absolute energies of the B3LYP-D3(BJ)/def2-TZVPP computations favor the *cis* isomer, the experimental study shows the *trans* isomer to be lowest in energy regardless of the substituents attached. Therefore, we conclude that an attenuation of intramolecular noncovalent interactions in DCM influences the equilibria of stilbene-type molecules significantly.^{30,31} This effect is not captured with solvent inclusion in the computations resulting in unsatisfactory computation of the absolute energy differences.

To investigate the origin of stabilization of the *cis*-alkene with bulky substituents attached, we conducted a qualitative analysis of noncovalent interactions. We generated intramolecular noncovalent interactions (NCI) plots³² to highlight attractive and repulsive regions between the disubstituted phenyl moieties. The results for the *cis* diastereomers of **2-H₂** (top) and **2-tBu₂** (bottom) are depicted in Figure 3. While the *trans*-alkenes show no NCI interactions between

the phenyl moieties (this is also confirmed by LED computations, see the SI), the *cis* isomers feature one large isosurface between adjacent phenyl moieties. With strong repulsive interactions color-coded in red and strong attractive interactions in blue, both alkenes show red isosurfaces in close proximity to the double bond, but blue ones in the exterior of both phenyl moieties. This is in line with the finding for hexaphenylethane.⁷ The incorporation of bulky substituents results in an additional green isosurface corresponding to LD interactions. Accordingly, *cis*-2-^tBu₂ is stabilized by close σ - σ contacts of around 2.3 Å in distance; these originate from the methyl groups of the *tert*-butyl substituents.

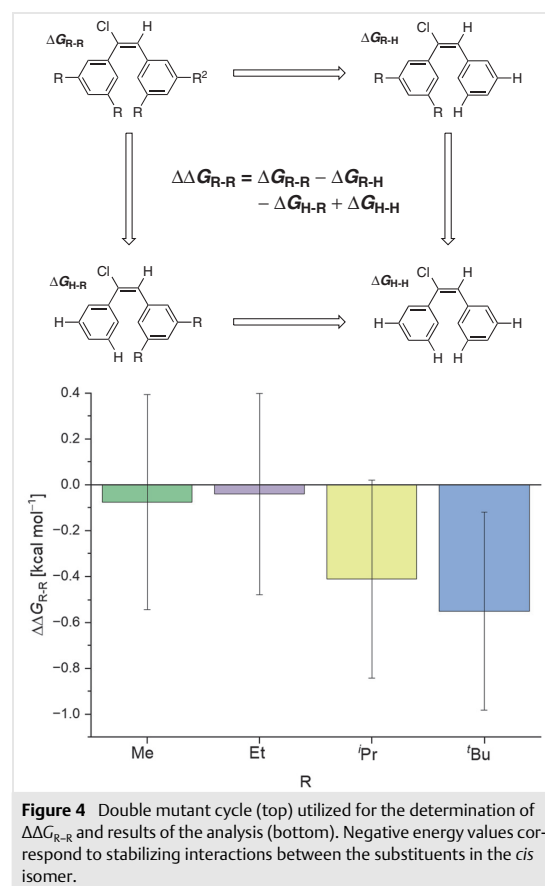


Apart from qualitative investigations, we quantitatively assessed the role DEDs play in the equilibrium. We performed a double-mutant cycle³³ (DMC) to dissect the interaction energy $\Delta\Delta G_{R-R}$ which corresponds to the energy gained or lost due to two substituents interacting with each other. $\Delta\Delta G_{R-R}$ is dissected from unsubstituted and singly substituted systems according to the following equation:

$$\Delta\Delta G_{R-R} = \Delta G_{R-R} - \Delta G_{R-H} - \Delta G_{H-R} + \Delta G_{H-H}$$

The results of the DMC give an experimental estimate of the attractive (negative energy values) or repulsive (positive energy values) interactions exclusively between DEDs, thereby, excluding interactions between substituent and the opposing phenyl moiety (Figure 4). Due to a large error estimate (summation of four ΔG errors) the results of the analysis have to be treated with caution (see the SI for error estimation). Nevertheless, the analysis qualitatively confirms the DED capacities of alkyl groups. The total interaction energies $\Delta\Delta G_{R-R}$ between the substituents are all attractive (negative) and, consequently, stabilizing for the *cis*-alkene. Both, Me–Me and Et–Et contacts ($\Delta\Delta G_{R-R} = \text{ca. } -0.1$ kcal mol⁻¹) only faintly favor the *cis*-alkene. This is not surprising since LD interactions are highly distance-dependent (r^{-6}). With a distance of around $d_{\text{Me-Me}} = \text{ca. } 4.2$ Å and $d_{\text{Et-Et}} = \text{ca. } 3.1$ Å, the substituents do not fall into the van der Waals

minimum ($d_{\text{ideal}} = \text{ca. } 2.5$ Å) range.^{31b} Additionally, the latter suffers an entropic penalty due to the increased flexibility of the Et substituent. A similar effect was observed in the conformational analysis of all-*meta*-substituted diphenylthiourea.³⁴ Azobenzene derivatives³⁵ as well as hierarchically assembled dinuclear titanium(IV) helicates³⁶ confirm the effect for longer alkyl chains. The highest stabilizing interaction in favor of the *cis*-alkene again is observed for the close ^tBu-^tBu ($d_{\text{tBu-tBu}} = \text{ca. } 2.3$ Å) contacts by $\Delta\Delta G_{\text{tBu-tBu}} = -0.6$ kcal mol⁻¹. The observed trends stem from a combination of attractive LD interactions between bulky DEDs and the solvophobic effect in polar solvents. Both effects increase with the size of alkyl substituent attached.



We performed a computational and experimental study on the role LD interactions play in the thermodynamic equilibrium of *cis*- and *trans*-alkenes, utilizing surface-mediated hydrochlorinations to study the effects of bulky substituents. In contrast to the notion that steric bulk favors the unfolded *trans*-alkene due to steric hindrance in the *cis*-olefin, we found a counterintuitive shift towards the more

crowded *cis*-alkene with increasing substituent size. We highlight LD interactions as the main source of stabilization. To confirm these findings, we evaluated a double-mutant cycle to quantify the stabilizing interactions between polarizable alkyl groups attached in all-*meta* positions. The most prominent effect was observed with *tert*-butyl substitution. By analogy, an LED analysis provides additional evidence that LD interactions only affect the folded *cis*-alkene via intramolecular σ - σ contacts.

Conflict of Interest

The authors declare no conflict of interest.

Funding Information

This work was supported by the priority program 'Control of London Dispersion in Molecular Chemistry' (SPP1807) of the Deutsche Forschungsgemeinschaft.

Acknowledgment

We thank Steffen Wagner for performing GC-MS measurements and Jan M. Schümann, Bastian Bernhardt, Henrik F. König, and Finn M. Wilming for fruitful discussions.

Supporting Information

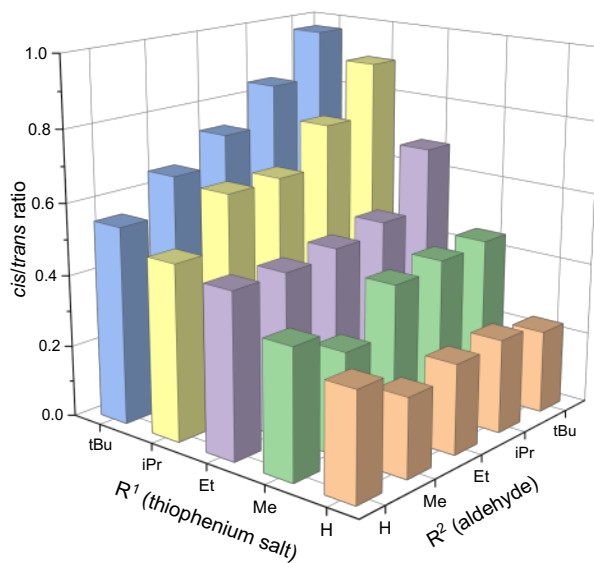
Supporting information for this article is available online at <https://doi.org/10.1055/a-1928-2473>.

References and Notes

- (1) Kwasniewski, S. P.; Claes, L.; François, J.-P.; Deleuze, M. S. *J. Chem. Phys.* **2003**, *118*, 7823.
- (2) (a) Malhotra, S. K.; Johnson, F. *J. Am. Chem. Soc.* **1965**, *87*, 5493. (b) Johnson, F.; Malhotra, S. K. *J. Am. Chem. Soc.* **1965**, *87*, 5492. (c) Johnson, F. *Chem. Rev.* **1968**, *68*, 375.
- (3) (a) Gotō, H.; Ōsawa, E.; Yamato, M. *Tetrahedron* **1993**, *49*, 387. (b) Scott, R. A.; Scheraga, H. A. *J. Chem. Phys.* **1966**, *44*, 3054. (c) Hoffmann, R. W.; Stahl, M.; Schopfer, U.; Frenking, G. *Chem. Eur. J.* **1998**, *4*, 559.
- (4) (a) Winstein, S.; Holness, N. J. *J. Am. Chem. Soc.* **1955**, *77*, 5562. (b) Jensen, F. R.; Bushweller, C. H.; Beck, B. H. *J. Am. Chem. Soc.* **1969**, *91*, 344.
- (5) (a) London, F. Z. *Phys.* **1930**, *63*, 245. (b) London, F. *Trans. Faraday Soc.* **1937**, *33*, 8b.
- (6) (a) Wagner, J. P.; Schreiner, P. R. *Angew. Chem. Int. Ed.* **2015**, *54*, 12274. (b) Solel, E.; Ruth, M.; Schreiner, P. R. *J. Org. Chem.* **2021**, *86*, 7701. (c) Solel, E.; Ruth, M.; Schreiner, P. R. *J. Am. Chem. Soc.* **2021**, *143*, 20837.
- (7) (a) Rösel, S.; Balestrieri, C.; Schreiner, P. R. *Chem. Sci.* **2017**, *8*, 405. (b) Rösel, S.; Becker, J.; Allen, W. D.; Schreiner, P. R. *J. Am. Chem. Soc.* **2018**, *140*, 14421. (c) Rummel, L.; Schümann, J. M.; Schreiner, P. R. *Chem. Eur. J.* **2021**, *27*, 13699. (d) Rösel, S.; Schreiner, P. R. *Isr. J. Chem.* **2022**, *62*, e202200002.
- (8) (a) Rösel, S.; Quanz, H.; Logemann, C.; Becker, J.; Mossou, E.; Cañadillas-Delgado, L.; Caldeweyher, E.; Grimme, S.; Schreiner, P. R. *J. Am. Chem. Soc.* **2017**, *139*, 7428. (b) Maué, D.; Strebert, P. H.; Bernhard, D.; Rösel, S.; Schreiner, P. R.; Gerhards, M. *Angew. Chem. Int. Ed.* **2021**, *60*, 11305.
- (9) (a) Wong, D. P.; Fink, W. H.; Allen, L. C. *J. Chem. Phys.* **1970**, *52*, 6291. (b) Schmittel, M.; Ruechardt, C. *J. Am. Chem. Soc.* **1987**, *109*, 2750.
- (10) Schweighauser, L.; Strauss, M. A.; Bellotto, S.; Wegner, H. A. *Angew. Chem. Int. Ed.* **2015**, *54*, 13436.
- (11) Grimme, S.; Huenerbein, R.; Ehrlich, S. *ChemPhysChem* **2011**, *12*, 1258.
- (12) (a) Kropp, P. J.; Daus, K. A.; Crawford, S. D.; Tubergen, M. W.; Kepler, K. D.; Craig, S. L.; Wilson, V. P. *J. Am. Chem. Soc.* **1990**, *112*, 7433. (b) Kropp, P. J.; Daus, K. A.; Tubergen, M. W.; Kepler, K. D.; Wilson, V. P.; Craig, S. L.; Baillargeon, M. M.; Breton, G. W. *J. Am. Chem. Soc.* **1993**, *115*, 3071. (c) Pienta, N. J.; Crawford, S. D.; Kropp, P. J. *J. Chem. Educ.* **1993**, *70*, 682. (d) Kropp, P. J.; Crawford, S. D. *J. Org. Chem.* **1994**, *59*, 3102. (e) Kropp, P. J.; Breton, G. W.; Craig, S. L.; Crawford, S. D.; Durland, W. F.; Jones, J. E.; Raleigh, J. S. *J. Org. Chem.* **1995**, *60*, 4146.
- (13) Saltiel, J.; Ganapathy, S.; Werking, C. *J. Phys. Chem.* **1987**, *91*, 2755.
- (14) Williams, R. B. *J. Am. Chem. Soc.* **1942**, *64*, 1395.
- (15) Fischer, G.; Muszkat, K. A.; Fischer, E. *J. Chem. Soc. B* **1968**, 1156.
- (16) Adrian, F. J. *J. Chem. Phys.* **1958**, *28*, 608.
- (17) **General Procedure for the Coupling Reactions**
Pd(PPh₃)₂Cl₂ (0.1 equiv.), 1,4-bis(diphenylphosphino)butane (0.1 equiv.), aryl halides (2 equiv.), and 2-butyne-1,3-diol (1 equiv.) were combined with DBU (2 equiv.) in a small round-bottomed flask. DMSO (15.0 mL) was added, and the flask was sealed with a septum. The resulting mixture was placed in an oil bath at 110 °C for 4 h. The reaction was poured into 25 mL of saturated aqueous ammonium chloride and extracted with Et₂O (4 × 20 mL). The combined ether extracts were washed with brine (90 mL), dried over MgSO₄, and filtered. The solvent was removed under reduced pressure, and the resulting crude product was purified by flash chromatography (n-hexane) on silica gel
Bis(3,5-di-*tert*-butylphenyl)acetylene (1'-Bu₂)
¹H NMR (400 MHz, CDCl₃): δ = 1.22 (s, 36 H, 1), 7.51 (t, 2 H, 2), 7.77 (d, 4 H, 3) ppm. ¹³C NMR [¹H] (101 MHz, CDCl₃): δ = 31.4, 34.9, 90.4, 122.8, 123.7, 126.7, 151.3 ppm.
- (18) (a) Eschmann, C.; Song, L.; Schreiner, P. R. *Angew. Chem. Int. Ed.* **2021**, *60*, 4823. (b) Shi, F.; Shen, J. K.; Chen, D.; Fog, K.; Thirstrup, K.; Hentzer, M.; Karlsson, J.-J.; Menon, V.; Jones, K. A.; Smith, K. E.; Smith, G. *ACS Med. Chem. Lett.* **2011**, *2*, 303.
- (19) Park, K.; Bae, G.; Moon, J.; Choe, J.; Song, K. H.; Lee, S. *J. Org. Chem.* **2010**, *75*, 6244.
- (20) **General Procedure for the Hydrochlorination Reaction**
A round-bottomed flask was charged with substituted diphenylacetylene (1 equiv.) and 10 g alumina. 20 mL DCM were added, and the mixture was stirred vigorously. To start the reaction oxalyl chloride (8 equiv.) was added via a syringe and the mixture sealed with a septum. The reaction procedure and product ratio was monitored via GC-MS.
- (21) Liu, T.; Schneider, H.-J. *Angew. Chem. Int. Ed.* **2002**, *41*, 1368.
- (22) Pracht, P.; Bohle, F.; Grimme, S. *Phys. Chem. Chem. Phys.* **2020**, *22*, 7169.
- (23) Frisch, M. J.; Trucks, G. W.; Schlegel, H. B.; Scuseria, G. E.; Robb, M. A.; Cheeseman, J. R.; Scalmani, G.; Barone, V.; Petersson, G. A.; Nakatsuji, H.; Li, X.; Caricato, M.; Marenich, A. V.; Bloino, J.; Janesko, B. G.; Gomperts, R.; Mennucci, B.; Hratchian, H. P.;

- Ortiz, J. V.; Izmaylov, A. F.; Sonnenberg, J. L.; Williams-Young, D.; Ding, F.; Lipparini, F.; Egidi, F.; Goings, J.; Peng, B.; Petrone, A.; Henderson, T.; Ranasinghe, D.; Zakrzewski, V. G.; Gao, J.; Rega, N.; Zheng, G.; Liang, W.; Hada, M.; Ehara, M.; Toyota, K.; Fukuda, R.; Hasegawa, J.; Ishida, M.; Nakajima, T.; Honda, Y.; Kitao, O.; Nakai, H.; Vreven, T.; Throssell, K.; Montgomery, J. A. Jr.; Peralta, J. E.; Ogliaro, F.; Bearpark, M. J.; Heyd, J. J.; Brothers, E. N.; Kudin, K. N.; Staroverov, V. N.; Keith, T. A.; Kobayashi, R.; Normand, J.; Raghavachari, K.; Rendell, A. P.; Burant, J. C.; Iyengar, S. S.; Tomasi, J.; Cossi, M.; Millam, J. M.; Klene, M.; Adamo, C.; Cammi, R.; Ochterski, J. W.; Martin, R. L.; Morokuma, K.; Farkas, O.; Foresman, J. B.; Fox, D. J. *Gaussian 16 Rev. C.01*; Gaussian: Wallingford, **2016**.
- (24) (a) Lee, C.; Yang, W.; Parr, R. G. *Phys. Rev. B* **1988**, *37*, 785. (b) Becke, A. D. *J. Chem. Phys.* **1993**, *98*, 5648.
- (25) (a) Grimme, S.; Antony, J.; Ehrlich, S.; Krieg, H. *J. Chem. Phys.* **2010**, *132*, 154104. (b) Grimme, S.; Ehrlich, S.; Goerigk, L. *J. Comput. Chem.* **2011**, *32*, 1456.
- (26) Schäfer, A.; Huber, C.; Ahlrichs, R. *J. Chem. Phys.* **1994**, *100*, 5829.
- (27) (a) Miertuš, S.; Scrocco, E.; Tomasi, J. *Chem. Phys.* **1981**, *55*, 117. (b) Tomasi, J.; Mennucci, B.; Cammi, R. *Chem. Rev.* **2005**, *105*, 2999.
- (28) Chai, J.-D.; Head-Gordon, M. *Phys. Chem. Chem. Phys.* **2008**, *10*, 6615.
- (29) (a) Riplinger, C.; Neese, F. *J. Chem. Phys.* **2013**, *138*, 034106. (b) Liakos, D. G.; Sparta, M.; Kesharwani, M. K.; Martin, J. M. L.; Neese, F. *J. Chem. Theory Comput.* **2015**, *11*, 1525.
- (30) Pollice, R.; Bot, M.; Kobylanski, I. J.; Shenderovich, I.; Chen, P. *J. Am. Chem. Soc.* **2017**, *139*, 13126.
- (31) (a) Pollice, R.; Fleckenstein, F.; Shenderovich, I.; Chen, P. *Angew. Chem. Int. Ed.* **2019**, *58*, 14281. (b) Schümann, J. M.; Wagner, J. P.; Eckhardt, A. K.; Quanz, H.; Schreiner, P. R. *J. Am. Chem. Soc.* **2021**, *143*, 41.
- (32) (a) Johnson, E. R.; Keinan, S.; Mori-Sánchez, P.; Contreras-García, J.; Cohen, A. J.; Yang, W. *J. Am. Chem. Soc.* **2010**, *132*, 6498. (b) Contreras-García, J.; Johnson, E. R.; Keinan, S.; Chaudret, R.; Piquemal, J.-P.; Beratan, D. N.; Yang, W. *J. Chem. Theory Comput.* **2011**, *7*, 625.
- (33) (a) Carter, P. J.; Winter, G.; Wilkinson, A. J.; Fersht, A. R. *Cell* **1984**, *38*, 835. (b) Adams, H.; Carver, F. J.; Hunter, C. A.; Morales, J. C.; Seward, E. M. *Angew. Chem., Int. Ed. Engl.* **1996**, *35*, 1542. (c) Yang, L.; Adam, C.; Nichol, G. S.; Cockroft, S. L. *Nat. Chem.* **2013**, *5*, 1006.
- (34) Rummel, L.; Domanski, M. H. J.; Hausmann, H.; Becker, J.; Schreiner, P. R. *Angew. Chem. Int. Ed.* **2022**, *134*, e202204393.
- (35) Strauss, M. A.; Wegner, H. A. *Angew. Chem. Int. Ed.* **2019**, *58*, 18552.
- (36) Van Craen, D.; Rath, W. H.; Huth, M.; Kemp, L.; Räuber, C.; Wollschläger, J. M.; Schalley, C. A.; Valkonen, A.; Rissanen, K.; Albrecht, M. *J. Am. Chem. Soc.* **2017**, *139*, 16959.

2.6 London Dispersion Favors cis-Selectivity in the Johnson-Corey-Chaykovsky Epoxidation



Abstract:

We present an experimental study on the role of dispersion energy donors on the cis/trans-selectivity of Johnson-Corey-Chaykovsky epoxidation. Whereas the generally accepted origin of diastereoselectivity is based on steric repulsion, we determined that London dispersion interactions are the main source of stabilization of the preferred transition structure. This was brought to the fore utilizing a series of nuclear magnetic resonance measurements to determine the role of noncovalent interactions.

Reference:

Lars Rummel, Marvin H. J. Domanski, Ephrath Solel, Heike Hausmann, and Peter R. Schreiner; *manuscript in preparation*.

London Dispersion Favors *cis*-Selectivity in the Johnson-Corey-Chaykovsky Epoxidation

Lars Rummel,[‡] Marvin H. J. Domanski,[‡] Ephrath Solel,[‡] Heike Hausmann, and Peter R. Schreiner^{*}

[‡] Authors contributed equally to this work.

^{*} Corresponding author

Institute of Organic Chemistry, Justus Liebig University, Heinrich-Buff-Ring 17, 35392 Giessen, Germany, E-mail: prs@uni-giessen.de

KEYWORDS. *Diastereoselectivity, Dispersion Energy Donors, Noncovalent Interactions, Steric Effects, Transition State*

ABSTRACT: We present an experimental study on the role of dispersion energy donors on the *cis/trans*-selectivity of Johnson-Corey-Chaykovsky epoxidation. Whereas the generally accepted origin of diastereoselectivity is based on steric repulsion, we determined that London dispersion interactions are the main source of stabilization of the preferred transition structure. This was brought to the fore utilizing a series of nuclear magnetic resonance measurements to determine the role of noncovalent interactions.

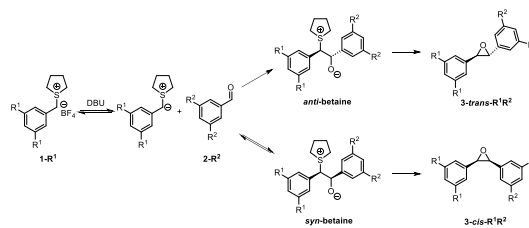
INTRODUCTION

In enantioselective catalysis, insights into reaction mechanisms are essential to maximize yields and stereoselectivities. Especially the latter requires extensive knowledge about how molecules interact and connect *via* elementary reaction steps. The applicability of a detailed understanding of reaction pathways ranges from basic S_N2 reactions¹ proceeding *via* stereospecific backside attack, to highly complex catalytic processes.² To date, the origin of stereoselectivity still is most often rationalized by repulsive steric interactions either between substrates or catalyst and substrate; this is particularly so in textbooks. While the concept of steric hindrance can typically explain the stereochemical outcome of reactions between *small* molecules and groups, bulky substituents counterintuitively sometimes have the opposite effect.³ This has been recently demonstrated, for example, for the Corey-Bakshi-Shibata reduction utilizing sterically highly encumbered oxazaborolidine catalysts.⁴ Here, the rate determining step of the reduction proceeds through the more *crowded* transition state that profits from *attractive* noncovalent interactions. For hydroamination reactions it was demonstrated that increasing steric bulk promotes catalyst-substrate interactions, thereby accelerating the reaction.⁵⁻⁷ Both studies highlighted the importance of London dispersion^{8,9} (LD) interactions as the key driving force for aggregation and as the essential interaction to rationalize experimental results. To maximize LD, bulky dispersion energy donor (DED) groups were introduced as a concept and in practice.^{3,10}

In comparison to ground-state stabilization *via* attractive σ - σ contacts, for example, in molecular balances,^{11,12} the stabilization of transition states has not been well investigated. Here,

we chose the Johnson-Corey-Chaykovsky (JCC) reaction¹³⁻¹⁶ to study the effect of DEDs on the stereodifferentiating transition states of this reaction. The JCC reaction takes place between an ylide and an aldehyde (Scheme 1). Numerous procedures¹⁷⁻²² exist that give a variety of products, for example, epoxides, cyclopropanes, and aziridines. Additionally, theoretical and experimental studies²³⁻²⁷ were performed on the mechanism of the JCC reaction. After a pre-equilibrium deprotonation with base to generate the ylide from sulfonium salt **1-R¹**, the ylide adds nucleophilically to the aldehyde **2-R²** in the rate-determining step. Subsequent bond rotation around the central C-C bond gives the *syn*- or *anti*-betaine, followed by elimination of sulfide to yield the *cis*- or *trans*-epoxide (**3-cis-R¹R²**), respectively.

Scheme 1. Currently accepted mechanism of the Johnson-Corey-Chaykovsky epoxidation.



Experimentally, the Gibbs free energy of activation was determined of around $\Delta G^\ddagger = 22.2$ kcal mol⁻¹ (with R¹ = H and R² = H) at 298 K for the nucleophilic addition of the ylide to

strated the torsional rotation around the central C–C bond of the betaine to be rate-determining for *cis*-epoxide.²⁶ The origin of the diastereoselectivity lies in the reversibility of the *syn*-betaine formation on the one hand and the irreversibility of the *anti*-betaine formation (from cross-over experiments) on the other hand. Accordingly, Aggarwal *et al.*²⁸ laid out four main principles to rationalize stereoselectivity. Apart from steric repulsion between the phenyl moieties in the *syn*-betaine structure, Aggarwal emphasized the stability of the ylide and the aldehyde and solvation effects to promote reversible *syn*-betaine formation. Herein, we study the role of DEDs on the JCC reaction demonstrating the importance of LD in this reaction in particular and in chemical reactions in general.

RESULTS

To study the impact of DEDs on the JCC epoxidation, we systematically varied the substituent at $1-R^1$ and $2-R^2$ in the logical series from methyl (Me), ethyl (Et), *iso*-propyl (*i*Pr), to *tert*-butyl (*t*Bu). We utilized 1-bromo-3,5-dialkyl-substituted benzene as starting material to generate all precursors. $2-R^2$ was prepared *via* a formylation reaction with DMF.²⁹ The aldehyde was reduced utilizing $LiAlH_4$ and the resulting alcohol was brominated *via* PBr_3 .^{30, 31} A Finkelstein-type reaction with tetrahydrothiophene and $NaBF_4$ yielded $1-R^1$.³² To probe the effects of DEDs on JCC, the reaction conditions were chosen in analogy to Crudden *et al.*²⁷ who experimentally investigated the mechanism of the JCC reaction. The epoxidations were performed in DCM under pseudo-first order (thus kinetic) conditions. Accordingly, the aldehyde was utilized in excess (0.5 M, 10 equiv.) with limiting sulfonium salt (1 equiv.) present. A buffer (1 equiv.) of 1,8-diazabicyclo(5.4.0)undec-7-ene (DBU) and *p*-toluenesulfonic acid (*p*-TSA) was utilized for a steady pH. Additionally, DBU (1 equiv.) was added as a base to generate the ylide and to start the reaction. The reaction progress was monitored by 1H -NMR at room temperature. The ratio of $3-cis-R^1R^2$ and $3-trans-R^1R^2$ was determined by integration of the *cis* and *trans* proton signals at the epoxide. Crudden *et al.*²⁷ already demonstrated irreversibility of the parent unsubstituted system. To see whether bulky substituents influence the reaction mechanism, we followed the reaction progress for $1-Me$ and $2-Me$ as well as $1-tBu$ and $2-tBu$ (see SI). In both cases the product concentration steadily increased while ratio between both epoxides remained constant. Additionally, we exposed a 1:1 mixture of $3-trans-HH$ and $3-cis-HH$ to the reaction conditions without observing a change ratio (see SI). Figure 1 shows the NMR signals of the symmetric epoxides with a chemical shift between 3.75–4.40 ppm.

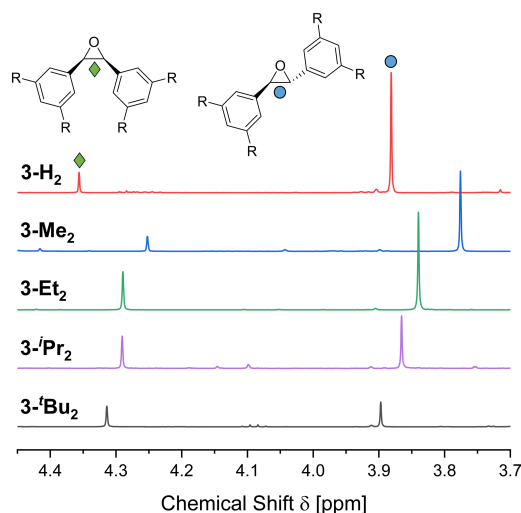


Figure 1. NMR measurements of symmetric $3-cis-R_2$ (green marking) and $3-trans-R_2$ (blue marking) as a result of the reaction of $1-R$ and $2-R$ in DCM at 273 K. For simplicity, the CH signals of the symmetric epoxides are depicted only.

The parent unsubstituted starting material resulted in a product ratio of 0.17:1 (*cis:trans*, Figure 1, red NMR). In accordance with the literature,²⁷ the larger signal (blue marking) was assigned to the unfolded $3-trans-HH$ and the smaller signal (green marking) to $3-cis-HH$. The generation of $3-trans-HH$ and $3-cis-HH$ from stilbene with *meta*-chloroperoxybenzoic acid (*m*CPBA) confirmed our assignment (see SI). To gather as much information as possible on the influence of DEDs on the reaction we followed our procedure for all possible $1-R^1$ and $2-R^2$ combinations. The results for the symmetric products are depicted in Figure 1. Counterintuitively, the epoxide ratio (*cis:trans*) shifts to the more crowded $3-cis-R^1R^2$ with increasing size of DEDs. Accordingly, the ratio of $3-trans-tBu^1Bu^2$ and $3-cis-tBu^1Bu^2$ (Figure 1, black NMR) is almost 1:1 (see SI for all ratios).

Figure 2 displays the experimentally determined $\Delta G_{R^1R^2-HH}^{\ddagger}$ values for the reaction between differently substituted tetrahydrothiophene salt $1-R^1$ and aldehyde $2-R^2$ to generate a mixture of $3-cis-R^1R^2$ and $3-trans-R^1R^2$. The energy values are derived from integration of the *cis* and *trans* proton signals at the epoxide. The unsubstituted system was utilized as reference reaction. $\Delta G_{R^1R^2-HH}^{\ddagger}$ refers to the energy between the transition states of the rate determining step relative to the parent unsubstituted reaction of $1-H$ and $2-H$. Therefore, the reaction of $1-H$ and $2-H$ is depicted as $\Delta G_{HH-HH}^{\ddagger} = 0.0 \pm 0.1 \text{ kcal mol}^{-1}$ (leftmost data point). With an absolute energy value of $\Delta G_{HH}^{\ddagger} = 1.0 \pm 0.0 \text{ kcal mol}^{-1}$ (see SI for absolute values) the reaction of $1-H$ and $2-H$ favors the less crowded $3-cis-HH$ over $3-trans-HH$ ($K_{HH}^{\ddagger} = 0.17$). In line with the argument that large groups such as phenyl moieties interact repulsively, the transition state leading to the unfolded $3-trans-HH$ is lower in energy by around $1.0 \text{ kcal mol}^{-1}$ than its more crowded counterpart. With this result and classic “steric repulsion thinking” in mind, bulkier groups, *e.g.*, with an all-*meta* substitution pattern, should shift the ratio even further to $3-trans-R^1R^2$ ($\Delta G^{\ddagger} > 0$).²⁸ In

stark contrast, Figure 2 shows the *opposite* trend. The attached substituents shift the ratio to the more crowded **3-cis-HH** ($\Delta G^\ddagger < 0$) contradicting the well-established rationale that increasing steric bulk predominantly favors **3-trans-R'R²**. However, our results are well in line with investigations focusing on attractive σ - σ and σ - π interactions.^{3, 33-38} Similar effects were observed in the enantioselective Corey-Bakshi-Shibata reduction⁴ and in the copper-catalyzed hydroamination^{5, 7} of unactivated olefins. In both cases, bulky substituents were utilized to lower the energy of the more crowded transition state by enforcing close σ - σ and σ - π contacts between catalyst and substrate. A similar effect appears to govern the JCC reaction as well.

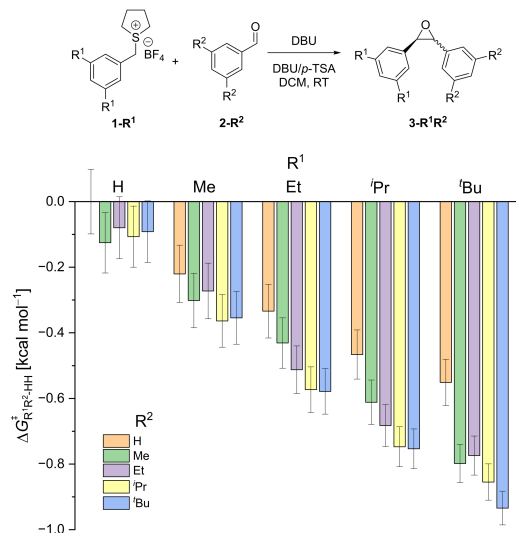


Figure 2. Experimentally determined relative Gibbs free energy values $\Delta G^\ddagger_{R^1R^2-HH}$ for the reaction of **1-R¹** and **2-R²** at room temperature relative to the parent case with $R^1 = R^2 = H$ (leftmost data point). The depicted energy values correspond to the energy differences of the transition states in the rate-determining step. $\Delta G^\ddagger < 0$ indicates favoring of **3-cis-R¹R²** formation with regards to the parent system. The gray lines indicate error bars.

To study the effect of LD on the transition state of the reaction, all combinations of **1-R¹** and **2-R²** were measured. The unsubstituted **1-H** always favors the reaction to **3-trans-HR²** (leftmost block of columns). The energy difference of the transition states does not change with increasing substituent size at **2-R²** ($\Delta G^\ddagger_{HR^2-HH} \approx -0.1 \pm 0.1$ kcal mol⁻¹). On the other hand, in a reaction with unsubstituted benzaldehyde **2-H** (orange bars) increasing substituent size at **1-R¹** decreases the energy gap between the two transition states. Stabilizing σ - π interactions appear to decrease the energy of the *more crowded* transition state. While the transition state to **3-cis-MeH** benefits by around $\Delta G^\ddagger_{MeH-HH} \approx -0.2 \pm 0.1$ kcal mol⁻¹ from stabilizing σ - π contacts, the incorporation of additional CH₃ substituents increases this effect by around -0.1 kcal mol⁻¹. In the series of singly substituted starting materials (orange bars and leftmost block of columns), the largest effect can be observed for the reaction of **1-tBu** and **2-H** ($\Delta G^\ddagger_{tBuH-HH} \approx -0.6 \pm 0.1$ kcal mol⁻¹). In stark contrast to the

well-established rule-of-thumb that steric hindrance governs the transition state of the JCC reaction, an increase in substituent size at **1-R¹** and **2-R²** shifts the *dr* towards the more crowded **3-cis-R¹R²**. The systematic increase of **2-R²** within each series of **1-R¹** identifies the *tert*-butyl substituent (blue bars) as the best DED. The strongest interaction can be observed for the reaction of **1-tBu** and **2-tBu** almost resulting in a 1:1 mixture ($K^\ddagger_{tBuBu} = 0.93$). Since we are under kinetic conditions, the transition state to the more crowded **3-cis-tBuBu** is favored by around $\Delta G^\ddagger_{tBuBu-HH} \approx -0.9 \pm 0.1$ kcal mol⁻¹ relative to its parent counterpart. Interestingly, the limit of stabilization was not reached with the substituents chosen since the *tert*-butyl derivative favors the *cis*-epoxide the most and no compensation due to steric repulsion can be observed. It is expected that even bulkier groups such as adamantyl will favor **3-cis-R¹R²** up to the point where steric interactions finally dominate. Unfortunately, the limit was set due to increasingly poor solubility of the adamantyl precursors, which we had attempted to include as well.

DISCUSSION

As described in the introduction, four main factors were made responsible for diastereoselectivity of the reaction between sulfur ylide and aldehyde. On the basis of our experimental data, three of these can be re-evaluated and refined (charge solvation is not part of our study).

Stability of the Carbonyl Group. Aggarwal *et al.*²⁸ observed a significant increase in *trans*-diastereoselectivity when utilizing aromatic instead of aliphatic aldehydes. While the formation of the *syn*-betaine structure is reversible (Scheme 1), stabilization of the starting material allows for an increase in *trans*-betaine formation. Aryl moieties stabilize the carbonyl form over the betaine structure. Accordingly, high *dr* is expected for benzaldehyde derivatives. Additionally, this effect should be amplified by electron-donor substituents due to an increase in electron density at the carbonyl carbon resulting in lower electrophilicity.²⁸ However, our experimental data show the opposite selectivity. While unsubstituted phenyl moieties favor **3-trans-R¹R²**, the attachment of DEDs clearly shifts the ratio towards **3-cis-R¹R²** (for example, $K^\ddagger_{tBuBu} = 0.93$). Accordingly, we deduce that the stability of the carbonyl group is less important and conclude that the action of increasingly larger alkyl groups at the aryl ring mainly act through stabilizing LD interactions.

Stability of the Ylide. In line with the argument above, Aggarwal *et al.*²⁸ found that the more stable the ylide, the higher the *trans* selectivity. Accordingly, electron-deficient functional groups increase diastereocontrol, whereas electron-rich groups yield lower *dr*. This statement is in line with our experimental findings. The attached alkyl groups decrease stereocontrol. The energy gap between both rate determining steps is equal in height to result in 1:1 mixture of *cis* and *trans* epoxide with bulky *tert*-butyl groups attached. Additionally, our experimental findings let us conclude that the stability of the ylide is not the only factor for stereocontrol but that this also depends on the fine balance between attractive and repulsive interactions. A combination of an increasing number of close LD contacts and a higher electron density maximize LD interactions in the more crowded transition state.

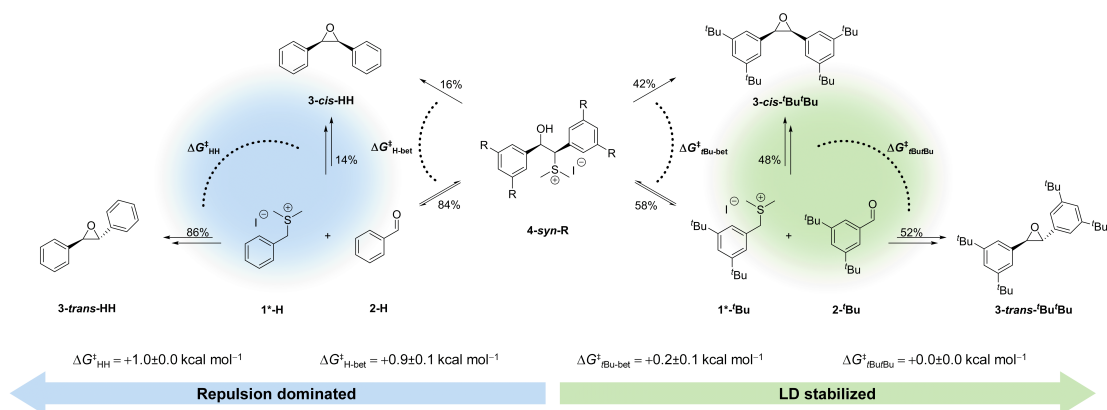
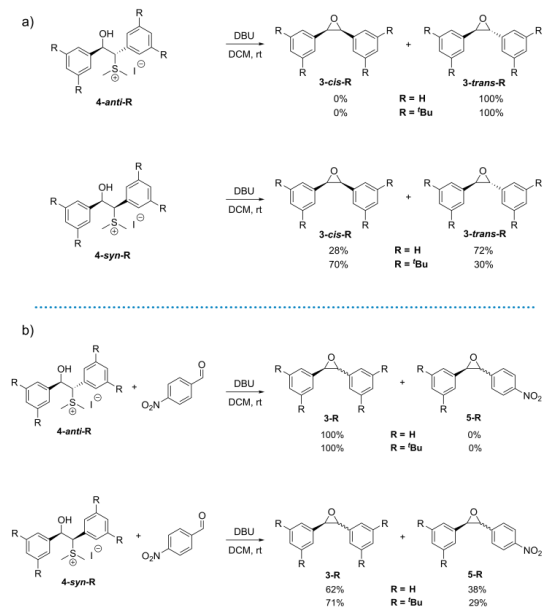


Figure 3. Reaction path for ring closure experiments of 4-syn-R with R = H (left, blue) and R = tBu (right, green). The percentage give the probability of conversion of 4-syn-R and recombination of 1*-R and 2-R. The Gibbs free energy values correspond to the difference in transition state of the conversion of 4-syn-R ($\Delta G^{\ddagger}_{\text{H-bet}}$) and for rate-determining transition states of recombination of 1*-R and 2-R ($\Delta G^{\ddagger}_{\text{R}^2}$).

Scheme 2. Ring closure experiments (top) and cross-over experiments (bottom) of 4-anti-R and 4-syn-R in DCM at room temperature with DBU as base. Para-nitrobenzaldehyde was utilized as trapping agent.



Since the first two principles are based on reversible betaine formation, we performed ring closure and cross-over experiments to investigate the reversibility for the unsubstituted and heavily substituted system. Hence, we synthesized the protonated diastereomers of betaine intermediates 4-anti-R and 4-syn-R (Scheme 2) to probe the epoxide formation starting with a single diastereomer. The starting materials were generated from *cis*- (4-syn-H) and *trans*-stilbene (4-anti-H).³⁹ After epoxidation of *cis*- and *trans*-stilbene and stereoselective ring opening with thiomethoxide, methyl-

ation with methyl iodide yields 4-syn-H and 4-anti-H selectively. The *tert*-butyl derivative was synthesized accordingly. Hereby, the *cis*- and *trans*-stilbene derivatives were prepared from hydrogenation of bis-(3,5-di-*tert*-butylphenyl) acetylene, which was the product of a coupling reaction with 2-butyne diacid.⁴⁰

The ring closure experiments (Scheme 2, top) of 4-anti-R and 4-syn-R were performed at room temperature in DCM by adding 1 equiv. of base (DBU). With 4-anti-R with R = H or tBu, the less crowded 3-trans-R¹R² forms exclusively. This implies that the rate-determining step for the JCC reaction has to occur *prior* to the final epoxidation step (thus the betaine formation). In line with earlier reports,^{21, 22, 39, 41-43} the epoxidation of 4-syn-H results in a 28:72 *cis:trans* product ratio. Thus, the rate-determining step of 3-cis-HH formation lies *after* betaine formation. Upon deprotonating 4-syn-H the *syn*-betaine can either be directly converted to 3-cis-HH or equilibrate to form the starting material (Figure 3). Recombination of 1*-R (asterisk indicates minor changes of the molecule to 1-R) and 2-R also result in a *cis* and *trans* product mixture. Under the assumption that molecular changes in 1*-R are minor and negligible, $\Delta G^{\ddagger}_{\text{R}^2\text{-HH}}$ (Figure 2) can be utilized to calculate the probability for the conversion of 4-syn-R. The ratio for the reaction of 4-syn-H in combination with results of the JCC epoxidation to form 3-cis/trans-HH (Figure 2) corresponds to an energy difference of $\Delta G^{\ddagger}_{\text{H-bet}} \approx +0.9 \pm 0.1 \text{ kcal mol}^{-1}$ for the transition states of the conversion (ring closure reaction or equilibration) according to probability calculations. This suggests that the majority of 4-syn-H ($\approx 84\%$) equilibrates while the remaining 16% are directly converted to 3-cis-HH (Figure 3). The same effect can be observed for 4-syn-tBu. Remarkably, now the final ratio for the consumption of 4-syn-tBu is 70:30 (*cis:trans*) in favor of the more crowded product 3-cis-tBu-tBu, suggesting a significant change in transition states for the conversion of 4-syn-tBu. The ratio corresponds to an energy difference of $\Delta G^{\ddagger}_{\text{tBu-bet}} \approx +0.2 \pm 0.1 \text{ kcal mol}^{-1}$, thereby, slightly favoring conversion to 1-tBu and 2-tBu. Accordingly, 42% of 4-syn-tBu are directly converted to 3-cis-tBu-tBu while the remaining 58% equilibrate to 1-R and 2-R (Figure

3). The direct formation of **3-cis-^tBu^tBu** from **4-syn-^tBu** significantly increases in comparison to parent **4-syn-H**. This can be related to additional LD interactions favoring the folded conformation **4-syn-^tBu** with the hydroxyl function in *anti*-position to the thioether functional group.

A similar DED-effect was already observed within hexaphenylethane.⁴⁴⁻⁴⁹ While the unsubstituted hexaphenylethane is not thermodynamically stable due to steric hindrance,⁴⁸ the *tert*-butyl substituted derivative offers multiple LD contacts to stabilize the molecule. Likewise, the unsubstituted reaction pathway of **4-syn-H** is governed by repulsive interactions. On the other hand, LD interactions stabilize the folded *syn*-betaine structure, thereby increasing the probability of direct conversion to **3-cis-^tBu^tBu**.

To demonstrate that an equilibration must occur by reopening the betaine structure, we performed cross-over experiments (Scheme 2, bottom).^{21, 22, 39, 41-43} Activated *para*-nitrobenzaldehyde was utilized as trapping agent for the ylide due to its higher reactivity (reactions proceed around 62 times faster than benzaldehyde).⁴⁵ Whereas **4-anti-R** with R = H or ^tBu solely results in the formation of **3-trans-R²** without incorporating nitrobenzaldehyde, **4-syn-R** gives a mixture of **3-trans-R²** and the corresponding nitro-product (**5-R**). This demonstrates that the equilibration of the *syn*-betaine has to occur by breaking the central carbon bond to give ylide and aldehyde.

Steric Hindrance of the Ylide/Aldehyde. Finally, steric hindrance is widely believed to affect the stereochemical outcome of the JCC reaction.²⁸ While this may be true for special cases, it is unlikely the sole contributor to selectivity because all bulky substituents used here (and elsewhere) show the opposite (Figure 2): The parent reaction of **1-H** with **2-H** yields the highest *trans* selectivity with a transition state energy difference of $\Delta G_{\text{HH}}^{\ddagger} = 1.0 \pm 0.0 \text{ kcal mol}^{-1}$. On the contrary, the reaction of **1-^tBu** with **2-^tBu** results in an approx. 1:1 mixture of **3-cis-^tBu^tBu** and **3-trans-^tBu^tBu** (i.e., $\Delta G_{\text{tBuEtBu}}^{\ddagger} \approx -0.0 \text{ kcal mol}^{-1}$). Consequently, the energy gap of around $1.0 \pm 0.0 \text{ kcal mol}^{-1}$ between the two diastereomeric transition states of the parent case vanishes due to the attachment of bulky *tert*-butyl groups.

To shed more light on the origin of the transition state stabilization, we dissected the $\Delta \Delta G_{\text{R}^1\text{R}^2}^{\ddagger}$ energy values by mutating all substituents separately. By comparing and applying this against energies of singly substituted reactions the interaction energy $\Delta \Delta G_{\text{R}^1\text{R}^2}^{\ddagger}$ can be dissected (Figure 4, top). $\Delta \Delta G_{\text{R}^1\text{R}^2}^{\ddagger}$ solely resembles the interaction energy between both alkyl groups R¹ and R², thereby disregarding the energy gain due to close σ - π contacts. For this procedure^{50, 51} (referred to as double mutant cycle, a practical application of Hess' law) we applied the following equation:

$$\Delta \Delta G_{\text{R}^1\text{R}^2}^{\ddagger} = \Delta G_{\text{R}^1\text{R}^2}^{\ddagger} - \Delta G_{\text{R}^1\text{H}}^{\ddagger} - \Delta G_{\text{HR}^2}^{\ddagger} + \Delta G_{\text{HH}}^{\ddagger} \quad (1)$$

The result gives an experimental estimate of the role DEDs play in the reaction of ylide and aldehyde. In contrast to the concept of steric repulsion, Figure 4 (bottom) qualitatively highlights the stabilizing effect (negative energy values) of each DED in the transition state of the reaction.

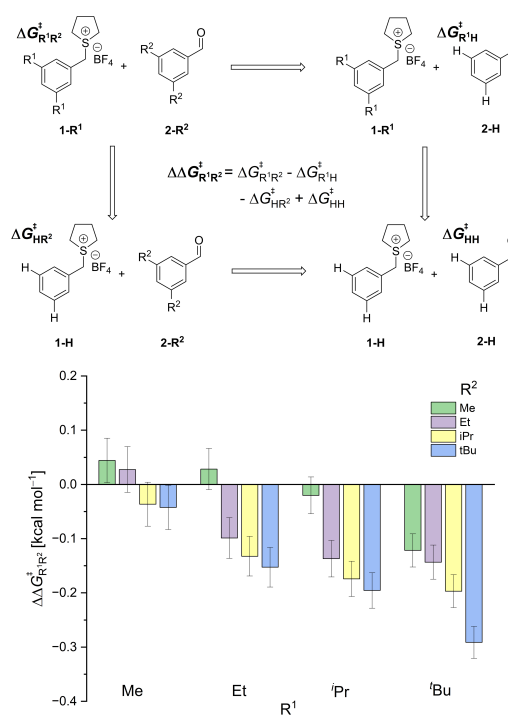


Figure 4. Double mutant cycle (top) and experimental results of the analysis (bottom). $\Delta \Delta G_{\text{R}^1\text{R}^2}^{\ddagger}$ illustrates the interaction energy between R¹ and R² in the reaction of **1-R¹** with **2-R²**. Negative energy values correspond to stabilizing interactions between R¹ and R². Grey lines indicate error bars.

Apart from Me-Et combinations, all energy values are negative corresponding to stabilizing interactions between the alkyl substituents. While this effect is small for **1-Me** (left-most block of columns), the stabilization increases with DED size, i.e., polarizability. Consequently, the largest effect can be observed for ^tBu-^tBu contacts $\Delta \Delta G_{\text{tBuEtBu}}^{\ddagger} = -0.3 \pm 0.1 \text{ kcal mol}^{-1}$. By comparing the relative Gibbs free energy values $\Delta G_{\text{R}^1\text{R}^2\text{-HH}}^{\ddagger}$ (Figure 2) to the results of the double mutant cycle (Figure 4), the interaction energy between each DED can be dissected into σ - σ (between DEDs) and σ - π (between DED and phenyl system) interactions. Accordingly, the energy difference $\Delta G_{\text{tBuEtBu-HH}}^{\ddagger} \approx -0.9 \pm 0.1 \text{ kcal mol}^{-1}$ for the reaction of **1-^tBu** with **2-^tBu** (Figure 2) contains stabilizing σ - σ interactions of $\Delta \Delta G_{\text{tBuEtBu}}^{\ddagger} = -0.3 \pm 0.1 \text{ kcal mol}^{-1}$ (Figure 4). Around 30% of the experimentally determined relative Gibbs free energies can be accounted for with LD attractive alkyl-alkyl contacts. The remaining 70% correspond to LD attractive σ - π interactions. These results qualitatively fit to measurements performed for molecular balances in the ground state.³⁸

Most recently, *N,N*-diphenylthiourea was shown to experience the same distribution of σ - σ and σ - π interactions to stabilize the most crowded *syn-syn* conformer.³⁸ Accordingly, the observations and values concerning the role of LD in molecular balances can be directly transferred to transition state stabilizations.¹¹ Since transition states are more loosely

bound than covalently bound structures, the effects of LD are somewhat reduced but can still be decisive.

CONCLUSION

We herein demonstrated the crucial role of LD on the transition states in the JCC reaction. Whereas the generally accepted sentiment that bulky groups repulse each other fails to rationalize the observed trends, attractive noncovalent interactions correctly predict a transition state stabilization due to attractive σ - σ interactions. The double mutant cycle qualifies and quantifies the interactions evoked by LD. Furthermore, the effects of LD were utilized in ring closure and cross-over experiments to study the reactions mechanism in detail.

AUTHOR INFORMATION

Corresponding Author

* Peter R. Schreiner
Institute of Organic Chemistry, Justus Liebig University,
Heinrich-Buff-Ring 17, 35392 Giessen, Germany, E-mail:
prs@uni-giessen.de, orcid.org/0000-0002-3608-5515

Author Contributions

‡ Authors contributed equally to this work.

ORCID:

Lars Rummel (orcid.org/0000-0002-3772-2109)
Marvin H. J. Domanski (orcid.org/0000-0002-1934-5223)
Ephrath Solel (orcid.org/0000-0002-0513-8995)
Heike Hausmann (orcid.org/0000-0003-0347-9064)
Peter R. Schreiner (orcid.org/0000-0002-3608-5515)

Funding Sources

This work was supported by the priority program "Control of London Dispersion in Molecular Chemistry" (SPP1807) of the Deutsche Forschungsgemeinschaft.

ACKNOWLEDGMENT

We thank Salome Wagner, Valeria Malynych, and Anna Shurando for synthetic support. Additionally, we like to thank Bastian Bernhardt, Finn M. Wilming, Jan M. Schümann, and Henrik F. König for fruitful discussions.

REFERENCES

- Cowdrey, W. A.; Hughes, E. D.; Ingold, C. K.; Masterman, S.; Scott, A. D., 257. Reaction kinetics and the Walden inversion. Part VI. Relation of steric orientation to mechanism in substitutions involving halogen atoms and simple or substituted hydroxyl groups. *J. Chem. Soc.* **1937**, (0), 1252-1271.
- Kozuch, S.; Shaik, S., How to Conceptualize Catalytic Cycles? The Energetic Span Model. *Acc. Chem. Res.* **2011**, *44* (2), 101-110.
- Wagner, J. P.; Schreiner, P. R., London Dispersion in Molecular Chemistry—Reconsidering Steric Effects. *Angew. Chem. Int. Ed.* **2015**, *54* (42), 12274-12296.
- Eschmann, C.; Song, L.; Schreiner, P. R., London Dispersion Interactions Rather than Steric Hindrance Determine the Enantioselectivity of the Corey–Bakshi–Shibata Reduction. *Angew. Chem. Int. Ed.* **2021**, *60* (9), 4823-4832.
- Lu, G.; Liu, R. Y.; Yang, Y.; Fang, C.; Lambrecht, D. S.; Buchwald, S. L.; Liu, P., Ligand–Substrate Dispersion Facilitates the Copper-Catalyzed Hydroamination of Unactivated Olefins. *J. Am. Chem. Soc.* **2017**, *139* (46), 16548-16555.
- Thomas, A. A.; Speck, K.; Kevlishvili, I.; Lu, Z.; Liu, P.; Buchwald, S. L., Mechanistically Guided Design of Ligands That Significantly Improve the Efficiency of CuH-Catalyzed Hydroamination Reactions. *J. Am. Chem. Soc.* **2018**, *140* (42), 13976-13984.
- Xi, Y.; Su, B.; Qi, X.; Pedram, S.; Liu, P.; Hartwig, J. F., Application of Trimethylgermyl-Substituted Bisphosphine Ligands with Enhanced Dispersion Interactions to Copper-Catalyzed Hydroboration of Disubstituted Alkenes. *J. Am. Chem. Soc.* **2020**, *142* (42), 18213-18222.
- London, F., Zur Theorie und Systematik der Molekularkräfte. *Z. Phys.* **1930**, *63* (3-4), 245-279.
- London, F., The General Theory of Molecular Forces. *Trans. Faraday Soc.* **1937**, *33*, 8b-26.
- Grimme, S.; Huenerbein, R.; Ehrlich, S., On the Importance of the Dispersion Energy for the Thermodynamic Stability of Molecules. *ChemPhysChem* **2011**, *12* (7), 1258-1261.
- Strauss, M. A.; Wegner, H. A., Molecular Systems for the Quantification of London Dispersion Interactions. *Eur. J. Org. Chem.* **2019**, 2019 (2-3), 295-302.
- Elmi, A.; Cockroft, S. L., Quantifying Interactions and Solvent Effects Using Molecular Balances and Model Complexes. *Acc. Chem. Res.* **2021**, *54* (1), 92-103.
- Johnson, A. W.; LaCount, R., 9-Dimethylsulfonium fluorenylide. *Chem. Ind.* **1958**, 1440-1441.
- Johnson, A. W.; LaCount, R. B., The Chemistry of Ylides. VI. Dimethylsulfonium Fluorenylide—A Synthesis of Epoxides. *J. Am. Chem. Soc.* **1961**, *83* (2), 417-423.
- Corey, E. J.; Chaykovsky, M., Dimethylsulfonium methylide, a reagent for selective oxirane synthesis from aldehydes and ketones. *J. Am. Chem. Soc.* **1962**, *84* (19), 3782-3783.
- Corey, E. J.; Chaykovsky, M., Dimethylsulfonium Methylide ((CH₃)₂S(O)CH₂) and Dimethylsulfonium Methylide ((CH₃)₂SCH₂). Formation and Application to Organic Synthesis. *J. Am. Chem. Soc.* **1965**, *87* (6), 1353-1364.
- Aggarwal, V. K.; Alonso, E.; Fang, G.; Ferrara, M.; Hynd, G.; Porcelloni, M., Application of Chiral Sulfides to Catalytic Asymmetric Aziridination and Cyclopropanation with In Situ Generation of the Diazo Compound. *Angew. Chem. Int. Ed.* **2001**, *40* (8), 1433-1436.
- Aggarwal, V. K.; Alonso, E.; Hynd, G.; Lydon, K. M.; Palmer, M. J.; Porcelloni, M.; Studley, J. R., Catalytic Asymmetric Synthesis of Epoxides from Aldehydes Using Sulfur Ylides with In Situ Generation of Diazocompounds. *Angew. Chem. Int. Ed.* **2001**, *40* (8), 1430-1433.
- Aggarwal, V. K.; Richardson, J., The complexity of catalysis: origins of enantio- and diastereoselectivity in sulfur ylide mediated epoxidation reactions. *Chem. Commun.* **2003**, (21), 2644-2651.
- Aggarwal, V. K.; Winn, C. L., Catalytic, Asymmetric Sulfur Ylide-Mediated Epoxidation of Carbonyl Compounds: Scope, Selectivity, and Applications in Synthesis. *Acc. Chem. Res.* **2004**, *37* (8), 611-620.
- Aggarwal, V. K.; Hebach, C., Carboxylate-stabilised sulfur ylides (thetin salts) in asymmetric epoxidation for the synthesis of glycidic acids. Mechanism and implications. *Org. Biomol. Chem.* **2005**, *3* (8), 1419-1427.
- Aggarwal, V. K.; Charmant, J. P. H.; Fuentes, D.; Harvey, J. N.; Hynd, G.; Ohara, D.; Picoul, W.; Robiette, R.; Smith, C.; Vasse, J.-L.; Winn, C. L., Highly Enantioselective Synthesis of Glycidic Amides Using Camphor-Derived Sulfonium Salts. Mechanism and Applications in Synthesis. *J. Am. Chem. Soc.* **2006**, *128* (6), 2105-2114.
- Volatron, F.; Eisenstein, O., Theoretical study of the reactivity of phosphonium and sulfonium ylides with carbonyl groups. *J. Am. Chem. Soc.* **1984**, *106* (20), 6117-6119.
- Volatron, F.; Eisenstein, O., Wittig versus Corey-Chaykovsky Reaction. Theoretical study of the reactivity of phosphonium methylide and sulfonium methylide with formaldehyde. *J. Am. Chem. Soc.* **1987**, *109* (1), 1-14.
- Lindvall, M. K.; Koskinen, A. M. P., Origins of Stereoselectivity in the Corey–Chaykovsky Reaction. Insights from Quantum Chemistry. *J. Org. Chem.* **1999**, *64* (13), 4596-4606.
- Aggarwal, V. K.; Harvey, J. N.; Richardson, J., Unraveling the Mechanism of Epoxide Formation from Sulfur Ylides and Aldehydes. *J. Am. Chem. Soc.* **2002**, *124* (20), 5747-5756.
- Edwards, D. R.; Montoya-Peleaz, P.; Crudden, C. M., Experimental Investigation into the Mechanism of the Epoxidation of Aldehydes with Sulfur Ylides. *Org. Lett.* **2007**, *9* (26), 5481-5484.
- Illa, O.; Namutebi, M.; Saha, C.; Ostovar, M.; Chen, C. C.; Haddow, M. F.; Nocquet-Thibault, S.; Lusi, M.; McGarrigle, E. M.;

- Aggarwal, V. K., Practical and Highly Selective Sulfur Ylide-Mediated Asymmetric Epoxidations and Aziridinations Using a Cheap and Readily Available Chiral Sulfide: Extensive Studies To Map Out Scope, Limitations, and Rationalization of Diastereo- and Enantioselectivities. *J. Am. Chem. Soc.* **2013**, *135* (32), 11951-11966.
29. Jadhav, P. D.; Lu, X.; Liu, R.-S., Gold-Catalyzed [5+2]- and [5+1]-Annulations between Ynamides and 1,2-Benzisoxazoles with Ligand-Controlled Chemoselectivity. *ACS Catal.* **2018**, *8* (10), 9697-9701.
30. Annunziata, R.; Benaglia, M.; Cinquini, M.; Cozzi, F.; Tocco, G., A Poly(ethylene glycol)-Supported Quaternary Ammonium Salt: An Efficient, Recoverable, and Recyclable Phase-Transfer Catalyst. *Org. Lett.* **2000**, *2* (12), 1737-1739.
31. Mohanty, A. D.; Bae, C., Mechanistic analysis of ammonium cation stability for alkaline exchange membrane fuel cells. *J. Mater. Chem. A* **2014**, *2* (41), 17314-17320.
32. Krief, A.; Swinnen, D.; Billen, D., Stereocontrolled synthesis of [3.1.0]bicyclohexanones by cyclopropanation of enones with benzylidene sulfuranes. *Tetrahedron Lett.* **2002**, *43* (33), 5871-5873.
33. Hwang, J.; Li, P.; Carroll, W. R.; Smith, M. D.; Pellechia, P. J.; Shimizu, K. D., Additivity of Substituent Effects in Aromatic Stacking Interactions. *J. Am. Chem. Soc.* **2014**, *136* (40), 14060-14067.
34. Schweighauser, L.; Strauss, M. A.; Bellotto, S.; Wegner, H. A., Attraction or Repulsion? London Dispersion Forces Control Azobenzene Switches. *Angew. Chem. Int. Ed.* **2015**, *54* (45), 13436-13439.
35. Hwang, J.; Li, P.; Smith, M. D.; Shimizu, K. D., Distance-Dependent Attractive and Repulsive Interactions of Bulky Alkyl Groups. *Angew. Chem. Int. Ed.* **2016**, *55* (28), 8086-8089.
36. Schumann, J. M.; Wagner, J. P.; Eckhardt, A. K.; Quanz, H.; Schreiner, P. R., Intramolecular London Dispersion Interactions Do Not Cancel in Solution. *J. Am. Chem. Soc.* **2021**, *143* (1), 41-45.
37. Soler, E.; Ruth, M.; Schreiner, P. R., London Dispersion Helps Refine Steric A-Values: Dispersion Energy Donor Scales. *J. Am. Chem. Soc.* **2021**, *143* (49), 20837-20848.
38. Rummel, L.; Domanski, M. H. J.; Hausmann, H.; Becker, J.; Schreiner, P. R., London Dispersion Favors Sterically Hindered Diarylthiourea Conformers in Solution. *Angew. Chem. Int. Ed.* **2022**, *n/a* (n/a).
39. Aggarwal, V. K.; Calamai, S.; Gair Ford, J., Additions of benzylium ylides to aldehydes and ketones: are they under kinetic or thermodynamic control? *J. Chem. Soc., Perkin Trans. 1* **1997**, (5), 593-600.
40. Park, K.; Bae, G.; Moon, J.; Choe, J.; Song, K. H.; Lee, S., Synthesis of Symmetrical and Unsymmetrical Diarylalkynes from Propiolic Acid Using Palladium-Catalyzed Decarboxylative Coupling. *J. Org. Chem.* **2010**, *75* (18), 6244-6251.
41. Yoshimine, M.; Hatch, M. J., Mechanism of the reaction of aqueous benzyldimethylsulfonium chloride and formaldehyde with sodium hydroxide. *J. Am. Chem. Soc.* **1967**, *89* (23), 5831-5838.
42. Aggarwal, V. K.; Charmant, J. P. H.; Ciampi, C.; Hornby, J. M.; O'Brien, C. J.; Hynd, G.; Parsons, R., Additions of stabilised and semi-stabilised sulfur ylides to tosyl protected imines: are they under kinetic or thermodynamic control? *J. Chem. Soc., Perkin Trans. 1* **2001**, (23), 3159-3166.
43. Edwards, D. R.; Du, J.; Crudden, C. M., Experimental Demonstration of Base-Catalyzed Interconversion of Isomeric Betaine Intermediates in the Corey-Chaykovsky Epoxidation. *Org. Lett.* **2007**, *9* (12), 2397-2400.
44. Stein, M.; Winter, W.; Rieker, A., Hexakis(2,6-di-tert-butyl-4-biphenyl)ethane—The First Unbridged Hexaarylethane. *Angew. Chem. Int. Ed.* **1978**, *17* (9), 692-694.
45. Kahr, B.; Van Engen, D.; Mislow, K., Length of the ethane bond in hexaphenylethane and its derivatives. *J. Am. Chem. Soc.* **1986**, *108* (26), 8305-8307.
46. Rösel, S.; Balestrieri, C.; Schreiner, P. R., Sizing the role of London dispersion in the dissociation of all-meta tert-butyl hexaphenylethane. *Chem. Sci.* **2017**, *8* (1), 405-410.
47. Rösel, S.; Becker, J.; Allen, W. D.; Schreiner, P. R., Probing the Delicate Balance between Pauli Repulsion and London Dispersion with Triphenylmethyl Derivatives. *J. Am. Chem. Soc.* **2018**, *140* (43), 14421-14432.
48. Rummel, L.; Schumann, J. M.; Schreiner, P. R., Hexaphenylditetrals – When Longer Bonds Provide Higher Stability. *Chem. Eur. J.* **2021**, *27* (55), 13699-13702.
49. Rösel, S.; Schreiner, P. R., Computational Chemistry as a Conceptual Game Changer: Understanding the Role of London Dispersion in Hexaphenylethane Derivatives (Gomberg Systems). *Isr. J. Chem.* **2022**, *62* (1-2), e202200002.
50. Carter, P. J.; Winter, G.; Wilkinson, A. J.; Fersht, A. R., The use of double mutants to detect structural changes in the active site of the tyrosyl-tRNA synthetase (*Bacillus stearothermophilus*). *Cell* **1984**, *38* (3), 835-840.
51. Adams, H.; Carver, F. J.; Hunter, C. A.; Morales, J. C.; Seward, E. M., Chemical Double-Mutant Cycles for the Measurement of Weak Intermolecular Interactions: Edge-to-Face Aromatic Interactions. *Angew. Chem. Int. Ed.* **1996**, *35* (13-14), 1542-1544.

3. Acknowledgement - Danksagung

Diese Arbeit wäre ohne einige Personen nicht zustande gekommen. Folgend möchte ich mich bei allen bedanken, die mich, nicht nur in wissenschaftlicher Hinsicht, tatkräftig unterstützt haben. Herzlich bedanken möchte ich mich bei:

Prof. Dr. Peter R. Schreiner, PhD für die Möglichkeit meine Arbeit in seiner Arbeitsgruppe durchzuführen, die gute Zusammenarbeit, die Freiheit in meiner Forschung und das Fördern meiner Fähigkeiten als Wissenschaftler.

Prof. Dr. Richard Göttlich für die Übernahme des Zweitgutachtens meiner Arbeit.

Jan M. Schümann für eine erfolgreiche Zusammenarbeit in zwei Publikationen und zahllose wissenschaftliche Diskussionen.

Marvin H. J. Domanski für seine Bereitschaft Projekte im Rahmen von Spezialisierungsmodulen und Masterarbeiten erfolgreich mit einer Publikation abzuschließen. Ich bin sehr dankbar, dass du viele der Experimente durchgeführt hast.

Henrik F. König für eine erfolgreiche und gute Zusammenarbeit beim Schreiben von zwei Publikationen. Auch dir danke ich, für die zahllosen Stunden im Labor und der ganzen Synthesearbeit, die du in unsere Projekte gesteckt hast.

Dr. Heike Hausmann, Dr. Jonathan Becker und Ephrath Solel, PhD für zahllose NMR-Messungen, Analysen von Einkristallen oder computerchemische Rechnungen, ohne die kein Projekt hätte abgeschlossen werden können.

Finn M. Wilming, Dr. Bastian Bernhardt, Henrik F. König und Marvin H. J. Domanski für eine wunderbare Arbeitsatmosphäre. Es hat mir jeden Tag Spaß gemacht mit euch zu arbeiten. Auch von mir bekommt ihr natürlich 25.000 Punkte.

Dr. Dennis Gerbig und **Dr. Raffael Wende** für die Unterstützung in wissenschaftlichen Fragestellungen im Bereich quantenchemischer Rechnungen oder massenspektrometrischer Probleme.

Michaela Richter für die tatkräftige Unterstützung in allen administrativen Angelegenheiten.

Kai Hanke, Salome Wagner, Valeria Malynych und Anna Shurando für das Interesse an meinen Projekten und die tatkräftige Unterstützung im Labor.

Der gesamten **PRS Group** sowie dem **OC-Institut** für die Arbeitsatmosphäre und Zusammenarbeit.

Dr. Leonie Lieber für die wunderbare Zusammenarbeit während des gesamten Studiums. Ich bin sehr stolz auf alles, was wir zusammen geschafft haben.

Meiner Familie, **Norbert**, **Karin** und **Annika Rummel** sowie meiner Freundin **Vanessa Rübmann** für die fortwährende berufliche und private Unterstützung. Ohne euch wäre diese Arbeit nie zustande gekommen.